

**EXAMINING ZINC RELEASE FROM PLATELETS AND ITS
MODULATION OF CLOT STRUCTURE AND FIBRINOLYSIS**

By:
SARA J. HENDERSON, B.Sc.

A Thesis
Submitted to the School of Graduate Studies in Partial
Fulfillment of the Requirements for the
Degree Doctor of Philosophy

McMaster University © Copyright by Sara J. Henderson, December 14, 2015

Ph.D. Thesis – S.J. Henderson; McMaster University – Biochemistry

DOCTOR OF PHILOSOPHY (2015)
(Biochemistry and Biomedical Sciences)

McMaster University
Hamilton, Ontario, Canada

TITLE: Examining Zinc Release from Platelets and its Modulation of Clot Structure and Fibrinolysis

AUTHOR: Sara J. Henderson, B.Sc. (University of Prince Edward Island)

SUPERVISOR: Jeffrey I. Weitz, M.D., F.R.C.P.(C), F.A.C.P.

NUMBER OF PAGES: i-xv, 1-266

ABSTRACT

Zinc (Zn^{2+}) is an abundant metal ion that circulates in the body. Within hemostasis, Zn^{2+} participates in platelet aggregation, coagulation, and fibrinolysis. At the site of injury, Zn^{2+} released from activated platelets accelerates coagulation and attenuates fibrinolysis. How Zn^{2+} regulates these processes on a molecular level has not been extensively examined. We hypothesized that Zn^{2+} released from platelets binds serine proteases involved in coagulation or fibrinolysis and modulates their proteolytic activity, thus controlling the rate of clot formation and lysis. We show that Zn^{2+} concentrations released from activated platelets are sufficient to modulate clot formation and fibrinolysis. We show *in vitro* that Zn^{2+} binds to fibrinogen with high affinity, accelerates fibrin monomer polymerization, and modifies clot structure. Zn^{2+} promotes clot stability by increasing fiber diameter, reducing fibrin fiber elasticity, and increases clot porosity. Although it might be predicted that these modifications would enhance clot degradation by enabling greater distribution of lytic enzymes through the more porous fibrin network, we showed the opposite. Thus, we demonstrated that Zn^{2+} binds to plasminogen activators and plasmin with high affinity and down-regulates their protease activity, which delays lysis. This adds to previous studies that showed that both coagulation and fibrinolysis are regulated by Zn^{2+} ions. These data support the functional role of Zn^{2+} in hemostasis.

ACKNOWLEDGEMENTS

I would like to thank my supervisor Dr. Jeffrey Weitz for his continual guidance, encouragement, and mentorship throughout my Ph.D. What I appreciate most about Dr. Weitz is that he is well connected and encourages collaboration. This has greatly contributed to the success of these projects, as a lot of techniques used were new concepts introduced into our lab. Dr. Weitz provided me with opportunity to collaborate with many top-notch labs around the world, which is a highlight in my research career. He also provided me with the knowledge and skills to pass on to others. Thank you for having confidence in my ability to teach others. It is truly a “domino effect” of success, reflecting that your best interest is in the accomplishments of your students.

Next, I would like to thank to my daily supervisor Dr. Jim Fredenburgh, who has been my academic coach throughout my Ph.D. Not only has Jim taught me the basic fundamentals of squash, but he also taught me a field of science that was completely foreign. Jim was my biggest fan and supporter, at all presentations, keeping me at ease. Although he was also my hardest critic as any coach is, he ensured that I was prepared to achieve any goal. Thank you Jim for your patience, continual guidance, perfectionism, and dropping everything when my projects were in a pickle. If there was something that Jim was unsure of technical wise, Beverly Leslie “Lab Mom” and Alan Stafford were called on. Both are tremendous lab technicians, they go above and beyond their job

descriptions, and are greatly appreciated. I am thankful to have experienced this amazing trifecta (Jim, Bev, and Alan). You all have made my Ph.D experience the best it could possibly be. I would also like to thank my committee members Dr. Geoff Werstuck and Dr. Patricia Liaw for your feedback on these projects. It is always great to have another perspective outside of the Weitz lab.

I would like to thank all the great people at TaARI that have made an east coaster feel right at home. The veteran Weitz members aka “The Docs”: Trang Vu, Paul Kim, Jonathan Yau, Calvin Yeh, and Iqbal Jaffer, my adopted Gross Lab members: Nima Vaezzadeh, Ran Ni, Shana Aalda Shaya, and my TaARI party planning partner: Kripa Raman. You all have made lab a fun place to come into on a daily bases.

Finally I would like to thank my PEI squad at home that still has no clue what I do. Regardless, they are all super proud and always rooting for me. To my family: Mom, Dad, and Chantel, thanks for your continual support of my student life. I swear I will get a “real” job after this. My friends: Luke Poirier, Megan Wood, and Brady McCloskey, thanks for visiting Hamilton. You can now check it off your top 10 must-see travel destinations.

Overall, my experience at TaARI has been a blast. As your one and only PEI connection, just remember, if you ever need access to lobsters, oysters, potatoes, or chocolate covered chips, you can always give me a shout. Thank you all!

TABLE OF CONTENTS

CHAPTER 1: INTRODUCTION

1.1 Overview of Hemostasis	1
1.2 Organelle and Granule Development in Megakaryocytes	3
1.3 Platelet Development from Megakaryocytes	7
1.4 Platelet Adhesion, Aggregation, and Activation.....	13
1.5 Platelet Granule Deficiencies.....	15
1.6 The Coagulation Cascade	16
1.7 Anticoagulation Pathways	21
1.8 Fibrinogen and Fibrin	23
1.9 Clot Structure	29
1.10 Fibrinolysis	34
1.11 Histidine-rich Glycoprotein	41
1.12 The Dynamic Role of Zn ²⁺ in Hemostasis	45

CHAPTER 2: THESIS OVERVIEW, RATIONALE, HYPOTHESIS, AND OBJECTIVE

2.1 Thesis Overview	51
2.2 Rationale of Studies	51
2.3 Central Hypotheses	52
2.4 Overall Objective	53

CHAPTER 3: ZINC PROMOTES CLOT STABILITY BY ACCELERATING CLOT FORMATION AND MODIFYING FIBRIN STRUCTURE

3.1 Forward	54
3.2 Objective	54
3.3 What is known	57
3.4 What this paper adds	57
3.5 Summary	57
3.6 Introduction.....	58
3.7 Materials and Methods	
3.7.1 Reagents	61
3.7.2 Clot formation in plasma.....	62
3.7.3 Clot time in purified systems	62
3.7.4 Preparation and polymerization of Fn monomers.....	63
3.7.5 Scanning electron microscopy (SEM)	63
3.7.6 Clot porosity.....	65
3.7.7 Clot strength.....	65
3.7.8 Statistical analysis	66

3.8 Results	
3.8.1 Effect of Zn ²⁺ on clot times in plasma	67
3.8.2 Effect of Zn ²⁺ on Fn clot formation	69
3.8.3 Effect of Zn ²⁺ on clot structure	78
3.8.4 Effect of Zn ²⁺ on clot porosity	82
3.8.5 Effect of Zn ²⁺ on clot rheology	82
3.9 Discussion	90
3.10 Acknowledgements	94

CHAPTER 4: ZINC DELAYS CLOT LYSIS BY ATTENUATING PLASMINOGEN ACTIVATION AND PLASMIN-MEDIATED FIBRIN DEGRADATION

4.1 Forward	95
4.2 Objective	95
4.3 What is known	98
4.4 What this paper adds	98
4.5 Summary	98
4.6 Introduction	99
4.7 Experimental Procedures	
4.7.1 Reagents	101
4.7.2 Quantification of Zn ²⁺ within and released from activated platelets	103
4.7.3 Binding of Zn ²⁺ to Fg, Fn, Glu-Pg, Lys-Pg, Pn, tPA, uPA, and trypsin	104
4.7.4 Effect of Zn ²⁺ on chromogenic activity of Pn, tPA, and uPA	105
4.7.5 Effect of Zn ²⁺ on Pg activation	106
4.7.6 Effect of Zn ²⁺ on the affinity of fibrinolytic proteins for Fg and Fn	107
4.7.7 Effect of Zn ²⁺ on the conversion of single-chain tPA and two-chain tPA	108
4.7.8 Effect of Zn ²⁺ on Fg degradation by Pn and trypsin	108
4.7.9 Clot lysis in a purified system	109
4.7.10 Clot lysis in plasma	109
4.7.11 Statistical analysis	110
4.8 Results	
4.8.1 Quantification of Zn ²⁺ in platelets and platelet releasate	110
4.8.2 Affinity of Zn ²⁺ for Fg, Glu-Pg, Lys-Pg, Pn, tPA, uPA, and trypsin	111
4.8.3 Effect of Zn ²⁺ on Pg activation	115
4.8.4 Effect of Zn ²⁺ on the affinities of Pg, VFK-Pn, and tPA for Fg and Fn	121
4.8.5 Effect of Zn ²⁺ on Fn clot lysis	125
4.8.6 Effect of Zn ²⁺ on plasma clot lysis	131
4.9 Discussion	133
4.10 Acknowledgements	137

CHAPTER 5: ZINC IS LOCATED IN PLATELET DENSE GRANULES AND RELEASED UPON ACTIVATION

5.1 Forward	138
5.2 Objective	138
5.3 Key points	141
5.4 Abstract	141
5.5 Introduction	142
5.6 Methods	
5.6.1 Reagents	143
5.6.2 Transmission electron microscopy (TEM)	144
5.6.3 High-resolution confocal laser immunofluorescence microscopy	145
5.6.4 Flame atomic absorption spectroscopy	146
5.6.5 Flow cytometry	148
5.6.6 Statistical analysis	148
5.7 Results	
5.7.1 Zn ²⁺ is located with Ca ²⁺ and phosphorus in platelet dense granules	148
5.7.2 Zn ²⁺ is not stored in the platelet cytoplasm or mitochondria	152
5.7.3 Zn ²⁺ colocalizes with Ca ²⁺ in select granules	154
5.7.4 Activated platelets release the majority of Ca ²⁺ stores, but only half of Zn ²⁺	156
5.7.5 Half of platelet Zn ²⁺ can be chelated with TPEN	157
5.8 Discussion	159
5.9 Acknowledgements	162

CHAPTER 6: ORIGIN AND RELEASE OF PLATELET HISTIDINE-RICH GLYCOPROTEIN

6.1 Forward	163
6.2 Objective	163
6.3 Key points	165
6.4 Abstract	165
6.5 Introduction	166
6.6 Methods	
6.6.1 Reagents	168
6.6.2 Preparation of megakaryocytes, proplatelets, and resting or activated platelets for immunofluorescence microscopy	170
6.6.3 Laser fluorescence spinning disk confocal microscopy	171
6.6.4 Western blot	172
6.6.5 Preparation of platelets for HRG quantification	173
6.6.6 Surface plasmon resonance	175
6.6.7 Blood collection from mice	175
6.6.8 Ex vivo perfusion assay	176

6.6.9 Statistical analysis	177
6.7 Results	
6.7.1 HRG is located in megakaryocytes, proplatelets and platelets	177
6.7.2 Activated platelets release little HRG	185
6.7.3 HRG is present in GPS patient platelet lysates	189
6.7.4 HRG binds to GPIb α in a Zn ²⁺ -dependent fashion	192
6.7.5 The role of HRG on platelet adhesion	194
6.8 Discussion	198
6.9 Acknowledgements	202

CHAPTER 7: GENERAL DISCUSSION AND FUTURE DIRECTIONS

7.1 General Discussion	203
7.2 Platelet Zn ²⁺	
7.2.1 Zn ²⁺ storage in platelets	204
7.2.2 Detecting Zn ²⁺ in HPS patient platelets	205
7.2.3 Zn ²⁺ transportation in platelets	206
7.2.4 Examining Zn ²⁺ release from platelets <i>in vivo</i>	214
7.3 Platelet HRG	
7.3.1 Examining the source of platelet HRG	215
7.3.2 Investigating the functional role of intracellular platelet HRG	216
7.4 Zn ²⁺ and Clot Formation	
7.4.1 Re-defining clot stability	221
7.4.2 Examining clot structure in cardiovascular disease patients	224
7.5 Zn ²⁺ and Clot Lysis	
7.5.1 Zn ²⁺ acts as a molecular brake on the fibrinolytic pathway	225
7.5.2 Localizing the Zn ²⁺ -binding domain on Pn	226
7.5.3 Identification of the Zn ²⁺ -binding domain on tPA	230
7.5.4 HRG may assist Zn ²⁺ in the attenuation of fibrinolysis	231
7.6 Recapitulating the effect of Zn ²⁺ on hemostatic reactions <i>in vivo</i>	232

CHAPTER 8: CONCLUSION

8.1 Concluding Remarks	234
------------------------------	-----

CHAPTER 9: APPENDIX

9.1 Methods	
9.1.1 Establishing a HRG dose-regiment in HRG ^{-/-} mice	237
9.1.2 Preparation of bone marrow from HRG ^{-/-} mice	238
9.1.3 Preparation of platelets from HRG ^{-/-} mice	248

CHAPTER 10: BIBLIOGRAPHY	247
---------------------------------------	-----

LIST OF FIGURES

CHAPTER 1: INTRODUCTION

Figure 1. Platelet biogenesis and secretory granule formation	5
Figure 2. Platelet structure and function	11
Figure 3. The blood coagulation cascade.....	18
Figure 4. The structure of fibrinogen and the polymerization of fibrin.....	27
Figure 5. The fibrinolytic system.....	35
Figure 6. The structure of histidine-rich glycoprotein	43

CHAPTER 3: ZINC PROMOTES CLOT STABILITY BY ACCELERATING CLOT FORMATION AND MODIFYING FIBRIN STRUCTURE

Figure 1. Effect of Zn ²⁺ on clotting.....	68
Figure 2. Effect of Zn ²⁺ and FXIII on clot formation	71
Figure 3. Effect of Zn ²⁺ on polymerization of Fn monomers	74
Figure 4. Comparison of the effect of Zn ²⁺ on clotting of Fg and fragment X.....	77
Figure 5. SEM of Fn clots formed in the absence or presence of Zn ²⁺ and FXIII.....	80
Figure 6. Effect of Zn ²⁺ on the rheological behavior of clots formed in the absence or presence of FXIII.....	84
Figure 7. Effect of Zn ²⁺ and FXIII on clot stability and rupture	87

CHAPTER 4: ZINC DELAYS CLOT LYSIS BY ATTENUATING PLASMINOGEN ACTIVATION AND PLASMIN-MEDIATED FIBRIN DEGRADATION

Figure 1. Effect of Zn ²⁺ on activation of Glu-Pg or Lys-Pg by tPA or uPA.....	116
Figure 2. Effect of Zn ²⁺ on Glu-Pg or Lys-Pg activation by tPA in the presence of Fn or Fg.....	119
Figure 3. Effect of Zn ²⁺ on Glu-Pg, Lys-Pg, VFK-Pn and tPA binding to immobilized Fg or Fn as determined by SPR	122
Figure 4. Effect of Zn ²⁺ on lysis of Fn clots	126
Figure 5. SDS-PAGE analysis of the effect of Zn ²⁺ on Fg degradation by Pn or trypsin	128
Figure 6. Effect of Zn ²⁺ on lysis of plasma clots	132
Supplementary Figure 1. Densitometric analysis of the effect of Zn ²⁺ on Pn-mediated cleavage of single-chain tPA.....	130

CHAPTER 5: ZINC IS LOCATED IN PLATELET DENSE GRANULES AND RELEASED UPON ACTIVATION

Figure 1. TEM and X-ray microanalysis of platelet dense granules.....	150
Figure 2. Detection of Zn ²⁺ in resting platelets.....	153

Figure 3. Detection of Zn ²⁺ and Ca ²⁺ in resting platelets.....	155
Figure 4. Zn ²⁺ release and chelation from activated and resting platelets	158
CHAPTER 6: ORIGIN AND RELEASE OF PLATELET HISTIDINE-RICH GLYCOPROTEIN	
Figure 1. HRG resides in megakaryocytes and proplatelets	179
Figure 2. HRG is located in the cytoplasm and outer surface of platelets	182
Figure 3. Little HRG is released in the absence and presence of a platelet agonist	186
Figure 4. GPS platelets contain HRG, CD61, and actin	191
Figure 5. HRG binds to GP1b α in the presence of Zn ²⁺	193
Figure 6. HRG and Zn ²⁺ increase platelet adhesion to vWF in HRG ^{-/-} mice.....	196
CHAPTER 7: GENERAL DISCUSSION AND FUTURE DIRECTIONS	
Figure 1. Transportation of Zn ²⁺ in mammalian cells.....	208
Figure 2. The structure of TRPM7 cation channel.....	210
Figure 3. TRPM7 is expressed in platelets	213
Figure 4. Bone marrow transplantation to examine platelet or plasma HRG	219
CHAPTER 9: APPENDIX	
Figure 1. HRG is rapidly cleared from the circulation of HRG ^{-/-} mice.....	239
Figure 2. Lys-Pn, Mini-Pg, and Micro-Pg bind to Ni ²⁺ in a dose-dependent fashion.....	241
Figure 3. Pg activation monitored by SDS-PAGE and fluorescence.....	243
Figure 4. Zn ²⁺ -binding to the catalytic site of Pn.....	245

LIST OF TABLES

CHAPTER 1: INTRODUCTION

Table 1. Modifiers that influence clot structure.....	31
Table 2. Zn ²⁺ -binding proteins in coagulation and anticoagulation.....	49

CHAPTER 3: ZINC PROMOTES CLOT STABILITY BY ACCELERATING CLOT FORMATION AND MODIFYING FIBRIN STRUCTURE

Table 1. The influence of Zn ²⁺ and FXIII on the mechanical properties of clots..	85
Table 2. The effect of Zn ²⁺ on clot stiffness under perturbation.....	89

CHAPTER 4: ZINC DELAYS CLOT LYSIS BY ATTENUATING PLASMINOGEN ACTIVATION AND PLASMIN-MEDIATED FIBRIN DEGRADATION

Table 1. Affinity of Zn ²⁺ for fibrinolytic proteins	112
Table 2. The effect of Zn ²⁺ on the kinetic parameters of Glu- or Lys-Pg activation by tPA in the absence and presence of Fg or Fn.....	117
Table 3. Affinities of fibrinolytic proteins for immobilized Fg and Fn determined by SPR	124
Supplementary Table 1. Effect of Zn ²⁺ on Pn-, tPA- or uPA-mediated hydrolysis of chromogenic substrates.....	114

CHAPTER 9: APPENDIX

Table 1. Affinity of Ni ²⁺ for fibrinolytic proteins.....	240
--	-----

LIST OF ABBREVIATIONS

ACD	acid citrate dextrose
ADP	adenosine diphosphate
AP	α_2 -antiplasmin
AP-1	adaptor protein-1
AP-3	adaptor protein-3
APC	activated protein C
Arg	arginine
ATP	adenosine triphosphate
BSA	bovine serum albumin
BLOC	biogenesis lysosome-related organelles complex
Ca ²⁺	calcium
CFH	complement factor H
CVD	cardiovascular disease
Da	Dalton
DNA	deoxyribonucleic acid
δ	loss tangent
DTS	dense tubular system
EDX	energy dispersive X-ray
EPCR	endothelial protein C receptor
ER	endoplasmic reticulum
F	factor
FDP	fibrin degradation products
Fg	fibrinogen
Fg ^{XIII}	FXIII-containing Fg
FI	fluorescent intensity
Fn	fibrin
FP	fibrinopeptide
G'	storage modulus
G''	loss modulus
Glu	glutamic acid
Glu-Pg	NH ₂ -terminal glutamic acid ₁ plasminogen
GP	glycoprotein
GPS	gray platelet syndrome
HBS	HEPES-buffered saline
His	histidine
HK	high molecular weight kininogen
HPS	Hermansky-Pudlack syndrome
HRG	histidine-rich glycoprotein
HRG ^{-/-}	histidine-rich glycoprotein deficient

HRR	histidine-rich region
HS	heparan sulfate
I	fluorescent intensity
IgG	Immunoglobulin
K _a	kallikrein
K _d	Binding affinity
K _s	Darcy's constant
LBS	lysine binding site
Lys	lysine
Lys-Pg	NH ₂ -terminal lysine ₇₈ plasminogen
Mg ²⁺	magnesium
MK	megakaryocyte
MMP	metalloproteinases
MNC	mononuclear cells
MVB	multivesicular body
<i>Nbeal2</i>	neurobeachin-like 2
NETS	neutrophil extracellular traps
NGP	non-granular protein
Ni ²⁺	nickel
OCS	open canalicular system
OD	optical density
PAI-1	plasminogen activator inhibitor-1
PAR	protease activated receptor
PBS	phosphate-buffered saline
PC	protein C
PFA	paraformaldehyde
PF4	platelet factor 4
Pg	plasminogen
PK	prekallikrein
Pn	plasmin
PPACK	Phe-Pro-Arg-chloromethylketone
PPP	platelet poor plasma
PRP	platelet rich plasma
PRR	proline-rich region
PS	protein S
R _{eq}	RU values at equilibrium
RLU	luminescence read
RNA	ribonucleic acid
RU	response unit
sc	single chain
SD	standard deviation

SE	standard error
SEM	scanning electron microscopy
Serpin	serine protease inhibitor
SPR	surface plasmon resonance
TAFI	thrombin activatable fibrinolysis inhibitor
TBS	Tris-buffered saline
tc	two chain
TcBS	Tricine-buffered saline
TEM	transmission electron microscopy
TF	tissue factor
TFPI	tissue factor pathway inhibitor
TM	thrombomodulin
tPA	tissue-type plasminogen activator
TPEN	N,N,N',N'-Tetrakis (2-pyridylmethyl) ethylenediamine
TRPM7	transient receptor potential melastatin-like 7
TRPM7 ^{-/-}	transient receptor potential melastatin-like 7 deficient
TxA ₂	thromboxane A ₂
uPA	urokinase-type plasminogen activator
uPAR	uPA receptor
VFK	Val-Phe-Lys-chloromethyl ketone
VLK	Val-Leu-Lys
vWF	von Willebrand factor
WT	wild-type
ZIP	Zrt-Irt-like protein
Zn ²⁺	zinc

CHAPTER 1: INTRODUCTION

1.1 Overview of Hemostasis

Hemostasis, the process that maintains the fluidity of blood, requires an intricate balance between coagulation and fibrinolysis. The natural wound healing process is initiated upon damage to the vascular endothelium. Bleeding is stopped through vasoconstriction of the blood vessels, primary hemostasis and secondary hemostasis. Primary hemostasis is initiated when platelets adhere to proteins such as collagen and von Willebrand factor (vWF) exposed on the subendothelium (Ruggeri and Mendolicchio, 2007; Sixma et al., 1995). Fibrinogen (Fg) tethers platelets together, resulting in aggregation and accumulation, thus forming a temporary plug within the injured area (Naimushin and Mazurov, 2004; Ruggeri, 2000). Damage to the endothelial cells exposes tissue factor to stimulate the coagulation cascade resulting in thrombin generation. Thrombin stimulates platelet activation, whereas the release of various stimuli, such as thromboxane A₂ (TxA₂), and adenosine diphosphate (ADP), augments activation (Li et al., 2010). With activation, the platelet secretory granule contents are released into the circulation. The concentration of proteins, small molecules, and ions, including Fg, vWF, ADP, calcium (Ca²⁺), and Zn²⁺ become elevated within the wound vicinity (Rendu and Brohard-Bohn, 2001). Components of the releasate such as ADP, positively feeds back to activate surrounding platelets, whereas Ca²⁺ and Fg propagate clot formation. Secondary hemostasis is the promotion of the

coagulation cascade to produce a fibrin (Fn) clot. Coagulation can be viewed as an ordered series of initiation and amplification processes through two main pathways that result in thrombin formation. The main driving force of coagulation begins with stimulation of the extrinsic pathway, as tissue factor (TF) is exposed on the subendothelial surface. This initiates a cascade of enzymatic activations leading to the production of the serine protease thrombin, which feeds back to activate upstream factors in the intrinsic pathway, and factor (F) V in the common pathway. Circulating Fg is converted to Fn via thrombin, and forms a thrombus to prevent bleeding at the site of injury. Once the damaged endothelium starts to repair, the third phase of hemostasis known as fibrinolysis begins. Fibrinolysis degrades the thrombus restoring blood flow, as plasminogen (Pg) is converted to its active form plasmin (Pn) by tissue-type plasminogen activator (tPA) and/or urokinase-type plasminogen activator (uPA) that is released or adhered to damaged endothelial cells (Suzuki et al., 2011). Pn binds to Fn and hydrolyzes Fn fibers, resulting in breakdown of the Fn network and eventual dissolution of the clot (Walker and Nesheim, 1999). Disruption of the hemostatic balance can lead to excessive coagulation or fibrinolysis that can result in either thrombosis or bleeding. Both outcomes may have lethal outcomes; therefore all processes in hemostasis are highly regulated.

1.2 Organelle and Granule Development in Megakaryocytes

Megakaryocytes (MK) develop in the bone marrow from hematopoietic stem cells and are ~50-100 μm in size (Figure 1A) (Thon et al., 2010; Thon and Italiano, 2010). A MK undergoes endomitosis as chromosomes duplicate, and a polyploid nucleus is synthesized (Figure 1B). Within a 5 day maturation period, deoxyribonucleic acid (DNA) amplification occurs and organelles such as mitochondria, endoplasmic reticulum (ER), Golgi-network, membranous systems, and secretory granules begin to develop (Figure 1C) (Patel et al., 2005; Thon et al., 2010; Thon and Italiano, 2010). Secretory granules that house proteins and ions are synthesized and sorted in the MK. MK synthesized granule contents are transported from the ER to the trans-Golgi network (Figure 1D). Here, proteins destined for the alpha granules are selectively sorted and encapsulated into clathrin-coated vesicles, containing adaptor protein-1 (AP-1) on their inner surface. Clathrin and AP-1 are essential for vesicle trafficking. Clathrin gives the vesicles a polyhedral lattice structure, which allows them to bud from the trans-Golgi network into the cytoplasm (Heijnen et al., 1998). The clathrin coat disassembles from the vesicles and exposes AP-1. The multivesicular bodies (MVB) arise from endosomes, and detect AP-1 (Blair and Flaumenhaft, 2009). The vesicle fuses with the MVB membrane where their contents are sorted into appropriate secretory vesicles (Italiano, Jr. and Battinelli, 2009). Contents destined for the dense granules are sorted in manner independent of clatherin.

Vesicles bud from the trans-Golgi network and form early endosomes coated with adaptor protein 3 (AP-3), which then develop into mature granules containing small molecules and ions. The remaining contents of the late endosomes that do not get packaged into the alpha or dense granules continue on to the last stage in the endocytosis pathway, which is the development of lysosomes. Lysosomes contain enzymes such as cathepsin, elastase and collagenase that degrade proteins and organelles that are not required for platelet formation.

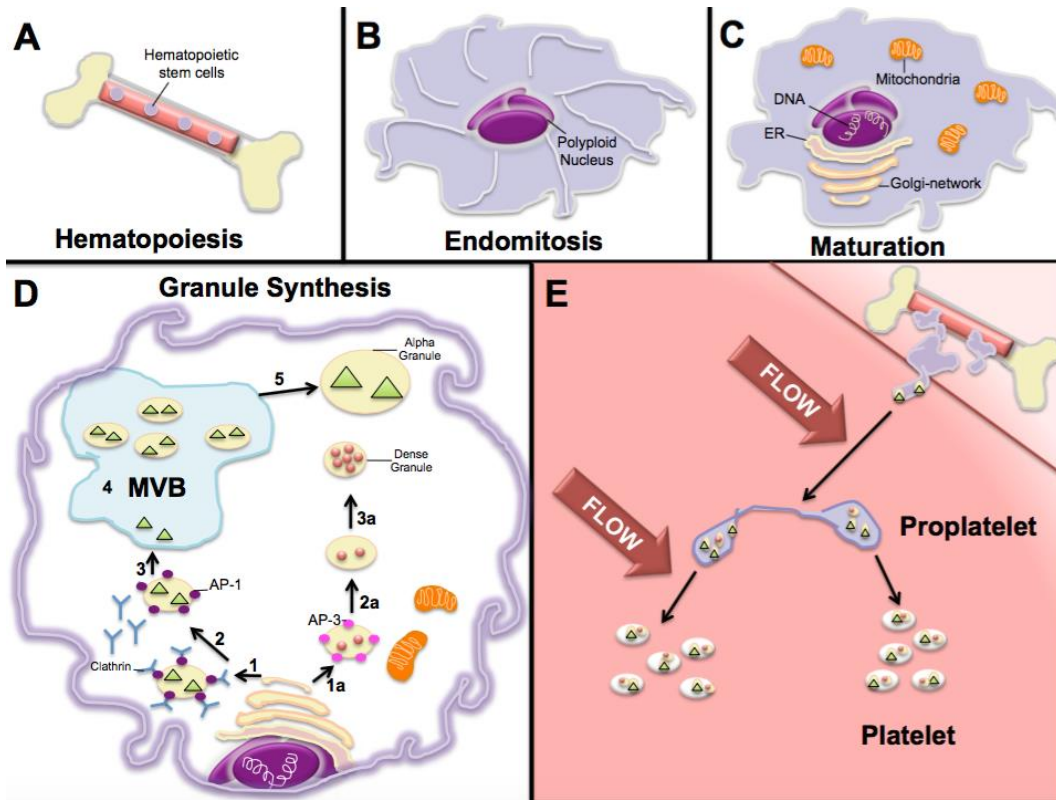


Figure 1. Platelet biogenesis and secretory granule formation

Platelets originate from membrane extensions from a MK. **(A)** MK develop in the bone marrow, and originate from hematopoietic stem cells. **(B)** The MK undergoes endomitosis, and develops a polyploid nucleus. Changes in the MK cytoskeleton generate pseudopodia-like structures on the outer membrane. **(C)** DNA amplification in the polyploid nucleus enables the development of cellular machinery. **(D)** Subsequently, synthesis of platelet granule contents begins in the ER of the MK. **(1)** Select contents are transported from the ER to the trans-Golgi network and encapsulated with a clathrin-coat containing AP-1. **(2)** The vesicle migrates towards the MVB and clathrin disassembles from the vesicle, exposing AP-1 to enable detection by the MVB. **(3)** The vesicle fuses with the MVB membrane, and **(4)** the alpha granule vesicle contents containing large proteins (*green triangles*) are sorted and compartmentalized into secretory granules. **(1a)** Small molecules and ions from the Golg-network bud to form a vesicle coated with AP-3. **(2a)** Contents are sorted forming an intermediate endosome, and **(3a)** which matures to develop a dense granule that contains small, charged molecules (*red dots*). **(E)** After maturation, the MK migrates into the sinusoidal vessels, moving towards circulatory blood vessels. Pseudopodia-like membrane extensions that enter the circulation generate proplatelets and fragment into platelets. Adapted from Thon and Italiano, 2009; and Blair and Flaumenhaft, 2010.

1.3 Platelet Development from Megakaryocytes

MK mature into proplatelets, and subsequently fragment into platelets (Figure 1E). Morphological changes in the cytoskeleton of the MK reflect its state of maturity. Microtubules in the cytoplasm elongate and migrate to the outer perimeter creating pseudopodia-like extensions (Machlus and Italiano, Jr., 2013; Patel et al., 2005). Organelles and granules synthesized in the MK move towards the outer periphery pseudopodia-like extensions. As the MK begins to enter the circulation, the pseudopodia-like extensions fragment due to shear flow changes (Figure 1E) (Italiano, Jr. et al., 2008; Machlus and Italiano, Jr., 2013). Here, fragmentation of MK pseudopodia-like extensions generate ~10-20 anuclear, dumbbell-shaped proplatelets, which are ~2-3 μm in diameter (Patel et al., 2005). Within the proplatelets, the granules continue to be transported to the lateral buds across a connecting microtubule track (Italiano, Jr. et al., 2008; Patel et al., 2005). The proplatelet buds further fragment to form platelets (Figure 1E).

In the quiescent state, circulating platelets are discoid in shape. Platelets contain two unique membrane systems, the dense tubular system (DTS) and the open canalicular systems (OCS) (Figure 2A) (Machlus and Italiano, Jr., 2013; Nispen tot et al., 2010; Rendu and Brohard-Bohn, 2001). The DTS is a closed membrane system that is the primary storage reservoir of intracellular Ca^{2+} (Machlus and Italiano, Jr., 2013; Nispen tot et al., 2010). The OCS is a continuous channel connected to the outer membrane surface, which allows the secretory

granule contents to exit the platelet (Nispen tot et al., 2010). As the MK reaches maturity, it enters the sinusoidal blood vessels of the bone marrow and migrates towards circulatory vessels (Machlus and Italiano, Jr., 2013).

Platelets contain two types of secretory organelles, known as alpha and dense granules, which together store over 300 different types of proteins and small molecules (Figure 2A) (Whiteheart, 2011). Granule contents are synthesized in the MK or taken up from plasma by the platelet OCS (Koseoglu and Flaumenhaft, 2013; Whiteheart, 2011). The alpha granules are the largest in size at ~200-500 nm, and are the most abundant constituting 50-80 per platelet (Blair and Flaumenhaft, 2009; Kahr et al., 2013; Wijten et al., 2013). The alpha granules contain proteins that participate in both coagulation and anticoagulation. More than 120 proteins have been detected in platelets, including high concentrations of vWF, platelet factor 4 (PF4), FV, FXIII, and plasminogen activator inhibitor-1 (PAI-1) (Mitchell et al., 2014; Wijten et al., 2013). These proteins are synthesized in the MK and released with activation (Rendu and Brohard-Bohn, 2001). In contrast, coagulation proteins such as Fg, HRG, high molecular weight kininogen (HK), α_2 -antiplasmin (AP), and α_2 -macroglobulin, are not synthesized by MK. Instead, these proteins are taken up from plasma (Handagama et al., 1993; Rendu and Brohard-Bohn, 2001). Compared with alpha granules, the dense granules are less abundant by ~10-fold, numbering 3-8 per platelet (Blair and Flaumenhaft, 2009; Heijnen and van der Sluijs, 2015). Dense granules are rich in electrons and

nucleotides, and contain an abundance of ions and signaling molecules such as ADP, adenosine triphosphate (ATP), serotonin, histamine, Ca^{2+} , magnesium (Mg^{2+}), pyrophosphate, and polyphosphate (Blair and Flaumenhaft, 2009; Heijnen and van der Sluijs, 2015). The dense granules are referred to as being electron-rich because they store ~70% of the total platelet content of Ca^{2+} , Mg^{2+} , and polyphosphates (Rendu and Brohard-Bohn, 2001). In addition, transmembrane proteins such as CD63, glycoprotein (GP) 1b, and $\alpha_2\beta_3$ are stored in the dense granules, and translocate to the membrane with activation (Israels et al., 1992). Finally, platelets contain 1-2 lysosomes that participate in macromolecule degradation because lysosomes store acid hydrolases that digest proteins, carbohydrates and lipids (Figure 2A) (Heijnen and van der Sluijs, 2015; Machlus and Italiano, Jr., 2013). However, some platelets lack lysosomes, indicating that these are not essential for platelet function. Platelet activation triggers the release of secretory granule contents into the circulation.

Normal circulating platelet counts in healthy individuals range from 150-400 x 10^9 L^{-1} (Daly, 2011). Patients with platelet counts below this range are considered thrombocytopenic, which may result in a bleeding diathesis (Thon and Italiano, 2010). Unless activation is induced, the lifespan of platelets in the circulation is 7-10 days (Patel et al., 2005). Platelets play an intricate role in coagulation to provide a surface on which clotting factors assemble to form

activation complexes that promote thrombin generation. Platelets further adhere and aggregate to form a temporary plug at the site of injury.

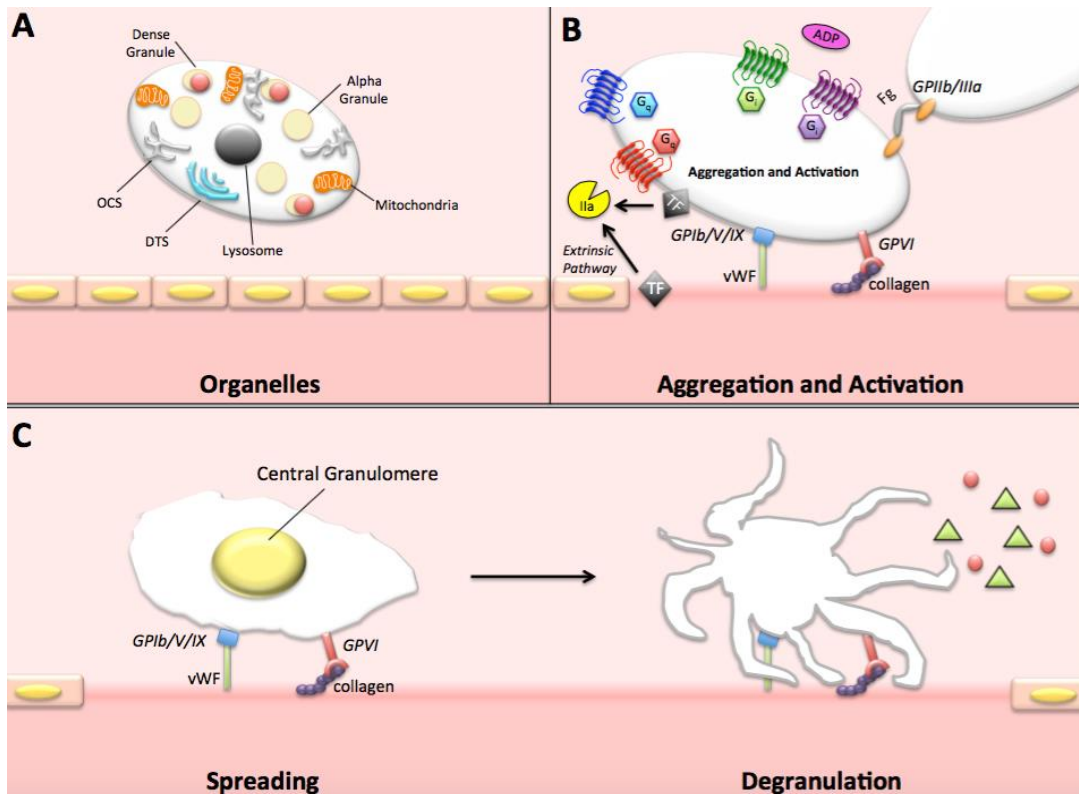


Figure 2. Platelet structure and function

(A) Platelets contain various organelles such as mitochondria, the OCS and DTS, two types of secretory granules, and variably a lysosome. (B) GP and transmembrane receptors located on the platelet surface participate in aggregation and activation. Platelets adhere to collagen and vWF exposed on the damaged subendothelium. Platelets aggregate as circulating Fg binds to GPIIb/IIIa surface receptors on neighbouring platelets. Endothelial and platelet surface TF both stimulate the extrinsic pathway to generate thrombin. Thrombin is a potent activator of platelets as it cleaves protease activator receptor (PAR)-1 (*red*) and (PAR-4) (*blue*), inducing intracellular G_q-protein signaling to initiate platelet activation. ADP released from endothelial cells or the dense granules of platelets binds to P₂Y₁ (*green*) and P₂Y₁₂ (*purple*) receptors, further augmenting intracellular G_i-protein signaling. (C) Stimulation of platelet activation causes the outer membrane to spread, and secretory granules to migrate to the center of the platelet. The central granulomere releases secretory contents by fusing with the OCS. Proteins (*triangle*), small molecules and ions (*circles*) are secreted into the circulation. The platelet cytoskeleton is modified with content release, resulting in long spicule-like extensions that aid in aggregation. Adapted from Offermans, 2006.

1.4 Platelet Adhesion, Aggregation, and Activation

Platelets serve as an initial plug at the site of injury to prevent bleeding under high shear arterial blood flow. Platelets circulate in a quiescent state unless stimulated with an agonist. At the site of vascular injury, platelets adhere to the damaged endothelium and are activated through a series of G-protein coupled signaling mechanisms (Figure 2B). This results in the release of proteins, chemical messengers, and ions that stimulate adjacent cells and activate coagulation.

Damage to endothelial cells exposes adhesive proteins vWF and collagen, which bind to GPIb/V/IX and GPVI on the platelet surface (Offermanns, 2006; Savage et al., 2001). Collagen binding induces outside-in signaling. This triggers a conformational change of the abundant transmembrane receptors GPIIb/IIIa and GPIa/IIa. GP receptors are important for activation as blocking IIb/IIIa inhibits aggregation in response to all agonists. Both receptors bind extracellular Fg to tether neighbouring platelets together to augment platelet aggregation (Offermanns, 2006; Whiss and Andersson, 2002). TF exposed on the subendothelium and platelet surface, initiates the extrinsic pathway of coagulation resulting in thrombin generation. Thrombin cleaves PAR-1 and PAR-4 on the platelet surface, triggering intracellular G_q -protein signaling to release initially TxA_2 (Offermanns, 2006). TxA_2 enhances platelet activation by binding to the TxA_2 receptor and stimulating intracellular G_{13} -protein signaling (Offermanns,

2006). In addition, small amounts of ADP are released from damaged endothelial cells to augment platelet activation. ADP binds to P_2Y_1 and P_2Y_{12} surface receptors, and triggers intracellular G_q - and G_i -protein signaling (Figure 2). P_2Y_1 stimulation by ADP enhances phospholipase C activity, which elevates intracellular Ca^{2+} levels (Offermanns, 2006). Furthermore, ADP release from the dense granules amplifies platelet aggregation and degranulation.

The main role of all G-protein signaling cascades is to initiate platelet granule secretion. This is critical as proteins and ions released augment coagulation to ensure proper wound healing. Elevation in intracellular platelet Ca^{2+} induces actin-myosin based contraction, causing a conformational change from the discoid shape to a rigid, active state (Figure 2C) (Heijnen and van der Sluijs, 2015). This causes granules to cluster at the center of the platelet as a circumferential ring of microtubules surrounds the granules, forming the central granulomere (Figure 2C) (Fitch-Tewfik and Flaumenhaft, 2013; Flaumenhaft, 2003; Flaumenhaft et al., 2005). The central granulomere contents fuse with the OCS and rapidly exit the platelet (Figure 2C) (Fitch-Tewfik and Flaumenhaft, 2013; Flaumenhaft, 2003; Flaumenhaft et al., 2005). However, essential cell surface components that reside in the dense granules, such as GP1b, are redistributed to the platelet surface, and not released into the circulation (Han et al., 2003).

1.5 Platelet Granule Deficiencies

Release of secretory granules from activated platelets is critical for augmenting platelet activation and aggregation. Patients that lack or have defective secretory granules have evidence of impaired aggregation, but normal coagulation, thus exhibiting minor to moderate bleeding problems (Rao, 2013). In contrast, the absence of platelet lysosomes is not problematic (Rendu and Brohard-Bohn, 2001). The first alpha granule deficiency reported is referred to as gray platelet syndrome (GPS) (Rao, 2013). GPS is a rare congenital or acquired disorder that results from a mutation in the neurobeachin-like 2 (*Nbeal2*) gene, located on chromosome 3p21 (Kahr et al., 2013). *Nbeal2* is responsible for sorting and packaging the granule contents in the MK (Kahr et al., 2013). A mutation in this gene results in alpha granules devoid of normal contents, thus displaying large empty vacuoles (Rendu and Brohard-Bohn, 2001). Granular contents do not get packaged in the MK, thus very little cargo makes it to the platelet (Rendu and Brohard-Bohn, 2001). This is because the contents continue through MVB development to the final lysosome stage, where contents become degraded. However, the empty vacuoles present in GPS platelets do contain P-selectin on the membrane surface, which allows for their identification (Rendu and Brohard-Bohn, 2001). GPS platelets still contain dense granules; therefore the platelets are not completely dysfunctional, because ADP and ions can be released upon activation.

Dense granule deficiency is characterized by a reduction in the number of dense granules in platelets (Rao, 2013). The subsequent reduction in the release of agonists such as ADP and Ca^{2+} impairs platelet aggregation. The most common dense granule deficiency is an inherited disorder known as Hermansky-Pudlack syndrome (HPS) (Rao, 2013; Rendu and Brohard-Bohn, 2001). HPS patient platelets lack dense granules, along with their small molecule cargo. However, because alpha granular contents are unaffected, platelet activation is not severely impaired. A defective gene on chromosome 10q2 allows HPS to exist as 9 different subtypes; HPS-1 is the most common form and is caused by a mutation in the protein biogenesis lysosome-related organelles complex 3 (BLOC-3) (Rao, 2013). HPS patients are characterized by hypopigmentation, resulting in albinism (Rao, 2013). Both alpha and dense granule deficiencies are not lethal; however platelet transfusions may be necessary, as the majority of these patients are thrombocytopenic.

1.6 The Coagulation Cascade

The coagulation cascade is divided into three pathways, known as the extrinsic, intrinsic, and common pathways (Figure 3). Here, a series of reactions convert zymogens to active serine proteases, which activate the zymogen of the subsequent step. TF is the primary driver of the coagulation cascade because it initiates the extrinsic pathway when it becomes exposed on the damaged vessel wall (Mackman et al., 2007). The intrinsic pathway, also termed the contact

pathway, is a less prominent pathway at stimulating coagulation, as its initiating factors must come in contact with negatively charged surfaces, such as DNA or ribonucleic acid (RNA) (Griffin, 1978). Both the extrinsic and intrinsic pathways converge at the common pathway, where thrombin is formed. Thrombin generates F_n, which serves as the as the main scaffolding of a clot, preventing bleeding until the endothelium of the injured area is restored back to its original state.

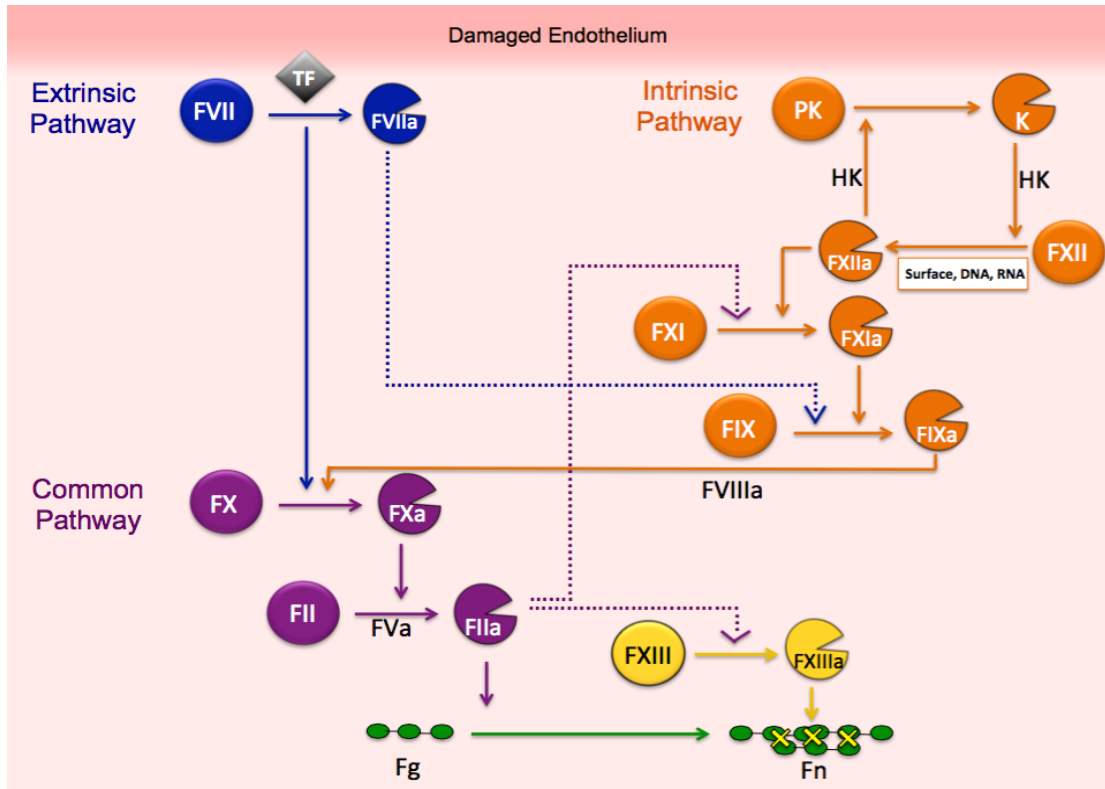


Figure 3. The blood coagulation cascade

Coagulation involves the extrinsic (*blue*) and intrinsic (*orange*) pathways that merge at the common pathway (*purple*) to generate thrombin. The extrinsic pathway begins with exposure of TF on the damaged endothelial surface. The intrinsic pathway amplifies coagulation when factors are exposed to polyanionic surfaces, such as DNA or RNA. Both pathways trigger a sequence of enzymatic reactions resulting in the formation of thrombin. The main substrate of thrombin is Fg (*green*), which forms Fn monomers that polymerize into a clot. In addition, thrombin activates FXIII (*yellow*), which cross-links the fibers to stabilize the clot. Zymogens (*circles*) are converted to active forms (*semi-circle*), indicated by arrows. Dotted line arrows represent factors that positively feedback to stimulate activation of zymogens to accelerate coagulation. Image was adapted from Gross et al., 2011.

The extrinsic pathway begins when endothelial cells, vascular smooth muscle cells, or adventitial fibroblasts expose TF on their surface (Smith et al., 2015). In addition, TF circulates in the blood stream on the surface of microparticles or platelets (Muller et al., 2003). TF initiates coagulation when it comes in contact with circulating FVII, the inactive zymogen of active FVIIa. However, FVII is also capable of auto-activation depending on the surface density of phospholipid TF (Morrissey et al., 1993). The TF/FVIIa complex has two main substrates, FIX and FX. Cleavage of these zymogens generates the serine proteases FIXa and FXa, respectively. The generation of FXa feeds into the common pathway, stimulating thrombin formation.

The common pathway is composed of FXa bound to its cofactor FVa, a complex referred to as the prothrombinase complex, which assembles on a phospholipid membrane surface in the presence of Ca^{2+} (Esmon et al., 1974). This enzyme complex converts the 72 kDa zymogen prothrombin (FII) to its serine protease form, thrombin (Esmon et al., 1974). Thrombin has high specificity for Fg, as it is the only coagulation factor that is able to convert Fg to Fn. Structurally, thrombin is a 37 kDa protease containing a light (A) and heavy (B) chain linked by a disulfide bridge (Esmon et al., 1974). The active site is flanked by two exosites responsible for determining its substrate specificity (Adams and Huntington, 2006). Exosite 1 is of particular importance as it recognizes Fg and PARs on platelets (Krishnaswamy, 2005). Thrombin also activates upstream

factors, such as FV, FVIII, and FXI, to amplify coagulation. FVIII and FIX are important in propagating coagulation, because their absence leads to hemophilia, and bleeding abnormalities. Clot stabilization occurs as thrombin activates FXIII to generate FXIIIa that covalently cross-links Fn (Kurniawan et al., 2014; Mitchell et al., 2014). With stable clot formation, bleeding comes to a halt.

Activation of the contact pathway begins through a “contact phase”. Upon vessel injury, circulating prekallikrein (PK), HK, FXI, and FXII are exposed to polyanionic surfaces, such as DNA or RNA (Griffin, 1978). FXII is capable of autoactivation to FXIIa when exposed to negatively charged surfaces. The release of negatively charged polyphosphate also activates FXII, and accelerates the activation of FV. Kallikrein (Ka), with its cofactor HK, initiates the conversion of FXII to its active form FXIIa, and stimulates a downstream cascade of sequential activations: FXI to FXIa, FIX to FIXa, followed by FX to FXa. Formation of the intrinsic prothrombinase complex requires FXa and its cofactor FVa, Ca^{2+} , and a phospholipid surface to assemble on. Furthermore, FXa feeds into the common pathway, and amplifies thrombin generation.

1.7 Anticoagulation Pathways

Coagulation must be highly regulated to prevent thrombus formation when or where it is not needed. This is carried out by natural anticoagulants, including the protein C system, antithrombin and tissue factor pathway inhibitor (TFPI).

The conversion of protein C (PC) to activated PC (APC) requires the binding of thrombin to its cofactor thrombomodulin (TM) which is constitutively expressed on the endothelial cell surface (Esmon, 1989). The endothelial protein C receptor (EPCR), also associates with TM (Esmon, 1989; Stearns-Kurosawa et al., 1996). The formation of PC/EPCR and thrombin/TM complexes initiates PC cleavage, generating its active form APC that binds to its cofactor protein S (PS). APC inactivates critical coagulation cofactors FVIIIa and FVa, down-regulating the intrinsic and common pathways, respectively (Heeb et al., 1993; Mohan Rao et al., 2014).

Antithrombin regulates thrombin activity, and is enhanced by heparin binding. Heparin is widely used as an anticoagulant for medicinal purposes but does not circulate freely in plasma (Weitz, 2003). However, its counterpart heparan sulfate (HS) also binds antithrombin, and acts as a natural anticoagulant due to its high distribution on the endothelial cell surface (Sasisekharan and Venkataraman, 2000). HS catalyzes the inhibition of thrombin, FIXa, FXa, FVII, FXIIa inhibition by antithrombin to augment anticoagulation.

The bulk (85%) of TFPI associates to the endothelial surface, whereas lower amounts (15%) circulate in plasma, in which both augment anticoagulation (Sandset et al., 1988). TFPI inhibits the TF/FVIIa complex in a FXa-dependent fashion (Ho et al., 1997). A deficiency in TFPI can lead to the development of thrombosis.

1.8 Fibrinogen and Fibrin

Fg is synthesized in the liver and circulates at $\sim 9 \mu\text{M}$ in plasma (Tennent et al., 2007). Fg is a 340 kDa glycoprotein that is symmetrical and composed of two pairs of three disulfide-linked polypeptide chains termed $A\alpha$, $B\beta$ and γ (Figure 4A) (Tennent et al., 2007; Weisel and Litvinov, 2013; Zavyalova et al., 2011). Folding of the chains creates the central E- and two lateral D-globular domains. The E-domain is formed by the convergence of the NH_2 -termini of all six chains. The D-domain is made up of the COOH -termini of the $B\beta$ - and γ -chains, with an internal segment of the $A\alpha$ -chain. The COOH -termini of the $A\alpha$ -chains exit the D-domains to form the αC -domain that resides near the E-domain (Collet et al., 2005; Gorkun et al., 1994; Weisel and Litvinov, 2013). In the circulation, the conversion of Fg to Fn is initiated by thrombin.

Fn formation begins as thrombin releases fibrinopeptides (FP) from two chains on Fg (Figure 4A). Thrombin initially releases FPA from the $A\alpha$ -chains, exposing new amino terminal Gly-Pro-Arg-Val motifs, termed knob “A” (Weisel and Litvinov, 2013). Knob “A” binds to complementary, pre-existing holes (hole “a”) located on the γ -nodules of D-domains on neighbouring Fn monomers (Figure 4B) (Weisel and Litvinov, 2013; Zavyalova et al., 2011). This forms an “A:a” interaction, which is the main driving force behind Fn monomer polymerization. The half-staggered double-stranded polymers are referred to as protofibrils (Figure 4B) (Weisel and Litvinov, 2013). The “A:a” interaction

between the Fn monomers is strong, however it is not a covalent linkage (Weisel and Litvinov, 2013). At a slower rate, thrombin releases FPB from the B β -chains, exposing a nascent Gly-His-Arg-Pro motif, termed knob “B” on the β -chain (Weisel and Litvinov, 2013). Knob “B” binds to complementary holes “b” on the β -nodule on the lateral D-domains (Weisel and Litvinov, 2013). The “B:b” interaction is not essential for polymerization, but enhances lateral association of protofibrils, increasing fiber diameter (Weisel and Litvinov, 2013). FPA release is sufficient to form a Fn clot, as observed in the presence of the serine protease batroxobin, a snake venom that clots Fg by only releasing FPA from the A α -chain (You et al., 2004). However, the fibers formed with batroxobin are thinner than those formed with thrombin because of the absence of the “B:b” interactions that promote lateral fiber association. The α C-domain also participates in the enhancement of lateral aggregation of fibers by self-association, involving β -hairpin swapping of NH₂- and COOH-termini with the α C-connector region (Tsurupa et al., 2012; Weisel and Litvinov, 2013). Confirming this concept, clots generated with Fg lacking the α C-domain exhibit thinner Fn fibers than those formed from intact Fg (Collet et al., 2005; Gorkun et al., 1994). Overall, polymerization of Fn monomers rapidly generates a network of fibers that provides scaffolding at the injured area and prevents bleeding.

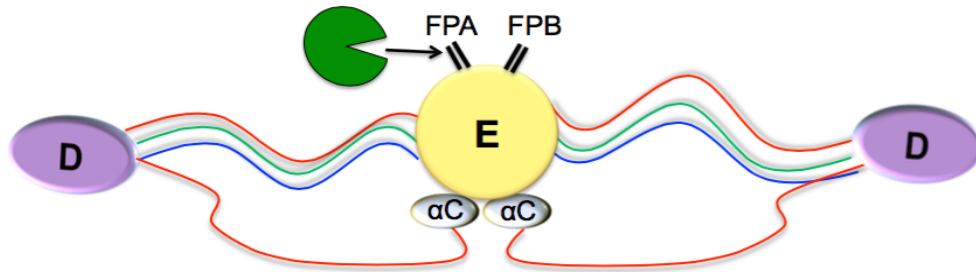
Fiber thickness influences the distribution and strength of fibers within a clot. The rate of FP release determines fiber thickness. A reduction in thrombin

concentration reduces the rate of FP cleavage, and increases the number of Fn monomers that associate laterally. Thus, a slower rate of clot formation results in thicker fibers. Conversely, increasing the concentration of thrombin limits lateral association and promotes longitudinal growth; as FP cleavage and polymerization occur at a rate faster than lateral aggregation (Ryan et al., 1999). Thin fibers tend to be more densely compacted within a clot compared with thick fibers, which are loosely woven. Regardless of fiber thickness, fiber strength is increased by covalent crosslinking by FXIIIa.

The concentration of FXIII in plasma is ~70 nM, and 90% is non-covalently bound to Fg (Aleman et al., 2014). Structurally, FXIII is a 312 kDa tetramer zymogen, containing two pairs of subunits (FXIII-A and FXIII-B) (Mitchell et al., 2014). The FXIII-A subunit contains the catalytic domain, whereas the FXIII-B subunit assists in regulation by protecting the active site, preventing activation when it is not needed (Mitchell et al., 2014). FXIII is converted to its active form FXIIIa when thrombin cleaves the NH₂-terminal activation peptide on the FXIII-A subunit at Arg₃₆-Gly₃₇ (Figure 4B) (Aleman et al., 2014; Lorand, 2001). Ca²⁺ binding induces a conformational change and causes the subunits to dissociate, which exposes the active site residue Cys₃₁₄ (Aleman et al., 2014). FXIIIa is a transglutaminase that stabilizes fibers by forming covalent cross-links between the proximal α - and γ -chains in adjacent Fn molecules at glutamic acid (Glu)- and lysine (Lys)-residues (Figure 4B) (Aleman

et al., 2014; Kurniawan et al., 2014). FXIIIa influences fiber formation as it links the α - α chains, allowing protofibrils to stack and form thicker fibers (Fraser et al., 2011; Weisel and Litvinov, 2013). The links generated between the γ - γ -chains promote longitudinal elongation of the fibers (Fraser et al., 2011; Weisel and Litvinov, 2013). Additional links between the α - γ -chains can form, but are not abundant in the clot (Helms et al., 2012; Weisel and Litvinov, 2013). The α - α -chain linkage is the main driver of clot rigidity by increasing clot stiffness (Helms et al., 2012; Weisel and Litvinov, 2013). In the presence of FXIII, clot stiffness is five times greater than in its absence (Ryan et al., 1999). Because FXIII compacts the Fn network, pore size is reduced. Clots composed of thick fibers tend to be less stiff, more porous, and susceptible to deformation (Weisel, 2007). Clots made up of thin densely packed fibers are more stiff and brittle, and less porous, which increases their susceptibility to rupture (Weisel, 2007). FXIIIa also impairs clot degradation by crosslinking the Pn inhibitor AP to the α -chain of Fn (Fraser et al., 2011).

A



B

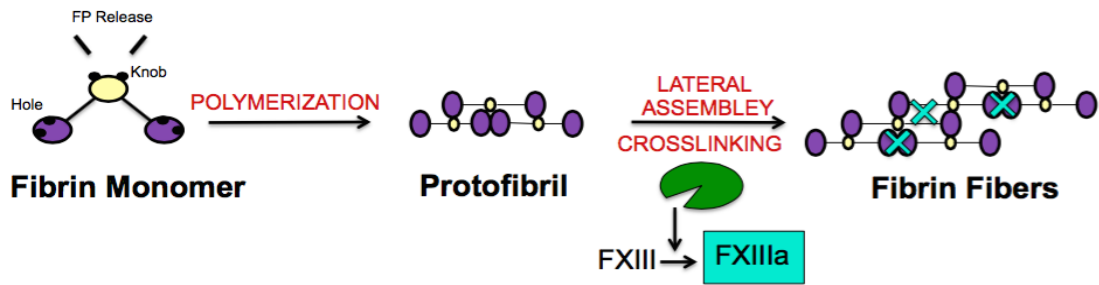


Figure 4. The structure of fibrinogen and the polymerization of fibrin

(A) Fg has three pairs of chains that form the central E-domain (*yellow*), which is flanked by two lateral D-domains (*purple*). The A α - (*red*), B β - (*green*), and γ - (*blue*) chains, are represented by lines. Remaining segments of the A α -chains connect the lateral D-domains to the central α C-domain (*grey*). Thrombin (*green semi-circle*) releases FPA and FPB from the α - and β -chains in the central E-domain. **(B)** FP release results in Fn monomers. Knobs on the central E-domain bind to complementary holes located on D-domains of a neighbouring monomer. This induces polymerization to generate a two-stranded protofibril, which associates laterally with other protofibrils to form Fn fibers. FXIII is converted to its active form FXIIIa (*blue rectangle*) by thrombin. FXIIIa covalently cross-links (*blue X*) Fn to stabilize the clot. Adapted from Weisel and Litvinov, 2013.

1.9 Clot Structure

Clot structure is an important determinant of clot stability and function. Stable clots are highly favourable in the vasculature as they are less likely to embolize and block downstream vessels (Weisel and Litvinov, 2013). Clot stability is defined as the ability of a Fn network to withstand applied mechanical stress (Weisel, 2007). From a rheology perspective, Fn is a unique material because it retains its mechanical properties when perturbed by a wide range of forces (Weisel, 2004). In the arterial and venous vascular systems, clots are exposed to high and low shear blood forces, respectively. Because clots are formed in both systems, Fn must withstand substantial changes in blood flow; therefore, its mechanical properties must be diverse.

The mechanical properties of a clot are influenced by its structural composition. Clots composed of thick fibers tend to be less stiff, more porous, and more susceptible to deformation (Weisel, 2007). Some deformation is beneficial as clots can retract back to their original form without breaking off and embolizing. Rigid clots made up of thin, densely packed fibers, tend to be less porous, and more stiff and brittle, thereby increasing their potential to rupture (Weisel, 2007). Clots that are highly permeable favour lysis because tPA and Pn can readily diffuse into the interstices of the Fn network (Collet et al., 2000). Overall, unstable clots can have negative consequences, the severity of which depends on the location at which a clot ruptures. Thus, clots in the deep vein of

the leg can embolize to the lungs, clots in the heart can travel to the brain, and clots in coronary arteries can embolize downstream to block small vessels.

Various modulators of clot structure are abundant at sites of injury (Table 1). Thrombin is one such modulator. Thus, the thrombin concentration is a major determinant of clot structure because it modulates the rate of FP release and FXIII activation. High levels of thrombin reduce clot times and stiffness, whereas high concentrations of Fg have an opposing effect. Elevated thrombin and Fg concentrations are found in patients with thrombosis (Wolberg et al., 2003). An elevation of Fg results in thin fiber formation, yet clot times are prolonged (Ryan et al., 1999). The increase in the substrate to enzyme ratio during clot formation may be the reason for delayed clot times (Ryan et al., 1999).

MODIFIER	FIBERS	FIBER DISTRIBUTION	POROSITY	LYSIS
ENZYME				
↑ [Thrombin]	Thin	Densely Packed	Decrease	Resistant
↓ [Thrombin]	Thick	Loosely Packed	Increase	Favoured
SUBSTRATE				
↑ [Fg]	Thin	Densely Packed	Increases	Resistant
↑ Fg [γA/γ']	Thin	Loosely Packed	Increase	Resistant
Fg Dusart	Thin	Densely Packed	Decrease	Resistant
NUCLEIC ACIDS				
DNA & Histones	Thick	N/A	Decrease	Resistant
IONS				
↑ Cations	Thick	Loosely Packed	Increase	Favoured
↑ Anions	Thin	Densely Packed	Decrease	Resistant
THROMBOSIS PROPHYLAXIS				
Heparin	N/A	N/A	Increased	Favoured
NOAC	Thick	Loosely Packed	Increased	Favoured
Aspirin	Thick	Loosely Packed	Increased	Favoured
Statin	Thick	N/A	Increased	Favoured

Table 1. Modifiers that influence clot structure

Clot formation can be affected *in vitro* and *in vivo* by various stimuli. The speed of the reaction, genetic mutations in Fg, the presence of proteins, nucleic acids, and ions, and therapeutic agents such as heparin, new oral anticoagulants (NOACS), aspirin, and statins, contribute to modifications in clot structure. Fiber diameter and distribution influence the rate of clot degradation. N/A represents data that are not available in the literature. This table was developed using data collected from Ryan et al. 1999; Collet et al. 1996; Di Stasio et al. 1998; Longstaff et al. 2013; and Bridge et al. 2014.

In addition to the rate of clot formation, structural alterations in Fg can affect clot morphology. A splice variant in the Fg γ -chain mRNA yields two Fg isoforms known as γ^A/γ^A and a γ^A/γ' (Allan et al., 2012; Walton et al., 2014). Only 8-15% circulates as the γ^A/γ' form (Allan et al., 2012; Walton et al., 2014). Previous reports show that the γ' -chain modifies clot structure (Allan et al., 2012). Clots generated with γ^A/γ' Fg exhibit thin fibers, reduced stiffness, and increased porosity (Allan et al., 2012). Variants with altered α -chains, such as Fg Dusart and Fg Marburg, exhibit abnormal Fn monomer polymerization, resulting in reduced fiber thickness (Collet et al., 2000; Koopman et al., 1992). A modification in the structure of Fg such as the removal of a domain and/or alteration of its α -chain or γ -chain can alter clot structure.

Ionic conditions also modify clot structure. The divalent cation Ca^{2+} circulates at ~ 2 mM in plasma (Marx, 1988a). Fg has high and low affinity binding sites for Ca^{2+} . Binding of Ca^{2+} to Fg accelerates clot times and modifies clot structure (Marx, 1988b; Marx, 1988c). Clots formed in the presence of 20 mM Ca^{2+} exhibit increased fiber diameter, even though the rate of clot formation is accelerated (Ryan et al., 1999). Therefore, the relationship between the rate of FP release and fiber thickness is not universal. Thus, Ca^{2+} modifies fiber thickness via an alternative mechanism. The mechanism through which Ca^{2+} alters clot structure remains controversial. Initial studies suggested that rapid release of FPA exposes a Ca^{2+} sensitive binding site, which enhances lateral association of Fn

fibers (Marx, 1988b). However, it is known that lateral association of fibers is mainly mediated through FPB release. Others have suggested that release of FPB by thrombin exposes a polymerization site that is sensitive to Ca^{2+} (Ryan et al., 1999). This site is thought to enhance Fn monomer association and promote lateral development of protofibrils (Marx et al., 1987; Marx, 1988b; Ryan et al., 1999). The binding of Ca^{2+} to sialic acid residues on the carbohydrate side chains of Fg was also hypothesized to decrease its charge and enhance lateral Fn association (Dang et al., 1989). These data suggest that Ca^{2+} modulates fiber thickness through various interactions. Other divalent metal ions such as nickel (Ni^{2+}) and Zn^{2+} also bind Fg independently of Ca^{2+} , and accelerate polymerization of Fn monomers (Kanaide et al., 1982; Marx, 1988a; Marx, 1988b). Divalent cations may have independent binding sites on Fg. However all appear to accelerate clot formation, but generate thick Fn fibers. Chlorine (Cl^-) has an opposing effect on clot structure compared with divalent cations. Studies reveal that at a Cl^- concentration of 200 mM, lateral aggregation of Fn monomers is reduced, and thin fibers are generated (Di Stasio et al., 1998). With both Ca^{2+} and Cl^- , the concentrations used to modify clot structure *in vitro* exceed the physiological concentrations (Di Stasio et al., 1998; Ryan et al., 1999). Therefore, both cations and anions can be used to manipulate clot structure, to allow for a better understanding of clot composition.

Recently, studies have demonstrated the impact of nucleic acids on clot structure. At the site of injury, neutrophils release DNA in the form of neutrophil extracellular traps (NETs), which are distributed throughout a developing thrombus (Longstaff et al., 2013; Varju et al., 2015). Studies indicate that DNA and histones promote thrombus formation by forming a complex with Fn (Longstaff et al., 2013). This results in an increase in fiber thickness, and enhanced clot stability, as clots formed with DNA and histones resist rupture (Longstaff et al., 2013; Varju et al., 2015). Therefore, the presence of inflammatory stimuli, DNA and histones is another *in situ* modifier of clot structure.

Modifying clot morphology and porosity can predict the rate of fibrinolysis. Therapeutics such as aspirin, statins, heparin, and NOACs all modulate clot structure by increasing clot porosity which favours lysis (Kotze et al., 2014). These studies suggest that various conditions within the vasculature can affect clot composition, and may alter the fate of unstable thrombi.

1.10 Fibrinolysis

Clot dissolution is known as fibrinolysis (Cesarman-Maus and Hajjar, 2005). Clot lysis is essential to prevent thrombus accumulation, which can occlude the vessel and obstruct blood flow. The fibrinolysis pathway begins when plasminogen activators convert Pg to its activated form Pn, which degrades the Fn network to restore blood flow (Figure 5) (Cesarman-Maus and Hajjar, 2005).

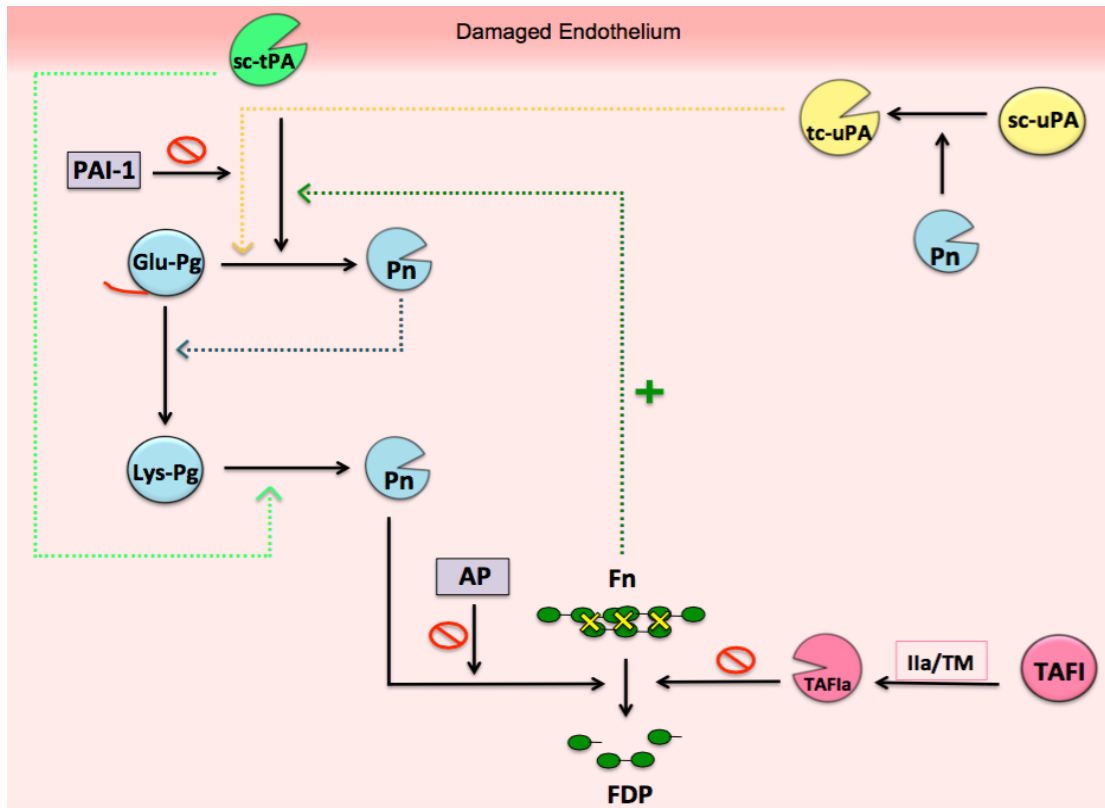


Figure 5. The fibrinolytic system

Damaged endothelial cells release tPA, which cleaves the activation sequence (Arg₅₆₁-Val₅₆₂) on Pg to generate Pn. Pn can positively feedback on Pg activation by cleaving Pg at Lys₇₇-Lys₇₈, removing the NH₂-terminus (*red line*) from Glu-Pg. This induces a conformational change in Glu-Pg from a closed form to its open more readily activated form, Lys-Pg. In addition, Pn converts single-chain (sc)-uPA to its active form two-chain (tc)-uPA, which also augments Pg activation. Fn generated from the coagulation cascade positively (+) feeds back to enhance Pg activation by binding both tPA and Pg. The main function of Pn is to hydrolyze Fn into soluble Fn degradation products (FDP). Fibrinolysis is regulated by serpins AP and PAI-1, which down regulate (⊗) Pn activity and Pg activation, respectively. Formation of the thrombin/TM complex during coagulation, results in the activation of TAFI to TAFIa. This removes COOH-terminal Lys-residues on Fn, hindering Pg, tPA, and Pn binding to Fn. Dotted line arrows represent positive feedback steps. Adapted from Gross et al., 2011.

The most important intravascular plasminogen activator is tPA. tPA is a 68 kDa serine protease that is synthesized by endothelial cells and stored within secretory vesicles until being released with endothelial damage (Stewart et al., 1998). Structurally, tPA is composed of a fibronectin finger-like domain, an epidermal growth factor domain, and two kringle domains, all located on the A-chain segment; followed by the serine protease domain positioned on the B-chain (Horrevoets et al., 1994). The finger-like domain acts as an anchor, as it initially binds to Fn (Stewart et al., 1998). In addition, the second kringle domain has a Lys-binding site (LBS) that mediates interactions with Fn by localizing to Lys-residues (Cesarman-Maus and Hajjar, 2005; Stewart et al., 1998). TPA binding to Fn increases its capacity to activate Pg by three orders of magnitude (Kim et al., 2012; Weitz and Leslie, 1990). tPA circulates in an active, single-chain form, but exhibits increased functionality in the presence of Fn (Weitz et al., 1988; Weitz and Leslie, 1990). Because tPA does not require activation, the concentration in plasma remains relatively low, ~0.2 nM (Schaller and Gerber, 2011). Pn cleaves Arg₂₇₅-Ile₂₇₆, converting sc-tPA to its tc-form that has a greater catalytic activity only in the absence of Fn (Husain, 1991).

tPA facilitates fibrinolysis in two phases. The first phase begins as tPA localizes to Fn and binds Pg to form a ternary complex, resulting in trace Pn generation (Gebbinck, 2011). In the second phase, Pn formed from the first phase, degrades Fn, which exposes new COOH-terminal Lys-residues on Fn (Gebbinck,

2011). These exposed Lys-residues enhance Pg activation by binding additional tPA, Pg, and Pn. Because tPA is effective at inducing proteolysis of occlusive thrombi in patients experiencing thrombosis, it is considered the gold standard for thrombolytic therapy (Lippi et al., 2013).

In addition to tPA, uPA circulates at a similar concentration in plasma (Schaller and Gerber, 2011). Synthesis of this Pg activator differs from tPA, as it is synthesized mainly in the lungs and kidneys, and by monocytes, macrophages, epithelial and endothelial cells (Bernik and Kwaan, 1969; Sappino et al., 1991). uPA is a 53 kDa serine protease that exhibits optimal catalytic activity in its tc-form (Baeten et al., 2010; Schaller and Gerber, 2011). Sc-uPA is a zymogen that mainly adheres to endothelial cells (Hoyer-Hansen et al., 1992). Sc-uPA is converted to its high molecular weight active form, tc-uPA, by Pn cleavage at Lys₁₅₈-Ile₁₅₉, which increases its catalytic activity 100 to 500 fold (Baeten et al., 2010). In addition, Pn cleaves uPA at Lys₁₃₅-Lys₁₃₆ generating a low molecular weight form that retains activity (Baeten et al., 2010). Unlike tPA, uPA activity is independent of Fn, as it lacks the fibronectin finger-like domain and a Lys-binding kringle domain. uPA localizes to cell surfaces by binding to the uPA receptor (uPAR) (Dano et al., 1985; Weitz and Leslie, 1990). Functionally, tPA and uPA catalyze the conversion of Pg to Pn by cleaving the scissile peptide bond at Arg₅₆₁-Val₅₆₂ on Pg (Camiolo et al., 1971; Schaller and Gerber, 2011).

NH₂-terminal glutamic acid₁ plasminogen (Glu-Pg) is a single-chain, 90 kDa glycoprotein that is synthesized in the liver and circulates in plasma at ~2 μM (Schaller and Gerber, 2011). Glu-Pg contains an activation and an NH₂-terminal peptide (Lys₇₇), along with five disulfide bonded kringle domains and the catalytic domain (Schaller and Gerber, 2011). Four of the five kringle domains contain an LBS (Marti et al., 1994; Sohndel et al., 1996). The kringle domains that possess an LBS bind to Lys-residues on Fn, which further promotes activation and cleavage of Fn. This generates a positive feedback mechanism, as additional Lys-residues become exposed. Pg kringle 1 domain is responsible for the initial localization of Pg on Fn. Following this step, kringles 2, 4, and 5 mediate additional interactions with Fn (Cesarman-Maus and Hajjar, 2005).

NH₂-terminal lysine₇₈ plasminogen (Lys-Pg) is 83 kDa, and formed upon cleavage of the Lys₇₇-Lys₇₈ peptide bond of Glu-Pg by Pn (Fredenburgh and Nesheim, 1992; Schaller and Gerber, 2011). Glu- and Lys-Pg differ only by the presence of the 1-77 peptide, yet they exhibit different conformations. Glu-Pg exists in a closed, spiral conformation, which makes it difficult for Pg activators to access the activation peptide (Xue et al., 2012). Lys-Pg, on the other hand, has an open linear conformation. Consequently, Pg activators can readily cleave the activation peptide to produce Pn. The purpose of Glu-Pg exhibiting a closed structure is to prevent lysis when it is not needed. However, once trace amounts of

Pn are generated, Pn positively feeds back on Glu-Pg to form Lys-Pg, allowing tPA to rapidly convert it to Pn.

The main role of Pn is the dissolution of Fn clots (Schaller and Gerber, 2011; Weinstein and Doolittle, 1972). Pn is an endopeptidase that hydrolyzes arginine (Arg)- and Lys-bonds. In addition to Fn, Pn can degrade other coagulation proteins such as FV, FVIII, FIX, FXI, and FXII. Because this can interfere with coagulation, it is important to regulate Pn activity or excessive bleeding can result (Kunamneni et al., 2007; Schaller and Gerber, 2011; Violand and Castellino, 1976).

Most steps in fibrinolysis have regulatory mechanisms to maintain hemostasis. A key inhibitor of fibrinolysis is AP, a 63 kDa serine protease inhibitor belonging to the serine protease inhibitor (serpin) family (Lu et al., 2011; Schaller and Gerber, 2011). The COOH-terminus of AP contains a Lys-residue that binds to the kringle 1 LBS of Pn (Lu et al., 2011). AP inhibits Pn by forming a covalent bond with Ser₇₄₁ at the catalytic site, thus impairing Pn function (Schaller and Gerber, 2011). FXIIIa cross-links AP to Fn during clot formation, impeding Pg activation. Other serpins present in the circulation provide additional regulatory mechanisms to protect the Fn clot from rapid degradation. The 50 kDa serpin PAI-1 is primarily released from the alpha granules of platelets during platelet activation, and is a potent tPA and uPA inhibitor (Podor et al., 2000). PAI-1 circulates in complex with vitronectin, which enhances its stability, and

localizes it to the surface of clots to modulate Pg activation (Podor et al., 2000). PAI-2 circulates in plasma at very low levels, thus PAI-1 is more efficient at inhibiting vascular Pg activation (Schaller and Gerber, 2011). A third regulator of fibrinolysis is thrombin activatable fibrinolysis inhibitor (TAFI), a latent carboxypeptidase that is crosslinked to the clot by FXIII (Valnickova and Enghild, 1998). TAFI is a 60 kDa zymogen that is activated by the thrombin/TM complex to form activated TAFIa (Schneider et al., 2004). TAFIa cleaves the COOH-terminal Lys-residues on Fn, hindering the binding of Pg, tPA, and Pn to Fn (Valnickova and Enghild, 1998). TAFIa also indirectly modulates clot lysis, as AP localization to Fn is reduced, which increases the amount of free AP to interact with Pn (Schneider et al., 2004). Thus, like coagulation, fibrinolysis is a cascade of regulated events that hydrolyze Fn clots. This pathway restores vascular integrity for proper wound healing.

1.11 Histidine-rich Glycoprotein

HRG is synthesized in the liver and circulates in plasma at a concentration of 1.3-2 μM (Jones et al., 2005; Kassar et al., 2015; Vu et al., 2011). Structurally, HRG is a 75 kDa glycoprotein consisting of two NH_2 -terminal cystatin-like domains, a histidine-rich region (HRR) flanked by two proline-rich regions (PRR), and a COOH-terminal domain (Figure 6) (Jones et al., 2005; Kassar et al., 2015). Due to the abundance of His-residues, $\sim 13\%$, the HRR provides metal-binding properties to HRG (Jones et al., 2005; Rydengard et al., 2008; Wakabayashi and

Koide, 2011). Zn^{2+} binding to the HRR modulates the function of HRG by inducing a conformational change. Zn^{2+} has been shown to enhance the affinity of HRG for ligands such as heparin and HS, which neutralizes their anticoagulant activity (Jones et al., 2005). Like albumin, HRG also acts as a reservoir by binding to other ligands such as Pg, immunoglobulin, heme, and transition metals (Horne, III et al., 2001).

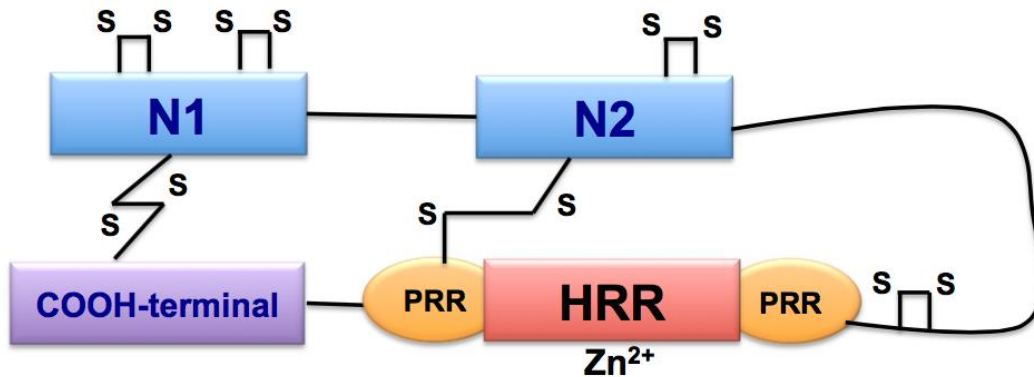


Figure 6. The structure of histidine-rich glycoprotein

HRG contains two NH₂-terminal cystatin-like domains (*blue*), connected to the HRR domain (*red*), which is flanked by two PRR (*orange*), and linked to the COOH-terminal domain (*purple*). The HRR region binds Zn²⁺ ions and induces a conformational change in HRG to enhance its affinity for ligands. The lines containing (S), represent disulphide bridges formed. Adapted from Jones et al., 2005.

The role of HRG was initially examined in inflammatory and innate immunity responses because HRG binds bacteria (Jones et al., 2005). Both processes were shown to be Fn-dependent mechanisms that trap bacteria and limit systemic infection (Jones et al., 2005). In plasma, HRG and Fg circulate in complex, as a Zn^{2+} -dependent interaction with a binding affinity (K_d) of ~6 nM (Jones et al., 2005; Vu et al., 2011). This interaction persists when Fg is converted to Fn. The γ' -chain on Fg is highly negatively charged, and binds to thrombin by exosite 2 (Meh et al., 2001). In the presence of Zn^{2+} , binding of HRG to the γ' -chain is enhanced; thus HRG competes with thrombin for binding to the γ' -chain (Vu et al., 2011). In addition, HRG also attenuates the intrinsic pathway by binding FXIIa and down-regulating its capacity to activate FXI (MacQuarrie et al., 2011). Recently, studies revealed that HRG hinders DNA and RNA mediated FXI and FXII activation. Therefore, HRG serves as a brake for the intrinsic pathway as evidenced by the fact that thrombosis is accelerated thrombosis in a HRG deficient mice (Vu et al., 2015a). These data suggest that HRG is an modulator of coagulation, especially in the presence of Zn^{2+} .

HRG not only circulates freely in plasma, but is also observed on the surface of macrophages and monocytes because it binds to immunoglobulins (Gorgani et al., 1999; Jones et al., 2005). HRG has been detected in platelets, and is thought to reside in the alpha granules along with Zn^{2+} and Fg (Lerch et al., 1988; Leung et al., 1983; Wijten et al., 2013). HRG is thought to be released from

activated platelets to elevate HRG concentrations at the site of injury where it is primed to modulate coagulation (Leung et al., 1983). Plasma HRG also binds to the surface of activated platelets where it binds to thrombospondin and Pg (Leung et al., 1984). In addition, HRG bound to the platelet surface can bind heparin and neutralize its anticoagulant properties (Leung et al., 1984). Therefore, HRG may have an important role in regulating platelet function by interacting with important mediators in the surrounding plasma.

1.12 The Dynamic Role of Zn²⁺ in Hemostasis

Zn²⁺ is the second most abundant metal ion in the body, after iron (Vu et al., 2013). Zn²⁺ enters the body by dietary consumption, and is essential for growth and development (Hambidge and Krebs, 2007). Zn²⁺ is a critical cofactor that interacts with more than 2000 transcription factors and 300 enzymes, thereby influencing protein structure, stability, and function (Beattie and Kwun, 2004; McCall et al., 2000). Only ~0.1% of total Zn²⁺ within the body circulates in plasma, where it serves as an important modulator of hemostasis (Roohani et al., 2013; Vu et al., 2013).

Zn²⁺ deficiency is prevalent in underdeveloped countries. Worldwide, ~2 billion people consume Zn²⁺-deficient diets, accounting for ~1-4% of deaths each year (Beattie and Kwun, 2004; Prasad, 2009). These deaths are mainly in infants having a compromised immune system, which increases their susceptibility to systemic infections (Black, 2003). Daily Zn²⁺ ingestion can be upwards of 14-30

mg/kg (Roohani et al., 2013). However, the body absorbs 20-40% of dietary Zn^{2+} through the gut, and residual Zn^{2+} is excreted (Roohani et al., 2013). The importance of Zn^{2+} in hemostasis was recognized in 1982, as Zn^{2+} -deficient men had bleeding and clotting abnormalities (Gordon et al., 1982). This was also demonstrated in Zn^{2+} -deficient rats, which exhibited impaired platelet function and prolonged bleeding times (Gordon et al., 1983). However, with Zn^{2+} sulphate supplementation, coagulation was fully restored (Gordon et al., 1983). The concentration of Zn^{2+} in plasma is 10-20 μ M (Stewart et al., 2009; Tubek, 2007). The majority of circulating Zn^{2+} is weakly bound to proteins, such as albumin and α_2 -macroglobulin (Lu et al., 2008; Vallee and Falchuk, 1993). Thus, only \sim 0.1-2 μ M Zn^{2+} circulates in a non-protein bound form, referred to as free Zn^{2+} (Bax and Bloxam, 1997; Lu et al., 2008; Mahdi et al., 2003; Vallee and Falchuk, 1993). Free Zn^{2+} may not be truly free, as it is thought to be bound to amino acids and other anions (Bax and Bloxam, 1997; Lu et al., 2008; Mahdi et al., 2003; Vallee and Falchuk, 1993). Local concentrations of free Zn^{2+} can vary depending on changes in the local microenvironment. Thus, Zn^{2+} concentrations are elevated at the site of injury with platelet granule secretion (Gorodetsky et al., 1993; Mahdi et al., 2003). Zn^{2+} levels also rise with elevated plasma lipid levels because fatty acids compete with albumin binding, thereby displacing weakly bound Zn^{2+} (Stewart et al., 2009).

Zn^{2+} participates as a regulatory cofactor in platelet aggregation, coagulation, anticoagulation, and fibrinolysis (Vu et al., 2013). Zn^{2+} is reported to be located in the alpha granules and cytoplasm of platelets, and is released with activation (Marx et al., 1993). As platelets accumulate, Zn^{2+} concentrations surge above local plasma concentrations by about 30- to 60-fold at the site of injury (Hughes and Samman, 2006; Rojkaer and Schmaier, 1999). Zn^{2+} mediates platelet aggregation stimulated by ADP or thrombin agonists because Zn^{2+} augments Fg binding to GPIIb/IIIa on the platelet surface (Heyns et al., 1985). These responses promote platelet aggregation, which is impaired in Zn^{2+} -deficient patients (Heyns et al., 1985).

Zn^{2+} regulates coagulation and anticoagulation mechanisms by binding to various ligands (Table 2). Zn^{2+} modulates amplification steps within coagulation, as it targets the intrinsic pathway. Zn^{2+} binds to FXII and HK and augments the intrinsic pathway by increasing their affinity for negatively charged surfaces (Lin et al., 2000; Rojkaer and Schousboe, 1997; Vu et al., 2013). However, Zn^{2+} can also attenuate contact activation by binding HRG, which down-regulates FXIIa activity, and its activation by DNA and RNA (MacQuarrie et al., 2011; Vu et al., 2015a). Zn^{2+} also attenuates coagulation through the extrinsic pathway by binding to FVIIa and reducing FVIIa/TF activity (Petersen et al., 2000). Zn^{2+} also modulates anticoagulation. In the presence of Ca^{2+} , Zn^{2+} promotes PC binding to EPCR, thereby enhancing PC activation to promote anticoagulation. Zn^{2+} binds to

APC, but does not interfere with APC anticoagulant activity to inactivate FVa (Fernandes et al., 2010; Sen et al., 2010). These studies provide evidence that Zn^{2+} plays a dynamic functional role in both coagulation and anticoagulation pathways.

Zn²⁺-Binding Protein	Binding Domain	Binding Affinity
COAGULATION		
FXII	Heavy-chain	1 μ M
FVIIa	Protease-domain	N/A
HK	Light-chain	0.8 nM
HRG	HRR	225 nM
Fg	α C- and D-domains	9.4 μ M
ANTICOAGULATION		
PC	Gla-domain	N/A
APC	Gla- and Protease-domain	7.4 μ M

Table 2. Zn²⁺-binding proteins in coagulation and anticoagulation

Zn²⁺ modulates both the coagulation and anticoagulation pathways by interacting with proteins through various binding domains. Zn²⁺ does not bind to all serine proteases domains with high affinity; therefore Zn²⁺-binding it is not a universal interaction observed in coagulation. The Gla-domains of vitamin-K antagonists tend to be ion sensitive, as both Ca²⁺ and Zn²⁺ bind. Binding affinities that have not been determined are indicated as N/A. Adapted from Vu et al., 2013.

The involvement of Zn^{2+} in fibrinolysis is not well established. Whether Zn^{2+} binds to tPA, uPA, Pg, or Pn, has yet to be elucidated. Previous reports indicate that Zn^{2+} inhibits tPA and Pn protease activity (Dang et al., 1985; Siddiq and Tsirka, 2004; Tubek et al., 2008). However, these experiments did not include Fg or Fn, and were performed with supra-physiological Zn^{2+} levels. Other reports suggest that Zn^{2+} delays fibrinolysis because it accelerates coagulation and induces a clot structure that is not favourable for lysis (Tubek et al., 2008; Vu et al., 2013). Mechanistic evidence to support the role of Zn^{2+} on fibrinolysis has yet to be reported.

CHAPTER 2: THESIS OVERVIEW, RATIONALE, HYPOTHESIS, AND OBJECTIVE

2.1 Thesis Overview

Previous studies indicate that plasma Zn^{2+} concentrations are elevated 30- to 60-fold at the site of injury, as it is released from activated platelets (Hughes and Samman, 2006). Here, Zn^{2+} accelerates clot formation by enhancing Fv monomer polymerization, yet delays fibrinolysis due to changes in clot structure (Vu et al., 2013). Mechanistic evidence in the literature to support these concepts is lacking, as conclusions were based on assumptions and speculation from limited data. The purpose of this thesis was to extensively re-examine existing evidence as to the location of Zn^{2+} in platelets, and its regulatory role in clot formation and degradation. In this thesis we **(A)** examined the effect of Zn^{2+} on the structural and mechanical properties of clots, **(B)** elucidated mechanistic evidence as to how Zn^{2+} prolongs clot lysis, and **(C)** determined the source of Zn^{2+} and HRG in platelets, and quantified their release from secretory granules.

2.2 Rationale for Studies

Zn^{2+} -deficiency is not a prevalent clinical problem in the developed world. However, Zn^{2+} -deficiency may arise in patients requiring massive transfusions. Blood is collected into citrate, which is a potent chelator of divalent ions and is added to prevent clotting. In addition to binding Ca^{2+} , citrate also chelates Zn^{2+} . Although Ca^{2+} is given to patients receiving massive blood transfusions because

of traumatic injury, however Zn^{2+} is not. Therefore, such patients could exhibit clotting abnormalities as a consequence of Zn^{2+} chelation. In virtually all experimental studies conducted *in vitro* Ca^{2+} is reconstituted back into plasma, whereas Zn^{2+} is typically not considered. Therefore, investigations reported by others may not reflect physiological conditions, as Zn^{2+} is absent. Regardless of variations in normal levels of Zn^{2+} , at the site of injury Zn^{2+} is released from platelets, such that physiological levels of Zn^{2+} may be exceeded locally. Therefore, it is important to re-examine reactions in the presence of Zn^{2+} , and determine its overall effect on clot formation and lysis.

2.3 Central Hypotheses

Zn^{2+} is an intricate modulator of hemostasis as it targets numerous reactions in hemostasis (Vu et al., 2013). Because Zn^{2+} binds to Fg with high affinity, we hypothesized that Zn^{2+} will affect clot structure independently of Ca^{2+} by altering fiber thickness and clot porosity. The function of zymogens and serine proteases are modulated through Zn^{2+} -binding. We hypothesized that Zn^{2+} will delay clot lysis by targeting Pg activators and Pn. Therefore, the delay in fibrinolysis caused by Zn^{2+} will be independent of changes in clot structure. Zn^{2+} storage and release from platelets has yet to be extensively examined. We hypothesized that Zn^{2+} will be located in the dense granules with other ions, and not the alpha granules with Fg. We predict that full release of intracellular platelet Zn^{2+} will be sufficient to effect clot formation and lysis.

2.4 Overall Objective

The physiological role of Zn^{2+} within hemostasis has been largely ignored because of Zn^{2+} removal through chelation, or failing to incorporate Zn^{2+} back into *in vitro* clotting reactions. The overall objective of this thesis was to re-examine Zn^{2+} storage in platelets, and mechanistically determine how Zn^{2+} accelerates clotting yet delays fibrinolysis. The four studies described in Chapters 3-6 reveal the progress in understanding the biological role of Zn^{2+} in hemostasis.

CHAPTER 3: ZINC PROMOTES CLOT STABILITY BY ACCELERATING CLOT FORMATION AND MODIFYING FIBRIN STRUCTURE

3.1 Forward

The effects of Zn^{2+} on the physical and mechanical properties of clot formation are described in this manuscript. We demonstrate that Zn^{2+} alters clot morphology, which increases clot stability and reduces rupture, independently of FXIIIa.

3.2 Objective: Determine whether Zn^{2+} modulates clot formation and influences clot stability

Understanding the structure of clots formed under physiological conditions can be used to predict thrombus stability, and its resistance to lysis. The aim of this study was to identify the effect of Zn^{2+} on the structural and mechanical properties of F_n clots. Divalent cations like Ca^{2+} bind F_g and augment coagulation resulting in an increased fiber thickness and porosity, but a reduction in clot stiffness. Because Zn^{2+} is a divalent ion and also binds F_g, we hypothesized that Zn^{2+} would have the same effect as Ca^{2+} on manipulating clot structure independently of FXIIIa. In order to test this hypothesis, Zn^{2+} and FXIIIa compared to in its absence were assessed in the following experiments: (A) clot times in purified and plasma systems, (B) visualization of clot structure, (C) clot physical properties such as fiber diameter and porosity were quantified, and (D)

mechanical properties were used to assess clot stiffness, stability, and rupture. These objectives were used to highlight the importance of Zn^{2+} on clot formation and its ability to influence clot stability.

Zinc Promotes Clot Stability by Accelerating Clot Formation and Modifying Fibrin Structure

Sara J. Henderson^{1,2}, Jing Xia⁵, Huayin Wu⁵, Alan R. Stafford^{1,3}, Beverly A. Leslie^{1,3}, James C. Fredenburgh^{1,3} David A. Weitz⁵, and Jeffrey I. Weitz^{1-4†}

Thrombosis and Atherosclerosis Research Institute¹ and the Department of Biochemistry and Biomedical Sciences², Medicine³ and Medical Sciences⁴, McMaster University, Hamilton, Ontario, Canada, School of Engineering and Applied Sciences⁵, Harvard University, Cambridge, Massachusetts, USA

Running title: Zinc modifies clot structure

Address correspondence: To whom correspondence should be addressed: Jeffrey I. Weitz, Thrombosis and Atherosclerosis Research Institute, 237 Barton Street East, Hamilton, ON, L8L 2X2. Tel: 905-521-2100 ext. 40721, e-mail: weitzj@taari.ca

Footnotes: This work was supported in part by the Canadian Institutes of Health Research and the Heart and Stroke Foundation. J.I.W. holds the Heart and Stroke Foundation J. Fraser Mustard Endowed Chair in Cardiovascular Research and the Canada Research Chair (Tier 1) in Thrombosis. The work by J.X., H.W., and D.A.W. was supported in part by the Harvard MRSEC (DMR 14-20570).

Authorship Contributions: SJH coordinated the study, performed experiments, and wrote the paper. JX performed rheology experiments in Figures 6 and 7, and HW assisted in rheology analysis. ARS contributed to experimental design in Figure 1. BAL prepared Fg and Fg^{XIII} and fragment X. JCF assisted in writing the paper, contributed to experimental design, and preparation of figures. DAW contributed to rheological experimental design and interpretation of the data. JIW assisted in writing, experimental design, and had the final approval of the manuscript for publication.

* **This manuscript is published in *Thrombosis and Haemostasis*:** Thromb Haemost. 2015 Oct 22;115(3). [Epub ahead of print]. Accepted September 14, 2015, assigned to the February 2016 Issue. This chapter is not a direct representation of the above referenced manuscript. All copyrights to the manuscript are effective, as the manuscript is published in *Thrombosis and Haemostasis* ©. Schattauer policy states that no copyright permission is necessary from original authors posting an accepted version of their manuscript for uploading it to institutional and/or centrally organized repositories.

References: References for this manuscript have been incorporated into the Bibliography (Chapter 10), at the end of this thesis.

3.3 WHAT IS KNOWN

- Zn^{2+} is released from activated platelets, and is abundant at sites of vascular injury.
- Zn^{2+} binds fibrinogen with high affinity.
- Zn^{2+} accelerates coagulation yet delays fibrinolysis

3.4 WHAT THIS PAPER ADDS

- Zn^{2+} increases fibrin fiber thickness at least in part by binding to the αC -domain of fibrinogen.
- Zn^{2+} increases pore size and porosity of fibrin clots.
- Zn^{2+} offsets the increase in clot stiffness induced by factor XIII thereby rendering cross-linked clots more elastic.

3.5 SUMMARY

Zinc released from activated platelets binds fibrin(ogen) and attenuates fibrinolysis. Although zinc also affects clot formation, the mechanism and consequences are poorly understood. To address these gaps, the effect of zinc on clot formation and structure was examined in the absence or presence of factor (F) XIII. Zinc accelerated (**A**) plasma clotting by 1.4-fold, (**B**) fibrinogen clotting by 3.5- and 2.3-fold in the absence or presence of FXIII, respectively, (**C**) fragment X clotting by 1.3-fold, and (**D**) polymerization of fibrin monomers generated with thrombin or batroxobin by 2.5- and 1.8-fold, respectively. Whereas absorbance increased up to 3.3-fold when fibrinogen was clotted in the presence of zinc,

absorbance of fragment X clots was unaffected by zinc, consistent with reports that zinc binds to the α C-domain of fibrin(ogen). Scanning electron microscopic analysis revealed a 2-fold increase in fiber diameter in the presence of zinc and in permeability studies, zinc increased clot porosity by 30-fold with or without FXIII. Whereas FXIII increased clot stiffness from 128 ± 19 Pa to 415 ± 27 Pa in rheological analyses, zinc reduced clot stiffness by 10- and 8.5-fold in the absence and presence of FXIII, respectively. Clots formed in the presence of zinc were more stable and resisted rupture with or without FXIII. Therefore, zinc accelerates clotting and reduces fibrin clot stiffness in a FXIII-independent manner, suggesting that zinc may work in concert with FXIII to modulate clot strength and stability.

3.6 INTRODUCTION

Fibrin (Fn), the main scaffold of blood clots, forms when thrombin cleaves fibrinopeptides (FP) A and B from the $A\alpha$ and $B\beta$ chains of fibrinogen (Fg) to expose knobs on the respective chains. The resultant Fn monomers polymerize when the knobs bind to pre-existing complementary holes of other Fn monomers to form two-stranded protofibrils. The protofibrils assemble laterally into long fibers that comprise the Fn clot (Weisel and Litvinov, 2013). Thrombin also converts FXIII to activated FXIII (FXIIIa), which covalently cross-links the protofibrils, thereby increasing clot stiffness by 2 to 5-fold to stabilize the clot by compacting the fibers (Kurniawan et al., 2014).

Clot stability, the ability to resist mechanical stress, is a critical property of Fn that is determined in part by the nature of the fibers that form upon polymerization (Weisel, 2007). Clot stiffness is represented by elastic and inelastic properties of Fn, and its development, which occurs much later than gelation, may reflect fiber re-arrangement (Weisel, 2004). Stiffer clots containing thinner fibers are less stable and more susceptible to rupture and embolization than softer clots, which can undergo reversible deformation (Weisel, 2007). In contrast, clots composed of thick fibers are more readily degraded by the fibrinolytic system (Gabriel et al., 1992). Therefore, the physical properties of Fn clots are critical determinants of their role in hemostasis.

Fn fibers formed in plasma are larger than those formed in purified systems (Carr, 1988), consistent with the concept that the structural and physical properties of a clot are a consequence of the conditions under which the clots form (Weisel, 2007; Weisel and Litvinov, 2013). In particular, the thrombin concentration and ionic conditions influence clot structure (Ryan et al., 1999). Calcium (Ca^{2+}) facilitates Fn monomer polymerization, thereby increasing fiber thickness (Kanaide et al., 1982; Marx, 1988a; Ryan et al., 1999), whereas chlorine opposes lateral aggregation and promotes thin fiber formation (Di Stasio et al., 1998). These observations suggest that the ionic milieu influences Fn monomer polymerization. Zinc (Zn^{2+}) is another cation that influences clot formation (Carr and Powers, 1991; Fatah and Hessel, 1998; Kanaide et al., 1982; Marx et al.,

1987; Marx and Eldor, 1985; Suzuki and Hashimoto, 1976). Zn^{2+} circulates in plasma at a concentration of $\sim 10\text{-}20\ \mu\text{M}$, however $\sim 80\%$ is weakly bound to albumin, leaving $\sim 0.1\text{-}2\ \mu\text{M}$ in a free, unbound state (Gorodetsky et al., 1993; Henderson et al., 2015a; Lu et al., 2008; Whitehouse et al., 1982). However, Zn^{2+} is abundant at sites of vascular injury because Zn^{2+} stores in platelets are released upon platelet activation, and platelets accumulate in thrombi in numbers 50- to 100-fold higher than those found in the circulating blood (Henderson et al., 2015a; Marx et al., 1993). Therefore, the Zn^{2+} concentrations in clots are likely to be higher than those in circulating plasma. These high levels enable Zn^{2+} to modulate the contact activation pathway at sites of vascular injury (Vu et al., 2013).

Previous studies have demonstrated that Zn^{2+} binds Fg and Fn with a K_d of $9\text{-}13\ \mu\text{M}$, and impairs proteolysis by plasmin and trypsin (Fredenburgh et al., 2013; Henderson et al., 2015a). Furthermore, a Zn^{2+} binding site has been identified on the αC -domain of fibrin(ogen) (Fredenburgh et al., 2013). Although Fn fibers formed in the presence of Zn^{2+} have been shown to be thicker than those formed in its absence (Marx et al., 1987), mechanistic information about how Zn^{2+} affects clot structure, the mechanical properties of Fn, and clot stability is lacking. To address these gaps in knowledge, we quantified the effect of Zn^{2+} on **(A)** Fg clot times in plasma and purified systems, **(B)** Fn fiber diameter, and **(C)** clot porosity, stiffness, and stability. Fragment X, a high molecular weight

plasmin degradation product of Fg that lacks the α C-domain, was used in place of Fg to examine the contribution of the α C-domain.

3.7 MATERIALS AND METHODS

3.7.1 Reagents

Human α -thrombin and Fg containing FXIII (FIB 1; herein termed Fg^{XIII}) were purchased from Enzyme Research Laboratories (South Bend, IN). A portion of the Fg^{XIII} was depleted of FXIII (herein termed Fg) by affinity chromatography using an immobilized antibody against FXIII (Fredenburgh et al., 2008). Both Fg and Fg^{XIII} were subjected to precipitation with 19% ammonium sulfate to ensure the highest integrity of the α -chains (Walker and Nesheim, 1999). SDS-PAGE analysis of thrombin-treated Fg or Fg^{XIII} under reducing conditions revealed absence and presence of cross-linked γ - γ dimers and α -polymers, respectively (data not shown). Plasmin was purchased from Haematologic Technologies Inc. (Essex Junction, VT, USA). Aprotinin was purchased from Cedarlane (Burlington, ON, Canada). Fragment X was prepared by digesting 4 ml of a solution containing 60 μ M Fg with 100 nM plasmin for 15 min at 37°C. Plasmin activity was inhibited by adding 500 KIU/mL aprotinin, and the digested mixture was then subjected to high-performance liquid chromatography to isolate fragment X as described (Schaefer et al., 2006). Thrombin was dialyzed against 20 mM Tris, pH 7.4, 150 mM NaCl (TBS) to remove citrate. Batroxobin, a thrombin-like enzyme from the venom of *B. atrox moojeni* that only releases FPA, was purchased from

Pentapharm (Basel, Switzerland). Experiments were performed in a Zn^{2+} buffering system containing 10 mM Tricine, 150 mM NaCl, pH 7.4, and 0.01% Tween 20 (TcBS). The desired free Zn^{2+} concentration in TcBS was obtained by adding ~100-fold higher concentration of $ZnCl_2$, as described (Henderson et al., 2015a).

3.7.2 Clot formation in plasma

Blood collected from 7 healthy volunteers into 5-ml tubes each containing 7.2 mg of EDTA was subjected to centrifugation at 2100 x g for 10 min at 23°C. The resultant platelet poor plasma was harvested, pooled, and dialyzed *versus* TBS at 4°C to remove Zn^{2+} and EDTA. Plasma Zn^{2+} concentrations were determined by atomic absorption spectrometry as described (Henderson et al., 2015a). For clotting experiments, 50 µl of dialyzed plasma pre-warmed to 37°C was placed into wells of a 96-well plate, and 50 µl of a solution containing 0.5 nM thrombin, 15 mM $CaCl_2$, and 0-10 µM free $ZnCl_2$ in TcBS was added. Absorbance was monitored at 350 nm at 3 s intervals up to 25 min at 37°C using a Spectromax plate reader (Molecular Devices, Sunnyvale, CA). The clot time, defined as the time to achieve half maximal absorbance, was obtained using instrument software.

3.7.3 Clot time in purified systems

Thrombin (0.5, 2, 5, or 10 nM) and 2 mM $CaCl_2$ were separately placed into wells of a 96-well plate, and clotting was initiated by adding aliquots of 3 µM

Fg in TcBS containing 0-5 μM free ZnCl_2 . In a separate experiment, 0.5 nM thrombin and 2 mM CaCl_2 were separately placed into wells of a 96-well plate, and clotting was initiated by adding 3 μM Fg or fragment X in TcBS with 0-5 μM free ZnCl_2 . Absorbance was monitored at 405 nm at 2 s intervals up to 33 min at 37°C using a plate reader and clotting time was determined as described above.

3.7.4 Preparation and polymerization of Fn monomers

After placing 3 ml of a 76.3 μM Fg solution in 12000-14000 molecular weight cut off dialysis tubing (VWR International), thrombin or batroxobin was added to 5 nM or 5 units/ml, respectively. The tubing was placed in a beaker containing 1 l of TBS and dialyzed for 3 h at 37°C. The buffer was changed to 20 mM acetic acid and dialysis was continued overnight at 4°C with one buffer change. The contents of the tubing were then removed and subjected to centrifugation at 5000 x g for 4 min at 23°C, after which the supernatant was collected and stored in aliquots at -80°C. After adding 10- μl aliquots of soluble Fn (final concentration 2 μM) to wells of a 96-well plate, polymerization was initiated by addition of 190 μl of TcBS containing 2 mM CaCl_2 and 0-6 μM free ZnCl_2 and absorbance was monitored at 405 nm at 2 s intervals up to 33 min at 37°C using a plate reader. Clot times were determined as described above.

3.7.5 Scanning electron microscopy (SEM)

Clots were formed in the absence or presence of Zn^{2+} and/or FXIII on 0.025 μm circular filter paper membranes (EMD Millipore) placed in wells of a

24-well plate. Thus, using a pipette, 50- μ l aliquots of a solution containing 3 μ M Fg or Fg^{XIII}, 10 nM thrombin, and 2 mM CaCl₂ in the absence or presence of 5 μ M free ZnCl₂ in TcBS were placed on each membrane. Three clots were formed under each of the four conditions. The wells were sealed, and the plate was incubated at 100% humidity for 30 min at 37°C. Membranes were fixed overnight in 2% glutaraldehyde in 0.1 M phosphate buffer, pH 7.4, rinsed twice with 0.1 M phosphate buffer and stained for 1 h with 1% osmium tetroxide in 0.1 M sodium cacodylate buffer. Samples were dehydrated using a series of graded ethanol washes (50%, 70%, 70%, 95%, 95%, 100%, 100% and 100%), and dried in a critical point dryer. The membranes were mounted onto SEM stubs, sputter-coated with gold, and viewed at 30,000x magnification using a Tescan Vega II LSU scanning electron microscope (Tescan, PA, USA) operating at 10 kV. Images were acquired with the VEGA/TESCAN software. Each clot was imaged at 5 different sites, and the fiber diameter in each image was quantified using Photoshop version 6 Extended (Adobe Systems, San Jose, CA). Contrast and brightness of the images were adjusted and changed from grey scale to black and white. An 11 x 11 inch grid was placed over each image to divide it into multiple cells and the thickness of fibers in each cell of alternate rows was measured manually in Photoshop using the ruler tool set to 2 μ m. The numbers of fibers quantified per image ranged from 72-207. After determining the fiber diameters in the 5 images, the mean fiber diameter for each clot was calculated.

3.7.6 Clot porosity

Samples containing 0.5 ml of 9 μM Fg or Fg^{XIII}, 2 mM CaCl₂ and 0 or 5 μM free ZnCl₂ were clotted in 3-ml syringes with 5 nM thrombin and incubated for 1 h at 23°C. Syringes were mounted vertically and 2.5 ml TcBS was then placed on top of each clot. The flow through was collected into tubes positioned below the syringes for 6 and 16 min with and without Zn²⁺, respectively. Darcy's constant K_s , a measure of clot porosity was then calculated using the following equation (Ariens et al., 2000).

$$K_s = \frac{Q \cdot L \cdot \eta}{t \cdot A \cdot \delta P}$$

where Q is the volume of TcBS collected (ml), L is the clot length (1.6 cm), η is the viscosity of flow through (10⁻² poise), t is the time of collection (s), A is the cross-sectional area of the syringe (0.232 cm²), and δP is the atmospheric pressure (1,012,950 dyne/cm²).

3.7.7 Clot strength

The viscoelastic properties of clots were determined using a Discovery Hybrid Rheometer-3 and TRIOS software (TA Instruments, New Castle, DE). Clots were formed by addition of 5 nM thrombin to a solution containing 9 μM Fg or Fg^{XIII} and 0-5 μM free ZnCl₂ in TcBS. Samples were gently mixed with a pipette for 3 s before adding 1230- μl aliquots between the Peltier plate and the nickel-coated cone (4° cone angle and 40 mm diameter). Samples were

surrounded with mineral oil to prevent dehydration and 3 sequential studies were then performed. Time sweep experiments were conducted under continuous oscillations at 1 rad/s with an imposed shear strain of 0.5% to monitor network polymerization. After the storage modulus (G') reached a plateau, a frequency sweep routine was applied under a shear strain of 0.5% with the angular frequency increasing from 0.1-10 rad/s. For both time and frequency sweep experiments, the storage modulus (G'), loss modulus (G'') and loss tangent (δ) were also calculated. The final peak hold experiment measured the stress-strain relationship by imposing steadily increasing strain on the Fn network.

3.7.8 Statistical analysis

Data are presented as mean \pm standard error (SE) unless otherwise indicated. Significance of differences was determined using the Mann-Whitney rank sum test or one-way analysis of variance followed by Tukey's test for multiple pair-wise comparisons (SigmaPlot version 11.0). A nested three-way (condition, clot, image) analysis of variance was performed to determine the dominant sources of variation in Fn fiber diameter. In particular, this analysis addressed the issue of whether there was additional variation in fiber diameter from image to image within a clot, and from clot to clot, relative to the inherent between fiber variation within an image. As a result of this analysis, subsequent comparisons of mean fiber diameter among the four conditions (i.e., with or without Zn^{2+} and/or FXIII) were based on the inter-clot variation in mean fiber

diameter. In all cases, p-values less than 0.05 were considered statistically significant.

3.8 RESULTS

3.8.1 Effect of Zn^{2+} on clot times in plasma

Zn^{2+} -depleted plasma was clotted with thrombin in the presence of $CaCl_2$ and concentrations of free Zn^{2+} up to 10 μM . In the presence of 5 and 10 μM free Zn^{2+} , clot times were significantly ($p < 0.01$ and $p < 0.001$) shortened by 1.2- and 1.4-fold respectively (Figure 1) Therefore, Zn^{2+} accelerates thrombin-mediated clotting in plasma.

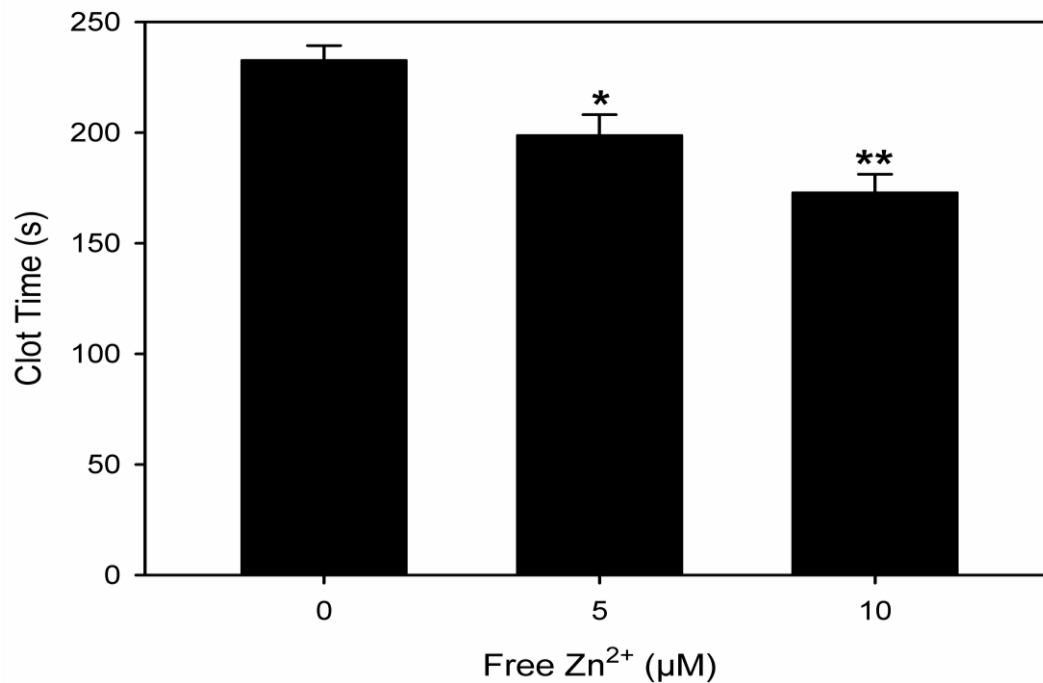


Figure 1. Effect of Zn²⁺ on clotting

Aliquots of dialyzed plasma were clotted with 0.5 nM thrombin in the presence of 15 mM CaCl₂ and 0-10 µM free Zn²⁺. Absorbance was monitored at 350 nm and clot times were determined. Bars represent means of three determinations each performed in duplicate, while the lines above the bars indicate SE. Based on parametric one-way analysis of variance, Zn²⁺ significantly ($p < 0.001$) accelerates clot time in a concentration-dependent fashion, and Tukey's test for multiple pairwise comparisons indicates that clot times at 5 µM (* $p < 0.01$) and 10 µM Zn²⁺ (** $p < 0.001$) are significantly shorter than that with no Zn²⁺.

3.8.2 Effect of Zn^{2+} on Fn clot formation

Fg was clotted with 0.5-10 nM thrombin in the presence of 0-5 μ M free Zn^{2+} . Zn^{2+} at 5 μ M produced an approximate 2-fold, concentration-dependent and statistically significant ($p < 0.001$) shortening of the clot time (Figure 2A); an effect similar to that observed on the plasma clot time. The Zn^{2+} -dependence was independent of thrombin concentration because the EC_{50} values for Zn^{2+} ranged from 1.5-1.9 μ M ($p = 0.8$) with thrombin concentrations ranging from 0.5-10 nM. At 5 μ M Zn^{2+} , there was a significant ($p < 0.001$) concentration-dependent reduction in relative clot time as the thrombin concentration increased from 0.5 nM to 10 nM; similar to the reduction of clot time with increasing thrombin concentration in the absence of Zn^{2+} . These results confirm previous reports that Zn^{2+} accelerates Fg clotting (Carr and Powers, 1991; Fatah and Hessel, 1998; Kanaide et al., 1982; Marx et al., 1987; Marx and Eldor, 1985; Suzuki and Hashimoto, 1976).

In the presence of Zn^{2+} , absorbance increased in a concentration-dependent manner. The increase ranged from 1.7 to 3-fold with thrombin concentrations of 0.5 and 10 nM, respectively (Figure 2A, inset); a difference that was statistically significant ($p < 0.001$). As expected, in the absence of Zn^{2+} , absorbance decreased with increasing concentrations of thrombin ($p < 0.001$), confirming that thrombin concentration affects clot formation (Ryan et al., 1999). By contrast, in the presence of 5 μ M Zn^{2+} , the thrombin dose-response was negated because the

changes in absorbance values were small and not statistically significant ($p=0.3$). Therefore, Zn^{2+} appears to negate the effect of thrombin concentration on absorbance. Together, these data suggest that Zn^{2+} is an independent modulator of clot structure.

Next, we examined the effect of Zn^{2+} in the presence of FXIII because cross-linking is an important determinant of Fn stability. The effect of Zn^{2+} was maintained in the presence of FXIII because clot times of Fg and Fg^{XIII} were significantly ($p<0.001$) accelerated by 3.5- and 2.3-fold, respectively (Figure 2B), and absorbance was significantly ($p<0.001$) increased by 3.3- and 1.7-fold, respectively (Figure 2B). Although Zn^{2+} accelerated Fg^{XIII} clotting to a lesser extent than Fg clotting, the EC_{50} values remained between 1 and 2 μM . Therefore, Zn^{2+} accelerates clotting in the absence and presence of FXIII.

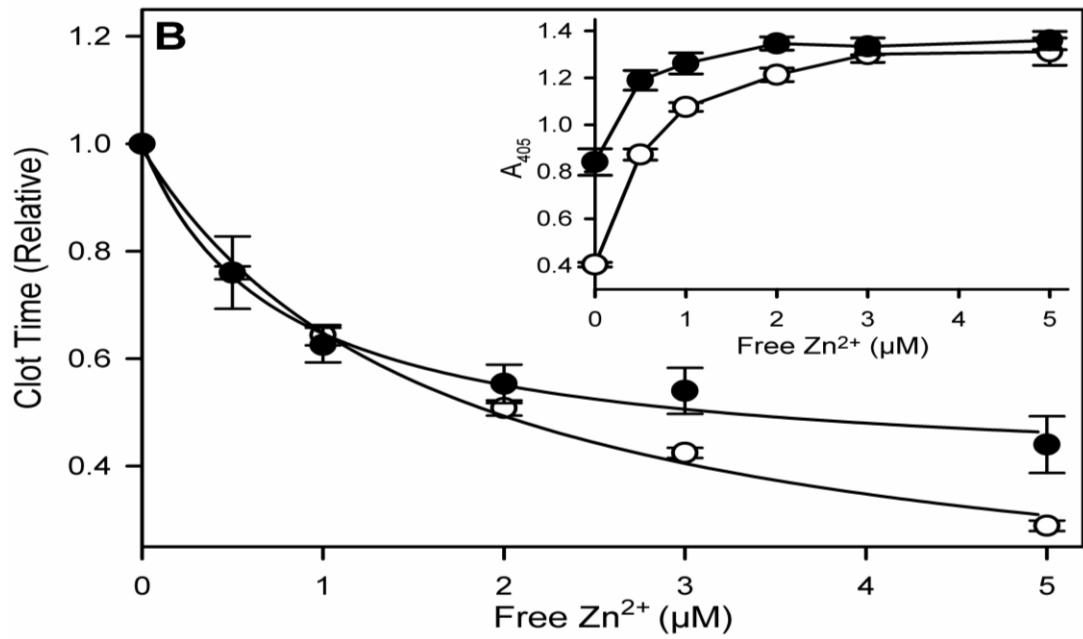
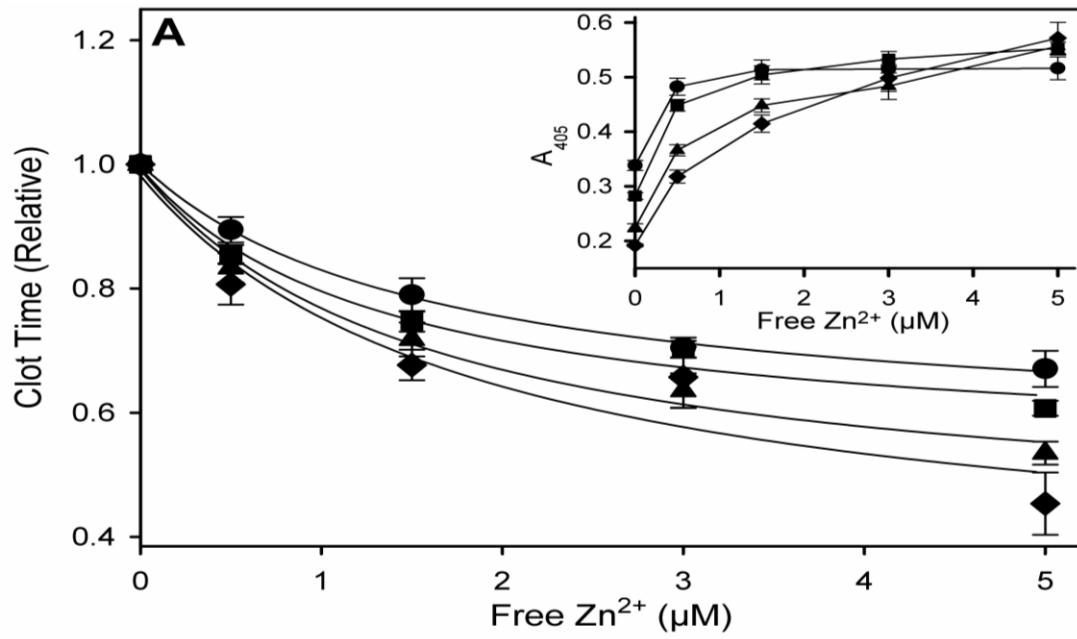


Figure 2. Effect of Zn²⁺ and FXIII on clot formation

(A) Samples containing 3 μM Fg, 2 mM CaCl₂, and 0-5 μM free Zn²⁺ were clotted with 0.5 (*circles*), 2 (*squares*), 5 (*triangles*), or 10 (*diamonds*) nM thrombin. Clot times were determined by monitoring absorbance at 405 nm and values measured in the presence of Zn²⁺ were normalized relative to that measured in its absence. Clot times in the absence of Zn²⁺ were 441.9 ± 25 , 122.1 ± 8 , 47.3 ± 1.7 , and 21.3 ± 1.1 s with 0.5, 2, 5, 10 nM thrombin respectively. Symbols represent the mean of three experiments each done in duplicate, while the bars reflect the SE. The data were fitted using nonlinear regression analysis of a rectangular hyperbola (*line*). Final absorbance values were determined from the experiments in **(A)** and mean values were plotted along with SE (*inset*). Arbitrary lines were used to connect the points. **(B)** Samples containing 0-5 μM free Zn²⁺, 2 mM CaCl₂, and 9 μM Fg with (*closed*) or without (*open*) FXIII, were clotted with 5 nM thrombin and clot times were determined as outlined above. Initial clot times in the absence of Zn²⁺ were 185.2 ± 16.1 and 144.5 ± 18 s without and with FXIII, respectively. Symbols (*circles*) represent the mean of three determinations each done in duplicate, while the bars reflect SE. The data were fitted by nonlinear regression analysis of a rectangular hyperbola (*line*). Final absorbance values from the experiments in **(B)** and mean values were plotted (*inset*).

In order to bypass the enzymatic steps involving thrombin, we examined the effect of Zn^{2+} on polymerization of preformed Fn monomers prepared with thrombin or batroxobin. In a concentration-dependent fashion, Zn^{2+} significantly ($p < 0.001$) accelerated polymerization of Fn monomers prepared with thrombin or batroxobin by 2.5- and 1.8-fold, respectively (Figure 3A). Furthermore, in the presence of Zn^{2+} , clot absorbance significantly ($p < 0.001$) increased by approximately 2- and 1.6-fold with thrombin- and batroxobin-generated monomers, respectively (Figure 3B), indicating that Zn^{2+} modulates Fn formation regardless of whether FPB is removed. Therefore, Zn^{2+} appears to influence Fn polymerization rather than fibrinopeptide release.

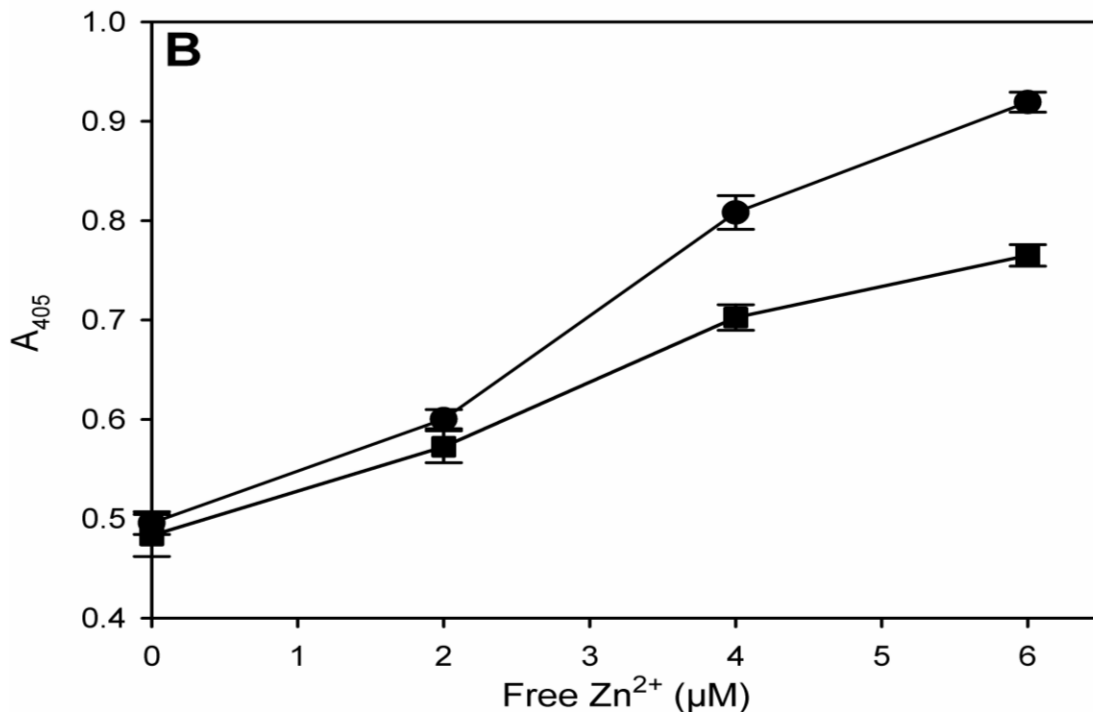
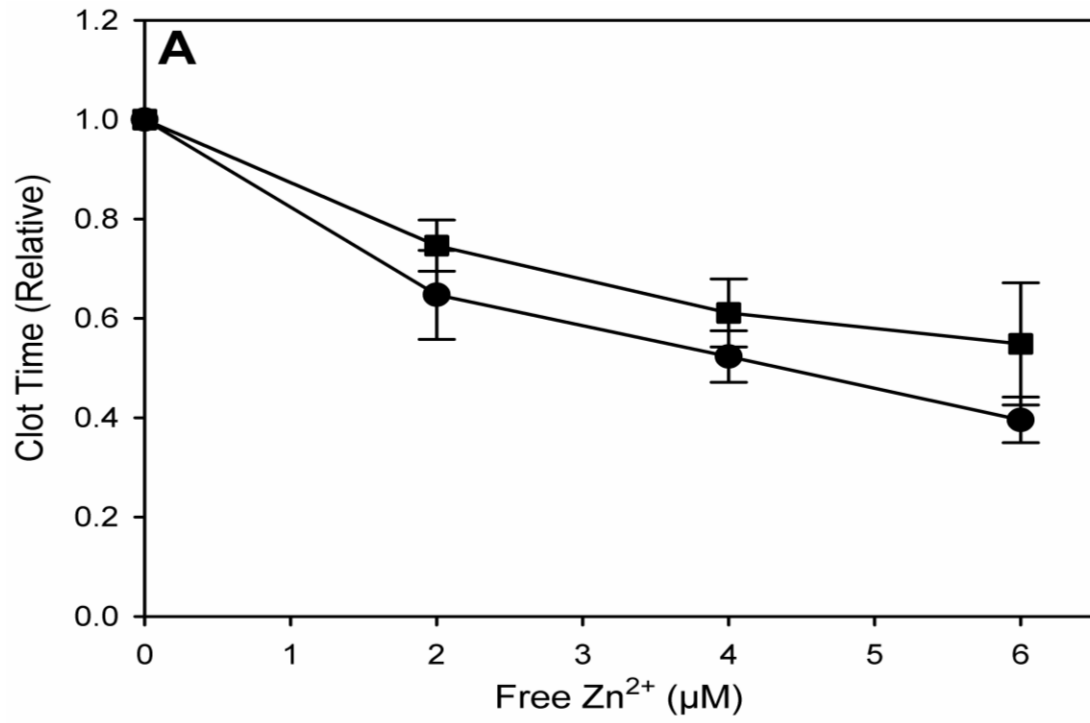


Figure 3. Effect of Zn²⁺ on polymerization of Fn monomers

(A) Samples containing 2 mM CaCl₂, 0-6 μM free Zn²⁺, were mixed with 2 μM Fn monomers generated with thrombin (*circles*) or batroxobin (*squares*). Clot times were determined by monitoring absorbance at 405 nm, and values measured in the presence of Zn²⁺ were normalized relative to that determined in its absence. Initial clot times in the absence of Zn²⁺ were 26.1 ± 4.2 and 27.3 ± 2.9 s for Fn monomers generated with thrombin or batroxobin, respectively. Symbols represent the mean of four determinations, while the bars reflect SE. Arbitrary lines were used to connect the points. **(B)** Final absorbance values were determined from the experiments in **(A)** and mean values and SE are plotted.

To determine the role of the α C-domain in the Zn^{2+} effect on clot formation, fragment X was used in place of Fg (Collet et al., 2005). At 5 μ M, Zn^{2+} significantly accelerated the clotting of Fg and fragment X by 1.5- ($p < 0.001$), and 1.3-fold ($p = 0.04$), respectively, (Figure 4), suggesting that the effect of Zn^{2+} on clot time is attenuated with fragment X. Although Zn^{2+} increased the absorbance of Fg clots by 2-fold ($p < 0.001$), the absorbance of fragment X clots was increased by only 1.2-fold ($p = 0.6$) (Figure 4, inset). Therefore, modulation of clotting and clot structure by Zn^{2+} appears to depend, at least in part, on the presence of the α C-domain of Fg.

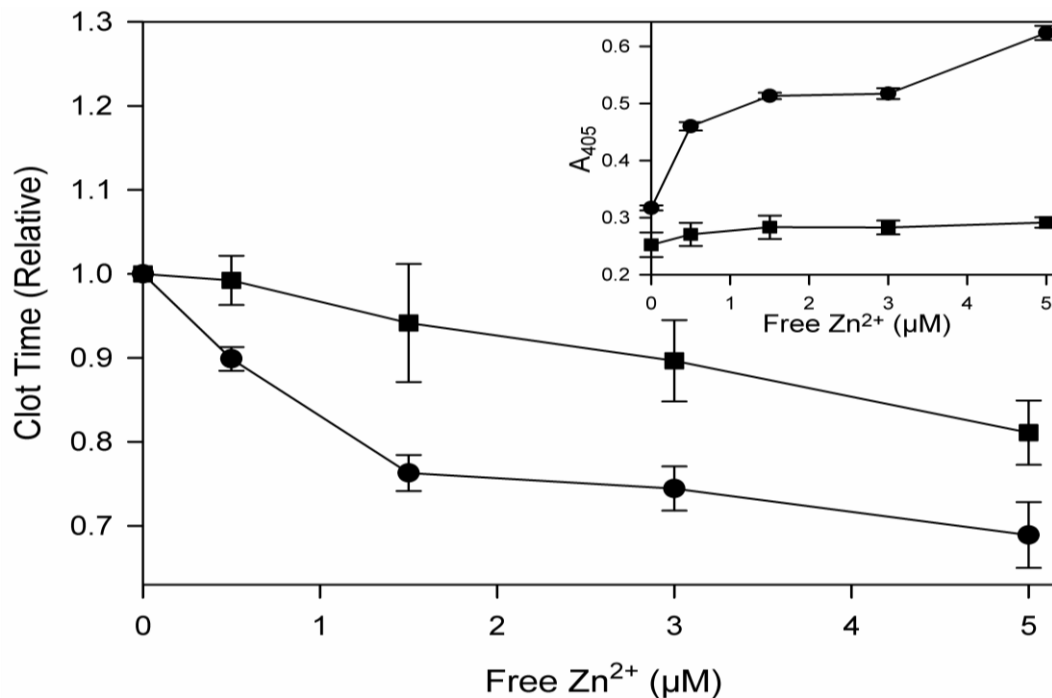


Figure 4. Comparison of the effect of Zn²⁺ on clotting of Fg and fragment X

Samples containing 3 µM Fg (*circles*) or fragment X (*squares*) and 2 mM CaCl₂ were clotted with 0.5 nM thrombin in the presence of 0-5 µM free Zn²⁺. Clot times were determined by monitoring absorbance at 405 nm, and values measured in the presence of Zn²⁺ were normalized relative to that determined in its absence. Initial clot times in the absence of Zn²⁺ were 476.2 ± 24.9 and 422.7 ± 67.9 s for Fg and fragment X, respectively. Final absorbance values were determined as above and plotted (*inset*). Symbols represent the mean of three determinations each performed in duplicate, while the bars reflect SE. Arbitrary lines were used to connect the points.

3.8.3 Effect of Zn^{2+} on clot structure

The effect of Zn^{2+} on 3-dimensional clot structure was examined using SEM. Clots prepared by clotting Fg or Fg^{XIII} with thrombin in the absence or presence of 5 μ M free Zn^{2+} were imaged at 30,000x magnification (Figure 5). Nested three-way analysis of variance indicated significant additional variation in Fn fiber diameter between images taken from the same clot ($p < 0.0001$) and in fiber diameters between clots ($p < 0.0001$), suggesting that the most appropriate statistical approach would be to use “clot” as the unit of analysis by firstly averaging all Fn fiber diameter measurements for a clot (giving 3 data points per condition). Comparisons between conditions were then based on the average of the 3 clot means per group and the pooled inter-clot SD of mean diameter. There was no significant interaction between the effects of Zn^{2+} and those of FXIII ($p = 0.18$) so that the results in all of the clots formed with Zn^{2+} or FXIII could be compared with those in all of the clots formed without Zn^{2+} or FXIII. Zn^{2+} had a strong effect on Fn fiber diameter ($p < 0.001$), increasing it by 2-fold (mean increase 0.069 μ m, 95% confidence interval 0.057 to 0.080). In contrast, FXIII had a non-significant effect on fiber diameter ($p = 0.20$, mean increase 0.006 μ m, 95% confidence interval -0.056 to 0.043); results that diverge from those of a previous study, which reported thinner fibers in the presence of FXIII (Hethershaw et al., 2014). Therefore, based on our findings, the Zn^{2+} -dependent increase in Fn fiber diameter is independent of FXIII. Because Zn^{2+} increases

fiber diameter and changes overall clot structure, studies were done to examine the effect of Zn^{2+} on the porosity of Fn clots.

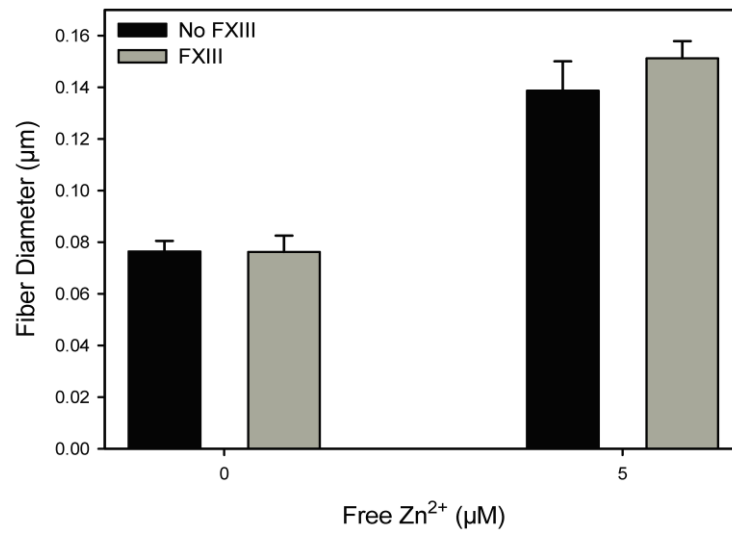
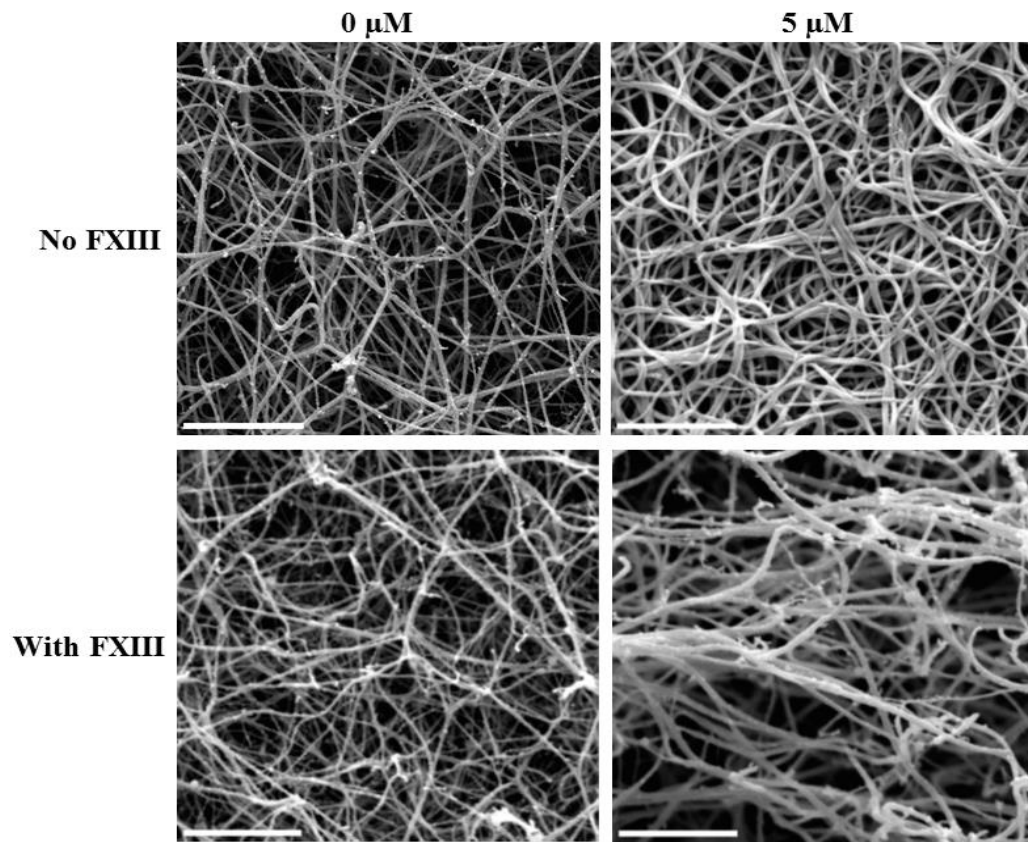


Figure 5. SEM of Fn clots formed in the absence or presence of Zn²⁺ and FXIII

Aliquots of 3 μM Fg containing **(A, B)** or lacking **(C, D)** FXIII were clotted with 10 nM thrombin in the presence of 2 mM CaCl₂ and in the absence **(A, C)** or presence **(B, D)** of 5 μM free Zn²⁺. Clots were incubated in 100% humidity for 30 min at 37°C prior to SEM analysis at a magnification of 30,000x. In all images the bar represents 2 μm . **(E)** Fiber diameters were quantified from the micrographs. The bars represent the mean values for 3 clots, imaged 5 times per clot, and lines above the bars reflect the inter-clot SD. The effect of Zn²⁺ on Fn fiber diameter was significant ($p < 0.001$), whereas neither the effect of FXIII nor the interaction of Zn²⁺ and FXIII was significant ($p = 0.20$ and $p = 0.18$, respectively).

3.8.4 Effect of Zn²⁺ on clot porosity

Clots formed with Fg yielded $K_s \pm SD$ values of $5.5 \pm 1.5 \times 10^{-12}$ and $1.9 \pm 0.5 \times 10^{-11} \text{ cm}^2$ in the absence or presence of Zn²⁺, respectively, whereas those formed with Fg^{XIII} had $K_s \pm SD$ values of $5.1 \pm 1.1 \times 10^{-12}$ and $2.4 \pm 0.2 \times 10^{-11} \text{ cm}^2$, in the absence or presence of Zn²⁺, respectively. Thus Zn²⁺ evoked a ~30-fold increase in clot porosity ($p=0.03$), and there was no significant effect of FXIII on porosity ($p=0.7$).

3.8.5 Effect of Zn²⁺ on clot rheology

Clots were formed by incubating 9 μM Fg or Fg^{XIII} with thrombin in the absence or presence of Zn²⁺ between the Peltier plate and cone geometry of the rheometer for viscoelasticity analysis. G' , G'' , and δ were continuously monitored in the time sweep phase to assess overall stiffness and rigidity as the clots formed. The storage modulus reached a plateau of $127.6 \pm 18.6 \text{ Pa}$ at about 2000 s in the absence of FXIII and Zn²⁺ (Figure 6A, Table 1). In the presence of FXIII, the storage modulus increased more slowly to $414.8 \pm 26.5 \text{ Pa}$; a value 3.3-fold higher ($p<0.001$) than that determined without FXIII (Figure 6B, Table 1). Thus, as shown previously, FXIII enhances the elastic properties of Fn, rendering the clots more rigid (Kurniawan et al., 2014).

In the presence of increasing concentrations of Zn²⁺, the time during which the storage modulus increased was accelerated, corresponding to faster clotting as observed by absorbance. However, the final storage modulus showed a

progressive decrease with increasing Zn^{2+} concentrations. This was observed in both the absence and presence of FXIII, resulting in a significant ($p < 0.001$) 10- and 8.5-fold reduction in the storage modulus for Fg and Fg^{XIII} clots, respectively, at 5 μM free Zn^{2+} (Figure 6C, Table 1). The amount of energy dissipated from the clot during deformation, known as the loss modulus, decreased significantly ($p < 0.001$) in a concentration-dependent manner, up to 6.5- and 2.6-fold with Fg and Fg^{XIII} clots, respectively, at 5 μM Zn^{2+} (Figure 6D, Table 1). The storage and loss moduli values were used to calculate the loss tangent, which is the ratio of energy dissipated to energy stored in a cyclic deformation. Zn^{2+} increased δ significantly ($p < 0.001$) by 2- and 3.5-fold with Fg and Fg^{XIII} clots, respectively (Table 1). Because the overall effects of Zn^{2+} on the mechanical properties of clots were similar in the absence and presence of FXIII, these data confirm the results of the absorbance studies and suggest that the capacity of Zn^{2+} to modulate clot structure is independent of FXIII.

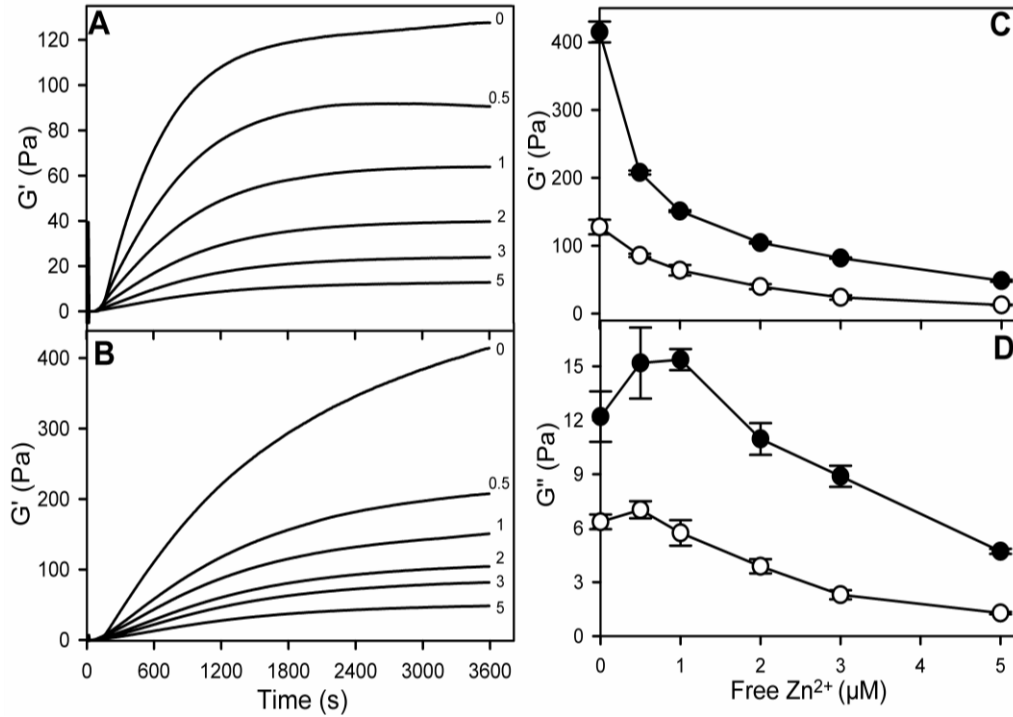


Figure 6. Effect of Zn²⁺ on the rheological behavior of clots formed in the absence or presence of FXIII

Clots were formed in a rheometer by incubating 9 μM Fg with 5 nM thrombin, 2 mM CaCl₂, and 0-5 μM free Zn²⁺ in the absence (A) or presence of FXIII (B). G' and G'' values at 1 h were averaged from the three sets of data and plotted (circles) without (open) and with (closed) FXIII.

Free Zn ²⁺ (μM)	No FXIII			With FXIII		
	G' (Pa)	G'' (Pa)	δ (Pa)	G' (Pa)	G'' (Pa)	δ (Pa)
0	127.6 ± 18.6	6.4 ± 0.7	0.05 ± 0.003	414.8 ± 26.5	12.2 ± 2.4	0.03 ± 0.006
0.5	90.6 ± 12.5*	7 ± 0.8	0.08 ± 0.005**	207.9 ± 5.2**	15.2 ± 3.4	0.07 ± 0.02*
1	63.8 ± 13.4**	5.7 ± 1.2	0.09 ± 0.007**	151 ± 2.3**	15.4 ± 1	0.1 ± 0.007**
2	39.7 ± 6.4**	3.9 ± 0.7*	0.1 ± 0.004**	104.4 ± 2.4**	11 ± 1.5	0.1 ± 0.01**
3	23.9 ± 5.6**	2.3 ± 0.4**	0.1 ± 0.006**	81.8 ± 1.4**	8.9 ± 1	0.1 ± 0.01**
5	12.8 ± 0.8**	1.3 ± 0.1**	0.1 ± 0.004**	48.5 ± 2.6**	4.7 ± 0.2*	0.1 ± 0.01**

Table 1. The influence of Zn²⁺ and FXIII on the mechanical properties of clots

Clots were formed by incubating 9 μM Fg or Fg^{XIII} with 5 nM thrombin, 2 mM CaCl₂, and 0-5 μM free Zn²⁺. The mean storage and loss modulus, loss tangent ratio and SD were determined at 3605 s from three separate experiments. Statistical significance was determined as p<0.05 (*) or p<0.001 (**).

Once the clots were formed, a sweep of frequency oscillations of up to 10 rad/s was applied to measure clot stability (Weisel, 2004a). Despite differing storage modulus values, no changes in the storage modulus with respect to frequency were observed with clots prepared in the absence or presence of Zn^{2+} or FXIII (Figure 7A, Table 2). This finding suggests that clots generated in the presence of Zn^{2+} remain stable upon perturbation despite the differences in clot structure.

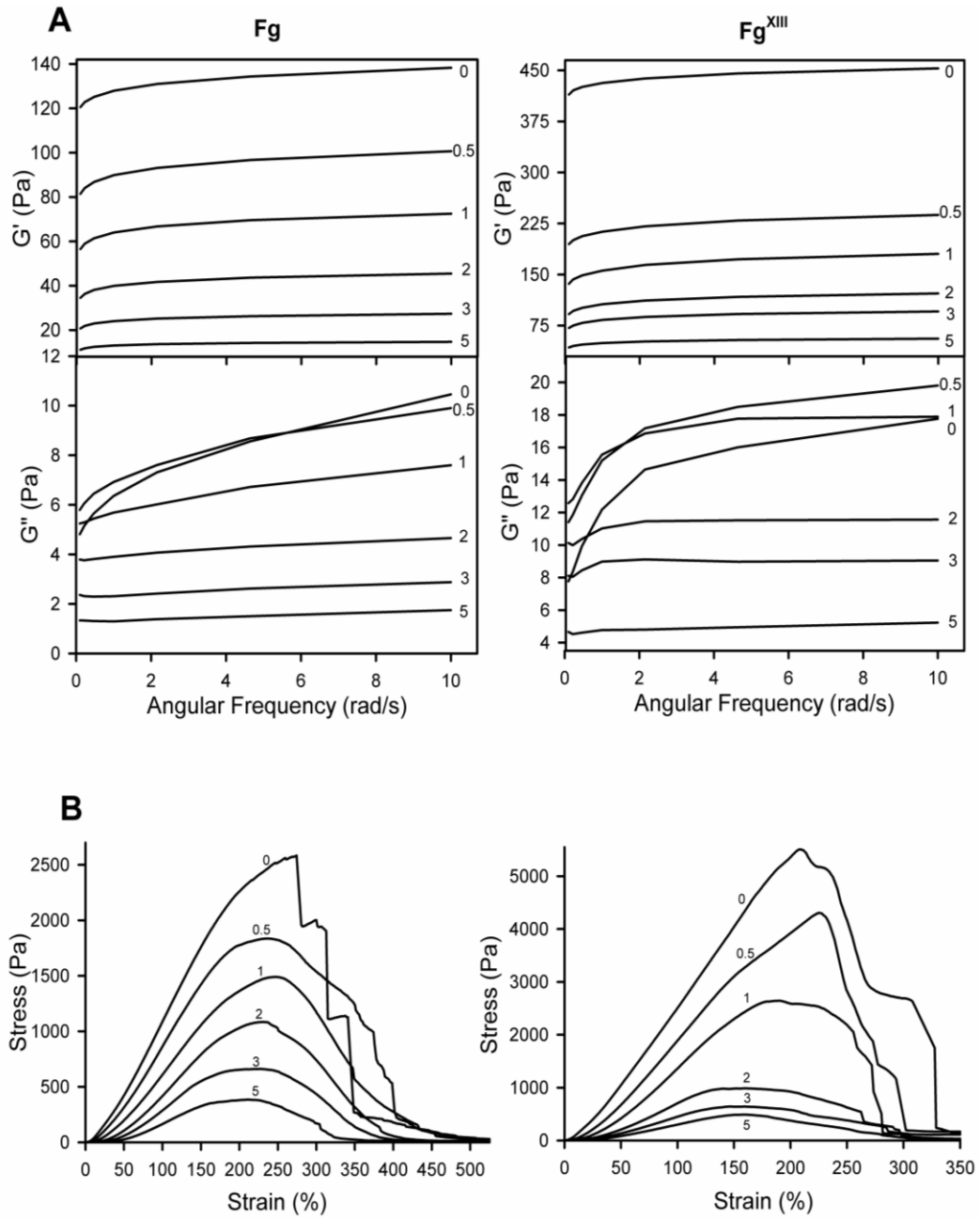


Figure 7. Effect of Zn^{2+} and FXIII on clot stability and rupture

(A) Clots from Figure 6 were perturbed with increasing forces to determine changes in G' or G'' . **(B)** After perturbation, the clots were compacted by increasing strain until the fibers broke causing the clots to rupture. Each plot represents the means of the three sets of data.

Free Zn ²⁺ (μ M)	No FXIII		With FXIII	
	G' (Pa; 0.1 rad/s)	G' (Pa; 10 rad/s)	G' (Pa; 0.1 rad/s)	G' (Pa; 10 rad/s)
0	120.5 \pm 19.1	138.3 \pm 21.9	414.3 \pm 31.1	452.8 \pm 35.9
0.5	81.4 \pm 12.3	100.6 \pm 14.6	194.8 \pm 8.3	237.7 \pm 3
1	56.5 \pm 12.1	72.5 \pm 15	136.3 \pm 3.3	180.3 \pm 2
2	34.5 \pm 5.4	45.5 \pm 7.4	91.8 \pm 1.3	122.2 \pm 4.1
3	20.8 \pm 5	27.4 \pm 6.2	71.4 \pm 2	95.7 \pm 2.5
5	11.1 \pm 0.6	14.7 \pm 0.6	42.8 \pm 3	55.9 \pm 2.6

Table 2. The effect of Zn²⁺ on clot stiffness under perturbation

Clots were formed under the same conditions as in Table 1. After formation, clots were perturbed with an initial frequency of 0.1 rad/s, and increased to maximal perturbation at 10 rad/s. The storage modulus and SD were determined for three individual experiments with varying Zn²⁺ concentrations.

By shearing Fn clots, the strain or deformation of the elastic network can be quantified. Thus, when torque is applied, the fibers become compacted because they are pulled apart, as demonstrated in the ascending phase of Figure 7B. As the network is stretched further, individual fibers begin to break until the clot is no longer able to support any additional stress (peak phase) and it then collapses (descending phase). In the ascending phase, more strain was required to reach a given level of stress in clots formed in the presence of Zn^{2+} compared with those formed in its absence, consistent with thicker fiber formation (Figure 7B). This is in agreement with the SEM and absorbance data, which indicate that Zn^{2+} increases fiber diameter because larger fibers of the same density and structure will require more force to strain than smaller ones. However, peak stress values decreased with increasing concentrations of Zn^{2+} (Figure 7B). In the descending phase, clots deformed in the presence of Zn^{2+} , but did not fully rupture, as evidenced by broadening of the descending phase. This suggests that Zn^{2+} renders clots more fluid-like, and less susceptible to rupture. The same Zn^{2+} phenomenon was observed in the presence of FXIII (Figure 7B), even though the initial stiffness of fibers formed in the presence of FXIII was greater than that of fibers formed in its absence.

3.9 DISCUSSION

Previous studies suggest that Zn^{2+} and other divalent ions accelerate clot formation by enhancing Fn assembly, resulting in increased fiber thickness (Carr

and Powers, 1991; Fatah and Hessel, 1998; Kanaide et al., 1982; Marx et al., 1987; Marx and Eldor, 1985; Suzuki and Hashimoto, 1976). However, no mechanism for this effect has been elucidated. In the current study, we confirm that Zn^{2+} accelerates Fn clot formation and increases fiber diameter both in the absence and presence of FXIII. Clots formed in the presence of Zn^{2+} are less stiff than those formed in its absence, are resistant to perturbation by mechanical forces and are more porous. Therefore, although FXIII promotes clot stiffness by compacting the Fn fibers, Zn^{2+} counters the effect of FXIII, such that cross-linked fibers remain in a more fluid-like state, possibly rendering clots more tolerant of deformation and less susceptible to rupture.

Cross-linking by FXIII is a critical determinant of the viscoelastic properties of Fn, and renders clots mechanically stronger by compacting the fibers (Schroeder and Kohler, 2013). This concept is supported by the bleeding diathesis and impaired wound healing exhibited by patients with congenital FXIII deficiency (Levy and Greenberg, 2013). Cross-linking of the α - and γ -chains of Fn increases clot stiffness and provides resistance to fibrinolysis (Bagoly et al., 2012; Hethershaw et al., 2014). However, stiff clots are more prone to rupture and embolization. Therefore, a balance between clot stiffness and elasticity is critical. Consequently, substances such as Zn^{2+} that modify the effect of cross-linking will impact on this balance.

Clot structure can be altered in several ways, including by changing the thrombin, Fg, and ion concentrations and by altering flow dynamics (Ryan et al., 1999). Therefore, local conditions can influence the size of the Fn fibers that are formed, and will impact on whether the fibers are densely or loosely distributed. Dense Fn clots composed of thin fibers are more rigid and brittle compared with porous soft clots containing loosely packed, thick fibers. Thus, with the same applied stress, stiff clots with a higher storage modulus will undergo less deformation and rupture more than soft clots (Weisel, 2007). These mechanical properties are particularly important for clots that form in the high shear environment of the arterial system. Zn^{2+} will be abundant in platelet-rich arterial thrombi because of its release from activated platelets (Henderson et al., 2015a).

We show that Zn^{2+} serves as a natural clot stabilizer because it offsets the rigidity induced by FXIII-mediated cross-linking by delaying the onset of strain stiffening of the clots. This is an important advantage because the balance between the elastic deformation and rupture of Fn networks determines in part whether clots remain intact and occlude major vessels or undergo fragmentation and subsequent embolization (Weisel, 2004).

Zn^{2+} participates in numerous hemostatic mechanisms, yet it is unclear how it modifies Fn structure. Because it affects clotting in the absence of thrombin, Zn^{2+} must exert its effect on Fn. Zn^{2+} binds to Fg at numerous sites; one in particular is in the α C-domain (Fredenburgh et al., 2013). Thus, histidine

residues 544 and 545 constitute a Zn^{2+} -dependent heparin-binding site that attenuates heparin-dependent thrombin inhibition by antithrombin (Fredenburgh et al., 2013). By examining clot formation with fragment X, we show that this Zn^{2+} -binding site is a likely candidate for altering fiber thickness. The Zn^{2+} effect on clot absorbance is abrogated with removal of the α C-domain, which is known to enhance lateral aggregation of protofibrils, thereby generating thick fibers with large pores (Collet et al., 2005). Consistent with this concept, histidine residues on Fg have been implicated in the regulation of Fn monomer polymerization (Fatah and Hessel, 1998). Although Fg binds Ca^{2+} and numerous other divalent cations, the Zn^{2+} binding site in the α C-domain may be particularly important because Zn^{2+} affects clot formation more than other positively charged ions (Carr and Powers, 1991; Kanaide et al., 1982). Therefore, by binding to Fg, Zn^{2+} may have important structural and functional roles in Fn formation and stabilization.

The current study demonstrates that Zn^{2+} modifies clot structure, and softens the stiffening that results from FXIII-mediated cross-linking. This modification in structure and pore size may facilitate the passage of plasma components into the interstices of the clot, thereby promoting clot maturation and subsequent fibrinolysis. Any enhancement of fibrinolysis via this mechanism will be offset, at least in part, by the fact that, independent of clot structure, Zn^{2+} slows fibrinolysis by attenuating plasminogen activation and Fn degradation by plasmin (Henderson et al., 2015a). Therefore, Zn^{2+} has competing effects on clot

formation and degradation via distinct mechanisms. These results provide additional evidence that Zn^{2+} serves as a dynamic modulator of numerous reactions in hemostasis, and contributes to the localized, rather than systemic, response to perturbation. They also suggest that ionic conditions should be considered when evaluating the effects of FXIIIa on clot properties.

3.10 AKNOWLEDGEMENTS

We would like to thank Iqbal Jaffer for blood collection, Marcia Reid for processing the SEM samples, and Professor Robin Roberts for help with the statistical analyses.

CHAPTER 4: ZINC DELAYS CLOT LYSIS BY ATTENUATING PLASMINOGEN ACTIVATION AND PLASMIN-MEDIATED FIBRIN DEGRADATION

4.1 Forward

The effect of Zn^{2+} on clot lysis is described in this manuscript. We demonstrated that Zn^{2+} is a dual mechanistic modulator of fibrinolysis, as it targets Pg activation and Pn-Fn hydrolysis to attenuate clot lysis. This suggests that the role of Zn^{2+} on fibrinolysis is independent of its effects on clotting, and changes in clot structure.

4.2 Objective: Identify fibrinolytic reactions that are influenced by Zn^{2+}

Uncovering mechanisms that are influenced by Zn^{2+} in clot lysis, may contribute to the advancements of new targets for thrombolytic therapy. Previous studies suggest that Zn^{2+} inhibits fibrinolysis by binding to Fg, and alters Fn clot structure (Marx et al., 1987; Marx, 1988c; Tubek et al., 2008; Vu et al., 2013). However, these studies lack mechanistic evidence to support this concept. The aim of this study was to identify components in fibrinolysis that are modulated by Zn^{2+} . Because Zn^{2+} affects tPA and Pn activity in the absence of Fg and Fn, we hypothesized that Zn^{2+} will modulate the fibrinolysis pathway at multiple levels (Vu et al., 2013). In order to test this hypothesis, the following reactions in the absence and presence of Zn^{2+} were assessed: **(A)** Zn^{2+} -binding to fibrinolytic zymogens and proteases, **(B)** Pg activation by tPA and uPA in the absence and

presence of Fg and Fn, **(C)** degradation of the α -chain on Fg by Pn and trypsin, and **(D)** clot lysis times in buffer and in plasma systems. These objectives were established to shed light on the dynamic role of Zn^{2+} regulation on the fibrinolysis pathway.

Zinc Delays Clot Lysis by Attenuating Plasminogen Activation and Plasmin-mediated Fibrin Degradation

Sara J. Henderson^{1,2}, Alan R. Stafford^{1,3}, Beverly A. Leslie^{1,3}, Paul Y. Kim^{1,3},
Nima Vaezzadeh^{1,4}, Ran Ni^{1,4}, James C. Fredenburgh^{1,3} and Jeffrey I. Weitz^{1,4†}

Thrombosis and Atherosclerosis Research Institute¹ and the Departments of
Biochemistry and Biomedical Science² and Medicine³ and Medical Sciences,⁴
McMaster University, Hamilton, Ontario, Canada

Running title: Zinc attenuates plasminogen activation and fibrin clot lysis

Footnotes: This work was supported in part by the Canadian Institutes of Health Research and the Heart and Stroke Foundation. J.I.W. holds the Heart and Stroke Foundation J. Fraser Mustard Endowed Chair in Cardiovascular Research and the Canada Research Chair (Tier 1) in Thrombosis.

Address Correspondence: Jeffrey I. Weitz, Thrombosis and Atherosclerosis Research Institute, 237 Barton Street East, Hamilton, ON, L8L 2X2. Tel: 905-521-2100 ext. 40721, e-mail: weitzj@taari.ca

Authorship Contributions: SJH coordinated the study, performed experiments, and wrote the paper. ARS performed experiments in Figure 3. BAL purified Fg required for the study. PYK provided assistance in kinetic analysis. NV and RI assisted in platelet isolation. JCF contributed to experimental design, analysis of all data, assisted in writing the manuscript. JIW provided insights on experimental design, writing of the manuscript, and had final approval for publication.

* **This manuscript is published in *Thrombosis and Haemostasis*: Thromb Haemost. 2015 Jun;113(6):1278-88. doi: 10.1160/TH14-09-0771. Epub 2015 Mar 19. This chapter is not a direct representation of the above referenced manuscript. All copyrights to the manuscript are effective as the manuscript is published in *Thrombosis and Haemostasis* ©. Schattauer policy states that no copyright permission is necessary from original authors posting an accepted version of their manuscript for uploading it to institutional and/or centrally organized repositories.**

References: References for this manuscript have been incorporated into the Bibliography (Chapter 10), at the end of this thesis.

4.3 WHAT IS KNOWN

- Zn^{2+} is an abundant metal ion that circulates in plasma where it is mostly protein-bound.
- Activated platelets release Zn^{2+} , thereby increasing local concentrations.
- Although Zn^{2+} modulates numerous hemostatic interactions, its role in fibrinolysis is poorly defined.

4.4 WHAT THIS PAPER ADDS

- Zn^{2+} binds tissue-type plasminogen activator and plasmin with high affinity and attenuates their activities.
- Zn^{2+} inhibits lysis of fibrin and plasma clots.

4.5 SUMMARY

By inhibiting plasminogen activation and fibrin degradation, release of zinc from platelets may attenuate fibrinolysis and promote clot stability. Zinc circulates free in plasma at a concentration of 0.1-2 μM , but its levels increase locally when it is released from activated platelets. Although zinc influences many processes in hemostasis, its effect on fibrinolysis has not been thoroughly investigated. Using a fluorescent zinc-binding probe, we demonstrated that zinc binds tissue-type plasminogen activator (tPA) and plasmin with high affinity (K_d values of 0.2 μM), and surface plasmon resonance studies revealed that zinc binds fibrin with a K_d of 12.8 μM . Zinc had no effect on the affinity of plasminogen or plasmin for fibrin, but increased the affinity of tPA by 2-fold. In the presence of 5 μM zinc, the catalytic efficiency of plasminogen activation by tPA was reduced

by approximately 2-fold, both in the absence or presence of fibrin. Zinc attenuated plasmin-mediated degradation of the fibrinogen alpha-chain by 43%, but had no effect on trypsin degradation. tPA-mediated fibrin clot lysis was prolonged 2.5-fold by zinc in a concentration-dependent fashion, and tPA-mediated plasma clot lysis was attenuated by 1.5-fold. Therefore, our data indicate that zinc modulates fibrinolysis by attenuating tPA-mediated plasminogen activation and plasmin-induced fibrin degradation. These findings suggest that local release of zinc by platelets attenuates fibrinolysis.

4.6 INTRODUCTION

Hemostasis, the arrest of bleeding, requires rapid hemostatic plug formation to seal leaks in injured blood vessels. Fibrin (Fn), the major protein component of hemostatic plugs, endows them with structural integrity. Fn is formed when tissue factor exposed at the site of injury initiates clotting and triggers thrombin generation. Thrombin binds to fibrinogen (Fg) and releases fibrinopeptides A and B, thereby generating Fn monomers. Fn monomers polymerize into protofibrils, which then aggregate laterally to form the Fn clot (Collet et al., 1996).

Once its barrier function has been served, the Fn clot must be degraded to restore vascular integrity in a process known as fibrinolysis, which is essential for wound healing. Fibrinolysis is initiated by the release of tPA from the damaged vessel wall (Levin et al., 1984; Sappino et al., 1991). tPA converts plasminogen

(Pg) to plasmin (Pn), and Fn serves as a template onto which tPA and Pg assemble (Schaller and Gerber, 2011). Therefore, hemostasis depends on coordination between Fn formation and degradation.

After iron, zinc (Zn^{2+}) is the next most abundant metal in the body (Tubek et al., 2008). Zn^{2+} is an important cation because of its involvement in cellular metabolism, protein stability and enzyme catalysis (Tubek et al., 2008). The total Zn^{2+} concentration in human plasma is 10-20 μM , but most is bound weakly to albumin and α_2 -macroglobulin, leaving 0.1-2 μM Zn^{2+} in a free, unbound state (Gorodetsky et al., 1993; Lu et al., 2008; Whitehouse et al., 1982). However, Zn^{2+} concentrations are not static because activated platelets release stored Zn^{2+} (Marx et al., 1993). As a result, the local Zn^{2+} concentration increases at sites of injury to levels that support activation of the plasma kallikrein system (Rojkjaer and Schmaier, 1999).

The role of Zn^{2+} in hemostatic reactions has often been overlooked because blood is usually collected into citrate, which not only binds calcium, but also Zn^{2+} . Although calcium is added back when evaluating clotting reactions, only a few studies have examined the effect of Zn^{2+} addition. Zn^{2+} binds Fg and shortens the thrombin clot time in a concentration-dependent fashion (Marx, 1988c; Marx and Eldor, 1985). This phenomenon is unlikely to be the result of altered thrombin activity because the rate of fibrinopeptide release is not accelerated in the presence of Zn^{2+} (Marx and Hopmeier, 1986). Instead, Zn^{2+}

appears to modulate Fn structure because Fn fibers formed in the presence of Zn^{2+} are thicker than those formed in its absence (Fredenburgh et al., 2013; Hopmeier et al., 1990; Marx et al., 1987; Marx, 1988c; Marx and Eldor, 1985). Although formation of thicker fibers may accelerate Fn degradation, the effects of Zn^{2+} on the reactions of fibrinolysis are poorly defined. To address this gap, we quantified the amount of Zn^{2+} released from activated platelets, measured the affinity of the fibrinolytic proteins for Zn^{2+} , and examined the effect of Zn^{2+} on (A) Pg activation by tPA and urokinase-type plasminogen activator (uPA), (B) Fg degradation, and (C) Fn clot lysis in buffer and plasma systems.

4.7 EXPERIMENTAL PROCEDURES

4.7.1 Reagents

D-Val-Leu-Lys-p-nitroaniline (D-VLK-pNA) was purchased from Molecular Innovations (Novi, MI), whereas S-2390 and S-2444 were from Chromogenix (Mölndal, Sweden), and CS 05(88) and CS 31(02) were from Biophen (Neuville, France). The fluorescent Zn^{2+} -binding probe FluoZin-1 was from Life Technologies (Burlington, ON). Human Fg (FIB 1) and α -thrombin were obtained from Enzyme Research Laboratories (South Bend, IN). Fg was depleted of factor XIII by affinity chromatography (Fredenburgh et al., 2008), and the fraction with an intact α -chain was selected by ammonium sulfate precipitation as described (Walker and Nesheim, 1999). Thrombin was dialyzed into 20 mM Tris, pH 7.4, 150 mM NaCl (TBS) to remove citrate. Pn was

purchased from Haematological Technologies Inc. (Essex Junction, VT). Collagen reagent HORM suspension was purchased from Nycomed (Linz, Austria) and prostaglandin E₁ was from Sigma Aldrich. Active site-blocked Pn was prepared by incubating Pn with a 10-fold molar excess of Val-Phe-Lys-chloromethyl ketone (VFK; EMD Millipore, San Diego, CA), followed by dialysis into 20 mM HEPES, pH 7.4, 150 mM NaCl (HBS). Trypsin was purchased from Cooper Biomedical Inc. (Malvern, PA). Glu-Pg was isolated from plasma and Lys-Pg was prepared as previously described (Kim et al., 2012; Stewart et al., 1998). Recombinant low-molecular-weight two-chain uPA was kindly provided by Dr. Jack Henkin (Abbott Laboratories, North Chicago, IL). Recombinant single-chain tPA was a gift from Dr. Bruce Keyt (Genentech Inc., South San Francisco, CA).

Experiments were performed in 10 mM Tricine, pH 7.4, 150 mM NaCl containing 0.01% Tween 20 (TcBS) unless indicated otherwise. Tricine serves as a Zn²⁺ buffering system, which maintains the free Zn²⁺ concentration at a constant level even in the presence of Zn²⁺-binding proteins (Low et al., 2000). We confirmed that the ratio of free to total Zn²⁺ in TcBS in the absence of Tween 20 is ~1:100 by first monitoring the fluorescence of 500 nM FluoZin-1 in TBS using a LS 50B fluorescence spectrometer (Perkin Elmer, Woodbridge, ON) with excitation and emission wavelengths of 495 and 525 nm, respectively, excitation and emission slit widths of 10 and 3.5 nm, and no emission filter (Low et al.,

2000). The titration was performed in a 10 x 10 mm quartz cuvette that was maintained at 25°C using a circulating water bath and mixed with a magnetic stir bar. Fluorescent intensity (I) was monitored as the sample was titrated with aliquots of 1 mM ZnCl₂ and I values were plotted *versus* the Zn²⁺ concentration. The titration was then repeated in TcBS in the absence of Tween 20, and the standard curve in TBS was used to determine the free Zn²⁺ concentrations from I values. A second plot of free Zn²⁺ *versus* total Zn²⁺ was used to prepare solutions with the desired free Zn²⁺ concentrations.

4.7.2 Quantification of Zn²⁺ within and released from activated platelets

After obtaining consent, 50 ml of blood was collected into acid citrate dextrose (9:1 vol/vol) from each of 3 healthy volunteers and subjected to centrifugation at 200 x g for 20 min at 23°C to generate platelet-rich plasma. To 25 ml of plasma was added 1 μM prostaglandin E₁ and the platelets were then pelleted by centrifugation at 1000 x g for 10 min at 23°C. After washing the pellet with Tyrode's salt solution lacking CaCl₂, but containing 1 μM prostaglandin E₁, the sample was again subjected to centrifugation at 1000 x g for 10 min and the washed pellet was suspended in a final volume of 5 ml Tyrode's salt solution lacking CaCl₂. Using a hemocytometer, the mean platelet count of the concentrate was obtained. To determine the total concentration of Zn²⁺ in platelets, a sample was subjected to centrifugation at 1000 x g for 10 min, and the pellet was sonicated for 5 min. Zn²⁺ concentrations were quantified by atomic absorption

spectroscopy (Varian 220FS, version 5.01 Pro). To determine the concentration of Zn^{2+} released from activated platelets, washed platelets were incubated with 10 nM thrombin and 20 μ g/ml collagen for 30 min at 37°C. After subjecting the sample to centrifugation at 1000 x g for 10 min to sediment the platelets, the supernatant was removed and Zn^{2+} concentrations were quantified.

4.7.3 Binding of Zn^{2+} to Fg, Fn, Glu-Pg, Lys-Pg, Pn, tPA, uPA and trypsin

The affinity of Zn^{2+} for proteins was determined using FluoZin-1 (Fredenburgh et al., 2013; Krezel et al., 2011). The initial fluorescence intensity (I_0) of 0.5 μ M FluoZin-1 and 5 μ M $ZnCl_2$ in TBS was determined as described above. Fluorescence was then monitored as the sample was titrated with aliquots of Fg, Glu- or Lys-Pg, Pn, tPA, uPA or trypsin. I/I_0 values were plotted *versus* the protein concentration and the data were subjected to nonlinear regression analysis of a rectangular hyperbola (Table Curve 2D, version 4, Jandel Scientific Software, San Rafael, CA) to determine the half maximal inhibitory concentration (IC_{50}). The IC_{50} value obtained was then corrected for the affinity of Zn^{2+} for FluoZin-1 to calculate the K_d value, using the Cheng-Prusoff equation by using a K_d of 32 μ M for Zn^{2+} binding to FluoZin-1, determined separately (Fredenburgh et al., 2013).

The affinities of Zn^{2+} for Fg and Fn were quantified using surface plasmon resonance (SPR) on a BIAcore T200 (GE Healthcare) (Fredenburgh et al., 2013). Using amine coupling, Fg in HBS containing 0.01% Tween 20 (HBS-Tw) was

immobilized on a CMD 50 I biosensor chip (XanTec Bioanalytics, Dusseldorf, Germany) to 10000 response units (RU). To convert immobilized Fg to Fn, 500 nM of thrombin was injected seven times for 3000 s into one flow cell. After washing, Zn^{2+} , in concentrations ranging from 0-26 μ M, was injected into the flow cells at a rate of 30 μ l/min. Flow cells were regenerated with 3.6% sodium citrate to remove Zn^{2+} . Sensorgrams of three runs were subjected to steady state kinetic analysis using the Biacore T200 Control Software (version 2.0) to quantify the maximal response units at equilibrium (R_{eq}). Plots of R_{eq} versus Zn^{2+} concentration were analyzed by nonlinear regression of a rectangular hyperbola to determine K_d values.

4.7.4 Effect of Zn^{2+} on chromogenic activity of Pn, tPA and uPA

The chromogenic activity of 15 nM Pn with 0-1000 μ M D-VLK-pNA or CS 31(02), or with 0-200 μ M S-2390 was determined in TcBS in the absence or presence of 2 μ M free $ZnCl_2$. Studies were performed in 96-well plates at 25°C with a final reaction volume of 100 μ l and absorbance was monitored at 405 nm for 5 min at 10 s intervals using a Thermomax plate reader (Molecular Devices, Sunnyvale, CA). Plots of rates versus the substrate concentration were subjected to nonlinear regression analysis to determine the V_{max} and K_m values using the Michaelis-Menten equation. The kinetic parameters for hydrolysis of 0-1400 μ M CS 05(88) by 50 nM tPA and 0-600 μ M S-2444 by 50 nM uPA were determined in a similar fashion.

4.7.5 Effect of Zn^{2+} on Pg activation

To determine the Zn^{2+} concentration dependence, activation of Glu- or Lys-Pg by tPA or uPA in the absence of a cofactor was assessed in wells of a 96-well plate using aliquots of a solution containing 1 μ M Glu-Pg or 0.5 μ M Lys-Pg and 400 μ M D-VLK-pNA in TcBS, in the absence or presence of free $ZnCl_2$ up to 5 μ M. Reactions with Glu-Pg were initiated by addition of 50 nM tPA or uPA, while those with Lys-Pg were initiated with 20 nM tPA or uPA. In all cases, the final volume was 100 μ l per well and temperature was maintained at 25°C. A_{405} was monitored at 10 s intervals for 45 min and slopes of the plots of absorbance *versus* time squared were calculated using SoftMax Pro (version 5.4). To quantify rates of Pn generation, slopes were divided by the specific activity of Pn for D-VLK-pNA, which was determined in a separate experiment to be 1.64 mOD/min/nM, and subsequently normalized relative to the value measured in the absence of Zn^{2+} . IC_{50} values for Zn^{2+} were calculated using nonlinear regression of a rectangular hyperbola.

To quantify the effect of Zn^{2+} on the kinetic parameters of Pg activation, experiments were repeated in the absence and presence of Fg or Fn by titrating Pg in the absence or presence of 5 μ M free Zn^{2+} . For studies in the absence of Fg cofactor, solutions containing 0-40 μ M Glu-Pg, 50 nM tPA, and 400 μ M D-VLK-pNA were prepared in the absence or presence of 5 μ M free $ZnCl_2$. Similar studies were done with 0-4 μ M Lys-Pg except that 20 nM tPA was used.

Experiments in the presence of 3 μM Fg were performed in a similar fashion, except with 0-10 μM Glu-Pg and 0.5 nM tPA, or 0-4 μM Lys-Pg with 2 nM tPA. For experiments with Fn, 3 μM Fg was clotted with 10 nM thrombin in the presence of 2 mM CaCl_2 , 400 μM D-VLK-pNA, 0-0.7 μM Glu-Pg or 0-0.6 μM Lys-Pg and 0.5 nM tPA. Absorbance was monitored at 405 and 450 nm for 140 min at 10 s intervals for experiments with Fn. To correct for turbidity, A_{corr} was calculated using $A_{405} - (1.7 \times A_{450})$ (Kim et al., 2012).

Rates of Pn generation were determined from plots of A_{corr} *versus* time squared and converted to k_{cat} values using the Pn chromogenic specific activity noted above, and the concentration of tPA (Kim et al., 2012). Rates of activation were plotted *versus* the concentration of Pg, and k_{cat} and K_m values were determined by nonlinear regression analysis of the Michaelis-Menten equation (Kim et al., 2012; Schneider and Nesheim, 2004). For activation experiments in the absence of Fg cofactor, catalytic efficiencies were determined by linear regression of the linear portions of the rate *versus* substrate concentration plots.

4.7.6 Effect of Zn^{2+} on the affinity of fibrinolytic proteins for Fg or Fn

The interaction of Glu-Pg, Lys-Pg, VFK-Pn, or tPA with immobilized Fg or Fn was assessed using SPR in the absence or presence of Zn^{2+} . Fg was immobilized to 4600 RU and converted to Fn as described above. Flow cells were washed with HBS-Tw containing 1 mM EDTA to remove all traces of Zn^{2+} . Aliquots containing 0-2500 nM Glu-Pg, 0-800 nM Lys-Pg, 0-750 nM VFK-Pn, or

0-2000 nM tPA in HBS-Tw containing 1 mM EDTA or 20 μ M ZnCl_2 were injected at a flow rate of 80 μ l/min. Between runs, flow cells were regenerated with 2 M NaCl, pH 7.4, containing 50 mM epsilon-aminocaproic acid and 50 μ M EDTA. R_{eq} values obtained from sensorgrams of each titration were normalized relative to the baseline values obtained without ligand and plotted *versus* the concentrations of titrated protein (Fredenburgh et al., 2013). K_d values were determined as described above.

4.7.7 Effect of Zn^{2+} on the conversion of single-chain tPA to two-chain tPA

Single-chain tPA (3 μ M) was incubated with 4 nM Pn at 23°C in the absence or presence of 12 μ M free ZnCl_2 in TcBS. At 10 min intervals, aliquots were collected and subjected to SDS-PAGE analysis on 4-15% polyacrylamide gels (Bio-Rad) in the presence of 1% SDS and 0.14 M β -mercaptoethanol to monitor the conversion of single-chain tPA to its two-chain form. Gels were stained with Coomassie Blue G250 (Bio-Rad, Hercules, CA) and imaged using Gel Dock (Bio-Rad). For densitometric analysis, mean peak intensities were calculated using Quantity One software (Bio-Rad, version 4.6.7) and normalized relative to the peak intensity of the control at time zero.

4.7.8 Effect of Zn^{2+} on Fg degradation by Pn or trypsin

Fg (3 μ M) was incubated with 10 nM Pn or 20 nM trypsin at 23°C in presence of 2 mM CaCl_2 and the absence or presence of 5 μ M free ZnCl_2 in TcBS. Aliquots taken at intervals were subjected to SDS-PAGE analysis under

reducing conditions, and gels were stained, imaged and analyzed as described above.

4.7.9 Clot lysis in a purified system

Aliquots of thrombin (10 nM) and 0.2 nM tPA or 2 nM uPA were placed separately in wells of a 96-well plate prior to addition of a solution containing 3 μM Fg, 1 μM Glu-Pg, 2 mM CaCl_2 , and 0-6 μM free ZnCl_2 in TcBS. A_{405} was monitored at 10 s intervals at 25°C and lysis times were defined as the time required for the maximum A_{405} to be reduced by 50%. Lysis times were plotted *versus* free Zn^{2+} concentrations and analyzed by nonlinear regression of a rectangular hyperbola. The experiment was then repeated using 18 nM Pn or 100 nM trypsin in place of Glu-Pg and tPA or uPA.

4.7.10 Clot lysis in plasma

Blood collected from the antecubital veins of healthy volunteers into EDTA blood collection tubes was subjected to centrifugation at 2100 x g for 10 min at 23°C to obtain platelet poor plasma. Plasma was harvested, pooled, and dialyzed against 5 changes of TBS to remove EDTA and Zn^{2+} . Zn^{2+} concentrations in plasma before and after dialysis were quantified using atomic absorption spectroscopy. For the lysis assays, 1 ml of plasma was preheated to 37°C, and diluted 3-fold with TcBS. After adding 50 μl aliquots to wells of a 96-well plate, reactions were initiated by addition of 50 μl of a solution that resulted in final concentrations of 5 nM thrombin, 15 mM CaCl_2 , 1.2 nM tPA and 0-15

μM free Zn^{2+} in TcBS. Absorbance at 350 nm was monitored in a plate reader at 10 s intervals at 37°C. Lysis times were determined as described above.

4.7.11 Statistical Analysis

Data are presented as mean \pm standard deviation (SD) unless noted otherwise. Significance of differences were determined by non-parametric methods using the Wilcoxon Rank Sum and Signed Rank Test, with a two-sided non-paired test with the statistical computing program R (version 3.0.1), or by one-way analysis of variance followed by Tukey's test for multiple pair-wise comparisons (SigmaPlot version 11.0). For all analyses, p-values less than 0.05 were considered statistically significant.

4.8 RESULTS

4.8.1 Quantification of Zn^{2+} in platelets and platelet releasate

A sample containing $1 \pm 0.2 \times 10^9$ washed platelets/ml had a Zn^{2+} concentration of $27 \pm 11.1 \mu\text{M}$. The concentration of Zn^{2+} in the releasate from a separate aliquot of platelets activated with thrombin and collagen was $14.4 \pm 1.4 \mu\text{M}$. Therefore, about half of the Zn^{2+} in platelets is released when platelets are activated. This represents $\sim 5 \mu\text{M}$ Zn^{2+} released by the equivalent number of platelets normally in blood, consistent with previous reports (Kiem et al., 1979; Mahdi et al., 2002). Therefore, when platelets are activated and aggregate at the site of injury, the local concentration of Zn^{2+} can increase above the 10-20 μM

reported in platelet-poor plasma (Gorodetsky et al., 1993; Lu et al., 2008; Whitehouse et al., 1982).

4.8.2 Affinity of Zn^{2+} for Fg, Glu-Pg, Lys-Pg, Pn, tPA, uPA and trypsin

The affinity of Zn^{2+} for various fibrinolytic proteins was determined using a fluorescent Zn^{2+} -binding probe (Fredenburgh et al., 2013; Krezel et al., 2011). The fluorescence of 0.5 μ M FluoZin-1 and 5 μ M $ZnCl_2$ was monitored throughout the titration with protein. Glu- and Lys-Pg titrations yielded non-saturable decreases, consistent with K_d values exceeding 100 μ M (data not shown). In contrast, titration with tPA or Pn resulted in a concentration-dependent and saturable decrease in fluorescence, indicating that Zn^{2+} bound tPA and Pn with K_d values of 0.2 ± 0.08 μ M and 0.2 ± 0.09 μ M, respectively (Table 1); values within the physiological range of 0.1 to 2 μ M free Zn^{2+} in plasma (Lu et al., 2008; Stewart et al., 2009; Vallee and Falchuk, 1993). Zn^{2+} bound uPA and trypsin with lower affinities; K_d values of 6.9 ± 0.9 and 30.1 ± 0.03 μ M (Fredenburgh et al., 2013). Using SPR, Zn^{2+} bound to immobilized Fg and Fn with K_d values of 9.3 ± 0.7 μ M and 12.8 ± 1.1 μ M, respectively. These findings indicate that Zn^{2+} binds numerous proteins in the fibrinolytic system.

Ligand	K_d (μM)
Fg	1.0 ± 0.3
Glu-Pg	NB
Lys-Pg	NB
Pn	0.2 ± 0.09
Trypsin	30.1 ± 0.03
tPA	0.2 ± 0.08
uPA	6.9 ± 0.9

Table 1. Affinity of Zn²⁺ for fibrinolytic proteins

The affinity of Zn²⁺ for each of the indicated fibrinolytic proteins was determined using a Zn²⁺-binding fluorophore. NB represents no binding to Zn²⁺. Values represent means ± SD of 3 separate determinations.

To examine the functional consequences of Zn^{2+} binding, we first assessed its influence on hydrolysis of chromogenic substrates. Zn^{2+} had no significant effect on the K_m or V_{max} values of tPA- or Pn-mediated hydrolysis of their respective chromogenic substrates (Supplementary Table 1). With uPA, the V_{max} was not affected; however Zn^{2+} increased the K_m value by 10%. Thus, Zn^{2+} had no effect on the chromogenic activity of Pn or tPA and only a minor effect on uPA chromogenic activity.

Reaction	V_{\max}		p-value	K_m		p-value
	-Zn ²⁺	+Zn ²⁺		-Zn ²⁺	+Zn ²⁺	
	<i>s</i> ⁻¹	<i>s</i> ⁻¹		μM	μM	
Pn + D-VLK-pNA	35.7 ± 0.1	35.0 ± 0.6	0.20	217.9 ± 3.2	243.8 ± 20.8	0.34
Pn + S2390	38.9 ± 2.4	34.8 ± 2.5	0.08	216.6 ± 16.7	190.0 ± 28.2	0.20
Pn + CS 31(02)	45.6 ± 7.1	43.8 ± 8.7	0.68	286.1 ± 40.9	276.3 ± 58.9	0.68
tPA + CS 05(88)	31.2 ± 5.0	27.2 ± 2.1	0.20	793.1 ± 183.2	789.3 ± 66.2	0.88
uPA + S2444	54.7 ± 0.8	53.3 ± 1.3	0.20	275.8 ± 2.1	305.0 ± 20.2	0.03

Supplementary Table 1. Effect of Zn²⁺ on Pn-, tPA- or uPA-mediated hydrolysis of chromogenic substrates

The chromogenic activity of 15 nM Pn or 50 nM tPA or uPA was determined using a range of concentrations of the indicated substrates in the absence or presence of 2 μM free Zn²⁺. V_{\max} and K_m values reflect the mean \pm SD of 4 determinations. The significance of differences between values measured in the absence and presence of Zn²⁺ was assessed using t-tests.

4.8.3 Effect of Zn^{2+} on Pg activation

Because Fg binds Zn^{2+} , the effect of this cation on Pg activation by tPA was initially examined in the absence of Fg. With increasing concentrations of Zn^{2+} , rates of Glu- and Lys-Pg activation decreased in a concentration-dependent fashion (Figure 1), with IC_{50} values for free Zn^{2+} of $2.1 \pm 0.6 \mu M$ and $1.6 \pm 0.3 \mu M$ ($p=0.13$), respectively. At $5 \mu M$ free Zn^{2+} , the catalytic efficiency values of activation of Glu- and Lys-Pg were reduced 1.8- and 2.2-fold respectively, compared with that in the absence of Zn^{2+} (Table 2). A similar response was observed when uPA was substituted for tPA, with IC_{50} values for free Zn^{2+} of $2.8 \pm 0.8 \mu M$ and $4.1 \pm 0.5 \mu M$, for Glu-Pg and Lys-Pg, respectively ($p=0.03$). These results indicate that Zn^{2+} attenuates Pg activation regardless of whether the activator binds Zn^{2+} with high affinity.

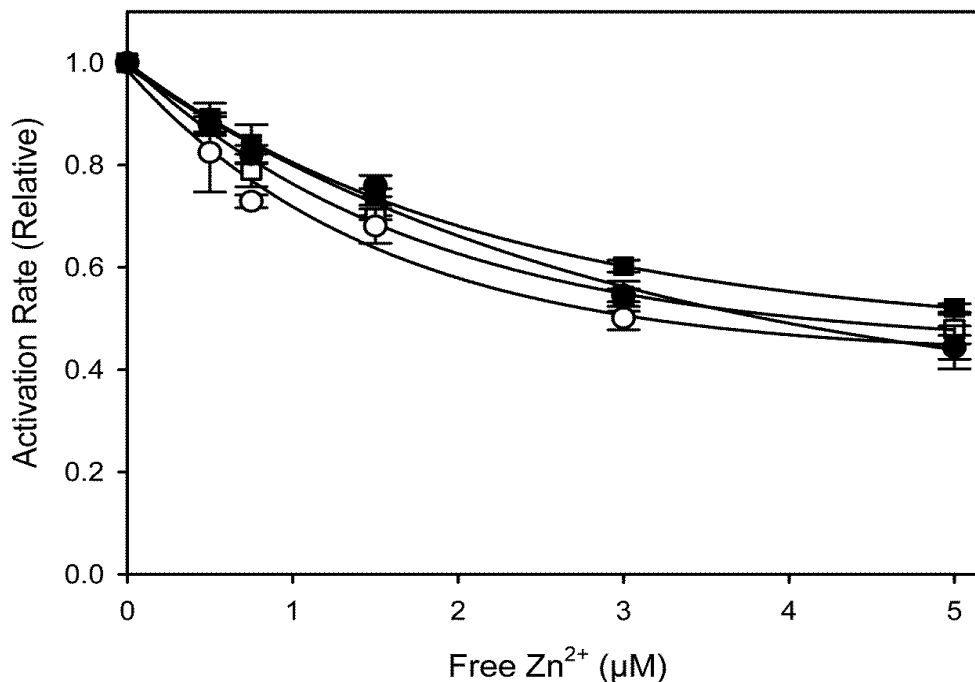


Figure 1. Effect of Zn²⁺ on activation of Glu-Pg or Lys-Pg by tPA or uPA

Activation of 1 µM Glu-Pg (*circles*) or 0.5 µM Lys-Pg (*squares*) by 50 nM tPA (*open*) or uPA (*closed*) was quantified in the absence or presence of Zn²⁺ at the indicated concentrations by monitoring the hydrolysis of D-VLK-pNA. Rates of Pg activation determined in the presence of Zn²⁺ were normalized relative to those measured in its absence. Data were analyzed by nonlinear regression analysis (*line*) to obtain IC₅₀ values. Symbols represent the mean of 3 experiments each done in duplicate, while the bars reflect the SD. Activation rates in the absence of Zn²⁺ were 0.34 ± 0.02, 1.64 ± 0.09, 2.48 ± 0.17, and 4.02 ± 0.05 nM/min for Glu-Pg/tPA, Glu-Pg/uPA, Lys-Pg/tPA, and Lys-Pg/uPA, respectively.

		No Zn ²⁺			With Zn ²⁺			
	Cofactor	K _m μM	k _{cat} s ⁻¹	CE (× 10 ⁻⁴) M ⁻¹ s ⁻¹	K _m μM	k _{cat} s ⁻¹	CE (× 10 ⁻⁴) M ⁻¹ s ⁻¹	CE Fold Change
Glu-Pg	None	N/A	N/A	0.009 ± 0.002	N/A	N/A	0.006 ± 0.001*	1.5
	Fg	4.0 ± 0.21	0.1 ± 0.01	2.5 ± 0.2	4.3 ± 0.5	0.05 ± 0.01*	1.1 ± 0.1*	2.3
	Fn	0.2 ± 0.02	0.008 ± 0.001	4.4 ± 0.2	0.2 ± 0.1	0.005 ± 0.001*	2.8 ± 0.8*	1.6
Lys-Pg	None	N/A	N/A	0.13 ± 0.008	N/A	N/A	0.06 ± 0*	2.2
	Fg	0.93 ± 0.12	0.03 ± 0.001	3.1 ± 0.4	0.99 ± 0.17	0.01 ± 0.001*	1.4 ± 0.2*	2.2
	Fn	0.06 ± 0.01	0.03 ± 0.001	49.7 ± 9.9	0.09 ± 0.003*	0.01 ± 0.001*	10.6 ± 0.6*	4.7

Table 2. The effect of Zn²⁺ on the kinetic parameters of Glu- or Lys-Pg activation by tPA in the absence or presence of Fg or Fn

Pg activation rates were determined in the absence or presence of 5 μM free Zn²⁺ (Figure 2). In the absence of Fg or Fn, the catalytic efficiencies (CE) were determined directly from rate *versus* substrate plots, whereas in the presence of Fg or Fn, k_{cat} and K_m values were determined and used to calculate CE. Values reflect the mean ± SD of 4 determinations. The fold reduction in CE in the presence of Zn²⁺ was calculated by dividing the CE in the absence of Zn²⁺ by that measured in its presence. The significance of the differences in the CE values in the absence or presence of Zn²⁺ was determined using the Wilcoxon Rank Sum and Signed Rank Test, with a two-sided non-paired test (*p<0.05).

Next, we examined the effect of Zn^{2+} on Pg activation by tPA in the presence of Fg or Fn. Because activation is enhanced in the presence of a cofactor, kinetic parameters were obtained from rate *versus* substrate concentration plots by Michaelis-Menten analyses (Figure 2). Free Zn^{2+} , at a concentration of 5 μ M, significantly reduced catalytic efficiency of Glu-Pg activation by tPA by 2.3- and 1.6-fold in the presence of Fg and Fn, respectively (Table 2). With Lys-Pg, Zn^{2+} reduced catalytic efficiency by 2.2- and 4.7-fold in the presence of Fg and Fn, respectively. The reductions resulted mainly from decreases in the k_{cat} values as evidenced in the rate plots. The only effect of Zn^{2+} on the K_m parameter was a 50% increase obtained with Lys-Pg in the presence Fn. Therefore, Zn^{2+} reduces Pg activation, but because the reduction in catalytic efficiency occurs in the absence and presence of Fg or Fn, the effect of Zn^{2+} on Pg activation is unlikely to be cofactor-mediated.

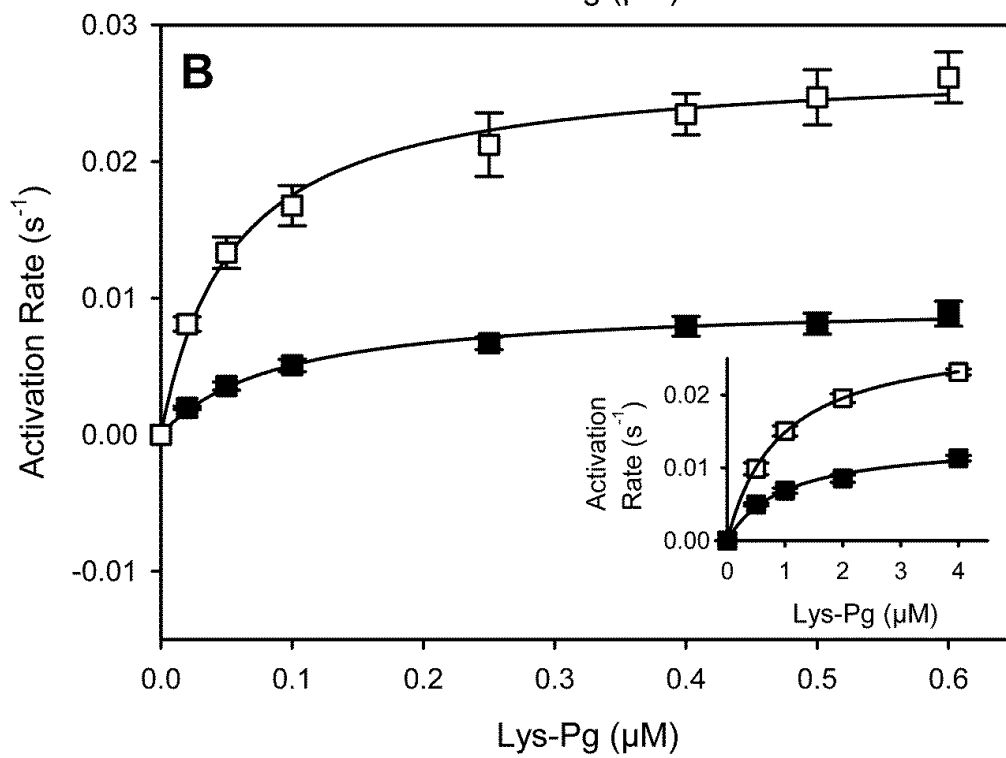
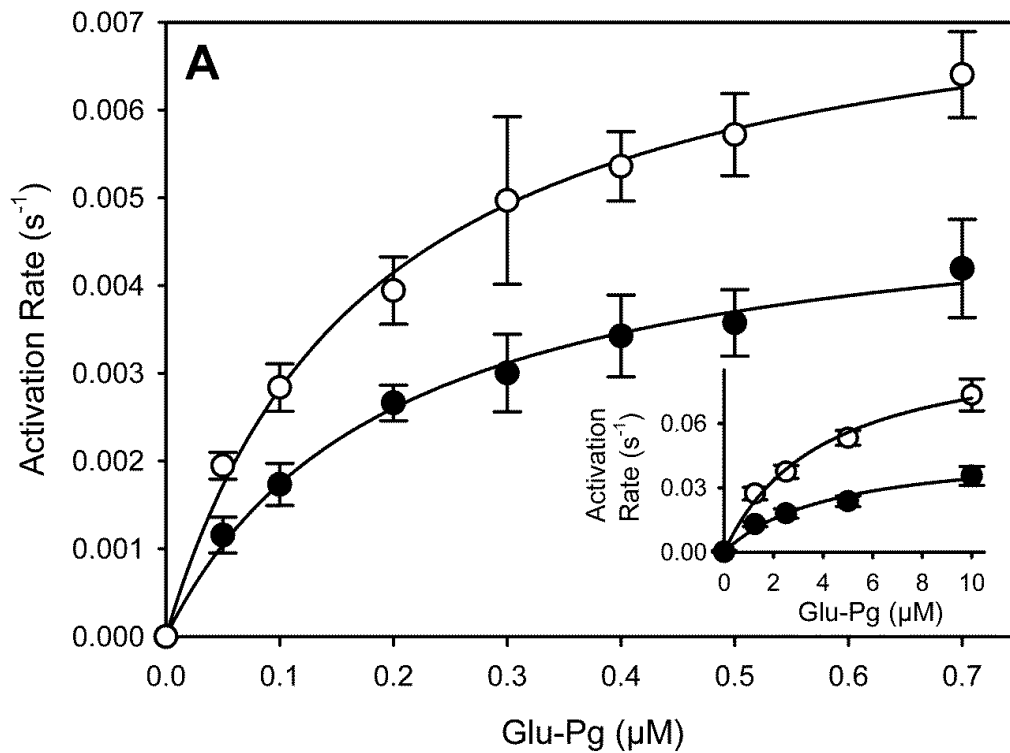


Figure 2. Effect of Zn^{2+} on Glu-Pg or Lys-Pg activation by tPA in the presence of Fn or Fg

(A) Samples containing 0-0.7 μ M Glu-Pg and 3 μ M Fg were incubated with 0.5 nM tPA, 10 nM thrombin, and 2 mM $CaCl_2$ in the absence (*open*) or presence of 5 μ M free Zn^{2+} (*closed*) and Pn generation was monitored by measuring the hydrolysis of D-VLK-pNA. Rates of activation are plotted *versus* Glu-Pg concentrations. Symbols represent the mean of 4 determinations, while the bars reflect the SD. Lines represent nonlinear regression analyses of the Michaelis-Menten equation. The inset shows activation with Fg in the absence of thrombin.

(B) Experiments were repeated using Lys-Pg in place of Glu-Pg in the presence of Fn or Fg (*inset*).

4.8.4 Effect of Zn²⁺ on the affinities of Pg, VFK-Pn and tPA for Fg and Fn

Next, we used SPR to determine the effect of Zn²⁺ on the affinities of Pg, VFK-Pn, and tPA for immobilized Fg or Fn. Glu-Pg, Lys-Pg, VFK-Pn, and tPA all demonstrated saturable binding to Fg and Fn (Figure 3). Analysis of the plots yielded binding affinities comparable to those reported previously (Table 3) (Stewart et al., 1998). Zn²⁺ did not significantly affect the affinity of Glu-Pg, Lys-Pg or VFK-Pn for Fg or Fn. The affinity of tPA for Fn was 2.2-fold higher (p=0.03) in the presence of Zn²⁺ than in its absence.

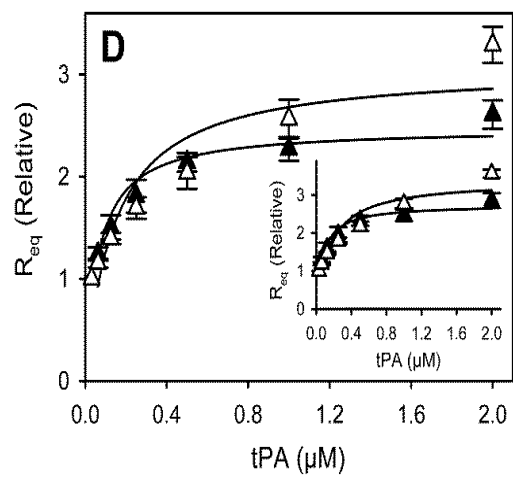
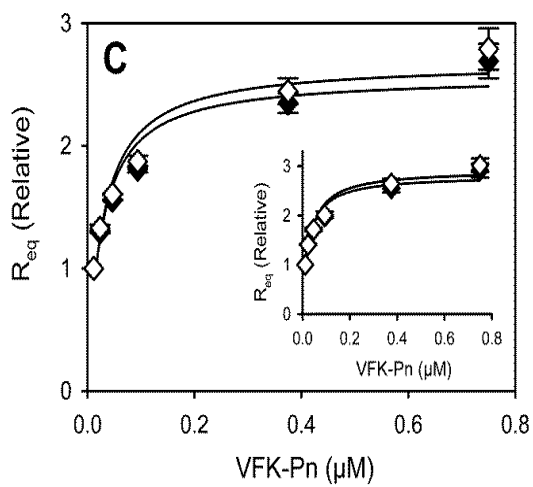
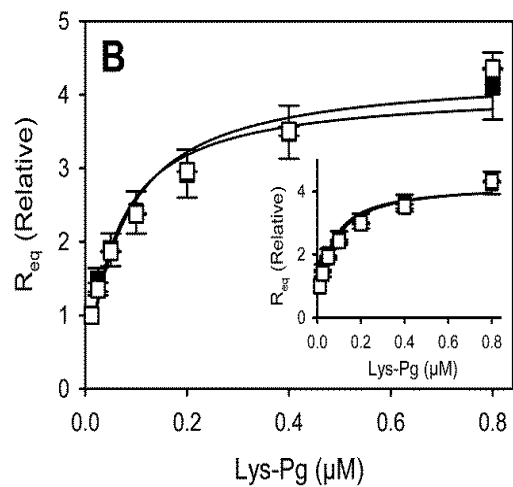
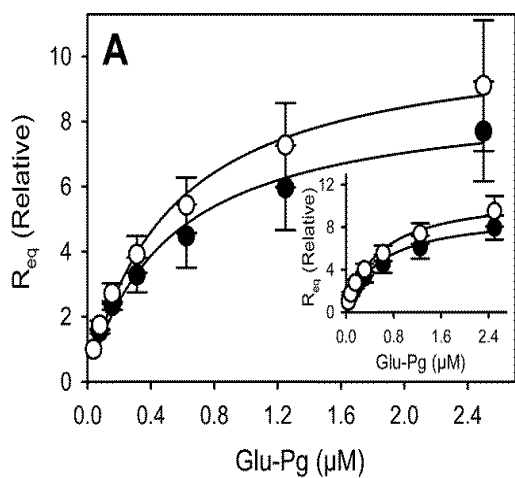


Figure 3. Effect of Zn^{2+} on Glu-Pg, Lys-Pg, VFK-Pn and tPA binding to immobilized Fg or Fn as determined using SPR

Fg was immobilized in flow cells of a biosensor chip. Glu-Pg (**A**), Lys-Pg (**B**), VFK-Pn (**C**) or tPA (**D**) was injected into the flow cells in concentrations up to 2500, 800, 750 and 2000 nM, respectively, in the presence of 1 μ M EDTA (*open*) or 20 μ M Zn^{2+} (*closed*). The insets show the experiment with immobilized Fn. R_{eq} values determined at equilibrium are plotted as a ratio of that determined prior to protein injection. Symbols represent the mean of duplicates, while the bars reflect the SD. The data were fitted using nonlinear regression of a rectangular hyperbola (*line*) to determine the K_d values.

K_d						
Ligand	Fg			Fn		
	No Zn ²⁺	With Zn ²⁺	p-value	No Zn ²⁺	With Zn ²⁺	p-value
	<i>nM</i>	<i>nM</i>		<i>nM</i>	<i>nM</i>	
Glu-Pg	526.6 ± 125.9	513.5 ± 135.3	0.07	554.1 ± 106.4	552.3 ± 123.2	1
Lys-Pg	67.9 ± 10.3	56.1 ± 10.5	0.3	62.7 ± 9.0	54.8 ± 8.7	0.3
VFK-Pn	26.7 ± 4.1	25.4 ± 4.0	0.7	29.0 ± 4.0	26.4 ± 3.5	0.2
tPA	143.4 ± 37.5	65.7 ± 10.1	0.3	164.8 ± 40.7	75.7 ± 11.4	0.03

Table 3. Affinities of fibrinolytic proteins for immobilized Fg and Fn determined by SPR

K_d values of various proteins for immobilized Fg and Fn were determined by SPR in the absence or presence of Zn²⁺. Values represent the mean ± SE of experiments performed in duplicate.

4.8.5 Effect of Zn^{2+} on Fn clot lysis

Because Zn^{2+} attenuates Pg activation by tPA or uPA, next we examined its effect on fibrinolysis. Fn clots containing increasing concentrations of Zn^{2+} were prepared in the presence of Glu-Pg with either tPA or uPA. By monitoring absorbance, lysis times were determined. Increasing concentrations of Zn^{2+} caused a concentration-dependent prolongation of clot lysis times. Thus, compared with no Zn^{2+} , lysis times with tPA and uPA were significantly ($p < 0.001$) prolonged 1.9- and 2.2-fold, respectively, in the presence of 6 μM free Zn^{2+} (Figure 4).

Because the prolonged lysis times may result from alterations in Pg activation and/or Fn breakdown, we used Pn in place of Pg and a Pg activator, to determine whether Zn^{2+} affects the capacity of Pn to degrade Fn. Zn^{2+} significantly ($p < 0.001$) prolonged Pn-mediated lysis times up to 2.5-fold; an effect that was concentration-dependent (Figure 4). To determine if the Zn^{2+} effect is Pn- or Fn-dependent, we examined Fn degradation by trypsin; a protease with weak affinity for Zn^{2+} ($K_d = 30.1 \pm 0.03 \mu M$). The lysis time with trypsin was only 1.4-fold ($p < 0.001$) longer in the presence of 6 μM Zn^{2+} than in its absence. These findings suggest that Zn^{2+} attenuates Fn clot lysis both by reducing the catalytic efficiency of Pg activation by tPA or uPA and by attenuating Fn degradation by Pn.

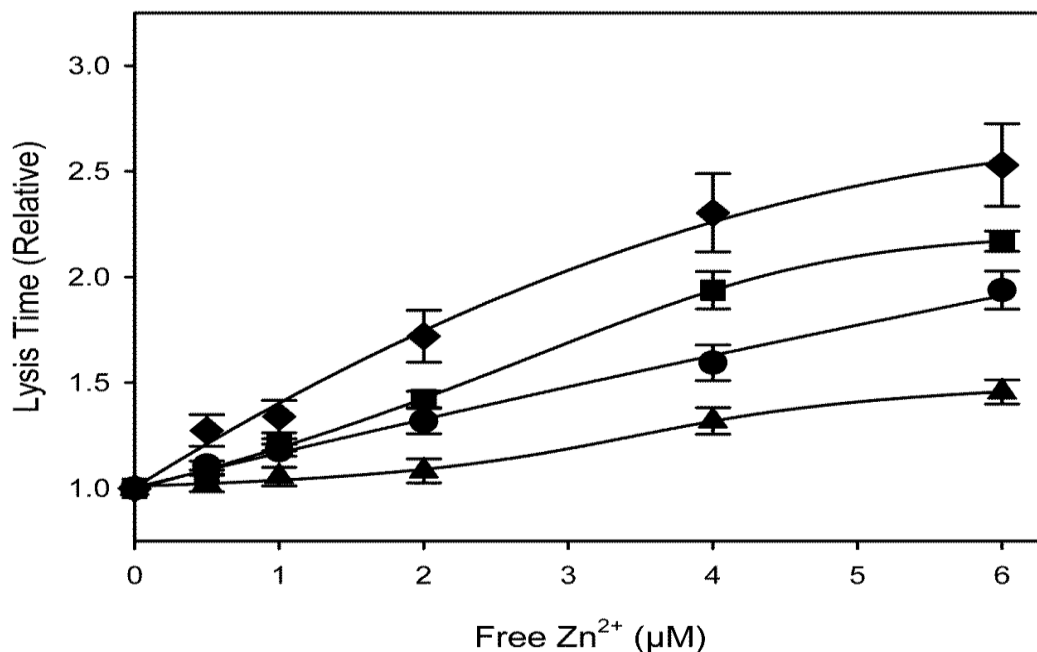


Figure 4. Effect of Zn²⁺ on lysis of fibrin clots

Samples containing 0.2 nM tPA (*circles*) or 2 nM uPA (*squares*), 1 μM Glu-Pg, 3 μM Fg, 2 mM CaCl₂, and 0-6 μM Zn²⁺ were clotted with 10 nM thrombin. Lysis times were determined by monitoring absorbance at 405 nm and determining the time to half-maximal decrease in absorbance. Values measured in the presence of Zn²⁺ were normalized relative to that measured in its absence. The experiment was then repeated using 18 nM Pn (*diamonds*) or 100 nM trypsin (*triangles*) in place of a plasminogen activator and Pg. Symbols represent the means of 3 experiments each done in triplicate, while the bars reflect the SE, and an arbitrary line was used to show the dose-response. Lysis times in the absence of Zn²⁺ were 1621.5 ± 78.8, 1800.6 ± 19.1, 955.3 ± 122.6, and 5047.2 ± 415 s with tPA, uPA, Pn, and trypsin, respectively.

To verify that Zn^{2+} attenuates the proteolytic activity of Pn, but has little effect on the activity of trypsin, Pn- or trypsin-mediated Fg degradation in the absence or presence of Zn^{2+} was assessed using SDS-PAGE analysis. In the absence of Zn^{2+} , Pn caused progressive proteolysis of all three chains, and the α -chain was completely degraded within 45 min (Figure 5A,E) (Liu et al., 1986). In the presence of 5 μM free Zn^{2+} , the α -chain was only degraded by $43 \pm 0.03\%$ at 60 min ($p < 0.001$ versus no Zn^{2+} , Figure 5B,E). In contrast, the time course of proteolysis of the α -chain by 20 nM trypsin in the presence of Zn^{2+} was similar to that in its absence ($p = 0.9$) (Figure 5C-E). These results suggest that the effect Zn^{2+} on Pn-mediated Fg degradation reflects interaction with Pn rather than Fg. Although Zn^{2+} attenuated Pn activity against Fg and Fn, Zn^{2+} had no effect on the rate of Pn-mediated conversion of single-chain tPA to its two-chain form (Supplementary Figure 1), which raises the possibility that the effect of Zn^{2+} on Pn activity is substrate specific.

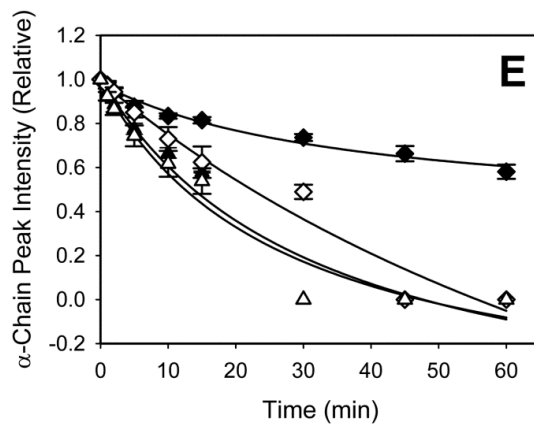
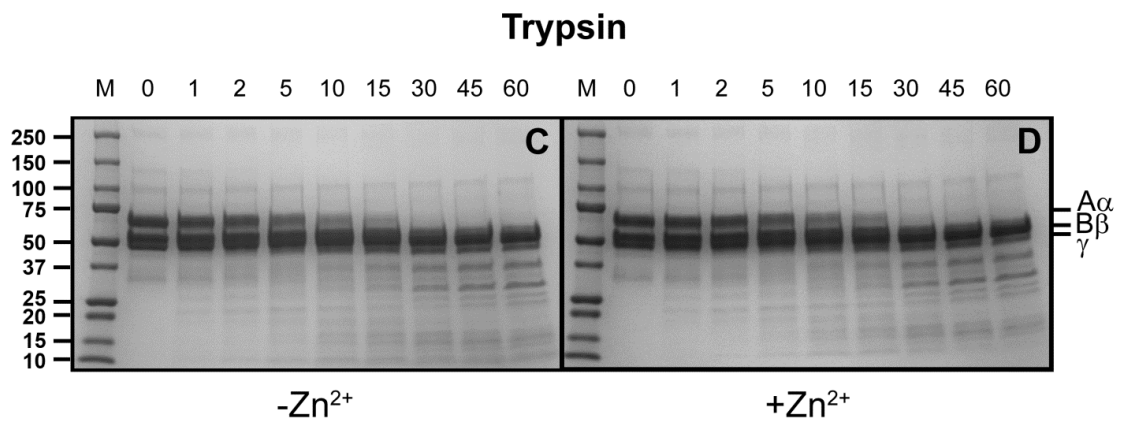
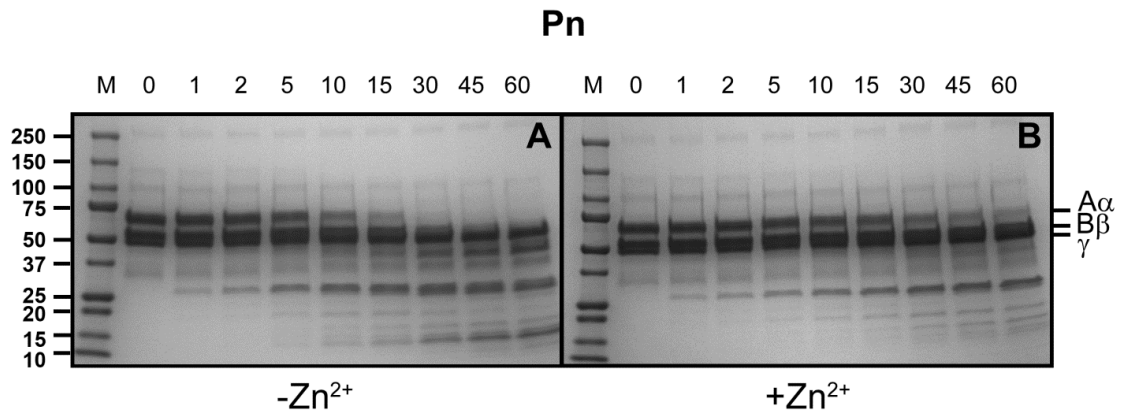
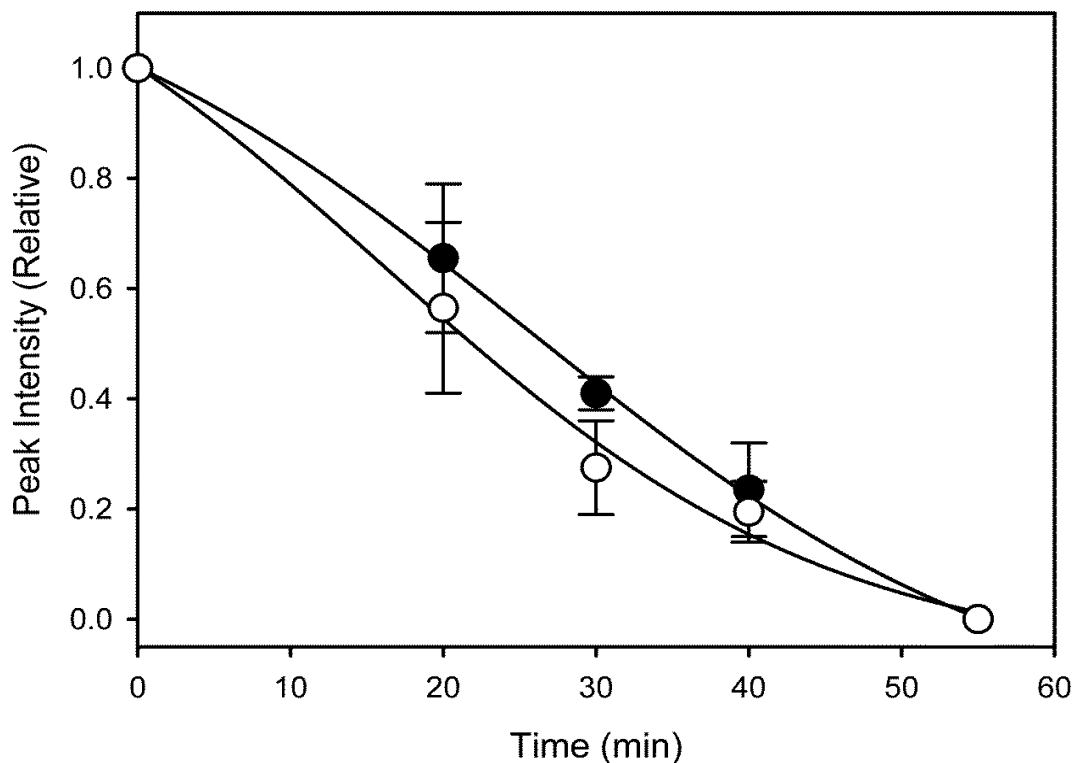


Figure 5. SDS-PAGE analysis of the effect of Zn^{2+} on Fg degradation by Pn or trypsin

Samples containing 3 μ M Fg and 2 mM $CaCl_2$ were incubated with 10 nM Pn (**A**, **B**) or 20 nM trypsin (**C**, **D**) in the absence (**A**, **C**) or presence (**B**, **D**) of 5 μ M free Zn^{2+} . Aliquots removed at the indicated time points (0-60 min) were subjected to SDS-PAGE analysis under reducing conditions. Markers (M) and Fg chains are indicated on the left and right, respectively. (**E**) The $A\alpha$ -chain band intensity was quantified by densitometry, normalized relative to that determined at time 0, and plotted *versus* time. Symbols for Pn (*diamonds*) and trypsin (*triangles*) in the absence (*open*) or presence (*closed*) of Zn^{2+} represent the mean of 3 determinations, while the bars reflect the SD.



Supplementary Figure 1. Densitometric analysis of the effect of Zn²⁺ on Pn-mediated cleavage of single-chain tPA

Single-chain tPA (3 μM) was incubated with 4 nM Pn in the absence or presence of 12 μM free Zn²⁺ and aliquots removed at the times indicated were subjected to SDS-PAGE analysis. Peak band intensity was quantified by densitometry, normalized relative to that at time 0 and values for the single-chain form were then plotted *versus* time. Symbols (*circles*) represent the mean of 2 determinations in the absence (*open*) or presence (*closed*) of Zn²⁺, while the bars reflect the SD, and an arbitrary line was used to show the trend.

4.8.6 Effect of Zn²⁺ on plasma clot lysis

To evaluate the effect of Zn²⁺ on plasma clot lysis, plasma was first dialyzed to remove the chelator. Aliquots of dialyzed plasma were clotted with thrombin in the presence of tPA and concentrations of free Zn²⁺ up to 15 μM, levels comparable to those attained when platelets are activated. Clotting and lysis were monitored by absorbance. Compared with its absence, Zn²⁺ significantly (p<0.001) prolonged the lysis times in a concentration-dependent fashion, up to 1.5-fold in the presence of 15 μM free Zn²⁺ (Figure 6). Therefore, Zn²⁺ has an inhibitory effect on clot lysis in plasma where Zn²⁺-binding proteins are abundant.

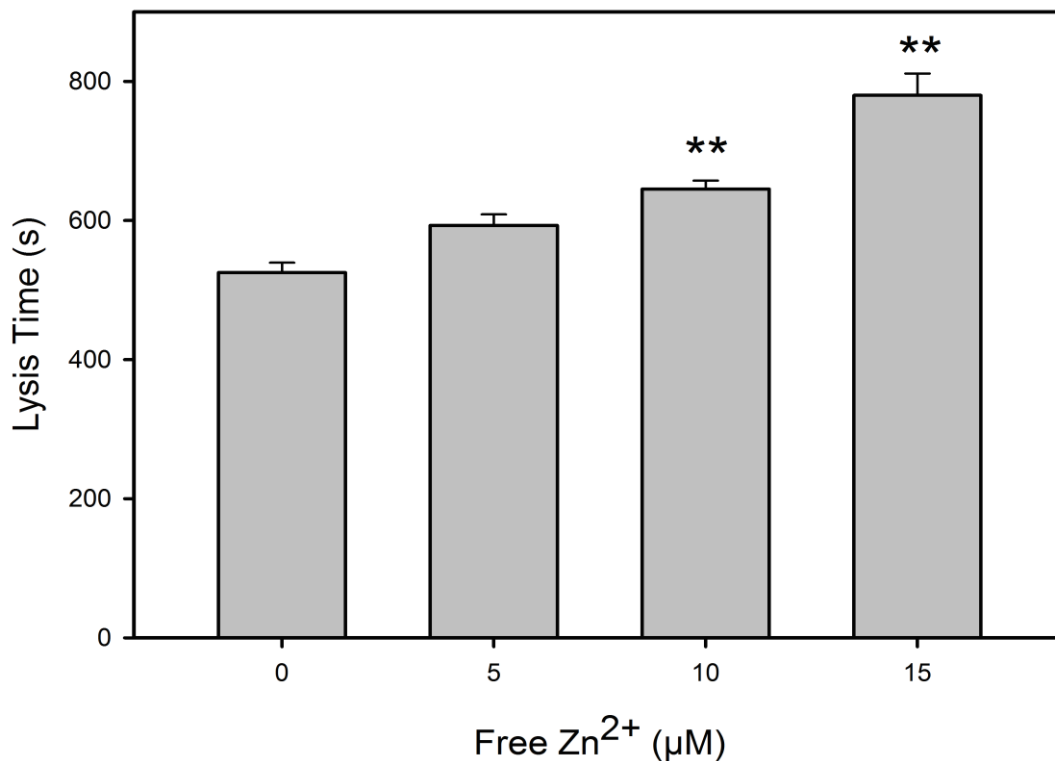


Figure 6. Effect of Zn²⁺ on lysis of plasma clots

Samples of dialysed platelet-poor plasma containing 1.2 nM tPA and 0–15 µM free Zn²⁺ were incubated with 5 nM thrombin and 15 mM CaCl₂. Absorbance was monitored at 350 nm. Data points represent mean lysis times while the bars reflect the standard error (SE) of three separate experiments each performed in triplicate. Based on the results of a parametric one-way analysis of variance, Zn²⁺ has a significant ($p < 0.001$) concentration-dependent effect on lysis times, and Tukey's test for multiple pairwise comparisons indicates that the lysis times with 10 and 15 µM Zn²⁺ are significantly (** $p < 0.001$) longer than that determined in the absence of Zn²⁺.

4.9 DISCUSSION

The goal of this study was to investigate the effect of Zn^{2+} on fibrinolysis. We show that Zn^{2+} inhibits fibrinolysis by attenuating two reactions in the fibrinolytic pathway. Firstly, Zn^{2+} reduces the catalytic efficiency of Pg activation by tPA or uPA; an effect that appears to be independent of the affinity of the activator for Zn^{2+} because the affinity of Zn^{2+} for tPA is 35-fold higher than that for uPA. Furthermore, the inhibitory effect of Zn^{2+} is independent of cofactors because similar attenuation was observed in the absence of Fg or Fn. Secondly, Zn^{2+} attenuates Pn-mediated lysis of Fg and Fn. This more likely results from the interaction of Zn^{2+} with Pn rather than with Fg or Fn because Zn^{2+} has minimal effects on Fg or Fn degradation by trypsin. These results suggest that Zn^{2+} is a regulator of fibrinolysis.

Zn^{2+} is a known regulator of hemostasis and is essential for activation of the contact system (Rojkjaer and Schmaier, 1999; Vu et al., 2013). The bulk of the 10-20 μ M total Zn^{2+} in plasma circulates bound to albumin and less abundant proteins such as α_2 -macroglobulin and histidine-rich glycoprotein (Foote and Delves, 1984; Guthans and Morgan, 1982). Most of the remainder is bound to free amino acids, such that free Zn^{2+} accounts for only ~1% of the total Zn^{2+} concentration (Bax and Bloxam, 1997). At sites of vascular injury, however, stored Zn^{2+} is released from activated platelets. Consistent with this concept, we observed that the physiological concentration of platelets release ~5 μ M Zn^{2+}

upon activation, which is about half of their total cellular Zn^{2+} content. Because platelets aggregate at sites of arterial injury to levels 50-100 times higher than those in circulating blood (Gorodetsky et al., 1993; Marx et al., 1993; Muthard and Diamond, 2012; Rojkjaer et al., 1998), Zn^{2+} levels within a clot may exceed 20 μ M. Consistent with this, sufficient Zn^{2+} is released by platelets to promote reactions regulated by Zn^{2+} , including contact pathway and platelet activation, and modulation of activated protein C and FVIIa activity (Rojkjaer et al., 1998; Rojkjaer and Schmaier, 1999; Vu et al., 2013).

To better understand the mechanisms by which Zn^{2+} modulates fibrinolysis, interactions of constituent proteins with the cation were quantified. Zn^{2+} binding to tPA and Fg has been studied previously, but the interaction of Zn^{2+} with other fibrinolytic proteins has not (Marx, 1988c; Rijken and Groeneveld, 1986; Siddiq and Tsirka, 2004; Vu et al., 2013). Although Zn^{2+} binds Pn, it does not bind Pg, suggesting that the Zn^{2+} -binding site is only exposed upon Pg activation. The affinity of Zn^{2+} for tPA and Pn (K_d values 0.2 μ M) is 35-fold higher than that for uPA. Thus, the Zn^{2+} -binding sites on tPA and Pn have the potential to be fully occupied at sites where Zn^{2+} is released from activated platelets (Rojkjaer and Schmaier, 1999).

Although Zn^{2+} binding to metalloproteases is well described, few interactions of Zn^{2+} with serine proteases have been reported (Nozaki et al., 2011). The affinity of Zn^{2+} for trypsin is 150-fold lower than that for Pn and tPA,

suggesting that domains distinct from the protease domain mediate the high affinity interaction. Although this contradicts the findings of a previous report that suggested that Zn^{2+} binds to the catalytic domain of tPA (Rijken and Groeneveld, 1986), the sites of interaction with Pn and uPA have not been identified. Regardless of the sites of interaction, Zn^{2+} has no effect on the chromogenic activity of these proteases. Previous studies that reported effects of Zn^{2+} on the chromogenic activity of tPA and Pn used much higher concentrations of Zn^{2+} (Siddiq and Tsirka, 2004; Tu and Liang, 2006). In contrast to results with chromogenic substrates however, Zn^{2+} does modulate the activity of tPA and Pn with macromolecular substrates. Thus, in addition to supporting initiation of coagulation by binding factors VIIa and XIIa and other contact proteins, Zn^{2+} attenuates lysis of clots through interaction with tPA and Pn. These results demonstrate that Zn^{2+} affects hemostasis by modulating the activity of numerous proteases.

The effect of Zn^{2+} is mediated through catalytic reactions involving tPA and Pn. Zn^{2+} elicits a 2-fold attenuation of Glu- and Lys-Pg activation by tPA. The Zn^{2+} effect is likely mediated through the activator because neither form of Pg binds Zn^{2+} . In support of this concept, Zn^{2+} reduced the catalytic efficiency of Glu- and Lys-Pg activation by tPA by decreasing k_{cat} , and by increasing the K_m for Lys-Pg. Furthermore, Zn^{2+} attenuates Pg activation by tPA to the same extent

in the presence of Fg or Fn as it does in their absence; a finding that suggests the effect is dependent on the Pg activator rather than the cofactor.

In addition to attenuating Pg activation, Zn^{2+} also modulates fibrinolysis at the level of Pn. Thus, Zn^{2+} binds Pn with high affinity and attenuates Pn-mediated degradation of Fg and Fn. This effect is unlikely to be the result of the interaction of Zn^{2+} with Fg or Fn because the cation has only a modest effect on trypsin-mediated Fn degradation and no effect on the degradation of Fg. The effect of Zn^{2+} appears to be limited to macromolecular substrates because Zn^{2+} has no effect on the chromogenic activity of Pn, tPA or uPA, and the effect may be substrate-specific because Zn^{2+} did not alter the rate of Pn-mediated conversion of single-chain tPA into its two-chain form. These results demonstrate that Zn^{2+} is a dual modulator of fibrinolysis because it attenuates both Pg activation by tPA and uPA and Pn-mediated Fg and Fn proteolysis.

Zn^{2+} retards clot lysis in buffer and plasma systems. Although previously attributed to Zn^{2+} -induced alteration in Fn clot structure (Tubek et al., 2008; Vu et al., 2013), the fact that Zn^{2+} attenuates the activities of tPA and Pn suggests that the Zn^{2+} effect extends beyond altered clot structure. Despite the abundance of Zn^{2+} -binding proteins in plasma, lysis of plasma clots is delayed in the presence of Zn^{2+} . This finding raises the possibility that fibrinolysis may be locally modulated when Zn^{2+} is released from activated platelets at sites of vascular injury (Rojkjaer and Schmaier, 1999; Vu et al., 2013); the sites where tPA, Pn and Fn accumulate.

Therefore, in addition to releasing type 1 plasminogen activator inhibitor, release of Zn^{2+} may represent a second mechanism through which activated platelets can locally modulate fibrinolysis.

Zn^{2+} has been shown to bind to numerous hemostatic proteins, including Fg, factor XIIa, VIIa, protein C, and protein S (Vu et al., 2013). We now have expanded this list by showing that Zn^{2+} also binds tPA and Pn. Furthermore, we demonstrate that Zn^{2+} down-regulates fibrinolysis by attenuating Pg activation and subsequent Pn activity. In addition to quantifying the extent of this attenuation and elucidating the mechanisms, we show that these effects occur with physiological concentrations of Zn^{2+} in buffer and plasma systems. Therefore, Zn^{2+} is well positioned to modulate fibrinolysis because it binds the principal components of the system. These findings add to the growing evidence that Zn^{2+} is an important regulator of hemostasis.

4.10 ACKNOWLEDGEMENTS

We would like to thank Vinai Bhagirath and Iqbal Jaffer for blood collection, Josephine Baldwin and Carol-Anne Wigmore of the Hamilton Regional Laboratory Medicine Program for performing the atomic adsorption analyses, and Professor Robin Roberts for statistical analyses.

CHAPTER 5: ZINC IS LOCATED IN PLATELET DENSE GRANULES AND RELEASED UPON ACTIVATION

5.1 Forward

A re-examination of platelet Zn^{2+} storage and release are described in this manuscript. We demonstrate that Zn^{2+} is located in the dense granules of platelets with other ions. However, only half of the platelet intracellular Zn^{2+} content can be removed via chelation or secreted with activation.

5.2 Objective: Re-examine platelet Zn^{2+} storage and release

Zn^{2+} modulates hemostasis at multiple levels by influencing platelet aggregation, coagulation, and fibrinolysis. It is important to understand Zn^{2+} release from activated platelets, as it results in a surge of Zn^{2+} at the vicinity of a clot. The aim of this study was to examine the location of Zn^{2+} and Ca^{2+} within human platelets and quantify their release upon activation. Previous studies suggest that Zn^{2+} is located in the alpha granules with Zn^{2+} -binding proteins (Marx et al., 1993). However, Ca^{2+} is located in the dense granules with other ions (Rendu and Brohard-Bohn, 2001). Both ions reside in different storage compartments, yet both granules secrete their contents during activation. We hypothesized that Zn^{2+} ions will be stored in platelet dense granules with Ca^{2+} , and exhibit full secretion when induced with a platelet agonist. In order to test this

hypothesis, **(A)** the location of Zn^{2+} and Ca^{2+} in platelets was identified, and **(B)** the amount of Zn^{2+} and Ca^{2+} ions in plasma and platelets were quantified.

Zinc is located in Platelet Dense Granules and Released upon Activation

Sara J. Henderson^{1,2}, Fred G. Pluthero^{5,6}, Harry F. G. Heijnen⁷, Willie J.C. Geerts⁷, Nima Vaezzadeh^{1,4}, Alan R. Stafford³, James C. Fredenburgh^{1,3}, Walter H. Kahr^{5,6}, and Jeffrey I. Weitz¹⁻⁴

Thrombosis and Atherosclerosis Research Institute¹ and the Department of Biochemistry and Biomedical Sciences², Medicine³ and Medical Sciences⁴, McMaster University, Hamilton, and the Department of Pediatrics, Division of Hematology/Oncology⁵, The Hospital for Sick Children⁶, University of Toronto, Toronto, Ontario, Canada, Departments of Clinical Chemistry and Hematology, University Medical Center Utrecht, Utrecht, Netherlands⁷.

Running Title: Zinc is located in the dense granules of platelets

Address correspondence to: Jeffrey I. Weitz, Thrombosis and Atherosclerosis Research Institute, 237 Barton St E, Hamilton, ON L8L 2X2, Canada; e-mail: weitzj@taari.ca

Footnotes: This work was supported in part by the Canadian Institutes of Health Research and the Heart and Stroke Foundation. J.I.W. holds the Heart and Stroke Foundation J. Fraser Mustard Endowed Chair in Cardiovascular Research and the Canada Research Chair (Tier 1) in Thrombosis.

Authorship Contributions: SJH coordinated the study, wrote the paper, performed ion quantifications and experiments in Figure 4. FGP captured platelet images in Figure 2 and 3. H.F.G.H and W.J.C.G acquired the images for the experiments shown in Figure 1, while NV and AS assisted in study design shown in Figure 4. JCF assisted in writing and preparation of the figures. WHK and JIW contributed to interpretation of the data, writing, and final approval of the manuscript. JIW obtained the funding for the project.

*** A modified version of this manuscript is in preparation for submission to the journal *Blood*.**

References: References for this manuscript have been incorporated into the Bibliography (Chapter 10), at the end of this thesis.

5.3 KEY POINTS

1. Like Ca^{2+} , Zn^{2+} is stored in the dense granules of human platelets.
2. Activated platelets secrete the majority of Ca^{2+} , whereas only half of Zn^{2+} is released.

5.4 ABSTRACT

Zinc (Zn^{2+}) and calcium (Ca^{2+}) ions are stored in platelet secretory granules, and are released upon platelet activation. Ca^{2+} is stored in the dense granules of platelets, whereas Zn^{2+} was reported to be stored in the alpha granules and the cytoplasm. However, Ca^{2+} and Zn^{2+} are divalent ions and should reside together in the dense granules. The purpose of this study was to confirm ion localization in human platelets. To do this, transmission electron microscopy combined with energy dispersive X-ray analysis was used to examine dense granular element content. Zn^{2+} , Ca^{2+} , phosphorus, and sodium were detected in dense granules. To confirm the dense granular localization of Zn^{2+} and Ca^{2+} , non-activated platelets were incubated with membrane-permeable Zn^{2+} and Ca^{2+} specific fluorescent probes, and imaged using high-resolution confocal laser fluorescence microscopy. Each resting platelet contained 1-3 Zn^{2+} -staining and 1-5 Ca^{2+} -staining foci. Ca^{2+} , but not Zn^{2+} , was also observed throughout the cytoplasm. Merged images revealed the presence of Zn^{2+} only in some of the Ca^{2+} -stained dense granules. Contrary to previous reports, Zn^{2+} was not observed in the platelet mitochondria or cytoplasm. Flame atomic absorption spectroscopy

was used to quantify Zn^{2+} and Ca^{2+} concentrations in platelet lysates and releasates. Whereas 90% of the intracellular Ca^{2+} was released when platelets were activated with thrombin and collagen, only 53% of the total Zn^{2+} concentration was released. The incomplete release of Zn^{2+} was confirmed using flow cytometry to study platelets that were pre-incubated with a Zn^{2+} -specific fluorescent probe. Compared with resting platelets, the fluorescent intensity was reduced by $54 \pm 2\%$ after platelet activation, and by $49 \pm 8\%$ with the addition of a Zn^{2+} -specific chelator. These studies suggest that only half of platelet intracellular Zn^{2+} is secreted with activation at the sites of vascular injury.

5.5 INTRODUCTION

After iron, Zn^{2+} is the second most abundant metal ion in the body (Vu et al., 2013). Zn^{2+} circulates in plasma at a concentration of $\sim 20 \mu M$, although most is weakly bound to albumin and other plasma proteins, leaving only $0.1-2 \mu M$ in a free, unbound state (Gorodetsky et al., 1993; Henderson et al., 2015a; Lu et al., 2008; Vu et al., 2013; Whitehouse et al., 1982). Zn^{2+} is an important ion because it participates in numerous hemostatic reactions, including those involved in platelet aggregation, coagulation, and fibrinolysis (Vu et al., 2013).

Ca^{2+} is found in the dense granules and cytoplasm of platelets, and is released when platelets are activated (Heijnen and van der Sluijs, 2015). Like Ca^{2+} , Zn^{2+} is stored in platelets, however, the site of Zn^{2+} storage and subsequent release upon activation is uncertain. A previous report suggested that Zn^{2+} is

stored in the alpha granules and cytoplasm of platelets because of its affinity for fibrinogen (Fg), histidine-rich glycoprotein, and factor XIII (Marx et al., 1993). However, direct evidence for storage in these sites is lacking. The purpose of this study was to **(A)** identify the location of Zn^{2+} in platelets, **(B)** determine whether Zn^{2+} and Ca^{2+} are localized to distinct regions, and **(C)** compare the extent of Zn^{2+} release from activated platelets with that of Ca^{2+} .

5.6 METHODS

5.6.1 Reagents

Fluorescent indicators FluoZin-3AM, Calcium Orange, Mitotracker Deep Red, and Lectin Wheat Germ Agglutinin conjugated with either Alexa Fluor 555 or 647 were purchased from Life Technologies (Burlington, ON, Canada). N,N,N',N'-Tetrakis (2-pyridylmethyl) ethylenediamine (TPEN) was purchased from Cedarlane (Burlington, ON, Canada). The fluorescent mounting media was purchased from Dako (Burlington, ON). An ADP assay kit, prostaglandin E_1 , and human or bovine serum albumin (BSA) were purchased from Sigma Aldrich. Collagen reagent HORM suspension was purchased from Nycomed (Linz, Austria). Human Fg and α -thrombin were obtained from Enzyme Research Laboratories (South Bend, IN, USA). Thrombin was dialyzed against 20 mM Tris, pH 7.4, 150 mM NaCl to remove citrate.

5.6.2 Transmission electron microscopy (TEM)

Blood was collected into 0.13 M (0.1 vol) sodium citrate, and platelet-rich plasma (PRP) was prepared by centrifugation at 180 x g for 10 min, at 23°C. Carbon-covered gold EM grids were coated by adding 200 mg/ml of Fg onto the grids, and stored at 4°C overnight. The Fg coated grids were blocked with 1% human serum albumin, and platelets were spread onto the grids using a pipette and left to adhere to immobilized Fg for 20 min. Grids with adherent platelets were fixed in 2% paraformaldehyde (PFA) and 0.2% glutaraldehyde in 0.1 M phosphate buffer, rinsed, and mounted in 1.8% methyl cellulose. Grids were subjected to TEM with a 200-kV Tecnai 20 microscope (FEI Company, Eindhoven, Netherlands) using a LaB6 gun (T20-LaB6), and images were acquired with a 4k x 4k Eagle camera (FEI Company).

Scanning TEM (STEM) data collection was performed on a 200-kV Tecnai 20 transmission electron microscope (FEI Company) with a Field Emission Gun (T20-FEG) and a twin objective lens. Data were acquired at an extraction voltage of 4.4 kV, gun lens setting 6, spot size 6, and with a 70- μ m C2 condenser aperture. These settings corresponded to a spot size of approximately 1.96 nm (Yakushevskaya et al., 2007).

Energy dispersive X-ray (EDX) analyses in combination with TEM (TEM-EDX) were performed on individual dense granules. EDX provides semi-quantitative data for samples that are not flat, polished, or homogenous. This

technique has limited sensitivity for low-Z elements, but is an excellent tool to decipher the elemental composition and ratios of organic material (van Niftrik et al., 2008; Zierold, 1997). The samples were mounted in a Beryllium specimen holder (Philips, Eindhoven, Netherlands). The EDX measurements were performed on the T20-FEG equipped with an EDAX CM-200ST X-ray detector. Spot and area spectra were interpreted using the FEI TEM imaging and analysis software package (version 4.8 SP1).

5.6.3 High-resolution confocal laser immunofluorescence microscopy

Blood was collected with consent from healthy donors into 3.2% citrate tubes and subjected to centrifugation at 140 x g for 15 min at 23°C. Platelet rich plasma (PRP) was harvested, and centrifuged at 1000 x g for 8 min to sediment the platelets. The pellet was suspended and washed with Tyrodes' salt solution, pH 6.5 containing 0.1% BSA, 1 mM CaCl₂, 1 mM MgCl₂, and 3 µM prostaglandin E₁. Platelets were incubated with 5 µM FluoZin3-AM and 1 µM Calcium Orange, membrane permeable fluorescent probes for the detection of Zn²⁺ and Ca²⁺, respectively. Cell-permeable MitoTracker Deep Red (200 nM) was used to detect mitochondria. Lectin Wheat Germ Agglutinin (10 µg/ml) was conjugated with either Alexa Fluor 555 or 647 and used to detect sialic acid. Stained platelet samples were fixed using a 1:1 vol/vol of 8% PFA in phosphate-buffered saline (PBS), and incubated for 15-30 min at 23°C. Fixed platelets were pelleted and suspended in PBS containing 1% BSA. Aliquots (25 µl) of the fixed

platelet suspensions were placed on poly-L-lysine coated glass coverslips, and incubated at 100% humidity for 90 min at 37°C in a water bath. Platelets adhered to the coverslips were washed with PBS. Adherent platelets were mounted using a fluorescent mounting medium prior to imaging.

Platelets were imaged using high-resolution Quorum spinning disc confocal inverted fluorescence microscope (Spectral Applied Research), with an oil immersion 60X objective and an internal 1.5X multiplier, resulting in a final 90X objective capturing mid-platelet Z-slices. Images were processed using Perkin Elmer Volocity software (versions 5.5-6.1) as described by Kahr *et al.* (Kahr et al., 2013).

5.6.4 Flame atomic absorption spectroscopy

Blood (4 ml) was collected into EDTA blood collection tubes, using a 21-gauge needle, from the antecubital vein of 3 donors. Normal platelet counts for each individual were quantified by the Hamilton Regional Medical Laboratory Program. After obtaining written consent, 50 ml of blood was collected from the 3 healthy volunteers into acid citrate dextrose (9:1 vol/vol). Platelets were isolated and washed with Tyrodes' salt solution lacking CaCl₂, but containing prostaglandin E₁ as described (Henderson et al., 2015a). Platelet counts for Zn²⁺ and Ca²⁺ experiments were 2.0 and 3.2 ± 0.4 × 10⁹, respectively, and determined using a hemocytometer. To quantify intracellular ion concentrations, a platelet lysate was generated by subjecting washed platelets to centrifugation at 1000 × g

for 10 min at 23°C. The platelet pellet was then sonicated for 5 min, until the pellet solubilized. To generate a releasate, platelets in Tyrodes' salt solution in the absence of CaCl₂, were incubated with thrombin (10 nM) and collagen reagent HORM suspension (20 µg/ml) for 30 min at 37°C. The activated platelet suspension was subjected to centrifugation at 1000 x g for 10 min at 23°C, and the supernatant was collected for ion quantification. To confirm that these conditions were suitable for complete dense body degranulation, the ADP concentration in a 100-µl aliquot of releasate was quantified using a ADP assay kit. ATP and ADP concentrations were quantified in a 96-well plate by monitoring luminescence at 578 nm with a SpectraMax Paradigm plate reader (Molecular Devices). Values obtained from the platelet supernatant samples were compared with the derived standard curve prepared using an ADP standard. Luminescence values (RLU) were used to determine the concentration of ADP per activated sample by the following formula:

$$[\text{ADP}] \mu\text{M} = \frac{\text{RLU ADP} - \text{RLU ATP}}{\text{Slope of ADP Standard}}$$

The concentrations of Zn²⁺ and Ca²⁺ obtained from the sonicates and activated samples, were quantified using flame atomic absorption spectroscopy at the Hamilton General Hospital and McMaster University (Varian 220FS, version 5.01 Pro).

5.6.5 Flow cytometry

Washed, isolated, platelet suspensions stained with FluoZin3-AM were diluted (1:100) in Tyrodes' salt solution lacking CaCl_2 , protected from light, and maintained at 23°C. At selected time points up to 20 min, an aliquot containing ~5000 platelets was counted using a FACSCalibur (BD Biosciences, Mississauga, ON), and mean fluorescent intensity (FI) was quantified using Cell Quest Pro (version 6.0) of samples untreated or treated with 10 nM thrombin and 20 $\mu\text{g/ml}$ of collagen, or 1 μM TPEN, a specific Zn^{2+} chelator.

5.6.6 Statistical analysis

Data are presented as mean \pm standard deviation (SD) or standard error (SE). Results were compared using one-way analysis of variance followed by Tukey's test for multiple pair-wise comparisons (SigmaPlot version 11.0). In these analyses, p-values less than 0.05 were considered statistically significant.

5.7 RESULTS

5.7.1 Zn^{2+} is located with Ca^{2+} and phosphorus in platelet dense granules

Platelets were imaged using TEM, and dense granules were identified by their electron-rich dense cores (Figure 1A). Non-dense and granular areas were subjected to elemental analysis (TEM-EDX) (Figure 1A). Peaks for carbon, phosphorus, oxygen, sodium, Ca^{2+} , and Zn^{2+} were detected in two dense granules of an individual platelet (Figure 1B). In the non-granule areas, Zn^{2+} , Ca^{2+} ,

phosphorus, and sodium levels did not exceed background levels (Figure 1B). However, carbon and oxygen were abundant in both the dense and non-dense granular areas (Figure 1B). When contents were chemically mapped to detect their distribution throughout the platelet, the STEM-EDX images show that carbon and oxygen were widely distributed throughout the platelet (Figure 1C). In contrast, Ca^{2+} and phosphorus appeared compartmentalized. Because Zn^{2+} and sodium peaks are indistinguishable on the spectra, it is difficult to determine whether Zn^{2+} is compartmentalized or distributed throughout the platelet in these images. Higher resolution analysis will be necessary to evaluate whether Zn^{2+} is present in the dense granules with Ca^{2+} .

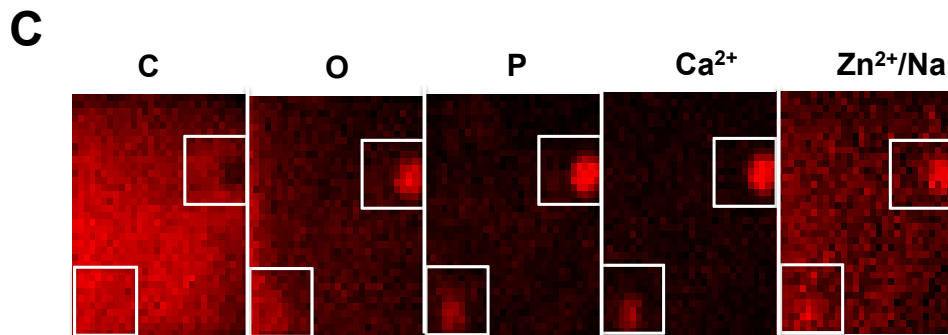
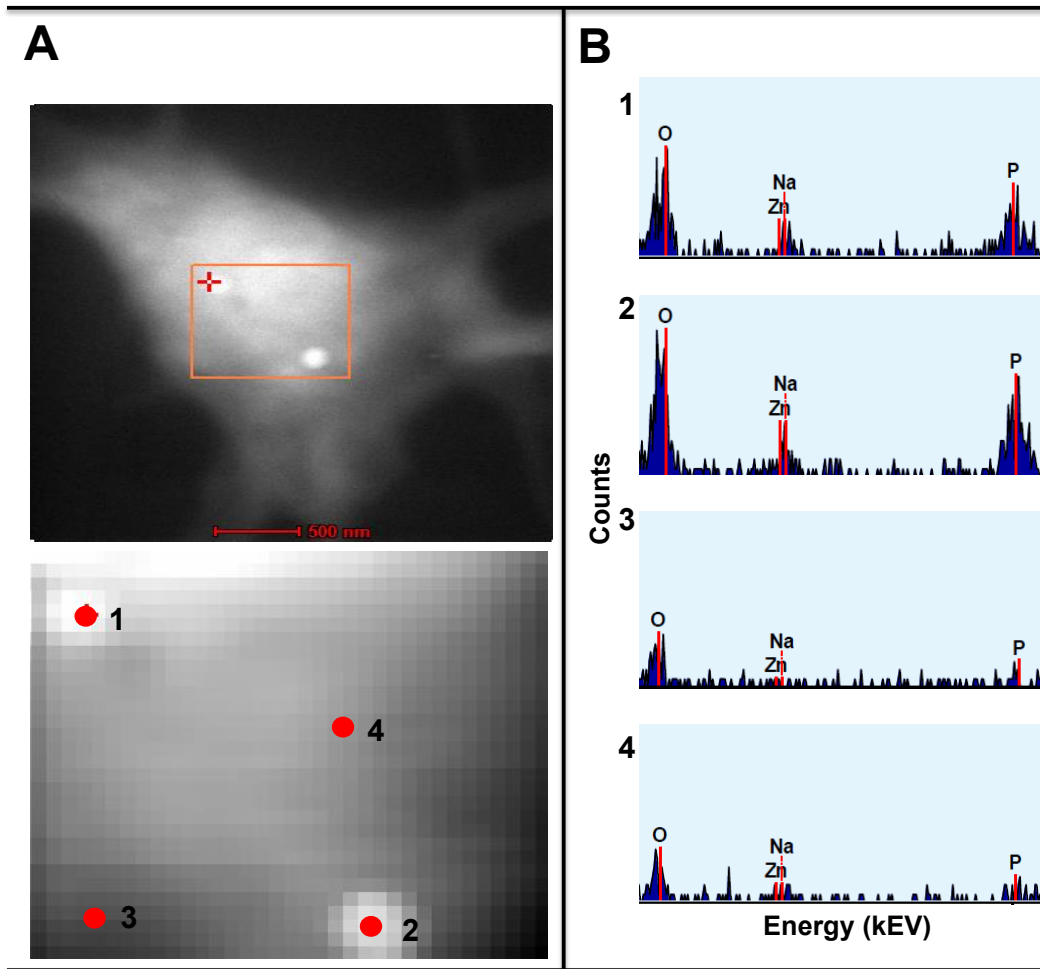


Figure 1. TEM and X-ray microanalysis of platelet dense granules

(A) Fixed platelets adhered to Fg were imaged using TEM (*top image*). A magnified image of a platelet is shown, with a box indicating the frame at higher magnification subjected to elemental analysis (*bottom, red dots*). Areas 1 and 2 represent dense granules, whereas areas 3 and 4 represent non-dense granular areas. **(B)** The EDX spectra for the four areas are shown. Energy (keV) and counts are shown on the X- and Y-axis, respectively. Peaks corresponding to element composition of carbon (C), oxygen (O), Zn^{2+} , sodium (Na), phosphorus (P), and Ca^{2+} are highlighted (*red boxes*). **(D)** The distribution of elements were mapped and represented in individual images for C, O, P, Ca^{2+} , Zn^{2+} and Na are shown (*red*), and the two dense granules selected are highlighted (*white boxes*).

5.7.2 Zn^{2+} is not stored in the platelet cytoplasm or mitochondria

Washed platelets were stained for platelet organelles, and imaged using high-resolution confocal laser immunofluorescence microscopy to confirm the location of Zn^{2+} and Ca^{2+} in the dense granules. There were 1.8 ± 0.8 Zn^{2+} staining foci/platelet (range 1-3, n=5 images) detected by FluoZin-3AM (Figure 2). Using Mitotracker Deep Red, each platelet contained a mean of 4 ± 1.9 mitochondria (range 2-6, n=5 images) (Figure 2), consistent with previous reports (Boudreau et al., 2014). Sialic acid located on platelet membranes was detected using Lectin Wheat Germ Agglutinin. Zn^{2+} was not observed in the mitochondria, nor was it located throughout the platelet membrane (Figure 2). Therefore, based on the number of fluorescent Zn^{2+} foci, it is highly likely that Zn^{2+} resides in the dense granules of platelets.

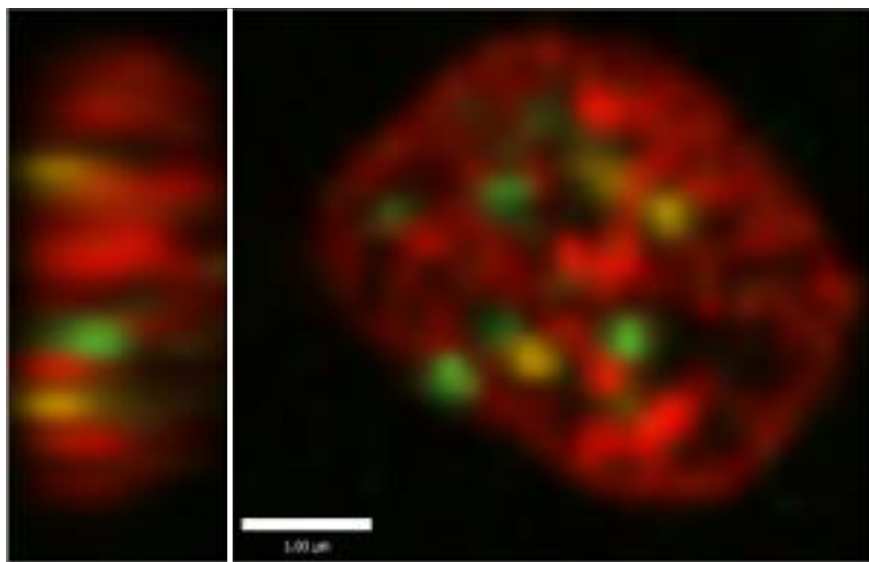


Figure 2. Detection of Zn²⁺ in resting platelets

Platelets were stained with combinations of membrane permeable fluorescent probes FluoZin3-AM (*green*), MitoTracker Deep Red (*yellow*), and Lectin Wheat Germ Agglutinin (*red*), for detection of Zn²⁺, mitochondria, and sialic acid respectively. High-resolution confocal laser immunofluorescence microscopy was used to capture lateral (*left*) and top (*right*) platelet slices at 90X magnification. The scale bar represents 1 μm.

5.7.3 Zn²⁺ colocalizes with Ca²⁺ in select granules

Next, Ca²⁺ was imaged using Calcium Orange to confirm localization of Zn²⁺ in the dense granules. Individual platelets contained 3.2 ± 1.6 Ca²⁺ foci (range 2-5, n=5 images) (Figure 3). In addition, diffuse background Ca²⁺ staining was observed in the platelet cytoplasm. When images were merged, Zn²⁺ colocalized with select Ca²⁺ foci, suggesting dense granule localization. However, Zn²⁺ did not colocalize with Ca²⁺ that was distributed throughout the cytoplasm or membrane with sialic acid. This confirms that Zn²⁺ is compartmentalized with other ions like Ca²⁺, in the dense granules of platelets.

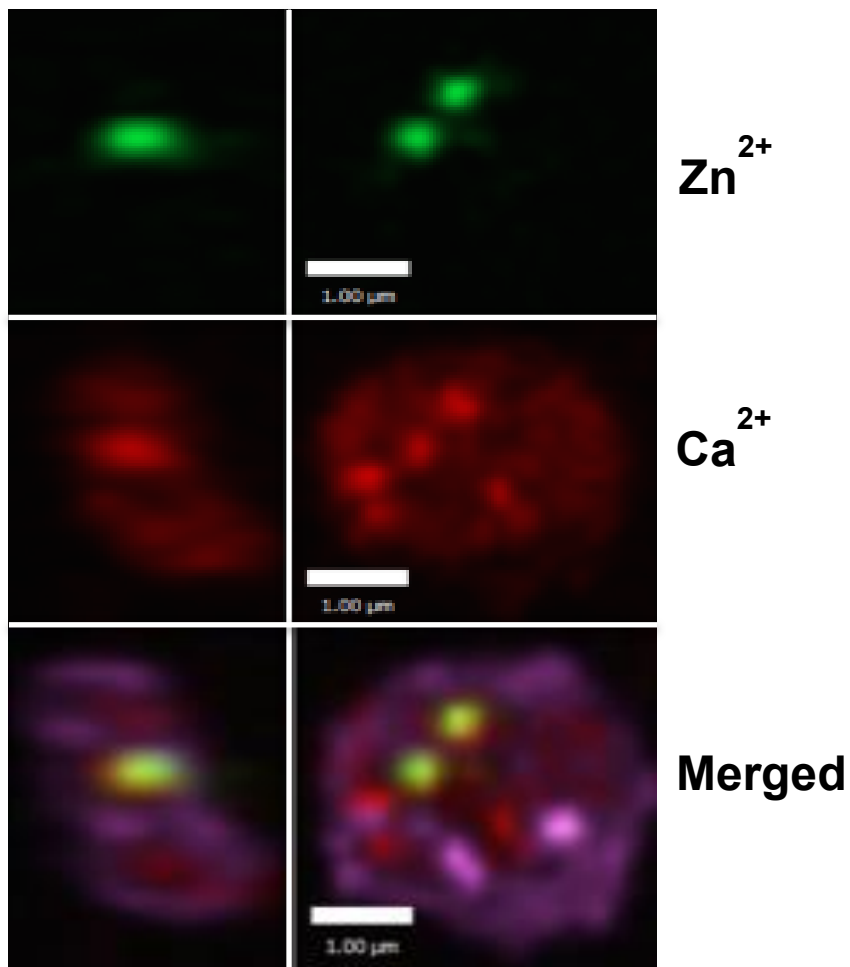


Figure 3. Detection of Zn²⁺ and Ca²⁺ in resting platelets

Platelets were stained using FluoZin3-AM (*green*), Calcium Orange (*red*), and Lectin Wheat Germ Agglutinin (*purple*), for the detection of Zn²⁺, Ca²⁺, and sialic acid, respectively. High-resolution confocal laser immunofluorescence microscopy was used to capture lateral (*left*) and top (*right*) platelet slices at 90X magnification. The scale bar represents 1 μm.

5.7.4 Activated platelets release the majority of Ca^{2+} stores, but only half of Zn^{2+}

Activated platelets release sufficient levels of Zn^{2+} to elevate plasma Zn^{2+} concentrations at the site of vessel injury (Henderson et al., 2015a). We observed that only half of the total Zn^{2+} concentration in resting platelets was released with activation and full dense degranulation (Henderson et al., 2015a). To complement this, platelet Ca^{2+} release was quantified using flame atomic absorption spectroscopy. Platelet poor plasma collected from three healthy individuals was used to determine plasma Zn^{2+} and Ca^{2+} concentrations. Plasma Zn^{2+} and Ca^{2+} concentrations were observed to be within normal range at $10.6 \pm 1.3 \mu\text{M}$ and $2.0 \pm 0.1 \text{ mM}$, respectively (Henderson et al., 2015a; Marx, 1988b). To determine intracellular ion levels, platelets were isolated and washed from blood collected from three healthy donors. For each donor, Zn^{2+} and Ca^{2+} concentrations were quantified in non-activated and activated platelet samples. Resting platelets ($\sim 1 \times 10^9 \text{ ml}^{-1}$) contained $27 \pm 11.1 \mu\text{M}$ and $220.1 \pm 65.7 \mu\text{M}$ Zn^{2+} and Ca^{2+} , respectively. In the presence of platelet agonists thrombin and collagen, the activated platelet supernatants contained $14.4 \pm 1.4 \mu\text{M}$ and $198.2 \pm 68.6 \mu\text{M}$ Zn^{2+} and Ca^{2+} , respectively. These results suggest that 90% of intracellular Ca^{2+} was released, whereas only 53% of Zn^{2+} was released from platelets upon activation. To confirm degranulation of the dense bodies, a fluorometric assay for ADP was quantified on platelet releasates. ADP release was $11.8 \pm 8.1 \mu\text{M}$ and 20.7 ± 8.1

μM for Zn^{2+} and Ca^{2+} releases. This reflects full dense degranulation, as released ADP values are expected to be $\sim 9.5\text{-}19 \mu\text{M}$ (Sigma Aldrich). This confirms platelet dense degranulation under the conditions used for activation.

5.7.5 Half of platelet Zn^{2+} can be chelated with TPEN

Next, we wanted to confirm that platelets release only a portion of their intracellular Zn^{2+} stores. Resting platelets were stained with FluoZin3-AM, and then incubated with the intracellular Zn^{2+} chelator TPEN or activated with thrombin and collagen. FI values at various times were determined by flow cytometry. Resting platelets that were stained with FluoZin-3AM had a $14 \pm 1.2\%$ reduction in FI after 20 min ($p < 0.001$). Activated platelets demonstrated a $54.3 \pm 2.1\%$ reduction in FI after 20 min ($p < 0.001$). These experiments correlate with our atomic absorption experiments, suggesting that only half of platelet intracellular Zn^{2+} is releasable upon activation (Figure 4). Next, we wanted to determine what quantity of platelet Zn^{2+} could be removed using a cell permeable Zn^{2+} -specific chelator. TPEN chelated $49.3 \pm 7.6\%$ of Zn^{2+} , which is comparable with active release ($p < 0.001$) (Figure 4). This suggests that only a portion of platelet intracellular Zn^{2+} remains freely available for release and/or chelation. These results confirm our previous data that only half of intracellular platelet Zn^{2+} is secreted with platelet activation (Henderson et al., 2015a).

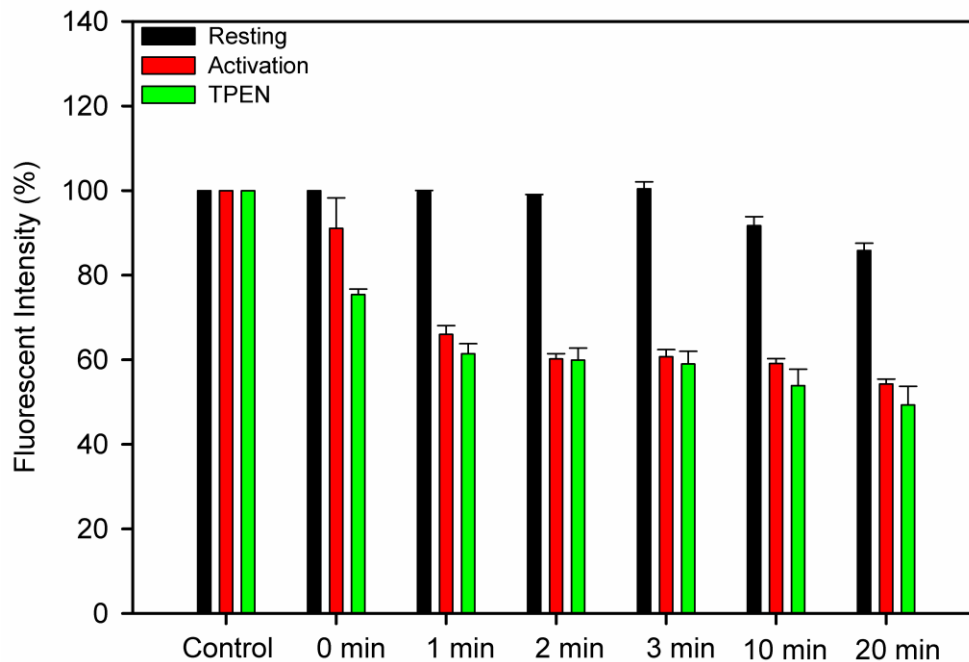


Figure 4. Zn^{2+} release and chelation from activated and resting platelets

Platelets isolated from 3 healthy individuals were stained with FluoZin3-AM (5 μ M), and ~5000 platelets were counted using a flow cytometer. Stained platelet samples were left to rest (*black*), activated with platelet agonists thrombin (10 nM) and collagen (20 μ g/ml) (*red*), or incubated with TPEN (1 μ M) (*green*), and monitored over time (0-20min). Changes in FI (%) were determined by comparing the FI measured at each time point to its resting control (Time 0). Bars represent the mean changes in FI of 3 donors, while the error bars reflect SE.

5.8 DISCUSSION

Zn^{2+} and Ca^{2+} are divalent ions that exhibit different intracellular locations in platelets as previously reported (Heijnen and van der Sluijs, 2015; Marx et al., 1993). The purpose of this study was to re-evaluate the discrepancy in Zn^{2+} and Ca^{2+} storage, and examine their release with platelet activation. We identified the intracellular location of Zn^{2+} using several technical approaches. Dense granule elemental analyses confirmed the presence of Ca^{2+} and phosphorus, consistent with previous data (Ruiz et al., 2004). We now provide novel evidence that Zn^{2+} is also stored in the dense granules of platelets. Immunofluorescence imaging revealed that Zn^{2+} and Ca^{2+} colocalize in select granules, but do not colocalize in the cytoplasm. Unlike Ca^{2+} , which is fully secreted with activation, only half of intracellular Zn^{2+} is releasable. Consistent with this, a similar fraction of Zn^{2+} was removed from the fluorescent probe using Zn^{2+} -specific chelation. Our results indicate that Zn^{2+} storage in platelets is tightly regulated, and concentrations released upon activation are sufficient to modulate hemostatic processes.

Platelet release of Ca^{2+} serves a signaling role because it is a cofactor for thrombin, which drives clot formation. Platelets elevate Zn^{2+} levels at the site of injury, and recent studies highlight the importance of Zn^{2+} regarding its ability to modulate the coagulation cascade, clot structure, and fibrinolysis reactions (Henderson et al., 2015a; Henderson et al., 2015b; Vu et al., 2013). However, concentrations required to modulate these processes are ~100-fold lower for Zn^{2+}

than Ca^{2+} (Ryan et al., 1999). Zn^{2+} binds to plasma proteins Fg and histidine-rich glycoprotein with high affinity, and was thought to reside with these proteins in the alpha granules (Marx, 1988c; Marx et al., 1993). In addition, others suggested that Zn^{2+} is also stored in the cytoplasm of platelets (Marx et al., 1993). Because of this discrepancy, we sought to identify the location of platelet Zn^{2+} . Our TEM results confirm those of Ruiz *et al.*, who demonstrated that dense granules contain carbon and oxygen, as it should be highly distributed in any membrane organelle (Ruiz et al., 2004). ADP, ATP, and polyphosphates are abundant in the dense granules, and contribute to phosphorus peaks observed (Heijnen and van der Sluijs, 2015; Ruiz et al., 2004). Zn^{2+} , sodium, and Ca^{2+} peaks were also detected in the dense granule segments. Thus, we can conclude that Zn^{2+} is most likely localized with Ca^{2+} and other charged molecules in the dense granules of platelets.

To confirm and examine other subcellular locations of Zn^{2+} , platelets were imaged using high-resolution confocal laser immunofluorescence microscopy. Images revealed the detection of 1-3 Zn^{2+} foci per platelet. This supports its dense granular location, as there are ~3-8 dense granules per platelet compared with ~50-80 alpha granules (Blair and Flaumenhaft, 2009; Fitch-Tewfik and Flaumenhaft, 2013; Heijnen and van der Sluijs, 2015). Unlike Ca^{2+} , we demonstrate that Zn^{2+} ions are specifically compartmentalized into few secretory granules, and do not freely circulate in the platelet cytoplasm. Ca^{2+} circulates in the cytoplasm to regulate signaling cascades, granule secretion, platelet activation,

adhesion, and aggregation (Ruiz et al., 2004). Unlike Ca^{2+} , it is unclear why Zn^{2+} is specific for dense granular populations; therefore Zn^{2+} might be a useful marker to identify these subgroups in future studies.

Next we wanted to quantify Ca^{2+} and Zn^{2+} storage and secretion from activated platelets. Images reveal that Zn^{2+} is strictly compartmentalized thus we were able to examine Zn^{2+} release and chelation. Atomic absorption spectroscopy and flow cytometry experiments examining platelet activation and Zn^{2+} chelation over time both resulted in half of platelet Zn^{2+} removal. What the remaining intracellular Zn^{2+} is interacting with after platelet activation has not been identified. Using immunofluorescence imaging approaches, we were unable to identify what Zn^{2+} may be binding, as antibodies used for protein detection require permeabilization of the platelet membrane, and cause the removal of ions. It is possible that Zn^{2+} binds with high affinity to intracellular proteins that are not secreted with activation. Previous reports indicate that platelets contain four Zn^{2+} -dependent metalloproteinases (MMP) including MMP-1, MMP-2, MMP-3, and MMP-9, which are endopeptidases responsible for extracellular matrix degradation (Jurasz et al., 2002). Structurally, MMPs contain a pro-peptide and catalytic metalloprotease domain, linked by a hinge region connected to a hemopexin domain (Jurasz et al., 2002). Active MMP-1 and MMP-2 are shown to play an important role in platelet function (Martinez et al., 2001). At the platelet surface, MMP-1 participates in tyrosine phosphorylation and grouping of integrin

$\beta 3$, whereas MMP-2 modifies glycoprotein 1b and glycoprotein IIb/IIIa, modulating platelet adhesion (Martinez et al., 2001). This may indicate why a portion of Zn^{2+} is not releasable with activation because it binds to Zn^{2+} -dependent matrix metalloproteinases on the platelet surface to mediate platelet function (Seizer and May, 2013). The functional role of intracellular Zn^{2+} that is not releasable upon activation has yet to be elucidated, and requires investigation.

Using a wide array of technical approaches, we provide an extensive assessment of platelet Zn^{2+} storage and release. Because platelets release Zn^{2+} into the microenvironment of a forming clot, Zn^{2+} is able to regulate numerous hemostatic processes. Concentrations of Zn^{2+} secreted from activated platelets are sufficient to modulate clot structure and fibrinolysis (Henderson et al., 2015a; Henderson et al., 2015b). These studies suggest that the role of Zn^{2+} as a key regulator in hemostasis should not be overlooked.

5.9 ACKNOWLEDGEMENTS

We would like to thank Iqbal Jaffer for blood collection, Alex Zimmer at McMaster University, and Carol-Ann Wigmore at the Hamilton General Hospital Core Laboratory for assisting in atomic absorption analysis.

CHAPTER 6: ORIGIN AND RELEASE OF PLATELET HISTIDINE-RICH GLYCOPROTEIN

6.1 Forward

The location of HRG in platelets and the extent of its release are described in this manuscript. We demonstrate that HRG is located in MK, proplatelets, and on the surface of platelets. The majority of HRG is not releasable with activation, because it participates in platelet adhesion by binding to GP1b α in a Zn²⁺-dependent fashion.

6.2 Objective: Re-examine platelet HRG storage and release

Previous studies suggest that HRG resides in the alpha granules of platelets (Leung et al., 1983). In Chapter 5, we demonstrated that Zn²⁺ is located in the dense and not the alpha granules of platelets as previously reported. Because HRG binds to Zn²⁺ with high affinity in plasma, we hypothesized that HRG may not reside in the alpha granules or cytoplasm. Therefore, HRG release from activated platelets is in question. To test our hypothesis we (A) determined the location of HRG in platelets, (B) quantified HRG concentrations in plasma and its release from activated platelets, and (C) investigated the involvement of HRG in platelet adhesion to vWF.

Origin and Release of Platelet Histidine-rich Glycoprotein

Sara J. Henderson^{1,2§}, Fred G. Pluthero^{5,6§}, Alan R. Stafford^{1,3}, Ran Ni^{1,4}, Ji Zhou^{1,3}, Nima Vaezzadeh^{1,4}, Peter L. Gross^{1,3,4}, James C. Fredenburgh^{1,3}, Walter H. Kahr^{5,6}, and Jeffrey I. Weitz^{1,4}

Thrombosis and Atherosclerosis Research Institute¹ and the Department of Biochemistry and Biomedical Sciences², Medicine³ and Medical Sciences⁴, McMaster University, Hamilton, and the Department of Pediatrics, Division of Hematology/Oncology⁵, The Hospital for Sick Children⁶, University of Toronto, Toronto, Ontario, Canada

§ Authorship note: Sara J. Henderson and Fred G. Pluthero contributed equally to this work and are co-first authors

Running title: Histidine-rich glycoprotein is not released with platelet activation

Address correspondence to: Jeffrey I. Weitz, Thrombosis and Atherosclerosis Research Institute, 237 Barton St E, Hamilton, ON L8L 2X2, Canada, e-mail: weitzj@taari.ca

Footnotes: This work was supported in part by the Canadian Institutes of Health Research and the Heart and Stroke Foundation. J.I.W. holds the Heart and Stroke Foundation J. Fraser Mustard Endowed Chair in Cardiovascular Research and the Canada Research Chair (Tier 1) in Thrombosis.

Authorship Contributions: SJH coordinated the study, wrote the paper, and performed experiments in Figures 3 and 6. FGP captured platelet images in Figures 1-3, and performed blots in Figure 4. ARS performed SPR experiments in Figure 5. JZ and RN performed blood collection from mice and assisted in perfusion assays. NV provided technical assistance for platelet HRG quantification. PLG assisted in experimental design and analysis for the perfusion assay. JCF contributed to writing and experimental design. WHK and JIW contributed to interpretation of the data and final approval of the manuscript. The authors have no conflicts to disclose.

***A modified version of this manuscript is in preparation for submission to the journal *Blood*.**

References: References for this manuscript have been incorporated into the Bibliography at the end of this thesis.

6.3 KEY POINTS

1. HRG is located in megakaryocytes, proplatelets, and platelets.
2. HRG resides on the platelet surface and is not released upon activation.

6.4 ABSTRACT

Histidine-rich glycoprotein (HRG) is thought to reside in the alpha granules of platelets, and secreted upon activation. Because HRG attenuates arterial thrombosis in a murine model, it was of interest to better characterize its origin and release in platelets. Using high-resolution laser fluorescence spinning disk confocal microscopy, HRG was detected **(A)** in the cytoplasm and surface of maturing megakaryocytes, **(B)** the buds of proplatelet extensions, and **(C)** the cytoplasm and surface of platelets. HRG did not colocalize with the alpha or dense secretory granules detected by P-selectin, or CD63. Activated platelets did not contain HRG in the central granulomere, detected by α -tubulin. HRG was present in platelet lysates of gray platelet syndrome patients, which do not contain alpha granule contents. This confirms that HRG does not reside in platelet alpha granules, as previously reported. The amount of HRG was 93-fold higher in resting platelets compared to activation, indicating that HRG is not secreted. Surface plasmon resonance revealed that HRG binds to full-length glycoprotein (GP) 1b α and GP1b α -269-286 peptide (K_d values of 2.8 ± 0.2 and 0.4 ± 0.01 nM,

respectively) in a zinc (Zn^{2+})-dependent fashion. Platelet adhesion to von Willebrand factor (vWF) was examined in blood collected from HRG deficient mice. Platelet adhesion was reduced in HRG deficient mice compared to wild-type mice. However, platelet adherence was improved in HRG deficient mice with the addition of HRG and Zn^{2+} . Our findings provide novel evidence to support the location of HRG in megakaryocytes, proplatelets, and platelets. Because HRG resides in the platelet cytoplasm and on the surface we have identified a new role for HRG as it participates in platelet adhesion by binding to $GP1b\alpha$ in the presence of Zn^{2+} .

6.5 INTRODUCTION

HRG has been shown to serve an antithrombotic role in a murine arterial thrombosis model (Vu et al., 2015b). This highlights a potential new role for this multifunctional plasma protein, and establishes a novel mechanism by which thrombosis may be regulated. HRG is a 75 kDa protein, composed of two NH_2 -terminal cystatin-like domains, a histidine-rich region (HRR) that is flanked by two proline-rich regions and linked to a $COOH$ -terminal domain (Rydengard et al., 2008; Vu et al., 2011; Vu et al., 2015a). HRG has been shown to interact with fibrinogen (Fg) and fibrin (Fn), heparin, DNA, factor (F) XIIa, kallikrein, and plasminogen (Jones et al., 2005; MacQuarrie et al., 2011; Rydengard et al., 2008; Vu et al., 2015a; Vu et al., 2011). Thus, HRG modulates coagulation by (A) circulating in complex with Fg, and competing with thrombin binding to the

γ_A/γ' -chain of Fn, **(B)** attenuating the intrinsic pathway by directly inhibiting FXIIa activity, and **(C)** down-regulating DNA and RNA induced activation of FXII and FXI (MacQuarrie et al., 2011; Vu et al., 2015a; Vu et al., 2011). Binding of Zn^{2+} to His-residues on the HRR, induces a conformational change in HRG that enhances ligand binding (Jones et al., 2005; Kassar et al., 2015; Kluszynski et al., 1997). Therefore, Zn^{2+} regulates HRG as it influences its ligand specificity.

HRG is synthesized in the liver and circulates in plasma at a concentration of ~ 1.5 - $2 \mu M$. However, this concentration may be elevated as HRG is thought to be released from activated platelets (Jones et al., 2005; Leung et al., 1983; Tsuchida-Straeten et al., 2005; Vu et al., 2011). Because HRG is an endogenous regulator of hemostatic processes, it is important to understand its release at the site of vascular injury. Previous reports suggest that HRG is located in megakaryocytes (MK) and resides in the alpha granules of platelets, where $\sim 80\%$ is released with activation induced by thrombin (Leung et al., 1983; Silverstein et al., 1985). HRG also has been reported to reside on the surface of activated platelets (Leung et al., 1984). Here, HRG binds thrombospondin, and regulates the anticoagulant function of heparin at the site of injury (Leung et al., 1984). Recently, Vu *et al.* showed that HRG is widely distributed in platelet-rich thrombi formed in a murine $FeCl_3$ arterial thrombosis model (Vu et al., 2015b). However, a thorough study of the intracellular location of HRG in platelets has yet to be undertaken. To address these gaps, we sought to **(A)** identify the cellular location

of HRG in MK, proplatelets, and platelets using high-resolution, laser fluorescence spinning disk confocal microscopy, **(B)** examine HRG storage and release from activated platelets, **(C)** determine whether HRG is present in gray platelet syndrome (GPS) patient platelets, and **(D)** identify a functional role of HRG in platelets.

6.6 METHODS

6.6.1 Reagents

Affinity-purified sheep polyclonal antibody against human HRG was purchased from Affinity Biologicals (Ancaster, ON, Canada), and purified as previously described (Vu et al., 2011). Human HRG was purified from plasma using metal-chelate chromatography as previously described (MacQuarrie et al., 2011). Mouse anti-human monoclonal LS-C127810 was purchased from LSBio (Seattle, WA, USA). Rabbit anti-complement factor H (CFH) was kindly provided by Dr. Peter F. Zipfel. Rabbit anti-human monoclonal EPR2417Y was purchased from AbCam Inc. (Toronto, ON, Canada). Mouse anti-CD63 was obtained from the Developmental Studies Hybridoma Bank at the University of Iowa (Iowa City, IA, USA). Hoechst 33342 and donkey anti-rabbit IgG or anti-mouse IgG conjugated with Alexa Fluor 488, 568, or 647 were purchased from Life Technologies (Burlington, ON, Canada). Mouse anti-CD42B was from BD Biosciences (San Jose, CA). PF4-rabbit polyclonal antibody was purchased from EMD Millipore (Etobicoke, ON, Canada). HRP-conjugated donkey anti-rabbit,

anti-mouse, or anti-goat primary antibodies were from Jackson ImmunoResearch Laboratories (West Grove, PA, USA). Mouse anti- α -tubulin, mouse anti- β -actin, U46619, bovine serum albumin (BSA), prostaglandin E₁, DiOC6, and TritonX-100 were purchased from Sigma Aldrich. The fluorescent mounting media was obtained from Dako (Burlington, ON). Human α -thrombin was from Enzyme Research Laboratories (South Bend, IN, USA). Abciximab was purchased from Eli Lilly (Mississauga, ON, Canada). Complete protease inhibitor was purchased from Roche (Mississauga, ON, Canada). Substrate o-phenylenediamine dihydrochloride was purchased from Cedarlane (Burlington, ON, Canada). GPIIb α extracellular domain was a gift from Raimondo de Cristofaro. A GPIIb α peptide, representing residues 269-286 with three phosphorylated Tyr-residues (GPIIb α -269-286PPP) was prepared by Mimotopes (Clayton, Victoria, Australia). Phe-Pro-Arg-chloromethylketone (PPACK) was purchased from Haematological Technologies Inc (Essex Junction, VT, USA). Purified, recombinant mouse vWF was kindly provided by Dr. David Ginsberg. Reagents for the sandwich ELISA were obtained from a VisuLize Buffer Pak purchased from Affinities Biologicals (Ancaster, ON, CA), and nickel coated 96-well plates were obtained from Thermo Fisher Scientific (Mississauga, ON, CA).

6.6.2 Preparation of megakaryocytes, proplatelets, and resting or activated platelets for immunofluorescence microscopy

Human cord blood was collected from healthy volunteers into 3.8% sodium citrate. Blood was passed over a Ficoll-Paque plus density gradient column to obtain mononuclear cells. Immunomagnetic beads were used to isolate progenitor CD34 cells, which were cultured in a serum-free suspension culture as described (Kahr et al., 2011). Maturing MKs were fixed, permeabilized, and stained as described previously with affinity purified polyclonal sheep anti-human IgG-HRG antibody, mouse anti-CD42B, and tagged with Alexa Fluor 647 conjugated IgG as described above for HRG and GPIIb α detection, respectively. MKs were stained with Hoechst 33342 for DNA detection. Stained platelet and MK coverslips were post-fixed with a 1:1 vol/vol of 4% PFA in PBS for 5 min, and mounted onto slides using a fluorescent mounting medium.

Platelets were isolated from blood collected with consent from healthy donors, as described in Chapter 5 (Henderson et al., unpublished 2015). Platelets were left to rest or subjected to activation with 8 nM thrombin for 10 min at 37°C, and fixed with 8% paraformaldehyde (PFA) (1:1 vol/vol) in phosphate-buffered saline (PBS) for 15-30 min at 23°C. Fixed platelets were pelleted and suspended in PBS containing 1% BSA. The fixed platelet suspensions (25 μ l) were spotted onto poly-L-lysine coated glass coverslips, and incubated at 100% humidity for 90 min at 37°C in a water bath. Platelets adhered to the coverslips were washed

with PBS and aspirated. Adherent platelets were mounted using a fluorescent mounting medium and immunostained immediately. Platelet suspensions were stained with antibodies for detection of various proteins. The mounted platelet membranes were either not permeablized or permeablized with 0.2% Triton X-100. Platelets were incubated overnight at 23°C with affinity-purified sheep polyclonal antibody against human HRG, mouse anti-human monoclonal LS-C127810, rabbit anti-CFH, mouse anti- α -tubulin, rabbit anti-human monoclonal EPR2417Y, or mouse anti-CD63 for detection of HRG, P-selectin, CFH, α -tubulin, CD61 antigen, or CD63 antigen, respectively. Stained coverslips were treated with 0.1% Triton X-100, washed with PBS, and labeled with fluorescent secondary antibodies for 60 min using donkey anti-rabbit IgG or anti-mouse IgG conjugated with Alexa Fluor 488, 568, or 647.

6.6.3 Laser fluorescence spinning disk confocal microscopy

Platelet images were captured as previously described in Chapter 5 (Henderson et al., unpublished 2015), using high-resolution Quorum spinning disc confocal inverted fluorescence microscope (Spectral Applied Research). Microscope conditions used are described by Kahr *et al.* (Kahr et al., 2013). A final 90X objective was used to capture mid-megakaryocyte, proplatelet, or mid-platelet Z-stack images, which were processed using Perkin Elmer Volocity software (versions 5.5-6.1).

6.6.4 Western blot

Platelets were isolated from blood as described in Chapter 5 (Henderson et al. unpublished 2015). Platelets were suspended at a concentration of 400 cells/nl in Tyrodes' salt solution containing 20 µg/ml Abciximab. Platelets were activated with 4 µM U46619 for 10 min at 37°C. Samples were subjected to centrifugation at 1000 x g for 8 min before harvesting the supernatants. Lysates were obtained by the addition of 0.1% Triton X-100 in PBS with 2X complete protease inhibitor to 1000 cells/nL solution of resting washed platelets. Samples from activated platelet supernatants or resting platelet lysates were electrophoresed on 4-20% acrylamide gradient gels (Bio-Rad), transferred onto a nitrocellulose membrane gel (Bio-Rad), and incubated with affinity purified polyclonal sheep anti-human IgG-HRG antibody, rabbit anti-human monoclonal EPR24174, or mouse anti-β-actin for the detection of HRG, CD61 antigen, and actin, respectively. Positive controls, secreted non-granule protein (NGP) and secreted alpha granule protein platelet factor 4 (PF4) were blotted on a separate gel. PF4 was detected using a PF4 rabbit polyclonal antibody. Secondary antibodies, HRP-conjugated donkey anti-rabbit, anti-mouse, or anti-goat were used for detection of primary antibodies. Blots were imaged using Western Lightning ECL (PerkinElmer Health Sciences) in Li-Cor Odyssey FC onto X-ray films.

6.6.5 Preparation of platelets for HRG quantification

An alternative platelet isolation protocol was used for HRG quantification. Blood was collected with consent from three healthy donors using a 21-gauge needle from the antecubital vein into 4 ml EDTA blood collection tubes to determine normal platelet counts by the Hamilton Regional Medical Laboratory Program. An additional 50 ml of blood was then drawn from the donors into acid citrate dextrose (ACD) (9:1 vol/vol). Blood was subjected to centrifugation at 200 x g for 20 min at 23°C. The PRP fraction was collected was supplemented with 1 µM of prostaglandin E₁, and subjected to centrifugation at 1000 x g for 10 min at 23°C. The platelet poor plasma (PPP) supernatant was removed and stored at -80°C for HRG quantification. The platelet pellet was washed with Tyrodes' salt solution lacking CaCl₂ but containing 1 µM prostaglandin E₁, and pelleted. The washed platelet pellet was suspended in 6 ml of the same solution and divided into two samples (3 ml per sample). All 3 ml samples were pelleted and concentrated by suspension into a final volume of 0.5 ml of Tyrodes' salt solution lacking CaCl₂. Platelet counts of the 0.5 ml solution were determined using a hemocytometer.

A 0.5 ml platelet suspension aliquot from each donor was activated by addition of 10 nM thrombin and 20 µg/ml HORM collagen suspension, or lysed by addition of 0.1% Triton X-100. After 30 min at 37°C, the activated and lysed samples were subjected to centrifugation at 1000 x g for 10 min at 23°C. The

supernatants of all samples were collected and dialyzed against 250 ml of PBS at 4°C with 2 hourly buffer changes, and an additional exchange overnight.

HRG concentrations were quantified by a sandwich ELISA with some modifications (MacQuarrie et al., 2011; Vu et al., 2011). Nickel coated 96-well plates were treated with 150 µl of blocking buffer containing 1% BSA in PBS, for 1 hr at 23°C, followed by aspiration. Purified HRG, donor PPP, and dialyzed platelet lysates and releasates (100 µl) were incubated in wells for 1 hr at 23°C. The wells were washed 3 times with PBS-Tween20, and aspirated. HRG was detected by adding 100 µl (1:1000 dilution) of affinity purified HRP-conjugated goat anti-human HRG antibody to the wells. After incubation for 1 h at 23°C, the antibody was aspirated, and the wells were washed 4 times with PBS-Tween20 then aspirated. The fluorescent substrate o-phenylenediamine dihydrochloride was dissolved in citrate-phosphate buffer containing 30% peroxide. Aliquots (100 µl) of the substrate were added to wells until a color change was observed. The reactions were stopped with the addition of 50 µl of 2.5 M H₂SO₄, and optical densities (OD) of the wells were read at 490 nm using a SpectraMax Paradigm plate reader (Molecular Devices). The background reading in the absence of HRG was subtracted from the values determined. OD values were corrected for dilution, and divided by the specific absorbance (0.0018 OD/ng/ml) obtained from the HRG standard curve to determine the plasma HRG concentration. The

concentrations of HRG in the platelet supernatants were determined from the standard curve.

6.6.6 Surface plasmon resonance

The affinity of HRG for extracellular domain of GPIb α (glycocalicin) was quantified using surface plasmon resonance (SPR) on a BIAcore T200 (GE Healthcare). Using amine coupling, GPIb α in 20 mM HEPES, pH 7.4, 150 mM NaCl (HBS) containing 0.01% Tween 20 (HBS-Tw), was immobilized on a CMD 50 I biosensor chip (XanTec Bioanalytics, Düsseldorf, Germany) resulting in 5000-7000 response units (RU). HRG (0-500 nM) was injected into flow cells in the absence and presence of 12 μ M ZnCl $_2$. Flow cells were regenerated with 3.6% sodium citrate to remove residual Zn $^{2+}$. Experiments were repeated by immobilizing the thrombin-binding GPIb α peptide. Sensorgrams were obtained and binding affinities (K_d) values were determined using a two-state reaction kinetic fit on BIAcore T200 Control Software (version 2.0).

6.6.7 Blood collection from mice

Wild-type (WT) C57BL/6 mice were obtained from Charles River Laboratories. HRG deficient (HRG $^{-/-}$) mice were obtained from W. Jahn-Dechent and propagated as described (Vu et al., 2015b). Females of similar weight were used for blood collection. Mice were anaesthetized with a 10% ketamine, 5% xylazine, 5% atropine cocktail. The carotid artery was cannulated and 1 ml of blood was drawn from WT or HRG $^{-/-}$ mice into a 1 ml syringe

containing PPACK (100 μM), and stored at 23°C. Animal utilization protocols were approved by the Animal Research Ethics Board at McMaster University and followed the Canadian Council on Animal Care guidelines.

6.6.8 Ex vivo perfusion assay

Mouse vWF was immobilized at a concentration of 50 $\mu\text{g/ml}$ into 4 channels of a Vena8 Fluoro⁺ biochip (Cellix, Dublin, Ireland). The remaining 4 channels were treated with BSA as controls (50 $\mu\text{g/ml}$). The biochip was incubated overnight at 4°C in a humidified chamber (Cellix, Dublin, Ireland). After immobilization, each channel was blocked with 3% BSA in Tyrodes' salt solution lacking CaCl_2 for 1 h at 23°C. Human HRG (2 μM) was added with or without 12 μM ZnCl_2 to blood collected from some HRG^{-/-} mice, and pre-incubated for 90 min at 23°C. Platelets were labeled by incubating whole blood samples with 1 μM of DiOC6 for 10 min at 37°C. Blood samples (320 μl) were loaded into channels of the BSA or vWF coated biochip, and the perfusion assay was performed using a Mirus Nanopump (Cellix, Dublin, Ireland). Blood perfusion was set to a shear rate of 2000 s^{-1} for 4 min, followed by a wash with Tyrodes' salt solution lacking CaCl_2 for 1 min. Biochip fluorescence was imaged under the 10X objective using confocal microscopy on an Olympus BX series microscope controlled by Slidebook (version 6.0) (Intelligent Imaging Innovations, Denver, Colorado). Three continuous images of each channel were

captured and converted to a montage image, and the mean sum fluorescent intensity (FI) per channel was quantified using Slidebook (version 6.0).

6.6.9 Statistical analysis

Data are presented as mean \pm standard error (SE). Significance of differences was determined using a Student's t-test or a one-way analysis of variance followed by Tukey's test for multiple pair-wise comparisons (SigmaPlot version 11.0). P-values less than 0.05 were considered statistically significant.

6.7 RESULTS

6.7.1 HRG is located in megakaryocytes, proplatelets and platelets

Human MK were imaged to determine the origin of HRG in platelets. Cells were cultured in serum-free media, isolated, and stained for HRG, CD42B, and DNA. MK contained a polyploid nucleus, and maturity state was identified as pre-mature by the lack of pseudopodia-like extensions on the outer surface (Figure 1A). HRG was distributed throughout the cytoplasm, and on the peripheral platelet-forming fields. HRG corresponded with the location of GP1b α , indicated by CD42B staining, which was not expected, as this suggests that HRG may reside on the surface and not be compartmentalized. After MK maturation, proplatelets developed, indicated by their dumbbell shape (Figure 1B). CD42B and HRG were detected in abundance throughout the proplatelet, corresponding with MK images. An abundance of HRG was concentrated in the lateral buds of the proplatelet, which are the precursor to platelets. These results highlight that

HRG resides in the MK, suggests that it is synthesized *de novo*. Because HRG and GP1b α are highly abundant in MK and proplatelets suggests that they may interact in platelets.

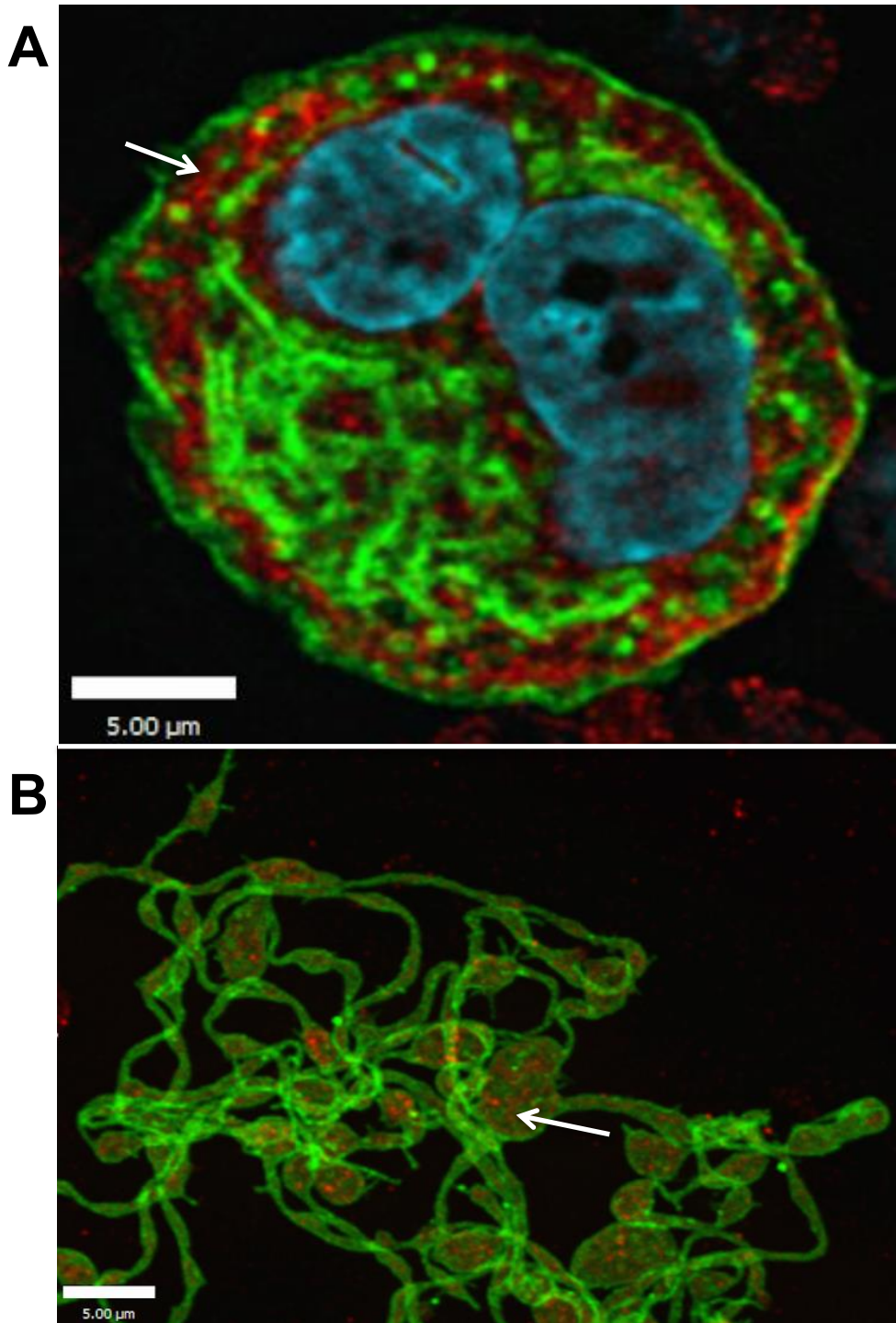


Figure 1. HRG resides in megakaryocytes and proplatelets

(A) MK were cultured in a serum free system, washed, fixed, permeablized, and stained with sheep anti-human HRG polyclonal IgG antibody tagged with Alexa Fluor 568 (*red*). DNA was stained with Hoechst 33342 (*blue*), and CD42B was stained with mouse anti-CD42B tagged with Alexa Fluor 488 (*green*). (B) Proplatelets and were imaged for HRG and CD42B as described above. Laser fluorescence spinning disk confocal microscopy images of mid-megakaryocyte Z-slices and proplatelets were captured at 90X magnification. White bars reflect a 5 μm scale.

Next we examined the location of HRG in platelets. Platelets were isolated from normal donors, permeabilized, and stained for the intracellular detection of HRG, CD61 antigen, and P-selectin. HRG fluorescence was observed in the platelet cytoplasm and on the platelet outer membrane. HRG shared a similar distribution as integrin $\beta 3$, which was not expected as HRG should be compartmentalized as previously reported (Figure 2A) (Leung et al., 1983). HRG was not contained within the alpha granule secretory matrix, identified by localization of P-selectin. This suggests that HRG may not reside in the alpha granules as previously reported (Leung et al., 1983).

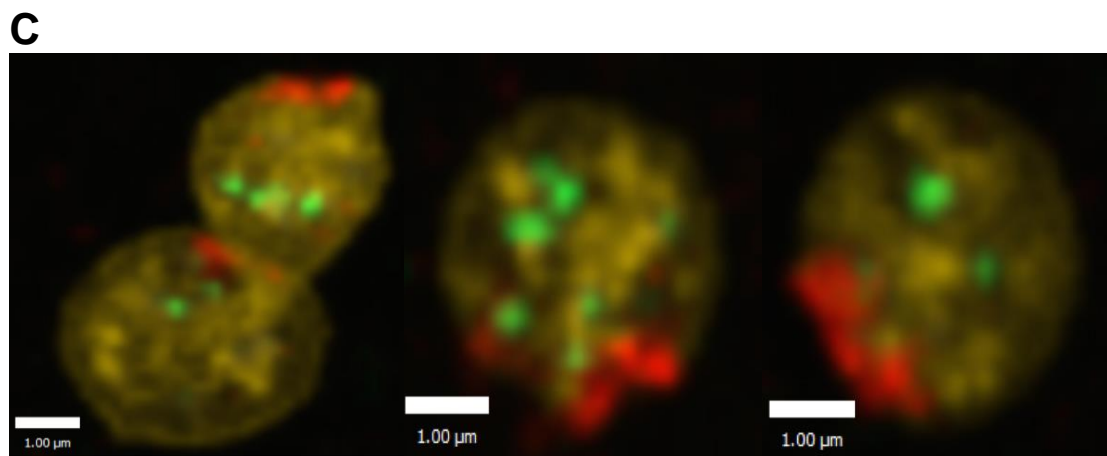
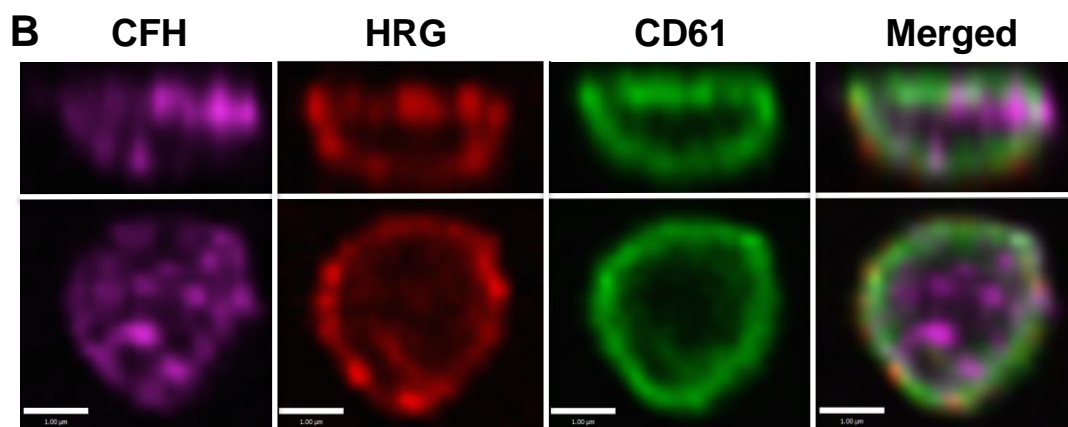
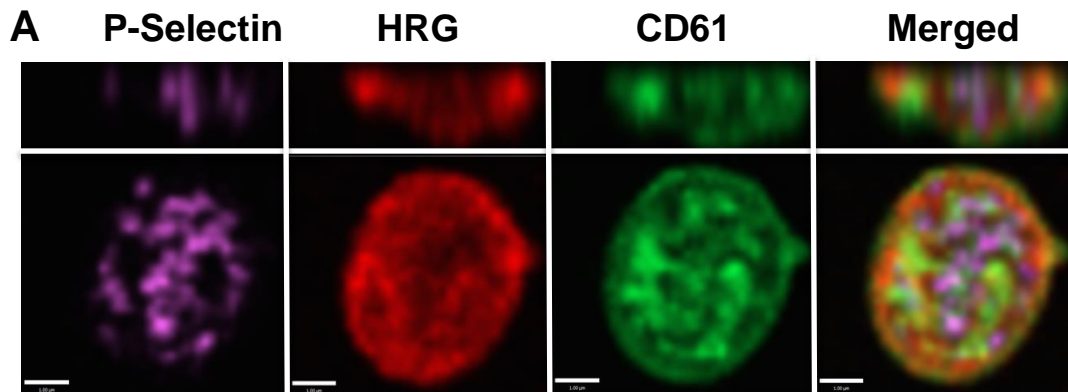


Figure 2. HRG is located in the cytoplasm and outer surface of platelets

Washed human platelets were fixed, and the membrane was either **(A,C)** permeablized or **(B)** not permeablized prior to staining. Platelets were incubated with sheep anti-human HRG IgG affinity purified polyclonal antibody, mouse anti-human monoclonal LS-C127810, or rabbit anti-human monoclonal EPR2417Y and labeled with secondary antibodies tagged with Alexa Fluor 488 (*green*), 568 (*red*), 647 (*violet*). **(A)** Permeablized resting platelets were stained for the HRG (*red*), CD61 (*green*), and P-selectin (*violet*), with overlapping of all three images reflecting colocalization (*yellow*). **(B)** Non-permeablized resting platelets were stained for HRG (*red*), CD61 (*green*), and CFH (*purple*), with colocalization of all images (*yellow*) **(C)** Permeablized resting platelets were washed several times prior to fixation and staining for HRG (*red*), CD61 (*yellow*), and CD63 (*green*). Platelets were imaged using laser fluorescence spinning disk confocal microscopy capturing mid-platelet Z-slices at 90X magnification. White bars reflect a 1 μm scale.

Because HRG circulates in plasma, we wanted to determine whether HRG could be detected on the outer surface of platelets. Platelets were stained but not permeabilized, allowing only extracellular HRG, CD61 antigen, and CFH to be detected. In earlier studies, CFH, a plasma protein, was reported to reside in the alpha granules of platelets (Devine and Rosse, 1987). However, in agreement with recent reports CFH was detected on the outer membrane surface and cytoplasm (Licht et al., 2009). Similarly, HRG was not located in the alpha granules via the detection of P-selectin, as HRG was on the platelet outer surface with CFH and integrin $\beta 3$ (Figure 2B). These data suggest that HRG is stored in the platelet cytoplasm, but plasma HRG also resides on the platelet outer surface.

Next, we wanted to determine whether plasma HRG was tightly bound to the outer surface of platelets. This was investigated by extensive washing of the platelets to see if HRG could be removed. Permeabilized platelets were incubated and washed several times for 3 h prior to fixing and staining. Platelets were stained for HRG, the dense granule membrane marker CD63, and CD61 antigen. Images revealed that after extensive washing, HRG was observed on the platelet outer surface in a defined polar cap-like region (Figure 2C). Integrin $\beta 3$ was not affected by washing, consistent with its location as an integral membrane protein. This indicates that HRG binds the outer surface, and is not anchored within membrane. HRG was not detected in the dense granular matrix, because colocalization was not observed with CD63. These data suggest that platelets

contain two HRG repositories as follows: 1. an intracellular source originating from the biosynthesis in the MK, and 2. plasma HRG docked on the outer surface of circulating platelets.

6.7.2 Activated platelets release little HRG

Next, we wanted to examine HRG release upon activation. Platelets were activated with thrombin in suspension, fixed, and stained for HRG, CD61 antigen, and α -tubulin. HRG and integrin β 3 were both observed on outer membrane surface (Figure 3A). This is not surprising as HRG colocalized with integrin β 3 in resting platelets. HRG did not colocalize with α -tubulin in the central granulomere, confirming that HRG is not located with secretory granules (Figure 3A). In contrast to previous studies, we show that platelet HRG is not located in the alpha granules, nor is it released upon activation (Leung et al., 1983). We demonstrate the HRG resides in the platelet cytoplasm and surface, and is not releasable.

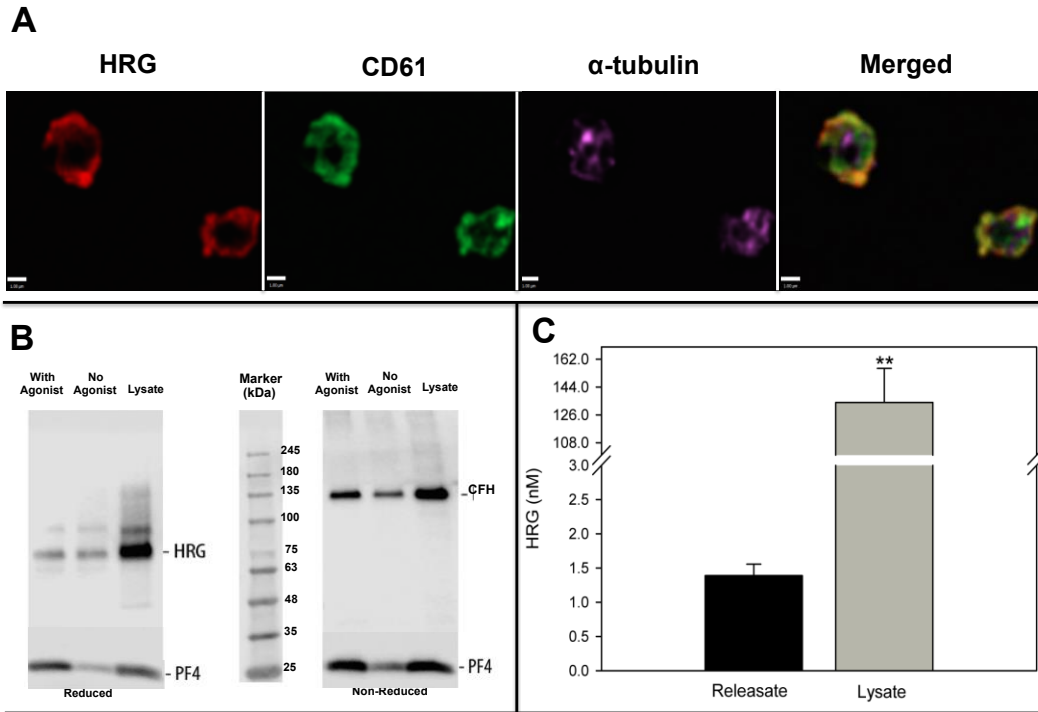


Figure 3. Little HRG is released in the absence and presence of a platelet agonist

(A) Platelets were activated with thrombin, fixed, stained for the detection of HRG (*red*) and integrin $\beta 3$ (*green*) and α -tubulin (*violet*). All three images were merged to examine colocalization (*yellow*). Platelets were imaged using laser fluorescence spinning disk confocal microscopy capturing mid-platelet Z-slices at 90X magnification. White bars reflect a 1 μm scale. **(B)** Platelets were incubated in the absence or presence of a platelet agonist U46619, or lysed with detergent. Platelet supernatants were collected and blotted under reduced (*left*) and non-reduced (*right*) conditions for HRG detection. Secreted contents for the detection of CFH and PF4 were used as controls. The molecular weight ladder is located in the center of the images. **(C)** Platelets were isolated, washed, activated with thrombin and collagen or lysed with detergent. Bars represent HRG levels in platelet lysates and releasates quantified using an ELISA, and error bars reflect SE between the three donors. Statistical significance was determined (** $p < 0.001$).

To confirm that HRG is not released upon activation, washed platelets were left untreated, lysed or activated with the mild platelet agonist U46619. After centrifugation, soluble fractions were then electrophoresed, blotted onto a membrane, and probed with antibodies for HRG. The lysed fraction exhibited HRG in the supernatant, confirming that HRG was present in platelets. However, there was little HRG in the control or activated platelet soluble fractions after centrifugation, indicating that the majority of HRG remained associated with the platelet (Figure 3B). A trace amount of HRG in the supernatants suggests that some release of HRG may occur, or that some plasma HRG was bound to the outer surface and released. These findings suggest that the majority of HRG remains within platelets and is not released with activation.

Next, we wanted to quantify the amount HRG stored and released from activated platelets. HRG levels were determined in PPP and in activated or lysed platelet samples using a modified sandwich ELISA (MacQuarrie et al., 2011; Vu et al., 2011). The concentration of HRG in PPP was $\sim 1.1 \pm 0.1 \mu\text{M}$, comparable with previous values (Corrigan, Jr. et al., 1990; Jones et al., 2005; Kassar et al., 2015; Vu et al., 2011). A lysed suspension of 1.5×10^9 platelets/ml yielded a HRG concentration of $146 \pm 53.6 \text{ nM}$ (Figure 3C). This is equivalent to 14.6 nM HRG in the number of platelets in normal plasma. Following platelet activation, $\sim 1.3 \pm 0.3 \text{ nM}$ HRG was detected in the platelet releasate (Figure 3C). The amount of HRG associated with the platelet aggregates could not be determined due to solubility limitations of the aggregate. These results confirm that the bulk of intracellular platelet HRG is not released, but remains associated with the platelet surface following activation.

6.7.3 HRG is present in GPS patient platelet lysates

Data to this point suggests that platelet HRG is not compartmentalized in secretory granules nor secreted with activation. GPS platelets lack alpha granule contents, and were used to confirm the location of HRG. GPS platelets were lysed with detergent and immunoblotted for HRG, actin, and CD61 antigen. Platelets isolated from three GPS donors all showed HRG bands comparable in intensity with the healthy control (Figure 4A). We believe that the slight mobility differences between healthy controls and GPS platelet lysates for HRG detection

appears to be an artifact, because it was evident for all probes in GPS platelet lysates. GPS and control platelet lysates contained comparable levels of integrin $\beta 3$ and actin, indicating comparable loading quantities (Figure 4B). These results confirm that HRG is not located in the secretory alpha granules of platelets as HRG is present in GPS platelet lysates that lack these granules and their respective contents.

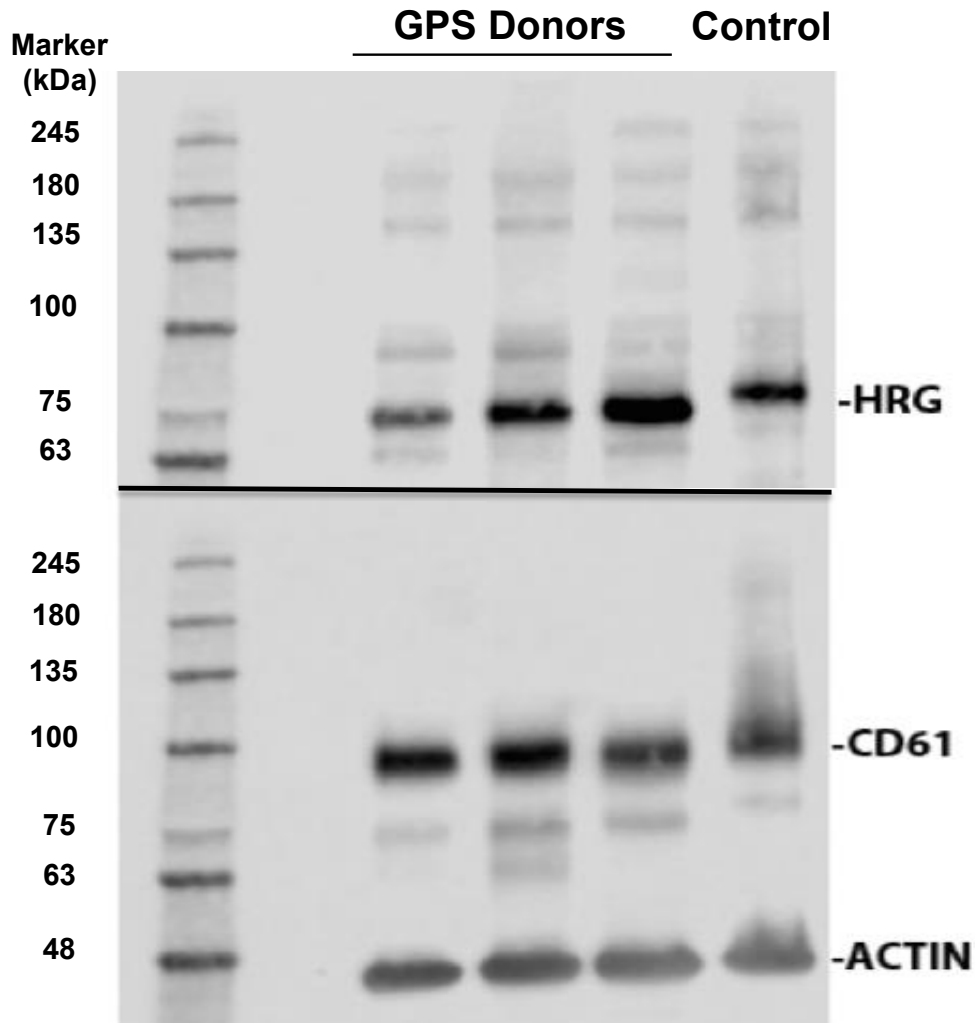


Figure 4. GPS platelets contain HRG, CD61, and actin

(A) Platelet lysates of three GPS patients and a healthy donor were blotted for HRG as described above. **(B)** Similar blots were probed for CD61 antigen and actin as controls. The molecular weight marker is indicated on the left.

6.7.4 HRG binds to GPIb α in a Zn²⁺-dependent fashion

Because images revealed that HRG colocalized with GPIb α in MK and proplatelets, we wanted to identify whether HRG binds to GPIb α . The extracellular domain of GPIb α glycofibrin was immobilized in a flow cell for SPR studies. Injection of increasing concentrations of HRG in the presence of Zn²⁺ resulted in elevated RU values (Figure 5). Analyses revealed that HRG binds to GPIb α with high affinity (K_d value of 2.8 ± 0.2 nM). HRG binding to the segment of GPIb α that interacts with thrombin, residues 269-286, was also examined. HRG bound to the peptide with higher affinity than to intact glycofibrin (K_d value of 0.4 ± 0.01 nM). Interestingly, no binding was observed to either glycofibrin or the peptide in the absence of Zn²⁺ (data not shown). This suggests that the HRG-GPIb α interaction is Zn²⁺-dependent, and is mediated by the thrombin-binding segment in GPIb α .

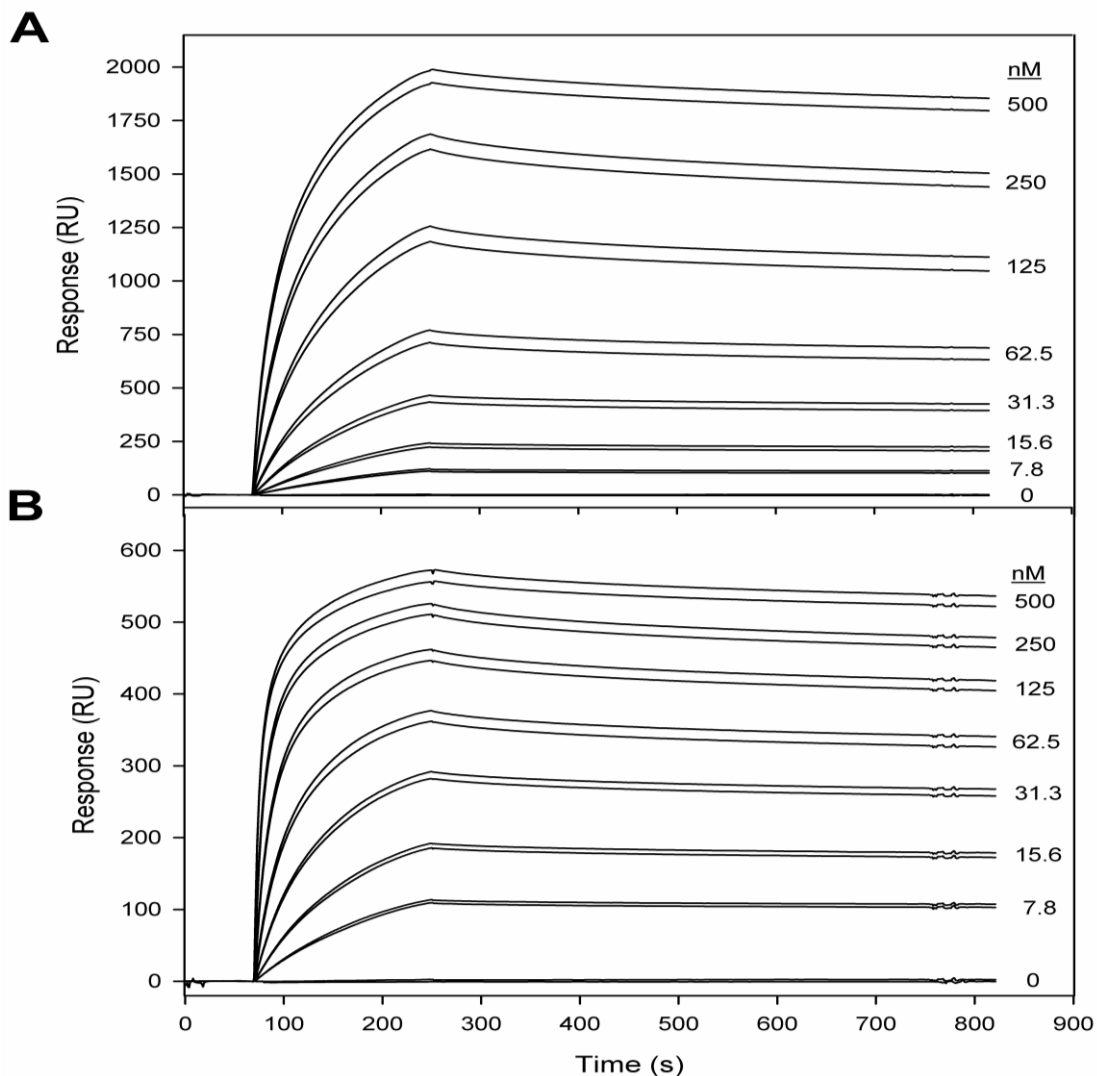


Figure 5. HRG binds to GP1ba in the presence of Zn^{2+}

Extracellular domain of GP1ba (**A**) or the thrombin binding peptide (**B**) was immobilized onto flow cells of a biosensor chip for SPR analysis. HRG was injected into the flow cells at concentrations of 0, 7.8, 15.6, 31.25, 62.5, 125, 250, and 500 nM, respectively, in the presence of $12 \mu\text{M Zn}^{2+}$. Sensorgrams of the duplicate runs are shown, with the HRG concentrations in nM beside the lines.

6.7.5 The role of HRG on platelet adhesion

Next we wanted to identify whether HRG modulates platelet adhesion to vWF through its interaction with GP1b α . Blood collected from WT or HRG^{-/-} mice were incubated with a platelet-specific dye DIOC6, and perfused over flow cells containing immobilized BSA or recombinant mouse vWF. Flow cells were washed and imaged by confocal microscopy to quantify platelet adhesion in WT and HRG^{-/-} mice (Figure 6A). Blood from some HRG^{-/-} mice was reconstituted with 2 μ M human HRG, or with HRG and 12 μ M Zn²⁺. FI for each flow channel was quantified and corrected for background fluorescence in the corresponding BSA channel for each blood sample. Experiments were performed 8 times per group, and the mean values are plotted (Figure 6E). Blood from WT mice had the highest adhesion of platelets to vWF, with a FI of $13.3 \pm 4.4 \times 10^7$ AUD, whereas the HRG^{-/-} mice had the lowest adhesion, with a FI of $4.2 \pm 0.7 \times 10^7$ AUD. However, differences in platelet adhesion between these groups was not statistically significant ($p=0.06$). FI of adhered platelets from the HRG^{-/-} mice increased to $5.2 \pm 1.4 \times 10^7$ AUD with HRG reconstitution, but was not statistically significant compared with its absence ($p=0.54$). Addition of Zn²⁺ and HRG to blood from HRG^{-/-} mice elicited a slight increase in FI to $7.3 \pm 1.6 \times 10^7$ AUD, but this value was also not statistically significant from HRG^{-/-} adhesion ($p=0.1$). These data suggest that HRG may modulate platelet adhesion to GP1b α in a Zn²⁺-dependent fashion. As a positive control, immobilization of collagen

instead of vWF could provide a direct comparison, and has yet to be examined. However, under these conditions platelet binding was not significantly different between the groups ($p=0.25$). Further studies will be needed to investigate the role of HRG on platelet function.

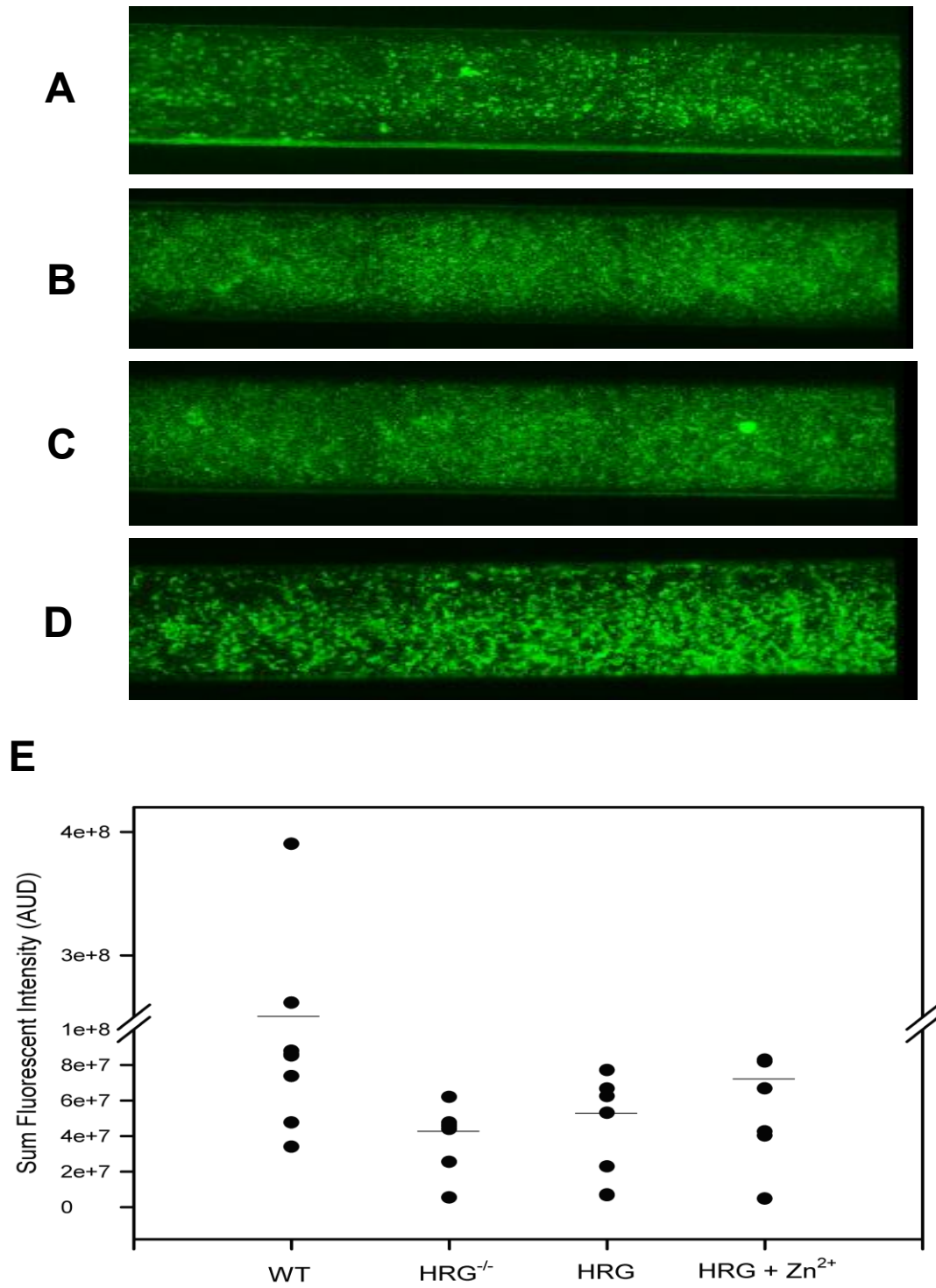


Figure 6. HRG and Zn²⁺ increase platelet adhesion to vWF in HRG^{-/-} mice

Blood was collected from 8 mice per group of (A) WT or (B,C,D) HRG^{-/-} mice and incubated with DiOC6, a fluorescent platelet marker. Some HRG^{-/-} blood samples were incubated with (C) 2 μM HRG or (D) 2 μM HRG and 12 μM Zn²⁺. Samples were perfused over flow cells containing immobilized recombinant mouse vWF. Flow cells were washed and imaged using confocal microscopy. Montage images were prepared for each condition. (E) FI was determined from images captured at 10X magnification, and plotted for each condition. Lines represent mean FI values.

6.8 DISCUSSION

Recent studies reveal that platelet-rich thrombi in WT mice contain an abundance of HRG (Vu et al., 2015b). It is known that HRG resides in platelets and is secreted upon activation by thrombin (Leung et al., 1983). As a result, HRG levels are thought to be elevated at the site of vascular lesions, where HRG binds Fn (Leung, 1986). Colocalization of HRG and Fn was confirmed in WT mice at the site of FeCl₃ induced injury, where platelets also were abundant (Vu et al., 2015b). Because HRG binds Fg, it was speculated that HRG is located in the alpha granules of platelets, where Fg resides (Leung, 1986). However, the origin and intracellular location of platelet HRG has yet to be defined. It is important to understand the location of HRG and its release, as HRG modulates coagulation through FXIIa and attenuates the intrinsic pathway (MacQuarrie et al., 2011; Vu et al., 2011; Vu et al., 2015a). This study was undertaken to address these gaps in our knowledge of platelet HRG storage and release. We show that: **(A)** HRG resides in MK, proplatelets, and platelets, **(B)** HRG is not located in the alpha granules of platelets, **(C)** little HRG is released in the presence of a platelet agonist, **(D)** HRG binds to GP1b α in the presence of Zn²⁺, and **(E)** attenuated platelet adherence to vWF in blood from HRG^{-/-} mice is restored with reconstitution of HRG and Zn²⁺.

Liver parenchymal cells are known to be the primary source of circulating HRG in plasma (Jones et al., 2005). Although HRG has also been detected in

immune cells such as monocytes and macrophages, and in MK. However, there is a lack of definitive evidence as to whether hematopoietic cells synthesize or acquire HRG from plasma (Hulett and Parish, 2000; Leung et al., 1983). Previous reports demonstrate that tissues harvested from the spleen, thymus, lymph nodes, bone marrow, and blood leukocytes do not contain HRG mRNA (Hulett and Parish, 2000). This suggests that HRG in platelets and immune cells enters from plasma. In the current study, imaging revealed that HRG was abundant in premature MK derived from human hematopoietic stem cells cultured in a serum free system. This suggests that MK have a capacity to synthesize HRG. With MK maturation, HRG was also observed in proplatelets, which are the precursors to platelets. In human platelets, HRG was detected in the cytoplasm and on the surface, but not in the secretory alpha or dense granules. Interestingly, plasma HRG bound weakly to the outer surface of platelets. This observation correlates with previous reports that HRG associates with the cell surface and extracellular matrix (Brown and Parish, 1994; Leung et al., 1984). With extensive washing, plasma HRG migrated to a polar cap-like region, which was observed with other plasma proteins such as plasminogen and PAI-1 (Whyte et al., 2015). HRG is known to bind to plasminogen, which may reflect its weak interaction with the outer cell surface (Jones et al., 2004). As to why these proteins localized to one specific region requires further examination.

In contrast to previous reports, HRG was not found in secretory granules (Leung et al., 1983). Thus, we wanted to determine whether intracellular HRG could be released upon activation. To investigate this, we examined the distribution of HRG in resting and activated platelets (Leung et al., 1983). HRG did not colocalize with alpha and dense granular markers P-selectin or CD63. In addition, we confirmed that HRG was not detected in GPS patient or healthy control lysates. This confirms that HRG is not present in platelet secretory granules. Furthermore, only minimal amounts of HRG were detected in platelet releasates in the absence and presence of platelet agonists. Minimal HRG detected probably accounts for plasma HRG that is bound to the outer surface of platelets.

It is unknown as to what HRG interacts with on the platelet surface. It is possible that HRG is bound to cell surface antigens or receptors. GP1b α is highly expressed on the cytoplasm and surface of platelets and had a similar cellular distribution of HRG in MK and proplatelets. We observed that HRG binds to GP1b α with high affinity in the presence of Zn²⁺. This interaction was most likely mediated through residues 269-286, since HRG bound to the corresponding synthetic peptide in the presence of Zn²⁺. Thus, the conformational change in HRG induced by Zn²⁺ may be required for GP1b α binding. We previously showed that intracellular Zn²⁺ is released from platelets with activation (Henderson et al., 2015a). This may signify that intracellular Zn²⁺ regulates platelet HRG. It remains to be investigated whether intracellular platelet

HRG/Zn²⁺ or extracellular plasma HRG/Zn²⁺ or both bind GP1b α , to modulate its function.

Recent studies have shown that HRG regulates arterial thrombosis (Vu et al., 2015b). Ringvall *et al.* demonstrated that platelets from HRG^{-/-} mice exhibit accelerated collagen, thrombin, and ADP stimulated platelet aggregation compared with WT mice (Ringvall et al., 2011). Vu *et al.* confirmed this by demonstrating that arterial thrombosis is accelerated in HRG^{-/-} mice (Vu et al., 2015b). These results suggest that HRG has antithrombotic properties. To investigate the functional role of platelet HRG, we examined platelet binding to vWF, which is mediated by GP1b α . Platelet adhesion was examined in blood collected from HRG^{-/-} mice. HRG^{-/-} mice had elevated adhesion to vWF with reconstitution of HRG and Zn²⁺ compared to its absence. This may support HRG/Zn²⁺-binding to GP1b α *in vitro*, and provide an explanation as to why HRG and a portion of Zn²⁺ are not released with platelet activation.

Emerging evidence has demonstrated that HRG is a key modulator in arterial thrombosis. HRG binds numerous plasma proteins, where it is proposed to modulate coagulation (Jones et al., 2005). HRG acts as a molecular brake by attenuating the intrinsic pathway through binding FXIIa and procoagulant nucleic acids DNA and RNA (MacQuarrie et al., 2011; Tsuchida-Straeten et al., 2005; Vu et al., 2015a). Because HRG is present in platelets, the origin and fate of platelet-derived HRG is of interest. Since HRG remains on the platelet surface via

interaction with glycoproteins, it is possible that HRG has a platelet-specific role independent of that of plasma HRG. This study demonstrates another avenue by which HRG may modulate hemostasis.

6.9 ACKNOWLEDGEMENTS

We would like to thank Iqbal Jaffer for blood collection and D'Andra Parker for assistance with the perfusion assay.

CHAPTER 7: GENERAL DISCUSSION AND FUTURE DIRECTIONS

7.1 General Discussion

Zn^{2+} provides regulation to numerous hemostatic interactions (Vu et al., 2013). Platelets accumulate at the site of vascular injury, and release Zn^{2+} from their secretory granules upon activation (Leung et al., 1983). Here, local levels of Zn^{2+} rise sufficiently above background levels exhibited in plasma (Rojkjaer and Schmaier, 1999). Consequently, elevated Zn^{2+} concentrations accelerate coagulation but delay fibrinolysis (Vu et al., 2013). The effect of Zn^{2+} on hemostatic reactions has been overlooked because of blood collection into divalent ion chelators. To correct for this, Zn^{2+} should be reconstituted into *in vitro* reactions. The main objective of this thesis was to re-evaluate Zn^{2+} storage and release in platelets, and evaluate the role of Zn^{2+} on clot formation and clot lysis. This thesis demonstrates that: Zn^{2+} accelerates clotting and modifies clot structure to promote stability (**Chapter 3**), Zn^{2+} attenuates fibrinolysis by down-regulating P_g activation and P_n-mediated F_n hydrolysis (**Chapter 4**), Zn^{2+} is located in the dense granules of platelets, but only half of its intracellular Zn^{2+} content is released with platelet activation (**Chapter 5**), and HRG resides in MK, proplatelets, the platelet cytoplasm and surface, and binds to GP1b α in a Zn^{2+} -dependent fashion to augment platelet adhesion in HRG^{-/-} mice (**Chapter 6**). The purpose of this Chapter is to (A) shed light on the physiological importance of

Zn²⁺ in hemostasis, **(B)** explore new avenues by which Zn²⁺ is regulated **(C)** provide future directions to expand on these projects, and **(D)** discuss the limitations and challenges of proposed work.

7.2 Platelet Zn²⁺

7.2.1 Zn²⁺ storage in platelets

Since it was believed that HRG and Fg reside in platelet alpha granules, it was reported that Zn²⁺ was also stored here, because it binds to these proteins with high affinity (Marx et al., 1993; Vu et al., 2011). However, Zn²⁺ is a divalent ion and could be compartmentalized in the dense granules with other ions, such as Ca²⁺ and Mg²⁺ (Heijnen and van der Sluijs, 2015). Due to the discrepancy in divalent ion storage, we re-evaluated the location of Zn²⁺ and Ca²⁺ in platelets, and examined their secretory release with activation. In contrast to previous reports, we showed that Zn²⁺ resides in the platelet dense granules with Ca²⁺ and phosphorus (Marx et al., 1993). Interestingly, unlike full Ca²⁺ release, only half of the Zn²⁺ content was secreted from activated platelets. By quantifying the amount of Zn²⁺ and Ca²⁺ stored in resting platelets, we demonstrated that the concentration of Zn²⁺ was ~10-fold lower than Ca²⁺. Plasma Zn²⁺ concentrations are also ~100-fold lower than Ca²⁺, yet Zn²⁺ has a greater potency in modulating clotting processes (Kanaide et al., 1982). Similarly to FV and PAI-1, Zn²⁺ requires strict compartmentalization in platelets, and regulates coagulation and fibrinolysis reactions (Rendu and Brohard-Bohn, 2001; Vu et al., 2013). Whether Zn²⁺

originates in MK or enters from plasma is in question. In this section we wanted to examine Zn^{2+} storage further, and investigate whether platelet Zn^{2+} originates from plasma or MK. This will highlight the discrepancies in storage of platelet divalent ions, and provide information regarding the regulated release of Zn^{2+} from activated platelets.

7.2.2 Detecting Zn^{2+} in HPS patient platelets

We have compelling evidence that Zn^{2+} is located in the dense granules of platelets (Chapter 5). To further confirm platelet storage of Zn^{2+} , we will examine HPS platelets. HPS patient platelets lack dense granules and their granular contents such as ADP, polyphosphates, and ions. However, platelet function is not completely abolished, as HPS patients contain functional alpha granules. The alpha granules contain coagulation proteins that drive clot formation, whereas the dense granules house small molecules and ions that augment platelet activation. Based on the evidence provided in Chapter 5, we hypothesize that Zn^{2+} will not be detected in HPS platelets, due to their lack of dense granules. Because Ca^{2+} was detected in the platelet cytoplasm, we hypothesize that Ca^{2+} will be found in HPS platelets. Zn^{2+} and Ca^{2+} in HPS platelets can be visualized using staining and imaging techniques described in Chapter 5. These experiments will further verify the storage of Zn^{2+} within platelet dense granules. It will also provide evidence that Zn^{2+} is unique, and requires strict compartmentalization unlike Ca^{2+} .

7.2.3 Zn^{2+} transportation in platelets

Zn^{2+} circulates in plasma at concentrations of 10-20 μ M. Platelets contain an open membranous system that allows plasma proteins and ions to enter. In Chapter 5, we did not detect Zn^{2+} in the cytoplasm or membrane system, thus Zn^{2+} must originate from the MK. Concrete evidence to support the origin of Zn^{2+} in the MK is lacking and the mechanism responsible for its compartmentalization into a secretory granule is unknown. To determine the origin of Zn^{2+} in platelets, MK can be stained with FluoZin3-AM as described in Chapter 6. This will indicate whether Zn^{2+} is strictly compartmentalized or dispersed throughout the cytoplasm of MK. Zn^{2+} cannot passively diffuse through a lipid bilayer cell membrane because Zn^{2+} is highly charged. Therefore Zn^{2+} requires transportation to enter, which is most likely mediated by an ion sensitive channel. Like any other cell, accumulation of Zn^{2+} can be toxic; therefore regulation of its transport into a MK is critical. Zrt-Irt-like protein (ZIP) transporters are abundant on the membrane and organelles of mammalian cells (Figure 1) (Kambe et al., 2015). Because ZIP transporters are selective for Zn^{2+} , we hypothesize that ZIP transporters are responsible for Zn^{2+} entry and movement in MK (Kambe et al., 2015). Future studies can investigate the presence of ZIP transporters in MK by lysing the cells with TritonX-100, and subjecting the lysates to inductively coupled plasma mass spectrometry for ZIP identification. Recognition of ZIP

transporters located on the cell membrane and organelles in MK is essential to understand Zn²⁺ origin and storage.

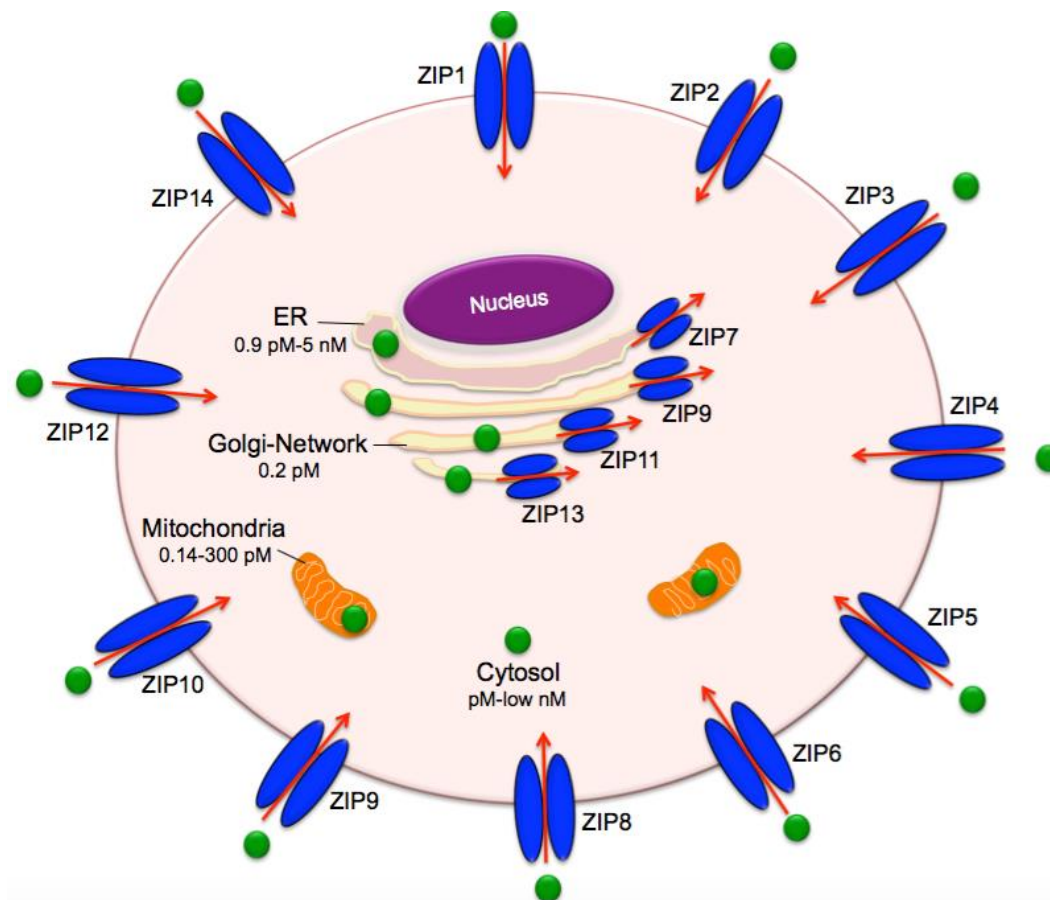


Figure 1. Transportation of Zn²⁺ in mammalian cells

Zn²⁺ transportation is essential for the regulation of various cellular functions. ZIP transporters mediate Zn²⁺ (green circles) influx into mammalian cells. The red arrows indicate the direction of Zn²⁺ transport. Values represent Zn²⁺ quantities in the cytosol, and organelles such as the mitochondria, Golgi-network, and ER. Adapted from Kambe et al., 2015.

The origin of platelet Zn^{2+} remains controversial. Thus, it is uncertain whether Zn^{2+} is endocytosed into cells from plasma. We have just explored the origin of Zn^{2+} from MK via ZIP transporters. Next we would like to explore the possibility of Zn^{2+} entry into platelets from plasma. Transient receptor potential melastatin 7 (TRPM7) is an ion transporter that is abundant on the surface of platelets (Mahaut-Smith, 2012). TRPM7 generates an inward current highly selective for Mg^{2+} ions (Figure 2). This enables Mg^{2+} entry through the phospholipid bilayer via a pore opening (Park et al., 2014; Yee et al., 2014; Zeng et al., 2015). In addition to Mg^{2+} , the influx of other divalent cations such as Ca^{2+} , Zn^{2+} , Ni^{2+} , manganese, and cobalt, also occurs via this channel (Yee et al., 2014).

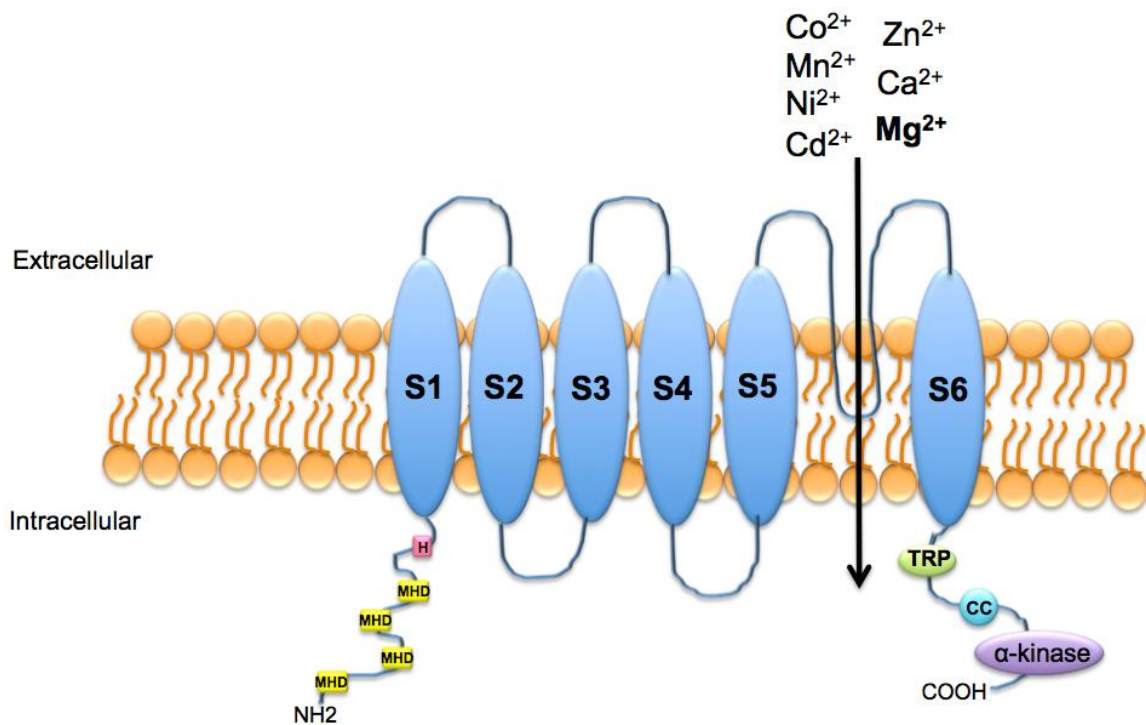


Figure 2. The structure of TRPM7 cation channel

The ion channel TRPM7 resides in the phospholipid bilayer. Structurally, TRPM7 contains 6 transmembrane subunits (S1-6). Between S5 and S6 there is a pore-forming loop, allowing extracellular ions to enter the channel. The intracellular NH₂-terminal region contains a hydrophobic region (H) and four melastatin homology domains (MHD). At the COOH-terminal region, a transient receptor potential domain (TRP), a coiled-coil region (CC), and α -kinase domain reside. TRPM7 is mainly responsible for transporting Mg²⁺ ions, although other ions like Zn²⁺, Ca²⁺, Ni²⁺, manganese (Mn²⁺), cobalt (Co²⁺), and cadmium (Cd²⁺) are also permitted. Adapted from Park et al., 2014.

Confocal images reveal that TRPM7 is highly expressed on the surface of mouse platelets (Figure 3) (Chen, 2015). This suggests that Zn^{2+} can enter a platelet through an alternative mechanism that is not the OCS. Examining these images further, TRPM7 appears to be present in few select foci. Future studies can examine these images further using high-resolution immunofluorescence confocal microscopy. Images can be used to identify TRPM7 on the dense granular membrane with colocalization of CD63, a dense granular marker. We hypothesize that TRPM7 will be located on the dense granular surface, where it transports cytosolic Zn^{2+} obtained from plasma into the dense granules to provide strict compartmentalization. This would explain why we were unable to detect a wide distribution of Zn^{2+} within the platelet cytoplasm. Next, we can use a TRPM7 deficient (-/-) murine model to examine Zn^{2+} secretion from the dense granules. Blood will be collected from WT and TRPM7^{-/-} mice, and platelets can be isolated and stained with FluoZin-3AM as described in Chapter 5. Flow cytometry can be used to assess platelet activation and Zn^{2+} release. If TRPM7 participates in plasma Zn^{2+} influx into platelets, the absence of this transporter would result in a reduction in the FI compared to WT mice. This would occur because Zn^{2+} entry into the platelet is abrogated in TRPM7^{-/-} mice. These experiments would provide concrete evidence that platelet Zn^{2+} may originate from plasma.

To establish the importance of Zn^{2+} secretion from activated platelets, this mouse model can be examined further. Tail bleeds can be used to assess coagulation in TRPM7^{-/-} mice compared to WT. TRPM7^{-/-} mice may lack dense granule Zn^{2+} stores, thus it is expected that clot times would be attenuated. This data would establish the regulatory role of Zn^{2+} in coagulation *in vivo*.

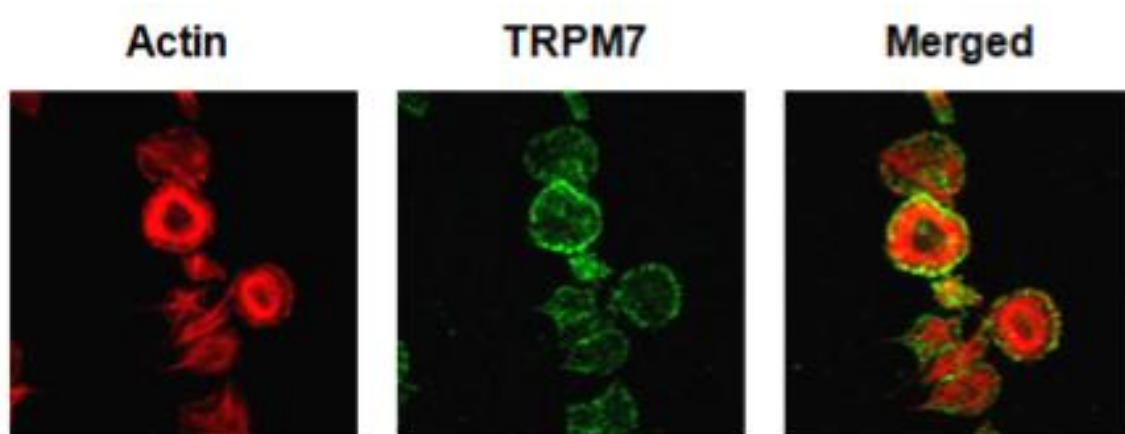


Figure 3. TRPM7 is expressed in platelets

Platelets obtained from WT mice were adhered to Fg, and activated with thrombin. Platelets were fixed, permeablized, and stained with Atto647N and TRPM7 antibodies to detect actin (*red*) and TRPM7 (*green*) respectively. Confocal images were captured to detect the location of actin and TRPM7. Images were merged to show colocalization between actin and TRPM7 (*yellow*). This image is a direct copy from Chen, 2015.

7.2.4 Examining Zn^{2+} release from platelets *in vivo*

The release of Zn^{2+} from platelets is thought to be critical for regulating clot formation and clot lysis. Accordingly, we want to identify whether platelet Zn^{2+} release can be demonstrated *in vivo*. Platelets from WT mice can be stained with FluoZin3-AM, and administered back into the circulation of another WT mouse. After inducing laser injury to arterioles in the cremaster muscle, the microcirculation can be visualized using intravital confocal microscopy. With fluorescently tagged platelet-directed antibodies, platelet accumulation at the site of injury can be monitored. Once the fluorescent platelets localize to the site of injury, we hypothesize that a reduction in fluorescence will be observed. This would indicate that Zn^{2+} is released from activated platelets *in vivo*, and dispersed into the circulation or forming thrombus. We can also detect Zn^{2+} within the thrombus using histological staining. The Rapid TimmStain Kit is widely used to detect the distribution of Zn^{2+} located in brain tissue. However, this methodology has not been used to identify Zn^{2+} within a vessel or thrombus. This approach could provide a visual examination as to how much Zn^{2+} is actually localized to a thrombus. These methodologies will support Zn^{2+} release from activated platelets *in vivo*, and demonstrate its localization to the site of vascular injury.

7.3 Platelet HRG

7.3.1 Examining the source of platelet HRG

Limited information is available regarding platelet HRG synthesis. Previous reports indicate that HRG resides in MK (Leung et al., 1983). However, others report that plasma proteins such as Fg, HRG, HK, AP, and α_2 -macroglobulin enter platelets from plasma (Handagama et al., 1993; Rendu and Brohard-Bohn, 2001). In Chapter 6, we wanted to re-examine the location of HRG in MK and platelets. We detected HRG in MK derived from human hematopoietic stem cells, suggesting that HRG is biosynthesized in the MK. Next, we wanted to determine whether MK and platelets permit HRG entry from plasma. We hypothesize that plasma HRG will not enter platelets by its OCS, as we show that HRG was detected in MKs cultured in a serum free system. We have preliminary data to support this hypothesis. HRG^{-/-} mice were injected with various doses of human HRG (Appendix Figure 1), and the bone marrow and platelets were extracted and fixed (Appendix Methods 9.1.2). Images revealed that HRG was not detected in MK or platelets harvested from HRG^{-/-} mice injected with HRG (Pluthero 2014, unpublished observation). This suggests that platelets may not permit HRG entry from plasma. We were unable to detect murine HRG in our WT control in either MK or platelets with the human HRG antibody, because of low cross reactivity. We are in the process of developing a suitable antibody to detect murine HRG to advance these studies.

Next we wanted to confirm that platelets do not allow the entry of plasma HRG via their OCS. Blood was collected from HRG^{-/-} mice, and platelets were isolated, washed, and incubated with FITC-labelled HRG for 4 h at 23°C. Platelet fluorescence was detected using flow cytometry as described in Chapter 5. We observed no changes in the FI when comparing platelets incubated with or without FITC-labelled HRG. This correlates with our *in vivo* experiments, suggesting that platelets do not have the capacity to take up HRG from plasma. Because it is not known how long it takes for a platelet to take up circulating HRG, thus increasing the incubation time may be considered. However, it is difficult to keep platelets in an inactive state over a long period of time without the requirement of fixation. In contrast to previous reports, this preliminary data indicates that platelet HRG originates in the MK and does not enter from endogenous plasma sources (Leung et al., 1983).

7.3.2 Investigating the functional role of intracellular platelet HRG

The functional role of HRG in platelets has not been extensively examined. In Chapter 6, we show that MKs contain HRG and GP1b α in the cytoplasm and on the cell surface. Next, we wanted to investigate whether HRG and GP1b α interact, to provide a rationale as to why HRG is abundant on the surface of resting and activated platelets. We demonstrated that HRG binds to full-length GP1b α and GP1b α ₂₆₉₋₂₈₆ peptide with high affinity. This suggests that HRG may compete with thrombin for binding to the GP1b α ₂₆₉₋₂₈₆ peptide sequence in a

manner analogous to how HRG competes with thrombin for binding to the γ -chain of Fg. To further investigate the involvement of platelet HRG on GP1b α , platelet adherence was examined using a blood perfusion assay. With the addition of HRG and Zn^{2+} to blood collected from HRG^{-/-} mice, platelet adherence to immobilized vWF was elevated compared with that measured in its absence. HRG and GP1b α both reside on the platelet surface, but bind only in the presence of Zn^{2+} . In Chapter 5, we highlight that platelets release only half of their Zn^{2+} content with activation. This supports the concept that a portion of Zn^{2+} is retained within platelets, which may augment HRG binding to GP1b α . Because HRG binding to GP1b α was examined *in vitro*, we do not know whether platelet or plasma HRG/ Zn^{2+} is responsible for binding GP1b α or modulates vWF binding.

We can differentiate the functional roles of platelet and plasma HRG by developing a chimeric mouse model. Mononuclear cells (MNC) can be harvested from the bone marrow of WT or HRG^{-/-} mice donors, and then injected back into irradiated acceptor mice of the opposite genotype (Figure 4). Therefore mice will contain only plasma or platelet HRG reservoirs. This model should be sufficient to distinguish between the two HRG stores, as it was used to differentiate between platelet-derived and endothelial cell-derived vWF (Verhene et al., 2015). Once we develop this mouse model, we can re-examine platelet adhesion to vWF using the blood perfusion assay described in Chapter 6. These studies will confirm the source of HRG that is responsible for modulating the function of GP1b α .

Interestingly, platelet adherence to vWF was reduced in HRG^{-/-} mice, however previous reports state that arterial thrombosis is accelerated (Vu et al., 2015b). We suspect that HRG has multiple roles on platelet function that have yet to be determined. This chimeric mouse model may be useful to determine what source of HRG is main driver in regulating arterial thrombus formation.

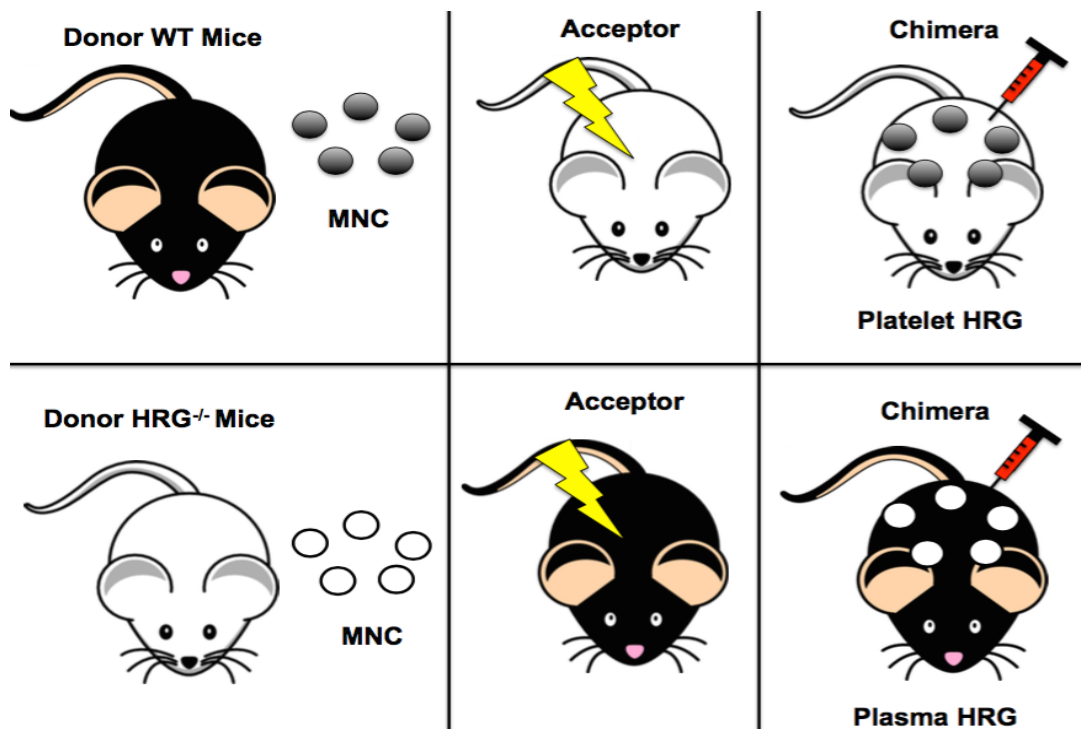


Figure 4. Bone marrow transplantation to examine platelet or plasma HRG

A chimeric mouse can be designed to specifically assess the involvement platelet or plasma HRG on the GP1b α interaction to vWF. After 6-10 weeks of age, bone marrow cells can be harvested from the femur and tibiae of WT and HRG^{-/-} mice as described (Appendix Methods 9.1.2). Isolated MNC can be transfused back into mice that were subjected to brief irradiation (*yellow*) to generate full chimerism. The HRG^{-/-} mice will contain platelet HRG, whereas the WT mice will have plasma HRG. Image adapted from Verhenne et al., 2015.

To further evaluate whether HRG participates in platelet adherence by GP1b α binding to vWF, this interaction can further be examined using the ristocetin cofactor assay. Ristocetin is an antibiotic that binds to vWF, and specifically triggers platelet agglutination through GP1b (Ermens et al., 1995). A platelet aggregometer can be used to detect platelet agglutination in blood collected from WT or HRG^{-/-} mice. Unfortunately, ristocetin is specific for triggering agglutination of human platelets; therefore batrocetin isolated from snake venom must be used for mouse platelets because it is not species specific. Because our perfusion assay examined platelet adherence to vWF and not activation, it is likely that full Zn²⁺ release was not acquired. Therefore we had to reconstitute Zn²⁺ into blood samples. In the batrocetin cofactor assay, platelet aggregation is examined as a consequence of activation. Therefore Zn²⁺ reconstitution is not required in this assay, because platelet Zn²⁺ release will be achieved. This experiment will directly compare platelet aggregation in the HRG^{-/-} and WT mice. Based on our findings, we hypothesize that platelet agglutination in blood from HRG^{-/-} mice will be less than that of WT mice. These experiments will confirm previous *in vivo* experiments and support the role of platelet intracellular Zn²⁺ that is not releasable with activation.

It would be of importance to colocalize GP1b α , HRG, and Zn²⁺ in resting and activated platelets to support our previous hypotheses. This is challenging from an imaging perspective because permeabilization of the platelet membrane is

required for staining, and triggers Zn^{2+} release. To overcome challenges with permeabilization, a new technology permits transient incorporation of proteins into cells without permeabilization of the membrane (Fuse-It, Ibidi, Beniag, Germany). Fuse-It generates small liposomal carriers that surrounds proteins, and fuses with plasma membrane delivering the protein of interest into the cell cytoplasm. This technology may enable antibodies to enter platelets allowing for the detection of GPIb α , HRG, and Zn^{2+} colocalization without membrane permeabilization. These experiments could provide concrete evidence to support the functional role of intracellular platelet HRG and Zn^{2+} on platelet adhesion.

7.4 Zn^{2+} and Clot Formation

7.4.1 Re-defining clot stability

It is important to re-establish the mechanical properties of clots formed, as it can be used to predict the fate of a thrombus (Weisel, 2004). Clot structure can be modified by altering enzyme, substrate, or ion concentration (Ferry and Morrison, 1947). In Chapter 3, we demonstrated that Zn^{2+} significantly accelerates clot formation by enhancing Fn monomer polymerization. By removing the α C-domain on Fragment X, we show that clot times remained accelerated, yet the effect of Zn^{2+} on fiber thickness was significantly attenuated. This implies that the Zn^{2+} -binding site on the α C-domain influences lateral assembly of protofibrils. In general, increasing fiber thickness is correlated with increased permeability. We demonstrate that the most potent effect of Zn^{2+} on clot

structure was its ability to increase porosity by ~30-fold. Increasing clot porosity favours stability, as these clots easily deform and retract under high shear forces to refrain rupture.

Divalent ions such as Zn^{2+} , Ca^{2+} and Mg^{2+} are stored in the dense granules of platelets, and secreted with activation (Heijnen and van der Sluijs, 2015). Divalent ions are elevated at the site of injury to accelerate clot formation (Carr and Powers, 1991; Marx, 1988b). However, the effect of divalent ions on clot structure and stability is not well defined. Previous reports indicate that Ca^{2+} significantly reduces clot stiffness (Ryan et al., 1999). With careful examination of this data, a biphasic response is actually demonstrated (Ryan et al., 1999). Physiologic Ca^{2+} concentrations (1.5 mM) caused an increase in clot stiffness, whereas supraphysiological Ca^{2+} concentrations (5-20 mM) resulted in a reduction in clot stiffness. The explanation of this response has not been addressed. Ca^{2+} circulates in plasma at ~2 mM, therefore clot stiffness should be increased, as we demonstrated that concentrated platelets release ~200 μM Ca^{2+} (Marx, 1988a). Therefore, Ca^{2+} concentrations at the site of injury will not exceed 5 mM and reduce clot stiffness. Our findings show that Zn^{2+} significantly reduces clot stiffness; therefore Zn^{2+} may counteract the effect of Ca^{2+} to promote clot stability. The effect of Mg^{2+} on the mechanical properties of clots has yet to be evaluated. Previous reports indicate that Mg^{2+} has a similar effect to Ca^{2+} on Fn structure (Carr and Powers, 1991). We hypothesize that Mg^{2+} will exhibit a

similar effect to Ca^{2+} and increase clot stiffness at low (mM) concentrations. The discrepancy between the responses of divalent cations on mechanical properties of clots requires investigation. It would be of interest to examine clot structure in the presence of all divalent ions, Zn^{2+} , Ca^{2+} and Mg^{2+} . Unlike Ca^{2+} and Mg^{2+} , Zn^{2+} binds Fn with high affinity. We believe that the effect of Zn^{2+} on clot structure will remain, however, Ca^{2+} and Mg^{2+} may reduce its potency to provide a fine balance on clot stiffness and stability. The effect of divalent ions on clot structure and stability should be re-evaluated using rheometry techniques, to improve our physiological understanding of clot development and stability.

FXIIIa cross-links Fn fibers providing clot stabilization. Currently, there are extensive studies on the mechanical properties of FXIIIa (Hethershaw et al., 2014; Kurniawan et al., 2014). However, none of these studies included Zn^{2+} reconstitution. We show that Zn^{2+} significantly modifies the structural and mechanical properties of clots independently of FXIIIa. FXIIIa increases clot stiffness, whereas Zn^{2+} has an opposing effect by increasing clot porosity. For stability purposes, Zn^{2+} may counteract the effects of FXIIIa, because FXIIIa compacts the Fn network to increase clot stiffness and rigidity. Clots that are highly porous with loosely woven fibers are advantageous for clot lysis, as Pn and Pg activators can permeate through the clot. As to how Zn^{2+} influences the mechanical properties of clots to reduce clot stiffness remains to be elucidated. Zn^{2+} and FXIIIa may work in unison, to provide an Fn network that is covalently

linked, yet porous to enhance stability, and favour lysis to reduce thrombosis. Regardless of divalent ions and FXIIIa, we show that Zn^{2+} plays a crucial role in clot stabilization.

7.4.2 Examining clot structure in cardiovascular disease patients

Patients afflicted with myocardial infarction or ischemic stroke form clots with densely packed fibers, reduced porosity, and experience prolonged lysis (Undas and Ariens, 2011). Limited data is available regarding the mechanical properties of clots developed in patients with cardiovascular disease (CVD). After examining individual processes in clot formation, we show that the most potent response of Zn^{2+} was demonstrated on clot porosity. Preventative therapies such as heparin, aspirin, NOACs, and statins, increase clot porosity in patients experiencing thrombosis (Bridge et al., 2014). Blood was collected from CVD patients into citrate, and then clot structures were compared. The effect of Zn^{2+} on clot structure was not accurately evaluated due to blood collection into citrate. Based on our results in Chapter 3, clot structure in CVD patients needs to be redefined. We hypothesize that the combination of Zn^{2+} with these therapies will modify clot structure to a greater extent by increasing porosity. Clots formed with prophylaxis and Zn^{2+} *in vitro* can be assessed using SEM, and by calculating Darcy's constant as described in Chapter 3. If Zn^{2+} enhances clot porosity beyond that of other therapies, CVD patients may want to consider dietary Zn^{2+} supplements to elevate plasma concentrations, and promote a more favourable

clot structure. However, the effect of Zn^{2+} supplementation *in vivo* will differ based on the rate of Zn^{2+} absorption and clearance per individual. The mechanical properties of CVD patients undergoing prophylaxes and Zn^{2+} supplementation can be assessed using a rheometer. Clots formed in Zn^{2+} -deficient PPP can be used to determine whether Zn^{2+} supplementation has an additive effect to prophylaxis alteration on clot structure and stability. Re-evaluating the effect of Zn^{2+} on clot formation in CVD patients is a new avenue that should be evaluated.

7.5 Zn^{2+} and Clot Lysis

7.5.1 Zn^{2+} acts as a molecular brake for the fibrinolytic pathway

Zn^{2+} modulation of the coagulation and anticoagulation pathways has been extensively examined (Vu et al., 2013). However, the influence of Zn^{2+} on components within fibrinolysis was not well defined. It was speculated that Zn^{2+} attenuates fibrinolysis, because it accelerates clotting, and alters clot structure (Tubek et al., 2008). However, individual reactions were not examined. We set out to investigate the role of Zn^{2+} on fibrinolysis in more detail. We identified that Zn^{2+} alters clot morphology to generate thick, loosely woven fibers, to form a highly porous clot (Chapter 3). Therefore, Zn^{2+} creates a clot structure that is more favourable to lysis. In Chapter 4, we examined the effect of Zn^{2+} on numerous interactions within the fibrinolysis pathway. Zn^{2+} prolonged clot lysis, however this effect was independent of changes that arise in clot structure.

Overall, Zn^{2+} can be viewed as a dual modulator of fibrinolysis, as it targets Pn-mediated Fn hydrolysis and Pg activation.

7.5.2 Localizing the Zn^{2+} -binding domain on Pn

An interesting finding in Chapter 4 was that Zn^{2+} binds to Pn but not Pg. This indicates that a Zn^{2+} -binding site on Pn is acquired with Pg activation. Lys-Pg and Lys-Pn are chemically identical, except for cleavage of the activation site peptide. Because Zn^{2+} -binding to Pn provides functional consequences on its activity, it would be of interest to identify its Zn^{2+} -binding site.

To confirm that Zn^{2+} binds to Pn but not Pg, we examined Pg activation using a fluorometer. We hypothesize that a Zn^{2+} -binding site on Pn will be exposed with Pg activation. Pg activation was initiated in the presence of Zn^{2+} bound to FluoZin-1, and changes in FI were observed over time. Preliminary data show that activation of Glu-Pg to Lys-Pn by uPA resulted in a concomitant decrease in fluorescence (Appendix Figure 3A) (Henderson 2013, unpublished observation). Thus Zn^{2+} was removed from the FluoZin-1 probe, as the Zn^{2+} -binding site on Lys-Pn was exposed. At various time points during activation, samples were removed from the fluorometer and subjected to SDS-PAGE analysis (Appendix Figure 3B). We confirmed that Zn^{2+} -binding coincides with Lys-Pn generation (Henderson 2013, unpublished observation). Because Zn^{2+} binds to Pn and attenuates its activity towards Fg and Fn, we investigated whether the Zn^{2+} -binding site resides at its active site. In the fluorometer, FluoZin-1 was

bound to Zn^{2+} , and the addition of Pn caused a decrease in FI because Pn binds to Zn^{2+} with a higher affinity than the fluorescent probe. Active site inhibitors VFK-CK or aprotinin were added to the sample to determine whether Zn^{2+} was displaced from the active site of Pn. However, the FI did not change when VFK-CK or aprotinin were added. Therefore, the active site directed inhibitors did not compete with Zn^{2+} -binding at the catalytic triad (Appendix, Figure 4). Thus the Zn^{2+} -binding site may be located elsewhere on the serine protease domain of Pn that impedes its ability to degrade Fn.

It remains unclear as to why Zn^{2+} binds to Pn but not Pg. In chapter 4, we show that the Zn^{2+} -binding site is specific for Pn, as Zn^{2+} did not bind trypsin with high affinity, nor did it affect the ability of trypsin to degrade Fg. In addition, we show that the Zn^{2+} -binding site was not kringle mediated, because Zn^{2+} did not influence Pg or Pn localization to Fg or Fn (Chapter 4). Preliminary data obtained using SPR analysis provided additional confirmation of a metal-sensitive binding site on Pn. A nitrilotriacetic acid (NTA) biosensor chip is a chelating divalent ion chip that enables metal ions to bind. However, this biosensor chip has a weak binding affinity for Zn^{2+} , thus Zn^{2+} cannot be immobilized without it being stripped by Zn^{2+} -binding proteins. As an alternative to Zn^{2+} , Ni^{2+} can be immobilized with high affinity. Ni^{2+} displays similar Zn^{2+} -binding properties to proteins such as HRG and Fg (Jones et al., 2005; Kanaide et al., 1982). Ni^{2+} may have the same ionic properties as Zn^{2+} , although it is not the same ion; thereby

these values are not directly proportional to Zn^{2+} -binding affinities (Thompson et al., 2011). Because Zn^{2+} bound to Pn but not Pg, we hypothesize that Ni^{2+} will have the same response establishing a metal-sensitive binding site. Preliminary data shows that similar to Zn^{2+} , Glu- or Lys-Pg did not bind Ni^{2+} , as K_d values could not be calculated (Appendix Table 2) (Henderson and Stafford 2013, unpublished observation). This data reveals that Pg does not contain a metal-binding site.

The structure of Pg can be modified by selective truncation of its kringle domains with proteases. This can be used to determine what domain on Pn is responsible for metal-binding. Removal of K1-K4 by elastase results in the formation of Mini-Pg, whereas the removal of K1-K5 by Pn generates Micro-Pg (Kim et al., 2012). We hypothesize that truncated forms of Pg will not bind Ni^{2+} , as the metal sensitive binding site is only exposed with Pg activation. Interestingly, Mini-Pg bound Ni^{2+} weakly with K_d values of 42.9 and 26 μ M (Appendix Figure 2, Table 1) (Henderson and Stafford 2013, unpublished observation). This reflects Ni^{2+} binding to the K5 and serine protease domain. This indicates that a metal sensitive binding site is exposed with heavy chain truncation. Removal of the K5 domain resulted in Micro-Pg, which bound Ni^{2+} with ~10- to 16-fold higher affinity than Mini-Pg (K_d value of 2.6 μ M) (Appendix Figure 2, Table 1) (Henderson and Stafford 2013, unpublished observation). These data suggest that a metal-binding site is readily exposed with the removal of the K5 domain.

Because Micro-Pg has a higher binding affinity for Ni^{2+} than Mini-Pg, reveals that the metal-binding site is likely located on the serine protease domain.

To further study the metal-binding site on the K5 domain alone, Lys-Pg could be digested with both elastase and Pn, removing the K1-K4 and K5 domains. By passing the digested fragments over a lysine-sepharose column, the kringle domains will bind via LBS, and can be eluted using epsilon-aminocaproic acid. A K5 metal-binding site can be identified using SPR analysis, as the isolated kringle domains may bind to immobilized Ni^{2+} if it possesses a metal sensitive binding site. Fragments that display Ni^{2+} -binding can be eluted with imidazole, and sent for mass spectrometry for sequence identification. Identification of a metal sensitive binding site on the K5 and protease domain of Pg may provide information regarding the functional consequences of Zn^{2+} on Pg activation.

In Chapter 4, we highlight that Zn^{2+} binds Lys-Pn, but not Glu- or Lys-Pg. We wanted to identify whether Pn also binds Ni^{2+} , as described with Mini- and Micro-Pg. Preliminary data show that Lys-Pn binds Ni^{2+} with high affinity (K_d value of 34.3 nM) (Appendix Figure 2, Table 1) (Henderson and Stafford 2013, unpublished observation). Therefore, activation of Pg to Pn probably exposes multiple metal-binding sites; one of which may be located on the serine protease domain, as Micro-Pg bound Ni^{2+} ~100-fold weaker than Lys-Pn. These preliminary investigations elucidate that a metal-sensitive binding site on Pn is exposed only after Pg is activated or truncated. To localize the binding site of

Zn^{2+} on Pn, we will digest Pn using trypsin or cyanogen bromide to cleave Pn into various sized peptide fragments. By flowing fragments over the Ni^{2+} biosensor chip, SPR analysis will identify fragment binding. Isolated fragments will be sequenced using mass spectrometry to locate the Zn^{2+} -binding site on Pn. A limitation of this experiment is that fragmenting native Pn could disrupt the Zn^{2+} -binding site, and prevent detection. Identification of the Zn^{2+} -binding site on Pn will add information to understand how Zn^{2+} modulates the function of Pn towards Fn degradation.

7.5.3 Identification of the Zn^{2+} -binding domain on tPA

In Chapter 4 we show that Zn^{2+} binds to tPA with high affinity, and impairs its ability to convert Pg to Pn. tPA is considered the gold standard for thrombolytic therapy, therefore it is important to recognize its Zn^{2+} -binding site that affects its function. This is physiologically relevant as tPA may not be as effective at stimulating the fibrinolysis pathway when Zn^{2+} concentrations are elevated at the site of injury. To reveal the Zn^{2+} -binding domain, tPA variants can be assessed using the FluoZin-1. tPA mutants that can be examined include delta-F, delta-EGF, delta-K1 and delta-K2, where each variant lacks their respective fibrinectin finger-like, epidermal growth factor, or kringle domains. Vampire bat plasminogen activator can also be assessed, as it has ~72% amino acid sequence identity to tPA, but lacks K2, and requires Fn to display optimal activity (Stewart et al., 1998). Once we determine which variants bind Zn^{2+} with high

affinity, Pg activation and clot lysis can be examined in the absence and presence of Zn^{2+} , and compared to the response of tPA. This will provide new information pertaining to the Zn^{2+} -binding domain on tPA that modulates its function towards Pg activation.

7.5.4 HRG may assist Zn^{2+} in the attenuation of fibrinolysis

The roles of Zn^{2+} and HRG in fibrinolysis were previously evaluated separately. Studies indicate HRG attenuates fibrinolysis, because lysis was accelerated ~3-fold in a HRG^{-/-} murine model (Tsuchida-Straeten et al., 2005). This delay was attributed to HRG binding to the K1-K3 domains on Pg (Jones et al., 2004). It was speculated that blockage of the kringle domains hinders Pg localization to Fn and reduces Pg activation (Horne, III et al., 2001). However, increased concentrations of HRG are not correlated with a reduction in the amount of Pn generated by tPA (Horne, III et al., 2001). These experiments were performed *in vitro* and lacked Zn^{2+} reconstitution. Therefore, these studies did not take into account that Zn^{2+} -binding to HRG can modulate its functionality. Because fibrinolysis was prolonged by ~2-fold in the presence of Zn^{2+} , we hypothesize that HRG in combination with Zn^{2+} may have a profound (>5-fold) inhibitory effect on fibrinolysis. Human Zn^{2+} -deficient plasma can be obtained via chelation and dialysis as described in Chapter 4. Passing Zn^{2+} -deficient plasma over a Ni^{2+} charged column will remove HRG by binding Ni^{2+} via its HRR. The effect of HRG and Zn^{2+} together on clot lysis can be examined with the

HRG/ Zn^{2+} -deficient plasma in the presence of tPA. Lysis times can be compared with a dose-dependent reconstitution of individual or combinations of HRG and Zn^{2+} . Metal-binding to Pn via the K5 and protease domain of Pg, and HRG binding to the K1-K3 domains on Pg suggests that HRG and Zn^{2+} may work together to down-regulate fibrinolysis. Re-evaluating the role of HRG/ Zn^{2+} regulation on clot lysis needs to be extensively investigated to identify new areas of fibrinolysis regulation.

7.6 Recapitulating the effect of Zn^{2+} on hemostatic reactions *in vivo*

The overarching goal of this thesis was to examine the *in vitro* effect of Zn^{2+} on individual hemostatic processes, such as platelet activation, clot formation, and fibrinolysis. Zn^{2+} is released from activated platelets where it substantially modifies clot structure and delays fibrinolysis. Because these reactions were performed in purified systems in the absence of Zn^{2+} -binding plasma proteins such as albumin and α_2 -macroglobulin, it would be ideal to establish an *in vivo* murine model to examine the effect of Zn^{2+} on these interactions. Limiting Zn^{2+} as a dietary source *versus* Zn^{2+} supplementation has generated a Zn^{2+} -deficient murine model (Reiterer et al., 2005). However, this reduces the concentration of total Zn^{2+} within the body, and does not completely eliminate circulating plasma Zn^{2+} levels. This makes it difficult to recapitulate our experiments *in vivo*, because we cannot completely remove Zn^{2+} from plasma *in vivo*, like *in vitro* using chelation and dialysis. The role of Zn^{2+} in the circulation highly complex, which

makes it difficult to assess individual reactions in hemostasis *in vivo*. It is challenging to strictly elevate Zn^{2+} concentrations to an individual process in the body; therefore examining individual reactions *in vitro* is the best way to understand Zn^{2+} regulation in hemostatic processes.

CHAPTER 8: CONCLUSION

8.1 Concluding Remarks

This thesis identifies Zn^{2+} and HRG storage and release in platelets, and the involvement of Zn^{2+} in regulating clot formation and fibrinolysis. We show that Zn^{2+} and HRG are not located where previously reported in platelets, whereas Zn^{2+} resided in the dense granules, and HRG remained in the cytoplasm and on the outer surface. We confirmed that Zn^{2+} accelerates clotting, and substantially modifies clot structure to favour stability. We also provide mechanistic evidence as to why fibrinolysis is delayed in the presence of Zn^{2+} . The effects of Zn^{2+} on hemostatic interactions have been overlooked due the presence of chelating agents for blood collection. Our re-evaluation of the role of Zn^{2+} in hemostasis supports the concept that Zn^{2+} should be incorporated into all *in vitro* reactions and indicates that more studies need to be conducted to explore the role of Zn^{2+} *in vivo*.

We have examined the location of HRG, Zn^{2+} and Ca^{2+} ions in platelets. We add evidence that goes against the central “dogma” of protein and ion storage in platelets. Not all large proteins get compartmentalized in the alpha granules, because HRG was identified in the cytoplasm and on the surface of platelets. In contrast, like Ca^{2+} , Zn^{2+} also is packaged in the dense granules, even though Zn^{2+} -binding proteins such as HRG and Fg are found in the cytoplasm and alpha granules, respectively. Because a molecule is located in a secretory granule does not definitively indicate that it will be fully secreted with platelet activation. This

was highlighted with Zn^{2+} , as it was only partially secreted from activated platelets. HRG and Zn^{2+} interact with an abundance of ligands in the body; therefore it is not surprising that both provide alternative functions in platelets compared with plasma.

We have determined that Zn^{2+} modifies clot structure. The interpretation that accelerated clot formation reflects thin fiber generation needs to be re-assessed. We show that Zn^{2+} accelerates clot times, but increases fiber thickness. Therefore, the rate of clot formation should not be used as a predictor of fiber thickness. We demonstrated that Zn^{2+} increases clot porosity and deformation, rendering clots to be more resistant to rupture. FXIIIa is the main stabilizer of clots because it compacts the Fn network. However, Zn^{2+} opposes the effect of FXIIIa because it reduced clot stiffness and increased deformation. Therefore, Zn^{2+} appears to be another important modulator of clot structure that enhances stability. A definitive explanation of “stability” and what essentially stabilizes a clot requires re-evaluation.

Changes in clot structure may not be the most accurate way to predict the rate of fibrinolysis. Increasing clot porosity facilitates the diffusion of lytic proteins into the interstices of a clot, thereby accelerating lysis. We show that Zn^{2+} increases clot porosity, which in theory should favour lysis. However, we show that fibrinolysis is attenuated because Zn^{2+} targets multiple components to

down-regulate fibrinolysis. Therefore, it should not be assumed that structure directly determines the rate of clot degradation.

Zn^{2+} has a potent effect on both coagulation and fibrinolysis reactions. Understanding the role of Zn^{2+} in these processes is only one avenue that has been explored. The addition of Zn^{2+} -binding proteins such as HRG into these reactions may cause an alternative response. The combination of HRG and Zn^{2+} to modulate clot structure and fibrinolysis remains to be investigated. Overall, this thesis reveals a greater complexity as to new areas of Zn^{2+} regulation within hemostasis.

CHAPTER 9: APPENDIX

* All preliminary data was conducted by Sara J. Henderson from 2011-2015. Ran Ni provided blood collection, and Laura Pepler and Ji Zhou performed and bone marrow isolation from WT and HRG^{-/-} mice. Alan Stafford provided the SPR experiments (Figure 3). Data collected from all figures below has not been published. This data may lead to future projects, as described in Chapter 7.

9.1 Methods

9.1.1 Establishing a HRG dose-regiment in HRG^{-/-} mice

To examine HRG entry from plasma into HRG^{-/-} MK and platelets, we needed to ensure that HRG levels remained elevated in HRG^{-/-} mice for 6 h. This time should be sufficient for MK or platelets to allow HRG entry from the circulation (Pluthero 2015, unpublished observation). Human HRG (6 mg/kg) was injected into the tail vein of HRG^{-/-} mice at 0, 0 and 2, or 0, 2, and 4 h. As controls, no treatment or saline injections were performed. At 6 h, mice were anesthetised as described in Chapter 6, and blood was collected from the carotid artery into 3.2% citrate. Blood was subjected to centrifugation 1000 x g for 10 min at 23°C, and the PPP was harvested. Plasma HRG levels were quantified using an ELISA as described in Chapter 6. At 6 h, 1.2 µM HRG was detected in the plasma from HRG^{-/-} mice receiving three injections (Appendix Figure 1). These results indicate

that HRG is rapidly cleared from the circulation in HRG^{-/-} mice. In the control groups, HRG was not detected in HRG^{-/-} mice as expected.

9.1.2 Preparation of bone marrow from HRG^{-/-} Mice

Once the dose-regiment was established (three HRG injections at 0, 2, and 4 h), blood was collected from the carotid artery of WT and HRG^{-/-} mice. To harvest the MK, the femurs and tibias were removed from the mice, and the bone marrow was flushed with 1 ml PBS containing 2.5% glutaraldehyde, incubated at 23°C for 1 h, and stored at 4°C. MK were stained for HRG and imaged as described in Chapter 6.

9.1.3 Preparation of platelets from HRG^{-/-} Mice

Blood collected into 3.2% citrate and diluted (1:10 vol/vol) in PBS containing citrate. Blood was subjected to centrifugation at 150 x g for 15 min. PRP was harvested and an equal volume of 8% PFA/PBS was added, and incubated for 15 min. Fixed PRP was subjected to centrifugation at 1000 x g for 8 min, and the supernatant was removed. The platelet pellet was reconstituted in PBS, washed twice with PBS/citrate, and stored at 23°C. Platelets were stained for HRG, and imaged as described in Chapter 6.

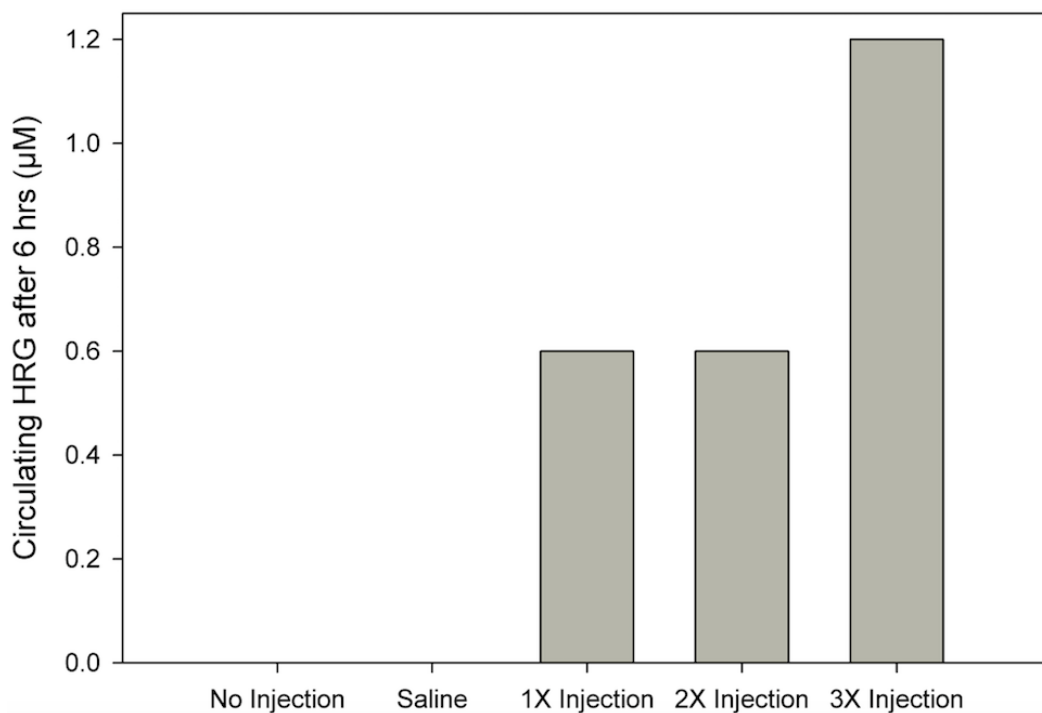


Figure 1. HRG is rapidly cleared from the circulation of HRG^{-/-} mice

HRG^{-/-} mice were injected with saline, or 1-3 doses of human HRG every 2 h. Blood was collected from the carotid artery, and the plasma was isolated. Plasma human HRG quantified using a modified sandwich ELISA (Chapter 6). HRG is rapidly cleared with from the circulation with 1-2 doses, thus 3 doses is optimal to restore physiological HRG levels at 6 h.

Protein	K_d (μM)
Glu-Pg	NB
Lys-Pg	NB
Lys-Pn	0.03
Mini-Pg	26
Micro-Pg	2.6

Table 2. Affinity of Ni²⁺ for fibrinolytic proteins

The binding affinities of various fibrinolytic proteins for immobilized Ni²⁺, were determined by SPR. NB represents no binding to Ni²⁺.

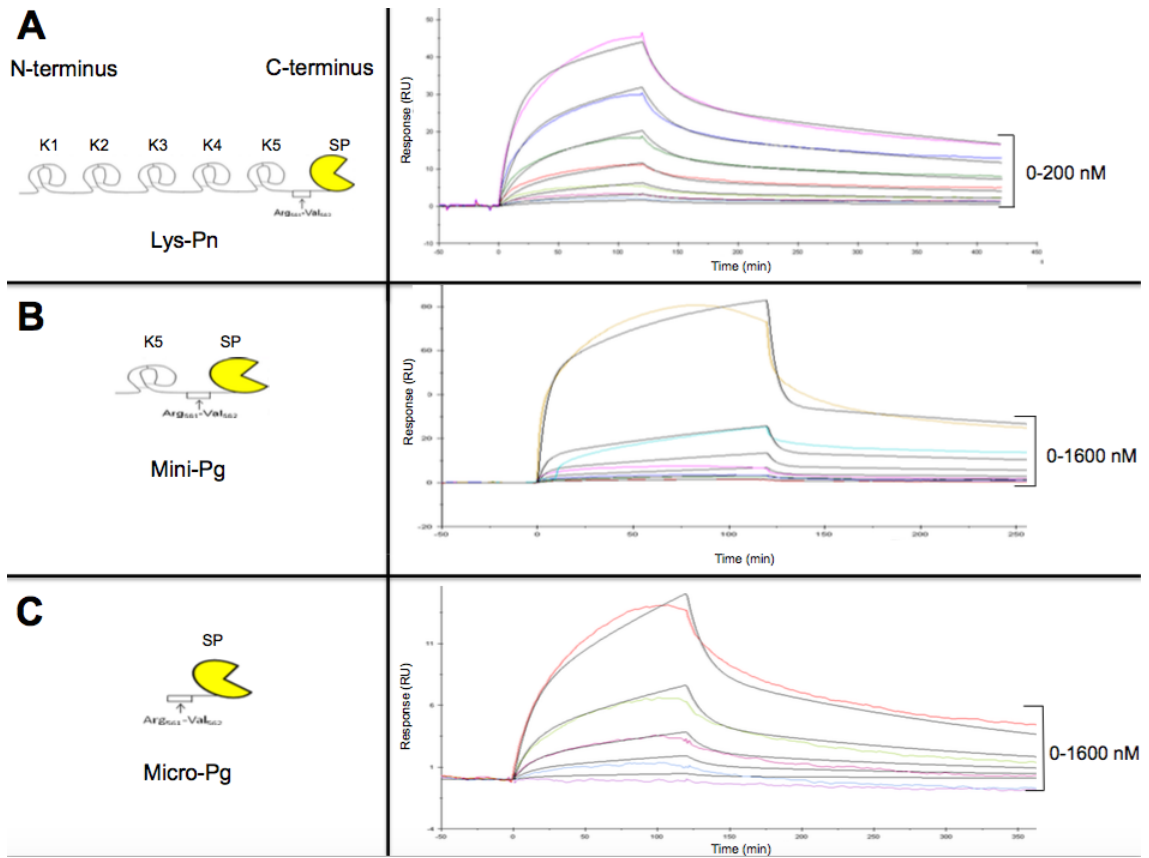
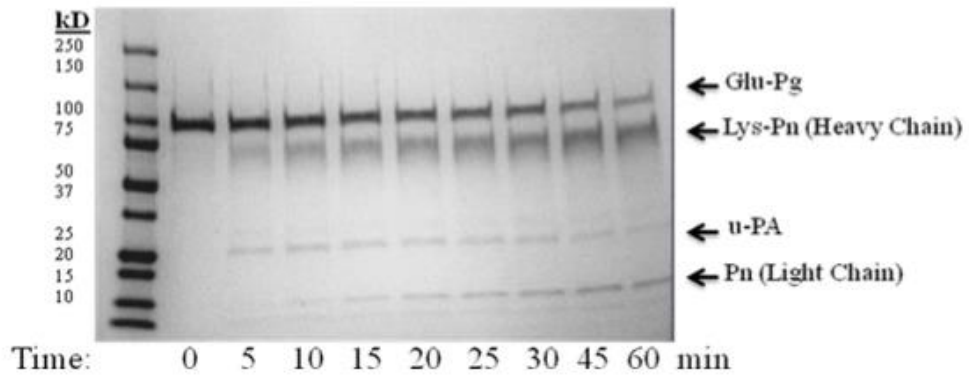


Figure 2. Lys-Pn, Mini-Pg, and Micro-Pg bind to Ni²⁺ in a dose-dependent fashion

The structure of (A) Lys-Pn, (B) Mini-Pg, and (C) Micro-Pg are displayed in panels on the left. Lys-Pn contains 5 kringle domains on its N-terminus, and a serine protease domain on its C-terminus. Truncation of the K1-4 domains, results in Mini-Pg. Removal of all kringle domains results in Micro-Pg, as it contains only the serine protease domain. Structurally, Lys-Pn is identical to Lys-Pg, except for the cleavage of a single peptide bond Arg₅₆₁-Val₅₆₂. This is the activation peptide sequence, that is targeted by Pg activators tPA or uPA. Cleavage of the activation peptide converts the zymogen Pg to its active protease form Pn. Lines represent doses of Lys-Pn (0, 3.1, 6.3, 12.5, 50, 100, and 200 nM), Mini-Pg (0, 25, 50, 100, 200, 400, 800, 1600 nM), and Micro-Pg (0, 25, 50, 100, 200, 400, 800, 1600 nM) passed over a Ni²⁺ coated biosensor chip, and binding affinities were determined. Lys-Pn binds Ni²⁺ in a dose-dependent fashion, indicated by the sensorgram on the right. With removal of K1-4 and K1-5 domains, Mini- and Micro-Pg were also able to bind to Ni²⁺ in a dose-response. This data suggests that the Ni²⁺ binding site on Pg and Pn is most likely located on the serine protease domain, and exposed by either activation of Pg to Pn, or through the removal of the kringle domains.

A



B

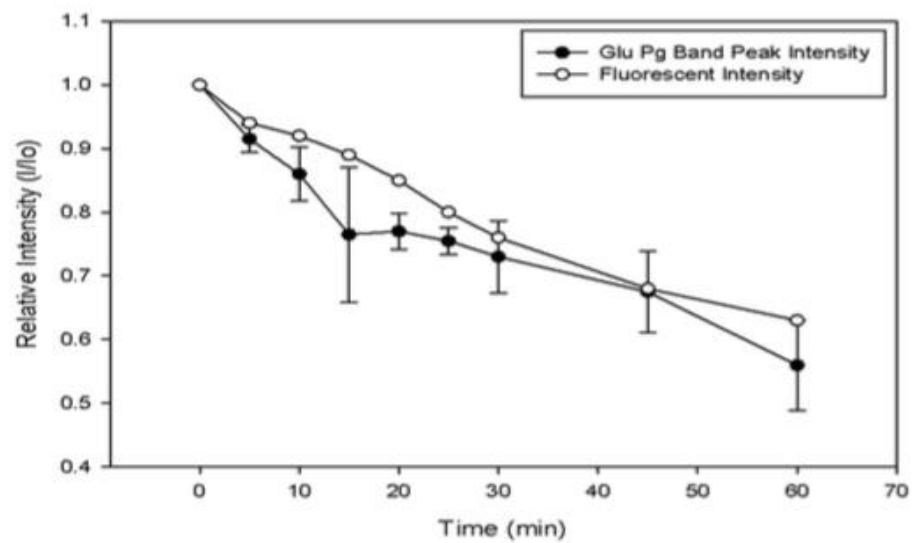


Figure 3. Pg activation monitored by SDS-PAGE and fluorescence

A reaction containing 0.5 μM FluoZin-1 and 5 μM Zn^{2+} in TBS was monitored at 37°C in a fluorimeter. After about 480 s, 4 μM of Glu-Pg was added to the mixture, followed by 0.5 μM u-PA addition. **(A)** Samples were taken over various periods of time from 0-60 min and subjected to SDS-PAGE analysis under reducing conditions. Molecular weight markers are labeled on the left. The identities of the protein bands are labeled on the right. **(B)** The FI at each time point from the raw data was normalized to give to that before uPA addition (I/I_0) and is represented in by the open circles. Densitometry values of Glu-Pg on SDS-PAGE from **(A)** were normalized and are represented by closed circles. Error bars indicate SE.

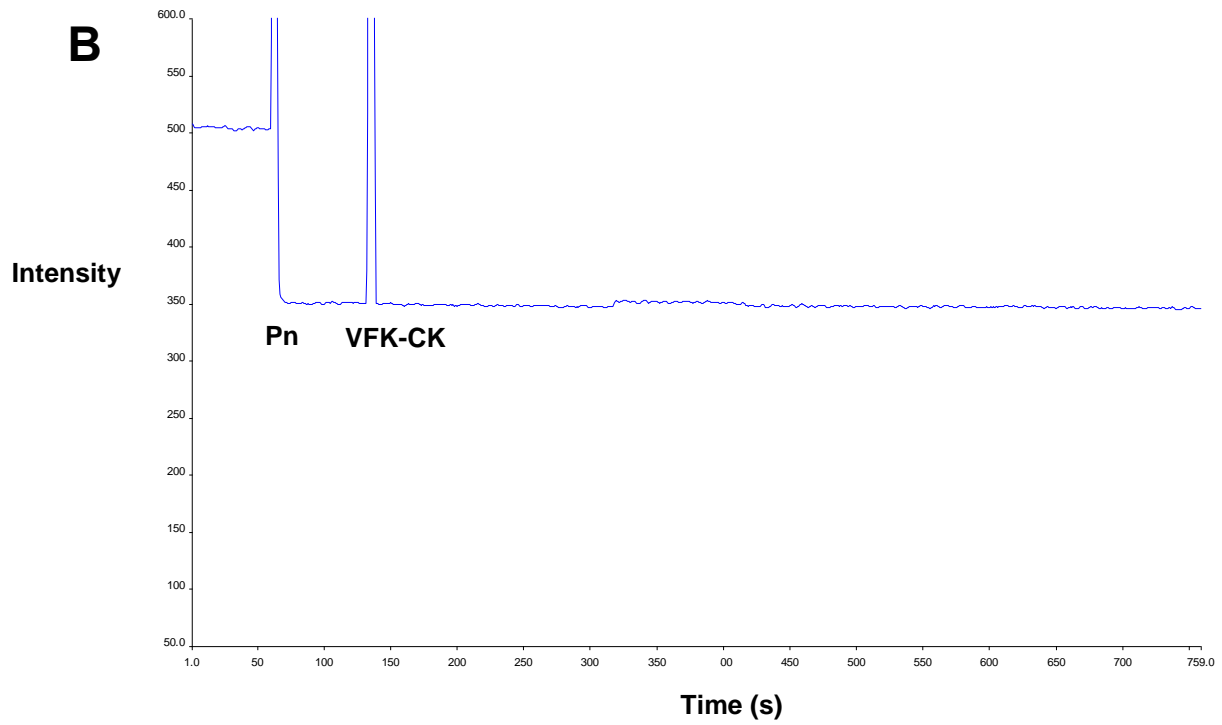
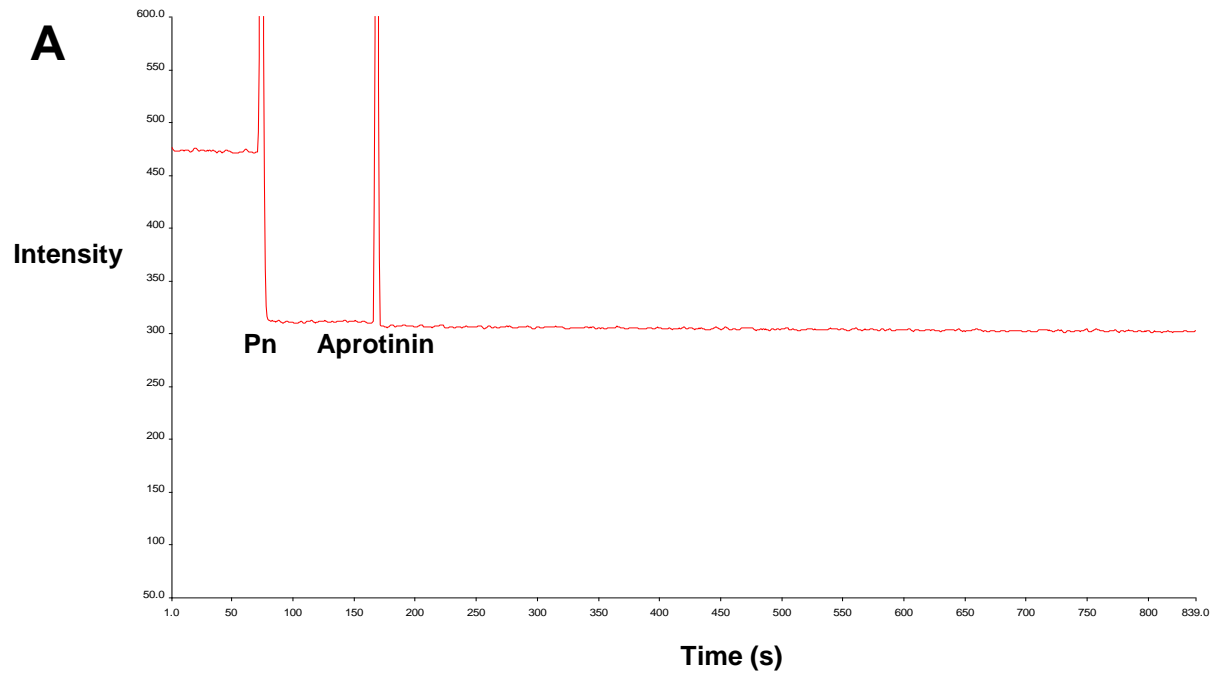


Figure 4. Zn²⁺-binding to the catalytic site of Pn

Zn²⁺ (5 μM) was incubated with FluoZin-1 (0.5 μM) in TBS, until the FI remained stable (*line*). Pn (0.25 μM) was added to the Zn²⁺ FluoZin-1 solution, resulting in a reduction in FI. This reflects Zn²⁺-binding to Pn. Once the FI signal remained stable, serine protease inhibitors (A) aprotinin (2 μM) or (B) VFK-CK (1.25 μM) were added respectively. No change in FI was observed with the addition of the serine protease inhibitors.

CHAPTER 10: BIBLIOGRAPHY

Adams,TE, J A Huntington, 2006, Thrombin-cofactor interactions: structural insights into regulatory mechanisms: *Arterioscler.Thromb.Vasc.Biol.*, v. 26, p. 1738-1745.

Aleman,MM, J R Byrnes, J G Wang, R Tran, W A Lam, J Di Paola, N Mackman, J L Degen, M J Flick, A S Wolberg, 2014, Factor XIII activity mediates red blood cell retention in venous thrombi: *J.Clin.Invest*, v. 124, p. 3590-3600.

Allan,P, d W Uitte, R H Abou-Saleh, S D Connell, R A Ariens, 2012, Evidence that fibrinogen gamma' directly interferes with protofibril growth: implications for fibrin structure and clot stiffness: *J.Thromb.Haemost.*, v. 10, p. 1072-1080.

Ariens,RA, H Philippou, C Nagaswami, J W Weisel, D A Lane, P J Grant, 2000, The factor XIII V34L polymorphism accelerates thrombin activation of factor XIII and affects cross-linked fibrin structure: *Blood*, v. 96, p. 988-995.

Baeten,KM, M C Richard, S M Kanse, N J Mutch, J L Degen, N A Booth, 2010, Activation of single-chain urokinase-type plasminogen activator by platelet-associated plasminogen: a mechanism for stimulation of fibrinolysis by platelets: *J.Thromb.Haemost.*, v. 8, p. 1313-1322.

Bagoly,Z, Z Koncz, J Harsfalvi, L Muszbek, 2012, Factor XIII, clot structure, thrombosis: *Thromb.Res.*, v. 129, p. 382-387.

Bax,CM, D L Bloxam, 1997, Human fetal endothelial cells acquire zinc(II) from both the protein bound and nonprotein bound pools in serum: *Biol.Trace Elem.Res.*, v. 56, p. 255-271.

Beattie,JH, I S Kwun, 2004, Is zinc deficiency a risk factor for atherosclerosis?: *Br.J.Nutr.*, v. 91, p. 177-181.

Bernik,MB, H C Kwaan, 1969, Plasminogen activator activity in cultures from human tissues. An immunological and histochemical study: *Journal of Clinical Investigation*, v. 48, p. 1740-1753.

Black,RE, 2003, Zinc deficiency, infectious disease and mortality in the developing world: *J.Nutr.*, v. 133, p. 1485S-1489S.

Blair,P, R Flaumenhaft, 2009, Platelet alpha-granules: basic biology and clinical correlates: *Blood Rev.*, v. 23, p. 177-189.

Boudreau,LH, A C Duchez, N Cloutier, D Soulet, N Martin, J Bollinger, A Pare, M Rousseau, G S Naika, T Levesque, C Laflamme, G Marcoux, G Lambeau, R W Farndale, M Pouliot, H Hamzeh-Cognasse, F Cognasse, O Garraud, P A Nigrovic, H Guderley, S Lacroix, L Thibault, J W Semple, M H Gelb, E Boilard, 2014, Platelets release mitochondria serving as substrate for bactericidal group IIA-secreted phospholipase A2 to promote inflammation: *Blood*, v. 124, p. 2173-2183.

Bridge,KI, H Philippou, R Ariens, 2014, Clot properties and cardiovascular disease: *Thrombosis & Haemostasis*, v. 112, p. 901-908.

Brown,KJ, C R Parish, 1994, Histidine-rich glycoprotein and platelet factor 4 mask heparan sulfate proteoglycans recognized by acidic and basic fibroblast growth factor: *Biochemistry*, v. 33, p. 13918-13927.

Camiolo,SM, S Thorsen, T Astrup, 1971, Fibrinogenolysis and fibrinolysis with tissue plasminogen activator, urokinase, streptokinase-activated human globulin, and plasmin: *Proc.Soc.Exp.Biol.Med.*, v. 138, p. 277-280.

Carr,ME, 1988, Fibrin formed in plasma is composed of fibers more massive than those formed from purified fibrinogen: *Thrombosis & Haemostasis*, v. 59, p. 535-539.

Carr,ME, P L Powers, 1991, Differential effects of divalent cations on fibrin structure: *Blood Coagul.Fibrinolysis*, v. 2, p. 741-747.

Cesarman-Maus,G, K A Hajjar, 2005, Molecular mechanisms of fibrinolysis: *Br.J.Haematol.*, v. 129, p. 307-321.

Chen,W. Studies on the role of calcium chnnels and the kinase domain of transient receptor potential melastatin-like 7 (TRPM7) in platelet function. 2015. Ref Type: Unpublished Work

Collet,JP, J L Moen, Y I Veklich, O V Gorkun, S T Lord, G Montalescot, J W Weisel, 2005, The alphaC domains of fibrinogen affect the structure of the fibrin clot, its physical properties, and its susceptibility to fibrinolysis: *Blood*, v. 106, p. 3824-3830.

Collet,JP, D Park, C Lesty, J Soria, C Soria, G Montalescot, J W Weisel, 2000, Influence of fibrin network conformation and fibrin fiber diameter on fibrinolysis speed: dynamic and structural approaches by confocal microscopy: *Arterioscler.Thromb.Vasc.Biol.*, v. 20, p. 1354-1361.

Collet,JP, J L Woodhead, J Soria, C Soria, M Mirshahi, J P Caen, J W Weisel, 1996, Fibrinogen Dusart: electron microscopy of molecules, fibers and clots, and viscoelastic properties of clots: *Biophys.J.*, v. 70, p. 500-510.

Corrigan,JJ, Jr., M A Jeter, D Bruck, W M Feinberg, 1990, Histidine-rich glycoprotein levels in children: the effect of age: *Thromb.Res.*, v. 59, p. 681-686.

Daly,ME, 2011, Determinants of platelet count in humans: *Haematologica*, v. 96, p. 10-13.

Dang,CV, W R Bell, R F Ebert, N F Starksen, 1985, Protective effect of divalent cations in the plasmin degradation of fibrinogen: *Archives of Biochemistry and Biophysics*, v. 238, p. 452-457.

Dang,CV, C K Shin, W R Bell, C Nagaswami, J W Weisel, 1989, Fibrinogen sialic acid residues are low affinity calcium-binding sites that influence fibrin assembly: *J.Biol.Chem.*, v. 264, p. 15104-15108.

Dano,K, P A Andreasen, J Grondahl-Hansen, P Kristensen, L S Nielsen, L Skriver, 1985, Plasminogen activators, tissue degradation, and cancer: *Adv.Cancer Res.*, v. 44, p. 139-266.

Devine,DV, W F Rosse, 1987, Regulation of the activity of platelet-bound C3 convertase of the alternative pathway of complement by platelet factor H: *Proc.Natl.Acad.Sci.U.S.A.*, v. 84, p. 5873-5877.

Di Stasio,E, C Nagaswami, J W Weisel, E Di Cera, 1998, Cl⁻ regulates the structure of the fibrin clot: *Biophys.J.*, v. 75, p. 1973-1979.

Ermens,AA, P J de Wild, H L Vader, G F van der, 1995, Four agglutination assays evaluated for measurement of von Willebrand factor (ristocetin cofactor activity): *Clinical Chemistry*, v. 41, p. 510-514.

Esmon,CT, 1989, The roles of protein C and thrombomodulin in the regulation of blood coagulation: *J.Biol.Chem.*, v. 264, p. 4743-4746.

Esmon,CT, W G Owen, C M Jackson, 1974, The conversion of prothrombin to thrombin. V. The activation of prothrombin by factor Xa in the presence of phospholipid: *J.Biol.Chem.*, v. 249, p. 7798-7807.

Fatah,K, B Hessel, 1998, Effect of zinc ions on fibrin network structure: *Blood Coagul.Fibrinolysis*, v. 9, p. 629-635.

Fernandes,N, L O Mosnier, L Tonnu, M J Heeb, 2010, Zn(2)(+) -containing protein S inhibits extrinsic factor X-activating complex independently of tissue factor pathway inhibitor: *J.Thromb.Haemost.*, v. 8, p. 1976-1985.

Ferry,JD, P R Morrison, 1947, Preparation and properties of serum and plasma proteins; the conversion of human fibrinogen to fibrin under various conditions: *J.Am.Chem.Soc.*, v. 69, p. 388-400.

Fitch-Tewfik,JL, R Flaumenhaft, 2013, Platelet granule exocytosis: a comparison with chromaffin cells: *Front Endocrinol.(Lausanne)*, v. 4, p. 77.

Flaumenhaft,R, 2003, Molecular basis of platelet granule secretion: *Arterioscler.Thromb.Vasc.Biol.*, v. 23, p. 1152-1160.

Flaumenhaft,R, J R Dilks, N Rozenvayn, R A Monahan-Earley, D Feng, A M Dvorak, 2005, The actin cytoskeleton differentially regulates platelet alpha-granule and dense-granule secretion: *Blood*, v. 105, p. 3879-3887.

Foote,JW, H T Delves, 1984, Albumin bound and alpha 2-macroglobulin bound zinc concentrations in the sera of healthy adults: *Journal of Clinical Pathology*, v. 37, p. 1050-1054.

Fraser,SR, N A Booth, N J Mutch, 2011, The antifibrinolytic function of factor XIII is exclusively expressed through alpha(2)-antiplasmin cross-linking: *Blood*, v. 117, p. 6371-6374.

Fredenburgh,JC, B A Leslie, A R Stafford, T Lim, H H Chan, J I Weitz, 2013, Zn²⁺ mediates high affinity binding of heparin to the alphaC domain of fibrinogen: *J.Biol.Chem.*, v. 288, p. 29394-29402.

Fredenburgh,JC, M E Nesheim, 1992, Lys-plasminogen is a significant intermediate in the activation of Glu-plasminogen during fibrinolysis in vitro: *J.Biol.Chem.*, v. 267, p. 26150-26156.

Fredenburgh,JC, A R Stafford, B A Leslie, J I Weitz, 2008, Bivalent binding to gammaA/gamma'-fibrin engages both exosites of thrombin and protects it from inhibition by the antithrombin-heparin complex: *J.Biol.Chem.*, v. 283, p. 2470-2477.

Gabriel,DA, K Muga, E M Boothroyd, 1992, The effect of fibrin structure on fibrinolysis: *J.Biol.Chem.*, v. 267, p. 24259-24263.

Gebbink,MF, 2011, Tissue-type plasminogen activator-mediated plasminogen activation and contact activation, implications in and beyond haemostasis: *J.Thromb.Haemost.*, v. 9 Suppl 1, p. 174-181.

Gordon,PR, J D Browning, B L O'Dell, 1983, Platelet arachidonate metabolism and platelet function in zinc-deficient rats: *J.Nutr.*, v. 113, p. 766-772.

Gordon,PR, C W Woodruff, H L Anderson, B L O'Dell, 1982, Effect of acute zinc deprivation on plasma zinc and platelet aggregation in adult males: *Am.J.Clin.Nutr.*, v. 35, p. 113-119.

Gorgani,NN, C R Parish, J G Altin, 1999, Differential binding of histidine-rich glycoprotein (HRG) to human IgG subclasses and IgG molecules containing kappa and lambda light chains: *J.Biol.Chem.*, v. 274, p. 29633-29640.

Gorkun,OV, Y I Veklich, L V Medved, A H Henschen, J W Weisel, 1994, Role of the alpha C domains of fibrin in clot formation: *Biochemistry*, v. 33, p. 6986-6997.

Gorodetsky,R, X Mou, A Blankenfeld, G Marx, 1993, Platelet multielemental composition, lability, and subcellular localization: *Am.J Hematol.*, v. 42, p. 278-283.

Griffin,JH, 1978, Role of surface in surface-dependent activation of Hageman factor (blood coagulation factor XII): *Proc.Natl.Acad.Sci.U.S.A*, v. 75, p. 1998-2002.

Guthans,SL, W T Morgan, 1982, The interaction of zinc, nickel and cadmium with serum albumin and histidine-rich glycoprotein assessed by equilibrium dialysis and immunoabsorbent chromatography: *Archives of Biochemistry and Biophysics*, v. 218, p. 320-328.

Hambidge,KM, N F Krebs, 2007, Zinc deficiency: a special challenge: *J.Nutr.*, v. 137, p. 1101-1105.

Han, Y, A Nurden, R Combrie, J M Pasquet, 2003, Redistribution of glycoprotein Ib within platelets in response to protease-activated receptors 1 and 4: roles of cytoskeleton and calcium: *J.Thromb.Haemost.*, v. 1, p. 2206-2215.

Handagama, P, R M Scarborough, M A Shuman, D F Bainton, 1993, Endocytosis of fibrinogen into megakaryocyte and platelet alpha-granules is mediated by alpha IIb beta 3 (glycoprotein IIb-IIIa): *Blood*, v. 82, p. 135-138.

Heeb, MJ, R M Mesters, G Tans, J Rosing, J H Griffin, 1993, Binding of protein S to factor Va associated with inhibition of prothrombinase that is independent of activated protein C: *J.Biol.Chem.*, v. 268, p. 2872-2877.

Heijnen, H, S P van der Sluijs, 2015, Platelet secretory behavior As diverse as the granulesor not?: *J.Thromb.Haemost.*

Heijnen, HF, N Debili, W Vainchencker, J Breton-Gorius, H J Geuze, J J Sixma, 1998, Multivesicular bodies are an intermediate stage in the formation of platelet alpha-granules: *Blood*, v. 91, p. 2313-2325.

Helms, CC, R A Ariens, d W Uitte, K F Standeven, M Guthold, 2012, alpha-alpha Cross-links increase fibrin fiber elasticity and stiffness: *Biophys.J.*, v. 102, p. 168-175.

Henderson, SJ, A R Stafford, B A Leslie, P Y Kim, N Vaezzadeh, R Ni, J C Fredenburgh, J I Weitz, 2015a, Zinc delays clot lysis by attenuating plasminogen activation and plasmin-mediated fibrin degradation: *Thrombosis & Haemostasis*, v. 113.

Henderson, SJ, J Xia, H Wu, A R Stafford, B A Leslie, J C Fredenburgh, D A Weitz, J I Weitz, 2015b, Zinc promotes clot stability by accelerating clot formation and modifying fibrin structure: *Thrombosis & Haemostasis*, v. 115.

Hethershaw, EL, A L Cilia La Corte, C Duval, M Ali, P J Grant, R A Ariens, H Philippou, 2014, The effect of blood coagulation factor XIII on fibrin clot structure and fibrinolysis: *J.Thromb.Haemost.*, v. 12, p. 197-205.

Heyns, AP, A Eldor, R Yarom, G Marx, 1985, Zinc-induced platelet aggregation is mediated by the fibrinogen receptor and is not accompanied by release or by thromboxane synthesis: *Blood*, v. 66, p. 213-219.

Ho, G, G J Broze, Jr., A L Schwartz, 1997, Role of heparan sulfate proteoglycans in the uptake and degradation of tissue factor pathway inhibitor-coagulation factor Xa complexes: *J.Biol.Chem.*, v. 272, p. 16838-16844.

- Hopmeier,P, M Halbmayr, M Fischer, G Marx, 1990, Zinc modulates thrombin adsorption to fibrin: *Thromb.Res.*, v. 58, p. 293-301.
- Horne,MK, III, P K Merryman, A M Cullinane, 2001, Histidine-proline-rich glycoprotein binding to platelets mediated by transition metals: *Thrombosis & Haemostasis*, v. 85, p. 890-895.
- Horrevoets,AJ, A Smilde, C de Vries, H Pannekoek, 1994, The specific roles of finger and kringle 2 domains of tissue-type plasminogen activator during in vitro fibrinolysis: *J.Biol.Chem.*, v. 269, p. 12639-12644.
- Hoyer-Hansen,G, E Ronne, H Solberg, N Behrendt, M Ploug, L R Lund, V Ellis, K Dano, 1992, Urokinase plasminogen activator cleaves its cell surface receptor releasing the ligand-binding domain: *J.Biol.Chem.*, v. 267, p. 18224-18229.
- Hughes,S, S Samman, 2006, The effect of zinc supplementation in humans on plasma lipids, antioxidant status and thrombogenesis: *J.Am.Coll.Nutr.*, v. 25, p. 285-291.
- Hulett,MD, C R Parish, 2000, Murine histidine-rich glycoprotein: cloning, characterization and cellular origin: *Immunol.Cell Biol.*, v. 78, p. 280-287.
- Husain,SS, 1991, A single-step separation of the one- and two-chain forms of tissue plasminogen activator: *Archives of Biochemistry and Biophysics*, v. 285, p. 373-376.
- Israels,SJ, J M Gerrard, Y V Jacques, A McNicol, B Cham, M Nishibori, D F Bainton, 1992, Platelet dense granule membranes contain both granulophysin and P-selectin (GMP-140): *Blood*, v. 80, p. 143-152.
- Italiano,JE, Jr., E M Battinelli, 2009, Selective sorting of alpha-granule proteins: *J.Thromb.Haemost.*, v. 7 Suppl 1, p. 173-176.
- Italiano,JE, Jr., J L Richardson, S Patel-Hett, E Battinelli, A Zaslavsky, S Short, S Ryeom, J Folkman, G L Klement, 2008, Angiogenesis is regulated by a novel mechanism: pro- and antiangiogenic proteins are organized into separate platelet alpha granules and differentially released: *Blood*, v. 111, p. 1227-1233.
- Jones,AL, M D Hulett, J G Altin, P Hogg, C R Parish, 2004, Plasminogen is tethered with high affinity to the cell surface by the plasma protein, histidine-rich glycoprotein: *J.Biol.Chem.*, v. 279, p. 38267-38276.

Jones,AL, M D Hulett, C R Parish, 2005, Histidine-rich glycoprotein: A novel adaptor protein in plasma that modulates the immune, vascular and coagulation systems: *Immunol.Cell Biol.*, v. 83, p. 106-118.

Jurasz,P, A W Chung, A Radomski, M W Radomski, 2002, Nonremodeling properties of matrix metalloproteinases: the platelet connection: *Circ.Res.*, v. 90, p. 1041-1043.

Kahr,WH, J Hinckley, L Li, H Schwertz, H Christensen, J W Rowley, F G Pluthero, D Urban, S Fabbro, B Nixon, R Gadzinski, M Storck, K Wang, G Y Ryu, S M Jobe, B C Schutte, J Moseley, N B Loughran, J Parkinson, A S Weyrich, J Di Paola, 2011, Mutations in NBEAL2, encoding a BEACH protein, cause gray platelet syndrome: *Nat.Genet.*, v. 43, p. 738-740.

Kahr,WH, R W Lo, L Li, F G Pluthero, H Christensen, R Ni, N Vaezzadeh, C E Hawkins, A S Weyrich, J Di Paola, C Landolt-Marticorena, P L Gross, 2013, Abnormal megakaryocyte development and platelet function in *Nbeal2(-/-)* mice: *Blood*, v. 122, p. 3349-3358.

Kambe,T, T Tsuji, A Hashimoto, N Itsumura, 2015, The Physiological, Biochemical, and Molecular Roles of Zinc Transporters in Zinc Homeostasis and Metabolism: *Physiol Rev.*, v. 95, p. 749-784.

Kanaide,H, T Uranishi, M Nakamura, 1982, Effects of divalent cations on the conversion of fibrinogen to fibrin and fibrin polymerization: *Am.J.Hematol.*, v. 13, p. 229-237.

Kassar,O, U Schwarz-Linek, C A Blindauer, A J Stewart, 2015, Plasma free fatty acid levels influence Zn(2+) -dependent histidine-rich glycoprotein-heparin interactions via an allosteric switch on serum albumin: *J.Thromb.Haemost.*, v. 13, p. 101-110.

Kiem,J, H Borberg, G V Iyengar, K Kasperek, M Siegers, L E Feinendegen, R Gross, 1979, Elemental composition of platelets. Part II. Water content of normal human platelets and measurements of their concentrations of Cu, Fe, K, and Zn by neutron activation analysis: *Clinical Chemistry*, v. 25, p. 705-710.

Kim,PY, L D Tieu, A R Stafford, J C Fredenburgh, J I Weitz, 2012, A high affinity interaction of plasminogen with fibrin is not essential for efficient activation by tissue-type plasminogen activator: *J.Biol.Chem.*, v. 287, p. 4652-4661.

Kluszynski,BA, C Kim, W P Faulk, 1997, Zinc as a cofactor for heparin neutralization by histidine-rich glycoprotein: *J.Biol.Chem.*, v. 272, p. 13541-13547.

Koopman,J, F Haverkate, J Grimbergen, R Egbring, S T Lord, 1992, Fibrinogen Marburg: a homozygous case of dysfibrinogenemia, lacking amino acids A alpha 461-610 (Lys 461 AAA-->stop TAA): *Blood*, v. 80, p. 1972-1979.

Koseoglu,S, R Flaumenhaft, 2013, Advances in platelet granule biology: *Curr.Opin.Hematol.*, v. 20, p. 464-471.

Kotze,RC, R A Ariens, Z de Lange, M Pieters, 2014, CVD risk factors are related to plasma fibrin clot properties independent of total and or gamma' fibrinogen concentration: *Thromb.Res.*, v. 134, p. 963-969.

Krezel,A, J Wojcik, M Maciejczyk, W Bal, 2011, Zn(II) complexes of glutathione disulfide: structural basis of elevated stabilities: *Inorg.Chem.*, v. 50, p. 72-85.

Krishnaswamy,S, 2005, Exosite-driven substrate specificity and function in coagulation: *J.Thromb.Haemost.*, v. 3, p. 54-67.

Kunamneni,A, T T Abdelghani, P Ellaiah, 2007, Streptokinase--the drug of choice for thrombolytic therapy: *J.Thromb.Thrombolysis.*, v. 23, p. 9-23.

Kurniawan,NA, J Grimbergen, J Koopman, G H Koenderink, 2014, Factor XIII stiffens fibrin clots by causing fiber compaction: *J.Thromb.Haemost.*, v. 12, p. 1687-1696.

Lerch,PG, U E Nydegger, C Kuyas, A Haeberli, 1988, Histidine-rich glycoprotein binding to activated human platelets: *Br.J.Haematol.*, v. 70, p. 219-224.

Leung,LL, 1986, Interaction of histidine-rich glycoprotein with fibrinogen and fibrin: *J.Clin.Invest*, v. 77, p. 1305-1311.

Leung,LL, P C Harpel, R L Nachman, E M Rabellino, 1983, Histidine-rich glycoprotein is present in human platelets and is released following thrombin stimulation: *Blood*, v. 62, p. 1016-1021.

Leung,LL, R L Nachman, P C Harpel, 1984, Complex formation of platelet thrombospondin with histidine-rich glycoprotein: *J.Clin.Invest*, v. 73, p. 5-12.

Levin,EG, U Marzec, J Anderson, L A Harker, 1984, Thrombin stimulates tissue plasminogen activator release from cultured human endothelial cells: *Journal of Clinical Investigation*, v. 74, p. 1988-1995.

Levy,JH, C Greenberg, 2013, Biology of Factor XIII and clinical manifestations of Factor XIII deficiency: *Transfusion*, v. 53, p. 1120-1131.

Li,Z, M K Delaney, K A O'Brien, X Du, 2010, Signaling during platelet adhesion and activation: *Arterioscler.Thromb.Vasc.Biol.*, v. 30, p. 2341-2349.

Licht,C, F G Pluthero, L Li, H Christensen, S Habbig, B Hoppe, D F Geary, P F Zipfel, W H Kahr, 2009, Platelet-associated complement factor H in healthy persons and patients with atypical HUS: *Blood*, v. 114, p. 4538-4545.

Lin,Y, R A Pixley, R W Colman, 2000, Kinetic analysis of the role of zinc in the interaction of domain 5 of high-molecular weight kininogen (HK) with heparin: *Biochemistry*, v. 39, p. 5104-5110.

Lippi,G, C Mattiuzzi, E J Favalaro, 2013, Novel and emerging therapies: thrombus-targeted fibrinolysis: *Semin.Thromb.Hemost.*, v. 39, p. 48-58.

Liu,CY, J H Sobel, J I Weitz, K L Kaplan, H L Nossel, 1986, Immunologic identification of the cleavage products from the A alpha- and B beta-chains in the early stages of plasmin digestion of fibrinogen: *Thrombosis & Haemostasis*, v. 56, p. 100-106.

Longstaff,C, I Varju, P Sotonyi, L Szabo, M Krumrey, A Hoell, A Bota, Z Varga, E Komorowicz, K Kolev, 2013, Mechanical stability and fibrinolytic resistance of clots containing fibrin, DNA, and histones: *J.Biol.Chem.*, v. 288, p. 6946-6956.

Lorand,L, 2001, Factor XIII: structure, activation, and interactions with fibrinogen and fibrin: *Ann.N.Y.Acad.Sci.*, v. 936, p. 291-311.

Low,CM, F Zheng, P Lyuboslavsky, S F Traynelis, 2000, Molecular determinants of coordinated proton and zinc inhibition of N-methyl-D-aspartate NR1/NR2A receptors: *Proc.Natl.Acad.Sci.U.S.A.*, v. 97, p. 11062-11067.

Lu,BG, T Sofian, R H Law, P B Coughlin, A J Horvath, 2011, Contribution of conserved lysine residues in the alpha2-antiplasmin C terminus to plasmin binding and inhibition: *J.Biol.Chem.*, v. 286, p. 24544-24552.

Lu,J, A J Stewart, P J Sadler, T J Pinheiro, C A Blindauer, 2008, Albumin as a zinc carrier: properties of its high-affinity zinc-binding site: *Biochem.Soc.Trans.*, v. 36, p. 1317-1321.

Machlus,KR, J E Italiano, Jr., 2013, The incredible journey: From megakaryocyte development to platelet formation: *J.Cell Biol.*, v. 201, p. 785-796.

Mackman,N, R E Tilley, N S Key, 2007, Role of the extrinsic pathway of blood coagulation in hemostasis and thrombosis: *Arterioscler.Thromb.Vasc.Biol.*, v. 27, p. 1687-1693.

MacQuarrie,JL, A R Stafford, J W Yau, B A Leslie, T T Vu, J C Fredenburgh, J I Weitz, 2011, Histidine-rich glycoprotein binds factor XIIa with high affinity and inhibits contact-initiated coagulation: *Blood*, v. 117, p. 4134-4141.

Mahaut-Smith,MP, 2012, The unique contribution of ion channels to platelet and megakaryocyte function: *J.Thromb.Haemost.*, v. 10, p. 1722-1732.

Mahdi,F, Z S Madar, C D Figueroa, A H Schmaier, 2002, Factor XII interacts with the multiprotein assembly of urokinase plasminogen activator receptor, gC1qR, and cytokeratin 1 on endothelial cell membranes: *Blood*, v. 99, p. 3585-3596.

Mahdi,F, Z Shariat-Madar, A H Schmaier, 2003, The relative priority of prekallikrein and factors XI/XIa assembly on cultured endothelial cells: *J.Biol.Chem.*, v. 278, p. 43983-43990.

Marti,D, J Schaller, B Ochensberger, E E Rickli, 1994, Expression, purification and characterization of the recombinant kringle 2 and kringle 3 domains of human plasminogen and analysis of their binding affinity for omega-aminocarboxylic acids: *Eur.J.Biochem.*, v. 219, p. 455-462.

Martinez,A, E Salas, A Radomski, M W Radomski, 2001, Matrix metalloproteinase-2 in platelet adhesion to fibrinogen: interactions with nitric oxide: *Med.Sci.Monit.*, v. 7, p. 646-651.

Marx,G, 1988a, Elasticity of fibrin and protofibrin gels is differentially modulated by calcium and zinc: *Thrombosis & Haemostasis*, v. 59, p. 500-503.

Marx,G, 1988b, Mechanism of fibrin coagulation based on selective, cation-driven, protofibril association: *Biopolymers*, v. 27, p. 763-774.

- Marx,G, 1988c, Zinc binding to fibrinogen and fibrin: Archives of Biochemistry and Biophysics, v. 266, p. 285-288.
- Marx,G, A Eldor, 1985, The procoagulant effect of zinc on fibrin clot formation: Am.J.Hematol., v. 19, p. 151-159.
- Marx,G, P Hopmeier, 1986, Zinc inhibits FPA release and increases fibrin turbidity: Am.J.Hematol., v. 22, p. 347-353.
- Marx,G, P Hopmeier, D Gurfel, 1987, Zinc alters fibrin ultrastructure: Thrombosis & Haemostasis, v. 57, p. 73-76.
- Marx,G, G Korner, X Mou, R Gorodetsky, 1993, Packaging zinc, fibrinogen, and factor XIII in platelet alpha-granules: Journal of Cell Physiology, v. 156, p. 437-442.
- McCall,KA, C Huang, C A Fierke, 2000, Function and mechanism of zinc metalloenzymes: J.Nutr., v. 130, p. 1437S-1446S.
- Meh,DA, K R Siebenlist, S O Brennan, T Holyst, M W Mosesson, 2001, The amino acid sequence in fibrin responsible for high affinity thrombin binding: Thrombosis & Haemostasis, v. 85, p. 470-474.
- Mitchell,JL, A S Lionikiene, S R Fraser, C S Whyte, N A Booth, N J Mutch, 2014, Functional factor XIII-A is exposed on the stimulated platelet surface: Blood, v. 124, p. 3982-3990.
- Mohan Rao,LV, C T Esmon, U R Pendurthi, 2014, Endothelial cell protein C receptor: a multiliganded and multifunctional receptor: Blood, v. 124, p. 1553-1562.
- Morrissey,JH, B G Macik, P F Neuenschwander, P C Comp, 1993, Quantitation of activated factor VII levels in plasma using a tissue factor mutant selectively deficient in promoting factor VII activation: Blood, v. 81, p. 734-744.
- Muller,I, A Klocke, M Alex, M Kotzsch, T Luther, E Morgenstern, S Zieseniss, S Zahler, K Preissner, B Engelmann, 2003, Intravascular tissue factor initiates coagulation via circulating microvesicles and platelets: FASEB J., v. 17, p. 476-478.
- Muthard,RW, S L Diamond, 2012, Blood clots are rapidly assembled hemodynamic sensors: flow arrest triggers intraluminal thrombus contraction: Arterioscler.Thromb.Vasc.Biol., v. 32, p. 2938-2945.

Naimushin, YA, A V Mazurov, 2004, Von Willebrand factor can support platelet aggregation via interaction with activated GPIIb-IIIa and GPIb: *Platelets.*, v. 15, p. 419-425.

Nispen tot, PH, F de Haas, W Geerts, G Posthuma, S van Dijk, H F Heijnen, 2010, The platelet interior revisited: electron tomography reveals tubular alpha-granule subtypes: *Blood*, v. 116, p. 1147-1156.

Nozaki, C, A M Vergnano, D Filliol, A Ouagazzal, A Le Goff, S Carvalho, D Reiss, C Gaveriaux-Ruff, J Neyton, P Paoletti, B L Kieffer, 2011, Zinc alleviates pain through high-affinity binding to the NMDA receptor NR2A subunit: *Nature Neuroscience*, v. 14, p. 1017-1022.

Offermanns, S, 2006, Activation of platelet function through G protein-coupled receptors: *Circ.Res.*, v. 99, p. 1293-1304.

Park, HS, C Hong, B J Kim, I So, 2014, The Pathophysiologic Roles of TRPM7 Channel: *Korean J. Physiol Pharmacol.*, v. 18, p. 15-23.

Patel, SR, J H Hartwig, J E Italiano, Jr., 2005, The biogenesis of platelets from megakaryocyte proplatelets: *J.Clin.Invest.*, v. 115, p. 3348-3354.

Petersen, LC, O H Olsen, L S Nielsen, P O Freskgard, E Persson, 2000, Binding of Zn²⁺ to a Ca²⁺ loop allosterically attenuates the activity of factor VIIa and reduces its affinity for tissue factor: *Protein Sci.*, v. 9, p. 859-866.

Podor, TJ, C B Peterson, D A Lawrence, S Stefansson, S G Shaughnessy, D M Foulon, M Butcher, J I Weitz, 2000, Type 1 plasminogen activator inhibitor binds to fibrin via vitronectin: *J.Biol.Chem.*, v. 275, p. 19788-19794.

Prasad, AS, 2009, Impact of the discovery of human zinc deficiency on health: *J.Am.Coll.Nutr.*, v. 28, p. 257-265.

Rao, AK, 2013, Inherited platelet function disorders: overview and disorders of granules, secretion, and signal transduction: *Hematol.Oncol.Clin.North Am.*, v. 27, p. 585-611.

Reiterer, G, R MacDonald, J D Browning, J Morrow, S V Matveev, A Daugherty, E Smart, M Toborek, B Hennig, 2005, Zinc deficiency increases plasma lipids and atherosclerotic markers in LDL-receptor-deficient mice: *J.Nutr.*, v. 135, p. 2114-2118.

- Rendu,F, B Brohard-Bohn, 2001, The platelet release reaction: granules' constituents, secretion and functions: *Platelets.*, v. 12, p. 261-273.
- Rijken,DC, E Groeneveld, 1986, Isolation and functional characterization of the heavy and light chains of human tissue-type plasminogen activator: *J.Biol.Chem.*, v. 261, p. 3098-3102.
- Ringvall,M, A Thulin, L Zhang, J Cedervall, N Tsuchida-Straeten, W Jahnen-Dechent, A Siegbahn, A K Olsson, 2011, Enhanced platelet activation mediates the accelerated angiogenic switch in mice lacking histidine-rich glycoprotein: *PLoS.One.*, v. 6, p. e14526.
- Rojkjaer,R, I Schousboe, 1997, Partial identification of the Zn²⁺-binding sites in factor XII and its activation derivatives: *Eur.J.Biochem.*, v. 247, p. 491-496.
- Rojkjaer,R, A A Hasan, G Motta, I Schousboe, A H Schmaier, 1998, Factor XII does not initiate prekallikrein activation on endothelial cells: *Thrombosis & Haemostasis*, v. 80, p. 74-81.
- Rojkjaer,R, A H Schmaier, 1999, Activation of the plasma kallikrein/kinin system on endothelial cells: *Proceedings of the Association of American Physicians*, v. 111, p. 220-227.
- Roohani,N, R Hurrell, R Kelishadi, R Schulin, 2013, Zinc and its importance for human health: An integrative review: *J.Res.Med.Sci.*, v. 18, p. 144-157.
- Ruggeri,ZM, 2000, Role of von Willebrand factor in platelet thrombus formation: *Ann.Med.*, v. 32 Suppl 1, p. 2-9.
- Ruggeri,ZM, G L Mendolicchio, 2007, Adhesion mechanisms in platelet function: *Circ.Res.*, v. 100, p. 1673-1685.
- Ruiz,FA, C R Lea, E Oldfield, R Docampo, 2004, Human platelet dense granules contain polyphosphate and are similar to acidocalcisomes of bacteria and unicellular eukaryotes: *J.Biol.Chem.*, v. 279, p. 44250-44257.
- Ryan,EA, L F Mockros, J W Weisel, L Lorand, 1999, Structural origins of fibrin clot rheology: *Biophys.J.*, v. 77, p. 2813-2826.
- Rydengard,V, O Shannon, K Lundqvist, L Kacprzyk, A Chalupka, A K Olsson, M Morgelin, W Jahnen-Dechent, M Malmsten, A Schmidtchen, 2008, Histidine-rich glycoprotein protects from systemic *Candida* infection: *PLoS.Pathog.*, v. 4, p. e1000116.

Sandset,PM, U Abildgaard, M L Larsen, 1988, Heparin induces release of extrinsic coagulation pathway inhibitor (EPI): *Thromb.Res.*, v. 50, p. 803-813.

Sappino,AP, J Huarte, J D Vassalli, D Belin, 1991, Sites of synthesis of urokinase and tissue-type plasminogen activators in the murine kidney: *Journal of Clinical Investigation*, v. 87, p. 962-970.

Sasisekharan,R, G Venkataraman, 2000, Heparin and heparan sulfate: biosynthesis, structure and function: *Curr.Opin.Chem.Biol.*, v. 4, p. 626-631.

Savage,B, M Cattaneo, Z M Ruggeri, 2001, Mechanisms of platelet aggregation: *Curr.Opin.Hematol.*, v. 8, p. 270-276.

Schaefer,AV, B A Leslie, J A Rischke, A R Stafford, J C Fredenburgh, J I Weitz, 2006, Incorporation of fragment X into fibrin clots renders them more susceptible to lysis by plasmin: *Biochemistry*, v. 45, p. 4257-4265.

Schaller,J, S S Gerber, 2011, The plasmin-antiplasmin system: structural and functional aspects: *Cellular and Molecular Life Sciences*, v. 68, p. 785-801.

Schneider,M, N Brufatto, E Neill, M Nesheim, 2004, Activated thrombin-activatable fibrinolysis inhibitor reduces the ability of high molecular weight fibrin degradation products to protect plasmin from antiplasmin: *J.Biol.Chem.*, v. 279, p. 13340-13345.

Schneider,M, M Nesheim, 2004, A study of the protection of plasmin from antiplasmin inhibition within an intact fibrin clot during the course of clot lysis: *J.Biol.Chem.*, v. 279, p. 13333-13339.

Schroeder,V, H P Kohler, 2013, New developments in the area of factor XIII: *J.Thromb.Haemost.*, v. 11, p. 234-244.

Seizer,P, A E May, 2013, Platelets and matrix metalloproteinases: *Thrombosis & Haemostasis*, v. 110, p. 903-909.

Sen,P, S Sahoo, U R Pendurthi, L V Rao, 2010, Zinc modulates the interaction of protein C and activated protein C with endothelial cell protein C receptor: *J.Biol.Chem.*, v. 285, p. 20410-20420.

Siddiq,MM, S E Tsirka, 2004, Modulation of zinc toxicity by tissue plasminogen activator: *Molecular and Cellular Neurosciences*, v. 25, p. 162-171.

Silverstein,RL, L L Leung, P C Harpel, R L Nachman, 1985, Platelet thrombospondin forms a trimolecular complex with plasminogen and histidine-rich glycoprotein: *J.Clin.Invest*, v. 75, p. 2065-2073.

Sixma,JJ, G H van Zanten, E U Saelman, M Verkleij, H Lankhof, H K Nieuwenhuis, P G De Groot, 1995, Platelet adhesion to collagen: *Thrombosis & Haemostasis*, v. 74, p. 454-459.

Smith,SA, R J Travers, J H Morrissey, 2015, How it all starts: Initiation of the clotting cascade: *Crit Rev.Biochem.Mol.Biol.*, v. 50, p. 326-336.

Sohndel,S, C K Hu, D Marti, M Affolter, J Schaller, M Llinas, E E Rickli, 1996, Recombinant gene expression and 1H NMR characteristics of the kringle (2 + 3) supermodule: spectroscopic/functional individuality of plasminogen kringle domains: *Biochemistry*, v. 35, p. 2357-2364.

Stearns-Kurosawa,DJ, S Kurosawa, J S Mollica, G L Ferrell, C T Esmon, 1996, The endothelial cell protein C receptor augments protein C activation by the thrombin-thrombomodulin complex: *Proc.Natl.Acad.Sci.U.S.A.*, v. 93, p. 10212-10216.

Stewart,AJ, C A Blindauer, P J Sadler, 2009, Plasma fatty acid levels may regulate the Zn(2+)-dependent activities of histidine-rich glycoprotein: *Biochimie*, v. 91, p. 1518-1522.

Stewart,RJ, J C Fredenburgh, J I Weitz, 1998, Characterization of the interactions of plasminogen and tissue and vampire bat plasminogen activators with fibrinogen, fibrin, and the complex of D-dimer noncovalently linked to fragment E: *J.Biol.Chem.*, v. 273, p. 18292-18299.

Suzuki,K, S Hashimoto, 1976, The influences of divalent metal ions on fibrin monomer polymerization: *Biochim.Biophys.Acta*, v. 439, p. 310-315.

Suzuki,Y, H Yasui, T Brzoska, H Mogami, T Urano, 2011, Surface-retained tPA is essential for effective fibrinolysis on vascular endothelial cells: *Blood*, v. 118, p. 3182-3185.

Tennent,GA, S O Brennan, A J Stangou, J O'Grady, P N Hawkins, M B Pepys, 2007, Human plasma fibrinogen is synthesized in the liver: *Blood*, v. 109, p. 1971-1974.

Thompson,LC, S Goswami, C B Peterson, 2011, Metals affect the structure and activity of human plasminogen activator inhibitor-1. II. Binding affinity and conformational changes: *Protein Sci.*, v. 20, p. 366-378.

Thon,JN, J E Italiano, 2010, Platelet formation: *Semin.Hematol.*, v. 47, p. 220-226.

Thon,JN, A Montalvo, S Patel-Hett, M T Devine, J L Richardson, A Ehrlicher, M K Larson, K Hoffmeister, J H Hartwig, J E Italiano, Jr., 2010, Cytoskeletal mechanics of proplatelet maturation and platelet release: *J.Cell Biol.*, v. 191, p. 861-874.

Tsuchida-Straeten,N, S Ensslen, C Schafer, M Woltje, B Denecke, M Moser, S Graber, S Wakabayashi, T Koide, W Jahn-Dechent, 2005, Enhanced blood coagulation and fibrinolysis in mice lacking histidine-rich glycoprotein (HRG): *J.Thromb.Haemost.*, v. 3, p. 865-872.

Tsurupa,G, I Pechik, R I Litvinov, R R Hantgan, N Tjandra, J W Weisel, L Medved, 2012, On the mechanism of alphaC polymer formation in fibrin: *Biochemistry*, v. 51, p. 2526-2538.

Tu,Z, J Liang, 2006, Zinc inhibits tumor metastasis by regulating plasminogen activation: *International Journal of Cancer Research*, v. 2, p. 376-382.

Tubek,S, 2007, Zinc supplementation or regulation of its homeostasis: advantages and threats: *Biol.Trace Elem.Res.*, v. 119, p. 1-9.

Tubek,S, P Grzanka, I Tubek, 2008, Role of zinc in hemostasis: a review: *Biol.Trace Elem.Res.*, v. 121, p. 1-8.

Undas,A, R A Ariens, 2011, Fibrin clot structure and function: a role in the pathophysiology of arterial and venous thromboembolic diseases: *Arterioscler.Thromb.Vasc.Biol.*, v. 31, p. e88-e99.

Vallee,BL, K H Falchuk, 1993, The biochemical basis of zinc physiology: *Physiology reviews*, v. 73, p. 79-118.

Valnickova,Z, J J Enghild, 1998, Human procarboxypeptidase U, or thrombin-activable fibrinolysis inhibitor, is a substrate for transglutaminases. Evidence for transglutaminase-catalyzed cross-linking to fibrin: *J.Biol.Chem.*, v. 273, p. 27220-27224.

van Niftrik,L, W J Geerts, E G van Donselaar, B M Humbel, A Yakushevskaya, A J Verkleij, M S Jetten, M Strous, 2008, Combined structural and chemical analysis of the anammoxosome: a membrane-bounded intracytoplasmic compartment in anammox bacteria: *J.Struct.Biol.*, v. 161, p. 401-410.

Varju,I, C Longstaff, L Szabo, A Z Farkas, V J Varga-Szabo, A Tanka-Salamon, R Machovich, K Kolev, 2015, DNA, histones and neutrophil extracellular traps exert anti-fibrinolytic effects in a plasma environment: *Thrombosis & Haemostasis*, v. 113, p. 1289-1298.

Verhenne,S, F Denorme, S Libbrecht, A Vandembulcke, I Pareyn, H Deckmyn, A Lambrecht, B Nieswandt, C Kleinschnitz, K Vanhoorelbeke, S F De Meyer, 2015, Platelet-derived VWF is not essential for normal thrombosis and hemostasis but fosters ischemic stroke injury in mice: *Blood*, v. 126, p. 1715-1722.

Violand,BN, F J Castellino, 1976, Mechanism of the urokinase-catalyzed activation of human plasminogen: *J.Biol.Chem.*, v. 251, p. 3906-3912.

Vu,T, B A Leslie, A R Stafford, J Zhou, J C Fredenburgh, J I Weitz, 2015a, Histidine-rich glycoprotein binds DNA and RNA and attenuates their capacity to activate the intrinsic coagulation pathway: *Thrombosis & Haemostasis*, v. 115.

Vu,TT, J C Fredenburgh, J I Weitz, 2013, Zinc: an important cofactor in haemostasis and thrombosis: *Thrombosis & Haemostasis*, v. 109, p. 421-430.

Vu,TT, A R Stafford, B A Leslie, P Y Kim, J C Fredenburgh, J I Weitz, 2011, Histidine-rich glycoprotein binds fibrin(ogen) with high affinity and competes with thrombin for binding to the gamma'-chain: *J.Biol.Chem.*, v. 286, p. 30314-30323.

Vu,TT, J Zhou, B A Leslie, A R Stafford, J C Fredenburgh, R Ni, S Qiao, N Vaezzadeh, W Jahnen-Dechent, B P Monia, P L Gross, J I Weitz, 2015b, Arterial thrombosis is accelerated in mice deficient in histidine-rich glycoprotein: *Blood*, v. 125, p. 2712-2719.

Wakabayashi,S, T Koide, 2011, Histidine-rich glycoprotein: a possible modulator of coagulation and fibrinolysis: *Semin.Thromb.Hemost.*, v. 37, p. 389-394.

Walker,JB, M E Nesheim, 1999, The molecular weights, mass distribution, chain composition, and structure of soluble fibrin degradation products released from a fibrin clot perfused with plasmin: *J.Biol.Chem.*, v. 274, p. 5201-5212.

Walton,BL, T M Getz, W Bergmeier, F C Lin, d W Uitte, A S Wolberg, 2014, The fibrinogen gammaA/gamma' isoform does not promote acute arterial thrombosis in mice: *J.Thromb.Haemost.*, v. 12, p. 680-689.

Weinstein,MJ, R F Doolittle, 1972, Differential specificities of the thrombin, plasmin and trypsin with regard to synthetic and natural substrates and inhibitors: *Biochim.Biophys.Acta*, v. 258, p. 577-590.

Weisel,JW, 2004, The mechanical properties of fibrin for basic scientists and clinicians: *Biophys.Chem.*, v. 112, p. 267-276.

Weisel,JW, 2007, Structure of fibrin: impact on clot stability: *J.Thromb.Haemost.*, v. 5 Suppl 1, p. 116-124.

Weisel,JW, R I Litvinov, 2013, Mechanisms of fibrin polymerization and clinical implications: *Blood*, v. 121, p. 1712-1719.

Weitz,JI, 2003, Heparan sulfate: antithrombotic or not?: *J.Clin.Invest*, v. 111, p. 952-954.

Weitz,JI, M K Cruickshank, B Thong, B Leslie, M N Levine, J Ginsberg, T Eckhardt, 1988, Human tissue-type plasminogen activator releases fibrinopeptides A and B from fibrinogen: *Journal of Clinical Investigation*, v. 82, p. 1700-1707.

Weitz,JI, B Leslie, 1990, Urokinase has direct catalytic activity against fibrinogen and renders it less clottable by thrombin: *Journal of Clinical Investigation*, v. 86, p. 203-212.

Whiss,PA, R G Andersson, 2002, Divalent cations and the protein surface coordinate the intensity of human platelet adhesion and P-selectin surface expression: *Blood Coagul.Fibrinolysis*, v. 13, p. 407-416.

Whiteheart,SW, 2011, Platelet granules: surprise packages: *Blood*, v. 118, p. 1190-1191.

Whitehouse,RC, A S Prasad, P I Rabbani, Z T Cossack, 1982, Zinc in plasma, neutrophils, lymphocytes, and erythrocytes as determined by flameless atomic absorption spectrophotometry: *Clinical Chemistry*, v. 28, p. 475-480.

Whyte,CS, F Swieringa, T G Mastenbroek, A S Lionikiene, M D Lance, P E van der Meijden, J W Heemskerk, N J Mutch, 2015, Plasminogen associates with phosphatidylserine-exposing platelets and contributes to thrombus lysis under flow: *Blood*, v. 125, p. 2568-2578.

Wijten,P, T van Holten, L L Woo, O B Bleijerveld, M Roest, A J Heck, A Scholten, 2013, High precision platelet releasate definition by quantitative reversed protein profiling--brief report: *Arterioscler.Thromb.Vasc.Biol.*, v. 33, p. 1635-1638.

Wolberg,AS, D M Monroe, H R Roberts, M Hoffman, 2003, Elevated prothrombin results in clots with an altered fiber structure: a possible mechanism of the increased thrombotic risk: *Blood*, v. 101, p. 3008-3013.

Xue,Y, C Bodin, K Olsson, 2012, Crystal structure of the native plasminogen reveals an activation-resistant compact conformation: *J.Thromb.Haemost.*, v. 10, p. 1385-1396.

Yakushevskaya,AE, M N Lebbink, W J Geerts, L Spek, E G van Donselaar, K A Jansen, B M Humbel, J A Post, A J Verkleij, A J Koster, 2007, STEM tomography in cell biology: *J.Struct.Biol.*, v. 159, p. 381-391.

Yee,NS, A A Kazi, R K Yee, 2014, Cellular and Developmental Biology of TRPM7 Channel-Kinase: Implicated Roles in Cancer: *Cells*, v. 3, p. 751-777.

You,WK, W S Choi, Y S Koh, H C Shin, Y Jang, K H Chung, 2004, Functional characterization of recombinant batroxobin, a snake venom thrombin-like enzyme, expressed from *Pichia pastoris*: *FEBS Lett.*, v. 571, p. 67-73.

Zavyalova,EG, A D Protopopova, A M Kopylov, I V Yaminsky, 2011, Investigation of early stages of fibrin association: *Langmuir*, v. 27, p. 4922-4927.

Zeng,Z, K Inoue, H Sun, T Leng, X Feng, L Zhu, Z G Xiong, 2015, TRPM7 regulates vascular endothelial cell adhesion and tube formation: *Am.J.Physiol Cell Physiol*, v. 308, p. C308-C318.

Zierold,K, 1997, Effects of cadmium on electrolyte ions in cultured rat hepatocytes studied by X-ray microanalysis of cryosections: *Toxicol.Appl.Pharmacol.*, v. 144, p. 70-76.